Journal of Chemistry

Analysis and Remediation of Pollutants in Water and Soil

Lead Guest Editor: Jun Wu
Guest Editors: Xia He and Song Jin

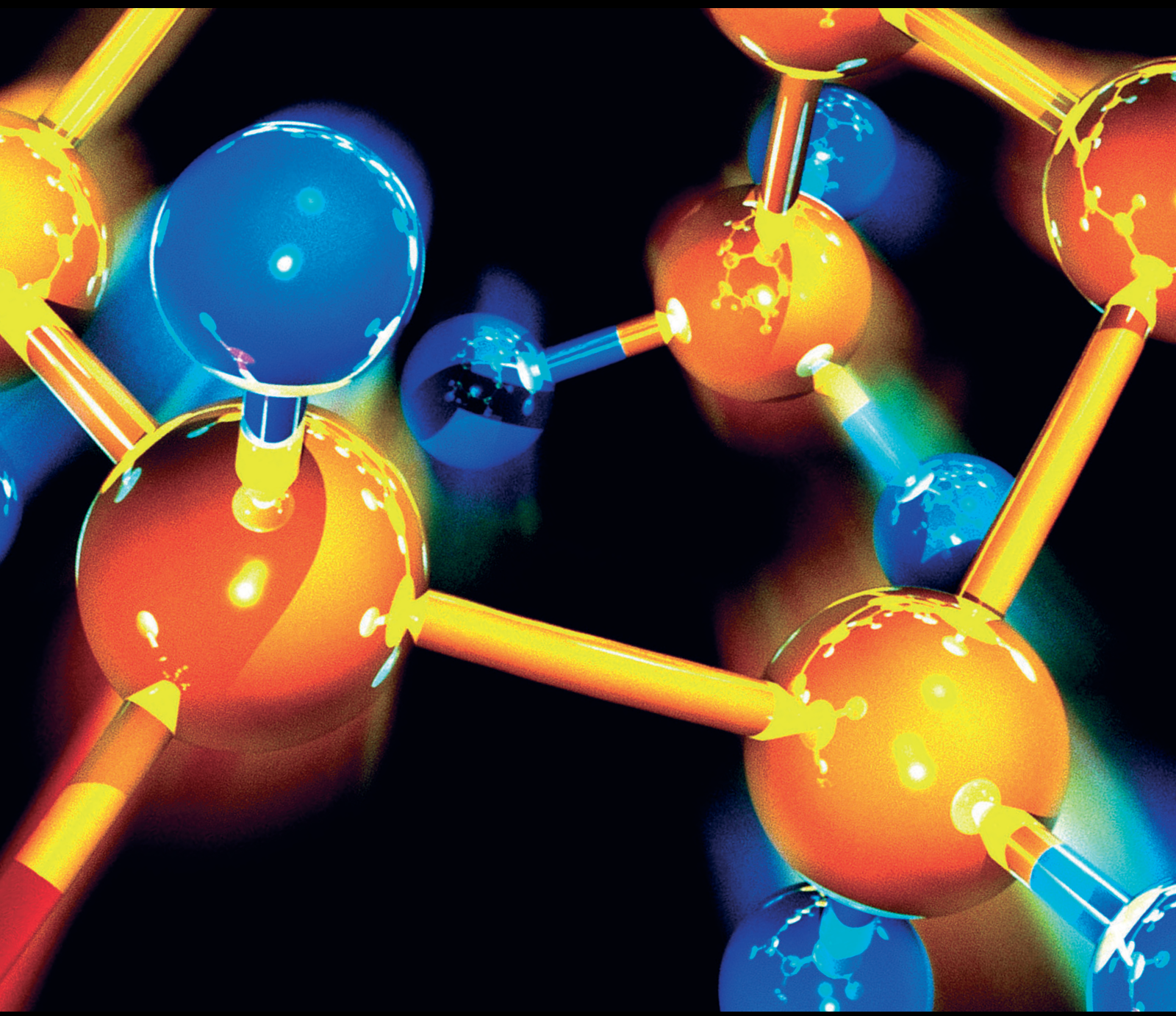

Analysis and Remediation of Pollutants in Water and Soil

Journal of Chemistry

Analysis and Remediation of Pollutants in Water and Soil

Lead Guest Editor: Jun Wu
Guest Editors: Xia He and Song Jin

Chief Editor

Kaustubha Mohanty, India

Associate Editors

Mohammad Al-Ghouti, Qatar
Tingyue Gu, USA
Teodorico C. Ramalho, Brazil
Artur M. S. Silva, Portugal

Academic Editors

Jinwei Duan , China
Luqman C. Abdullah, Malaysia
Dr Abhilash, India
Amitava Adhikary, USA
Amitava Adhikary, USA
Mozhgan Afshari, Iran
Daryoush Afzali, Iran
Mahmood Ahmed, Pakistan
Islam Al-Akraa, Egypt
Juan D. Alché, Spain
Gomaa A. M. Ali, Egypt
Mohd Sajid Ali, Saudi Arabia
Shafaqat Ali, Pakistan
Patricia E. Allegretti, Argentina
Marco Anni, Italy
Alessandro Arcovito, Italy
Hassan Arida, Saudi Arabia
Umair Ashraf, Pakistan
Narcis Avarvari, France
Davut Avci, Turkey
Chandra Azad, USA
Mohamed Azaroual, France
Rasha Azzam, Egypt
Hassan Azzazy, Egypt
Renal Backov, France
Suresh Kannan Balasingam, Republic of Korea
Sukanta Bar, USA
Florent Barbault, France
Maurizio Barbieri, Italy
James Barker, United Kingdom
Salvatore Barreca, Italy
Jorge Barros-Velázquez, Spain
THANGAGIRI Baskaran, India
Haci Baykara, Ecuador
Michele Benedetti, Italy
Laurent Billon, France
Marek Biziuk, Poland
Jean-Luc Blin, France
Tomislav Bolanca, Croatia
Ankur Bordoloi, India
Cato Brede, Norway
Leonid Breydo, USA
Wybren J. Buma, The Netherlands
J. O. Caceres, Spain
Patrizia Calaminici, Mexico
Claudio Cameselle, Spain
Joaquin Campos, Spain
Dapeng Cao, China
Domenica Capasso, Italy
Stefano Caporali, Italy
Zenilda Cardeal, Brazil
Angela Cardinali, Italy
Stefano Carli, Italy
Maria F. Carvalho, Portugal
Susana Casal, Portugal
David E. Chavez, USA
Riccardo Chelli, Italy
Zhongfang Chen, Puerto Rico
Vladislav Chrastny, Czech Republic
Roberto Comparelli, Italy
Filomena Conforti, Italy
Luca Conti, Italy
Christophe Coquelet, France
Filomena Corbo, Italy
Jose Corchado, Spain
Maria N. D.S. Cordeiro, Portugal
Claudia Crestini, Italy
Gerald Culioli, France
Nguyen Duc Cuong, Vietnam
Stefano D'Errico, Italy
Matthias D'hooghe, Belgium
Samuel B. Dampare, Ghana
Umashankar Das, Canada
Victor David, Romania
Annalisa De Girolamo, Italy
Antonio De Lucas-Consuegra, Spain
Marcone A. L. De Oliveira, Brazil
Paula G. De Pinho, Portugal
Damião De Sousa, Brazil
Francisco Javier Deive, Spain
Tianlong Deng, China

Contents

Hindawi
Journal of Chemistry
Volume 2024, Article ID 2510050, 12 pages
https://doi.org/10.1155/2024/2510050

Research Article

Characterization Analysis of Mudstone and Study of Its Pb (II) Adsorption Characteristics in Polluted Water Bodies

Baoqiang Zhang,[1,2,3,4,5] **Bo Zhao**,[1,2,3,4,5] **Longfei Xia**,[1,2,3,4,5] **Yingying Sun**,[1,2,3,4,5] **Tianqing Chen**,[1,2,3,4,5] **and Hailan Shi**[1,2,3,4,5]

[1]*Shaanxi Provincial Land Engineering Construction Group Co., Ltd., Xi'an 710075, China*
[2]*Land Engineering Quality Testing of Shaanxi Land Engineering Construction Group Co., Ltd., Xi'an 710021, China*
[3]*Institute of Land Engineering and Technology, Shaanxi Provincial Land Engineering Construction Group Co., Ltd., Xi'an 710021, China*
[4]*Key Laboratory of Degraded and Unused Land Consolidation Engineering, Ministry of Natural Resources, Xi'an 710021, China*
[5]*Shaanxi Engineering Research Center of Land Consolidation, Xi'an 710021, China*

Correspondence should be addressed to Baoqiang Zhang; 1610727540@qq.com

Received 3 May 2022; Revised 31 July 2023; Accepted 7 March 2024; Published 25 March 2024

Academic Editor: Abhilash

In order to explore a medium material for the efficient treatment of Pb(II) pollutants in groundwater, in this paper, mudstone is selected as the medium material, and the morphological structure of the mudstone is characterizes via X-ray diffraction (XRD), scanning electron microscopy (SEM), and Brunauer–Emmett–Teller (BET) analyses to study the feasibility of the mudstone adsorbing Pb(II) ions. Then, static adsorption experiments are carried out to investigate the removal effect of mudstone on Pb(II) in aqueous solutions under different conditions and to determine the optimal adsorption conditions. Finally, the results are fitted and analyzed using a thermodynamic model to explore the adsorption mechanism of the mudstone. The main results of this study are as follows. The main mineral composition of the mudstone used in the experiments includes $CaCO_3$, SiO_2, $CaAl_2O_4{\cdot}10H_2O$, and $CaFe_4O_7$. The specific surface area of the mudstone is as high as 23.027 $m^2{\cdot}g^{-1}$, the pore size is 9.145 nm, and its surface structure is rough, with pores and fissures developed. The pore space and adsorption capacity of the mudstone were enhanced. When 1 $g{\cdot}L^{-1}$ of mudstone was added, the pH value of the solution was 6, the reaction time was 60 min, and the initial concentration of Pb(II) was 30 $mg{\cdot}L^{-1}$. The removal efficiency of Pb reached 84.5%, and the adsorption amount was 25.352 $mg{\cdot}g^{-1}$. For the removal of Pb(II) from the aqueous solution by the mudstone under different concentrations of Pb(II), the reaction was in accordance with the Langmuir adsorption isotherm model, and the maximum adsorption amount reached 54.975 $mg{\cdot}g^{-1}$. The relationship between the removal of Pb(II) and the reaction time was in accordance with the pseudo-second-order rate model. The results of this study suggest that mudstone can be used for the removal of Pb(II) from aqueous media.

1. Introduction

Water is an indispensable natural resource in human life and is an integral part of the ecological and environmental system [1]. Currently, due to the rapid development of agriculture and industry, the excessive use of chemical fertilizers and pesticides in the agricultural field has caused serious pollution of water bodies with Pb(II) ions [2, 3]. Pb(II) ions in water bodies are difficult to degrade, and they have a high toxicity. Long-term consumption of water with a high lead content is likely to cause cancer. The lead pollution cycle is long, and it is easily bioaccumulated. Through its gradual accumulation in the food chain, it causes serious harm to the human living environment, biosphere, and human health [4–7]. Therefore, the purification of polluted water bodies has become a research hotspot in the field of environmental science, and it is of great significance to apply clay mineral materials to the study of the adsorption of heavy

metals in water bodies [8, 9]. There are two treatment methods for water bodies polluted by Pb(II) ions: one is to reduce the bioavailability of the Pb(II) ions in the water body, and the other is to directly remove the Pb(II) ions from the water body [10, 11]. Therefore, some efficient water treatment technologies, for example, physical adsorption, electrochemical adsorption, ion exchange, chemical precipitation, and a series of other treatment methods and technologies, are used in the treatment of Pb(II) in water bodies [12].

In the method of absorbing Pb(II), the choice of the adsorbent is extremely important. Clay minerals have a super-self-purification capacity in the restoration of water bodies polluted by Pb(II) ions [13]. The common clay minerals used to restore water bodies heavily polluted by Pb(II) ions include montmorillonite, attapulgite, zeolite, kaolinite, sepiolite, vermiculite, and illite [14–17]. As a mineral material with abundant reserves and a low price, mudstone is a composite clay mineral material composed of layered porous silicate-rich minerals. Mudstone is mainly composed of minerals such as illite, kaolinite, montmorillonite, quartz, feldspar, mica, epidote, chlorite, ferromanganese oxide, and organic matter [18]. There are certain differences in the mineral components contained in different regions [19]. Mudstone has a strong viscoelasticity, is easily weathered into fine particles, is easy to crush, easy to mine, cheap, and easy to obtain. In addition, as a composite clay mineral material, mudstone is a good soil-forming parent material, and its basic characteristics determine that it will not generate secondary pollution when used as an adsorbent. In addition, the restoration cost of this method is low, it is simple and easy to operate, and it has broad application prospects.

In this study, the adsorption method was used to remove the Pb(II) in a water body. The aim was to develop an environmentally friendly adsorption material with a high adsorption efficiency, good performance, and no secondary pollution. Therefore, in this study, through the characterization analysis of mudstone, the possibility of its adsorption of the heavy metal Pb(II) was explored, and the adsorption effect of the mudstone on Pb(II) in a water body under different influencing factors was investigated so as to provide a theoretical scientific basis and technical support for the efficient use of mudstone material.

2. Materials and Methods

2.1. Materials. The mudstone used in this study was collected from Yaoqu Village, Yaoqu Town, Yaozhou District, Tongchuan City, Shaanxi Province, and the chemical agent used was purchased from the Aladdin Reagent Co., Ltd. (Shanghai, China).

2.2. Preparation of Mudstone Material. First, the mudstone protolith collected was air dried, and the air-dried clay mineral material mudstone was refined. Then, the refined mudstone was cleaned with deionized water for three times to remove the impurities in the sample. The washed sample was air dried again and sieved through a 100-mesh screen to make the mudstone material required for the experiment. The prepared mudstone material was placed in a plastic bag and stored under dry conditions for later use. The basic physical and chemical properties of the mudstone material are presented in Table 1. The Pb content of the mudstone was far lower than the soil pollution risk screening value, and it did not carry the target heavy metal when adsorbing the Pb(II) in the polluted water body.

2.3. Characterization of Mudstone. The surface morphology and elements composition of the mudstone were analyzed using X-ray diffractometers (America -FEI-Quanta FEG 250 and Japan-Rigaku-Smart Lab 9KW models), and the specific surface area and pore size of the mudstone were determined using an America - Mack -ASAP 2020HD8.

2.4. Adsorption Experiment. A batch experiment was conducted to study the adsorption effect of the mudstone on Pb(II) in 100 mL of water contaminated with Pb(II) at a concentration of 30 $mg{\cdot}L^{-1}$, Experiment 1: Different amounts of mudstone (0.25 $g{\cdot}L^{-1}$, 0.5 $g{\cdot}L^{-1}$, 0.75 $g{\cdot}L^{-1}$, 1 $g{\cdot}L^{-1}$, 1.25 $g{\cdot}L^{-1}$, and 1.5 $g{\cdot}L^{-1}$) were added to the contaminated water under constant temperature shaking. Experiment 2: The best adsorption amount of mudstone from experiment 1 was added to the polluted water, the pH of the solution was adjusted (2, 3, 4, 5, 6, 7, and 8), and the reaction time was 120 min. Adsorption experiments were conducted to determine the best pH value for heavy metal adsorption by the mudstone. Experiment 3: The best adsorption amount of mudstone from experiment 1 was added, and the pH was adjusted to the ideal value obtained from experiment 2. Then, experiments on Pb(II) adsorption by the mudstone were conducted to study the effect of the adsorption reaction time on the adsorption effect by collecting samples at different times (5 min, 10 min, 20 min, 30 min, 40 min, 50 min, 60 min, 70 min, 80 min, 90 min, 100 min); Experiment 4: Under the optimal conditions determined in Experiment 1, Experiment 2, and Experiment 3, mudstone was add to solutions with various initial Pb(II) concentration (10, 20, 30, 40, 50, and 60 $mg{\cdot}L^{-1}$) to observe the Pb(II) adsorption effect of the mudstone under different initial concentrations. The supernatant of the adsorbed mixture was filtered, and the Pb(II) concentrations of the filtrate was determined via multicollector inductively coupled plasma mass spectrometry (MC-ICP-MS). To ensure the accuracy of the experiments, each experiment was repeated three times.

The removal rate and adsorption amount are important indicators of the performance of adsorbent materials. The adsorption amount (q_e) and removal rate (R) of lead by the mudstone were calculated as follows:

$$q_e = \frac{(C_0 - C_e)}{m} \times V,$$
$$R = \frac{C_0 - C_e}{Co} \times 100\%, \quad (1)$$

Table 1: Basic physical and chemical properties of the mudstone.

Material	pH	Conductivity ($mS \cdot m^{-1}$)	Particle size composition (%)			Pb content ($mg \cdot kg^{-1}$)	Cation exchange capacity ($mmol \cdot kg^{-1}$)	Expansion rate (%)
			Clay particle	Powder particle	Sand			
Mudstone	8.29	14.8	16.33	83.40	0.27	0.322	101.44	25.36

where q_e is the unit adsorption capacity of the composite clay mineral material for Pb (II) after adsorption equilibrium ($mg \cdot L^{-1}$); C_0 is the initial concentration of Pb(II) ($mg \cdot L^{-1}$); C_e is the concentration of Pb(II) in the adsorption equilibrium state ($mg \cdot L^{-1}$); V is the volume of the sewage solution poured into the conical bottle initially (mL); m is the amount of mudstone used (g) [20].

3. Results and Discussion

3.1. Characterization Analysis of Mudstone. The scanning electron microscopy (SEM) morphology results for the mudstone are shown in Figures 1(a)–1(d). Figures 1(a)–1(d) present SEM photos of the mudstone collected from the Tongchuan area, Shaanxi, under magnifications of 5000x, 10000x, 20000x, and 50000x, respectively. It can be seen from Figure 1 that the surface structure of the mudstone is rough and consists of aggregates of irregular flakes; the particles are connected by irregular surface-to-surface and surface-to-edge contacts; and the pore channels of the mudstone are unobstructed. This scattered structure helps in the generation of pores, interstices, voids, cracks, fissures, and the connections between them. The pores, interstices, voids, cracks, and fissures are mostly formed via stacking of the irregular mineral particles contained in the mudstone, so there is a certain difference in the pore size and pore wall thickness. The size of the space between the pores also varies, which not only increases the free adsorption group of the mudstone but also helps the mudstone to form a pore channel structure. There are pores and fissure structures of different sizes distributed on the surfaces of the mudstone particles, which are aggregated in a disorderly manner. The well-developed pores and rough pore walls on the mudstone surface and the good connection between the pores enhance the effective space and adsorption capacity of the mudstone pore channels and improve the physical adsorption and chemisorption capacity of the mudstone.

Phase analysis of the mudstone material was carried out. The X-ray diffraction (XRD) results for the mudstone are shown in Figure 2. The results show that the minerals contained in mudstone mainly include $CaCO_3$, SiO_2, $CaAl_2O_4 \bullet 10H_2O$, and $CaFe_4O_7$. This is because clay minerals are the main rock forming minerals in mudstone, and the clay minerals are mainly aluminum-silicate minerals. Therefore, the Si and Al contents of the mudstone are large. In addition, the shapes and positions of all of the main diffraction peaks of the mudstone are prominent, the XRD diffraction peaks of the crystals are sharp and symmetrical, and the crystal structure is complete. The strong binding capacity of the silicate minerals contained in the mudstone for Pb (II) can be used to improve the adsorption capacity of the mudstone for the heavy metal Pb (II) to a large extent.

Figure 3 shows the nitrogen adsorption curve of the mudstone. Based on analysis of the nitrogen adsorption curve, the adsorption isotherm belongs to the second category of the Brunauer-Emmett-Teller (BET) classification, with a small slope and slow rise in the first half and a sharp rise in the second half. As the relative pressure increases, capillary condensation occurs simultaneously with multilayer adsorption. When $P/P_0 = 0$, the curve intersects with the ordinate (representing the adsorption volume) at a nonzero value, the intercepts are not equal, so there are micropores and the micropore volumes are not equal. The average specific surface area obtained using methods such as the BET method is 23.027 $m^2 \cdot g^{-1}$, and the average pore size is 9.145 nm.

3.2. Adsorption of Pb(II) Ions in Batch Systems. The Pb(II) adsorption performance of the mudstone is not only related to its surface structure but is also influenced by external factors. Mudstone was used as the adsorption material to investigate the effects of the pH, amount of mudstone addition, reaction time, and initial Pb(II) concentration of solution on the heavy metal ion adsorption performance of the mudstone.

3.2.1. Effect of Mudstone Dosage on Absorption Effect. The results of the effect of the mudstone dosage on the removal of Pb(II) are shown in Figure 4. This is mainly due to the fact that the Pb(II) concentration of the solution was fixed, and the removal efficiency of Pb(II) increased gradually as the amount of mudstone increased, which caused the mudstone to reach adsorption equilibrium. The removal efficiency increased linearly as the amount of mudstone added increased from 0.25 $g \cdot L^{-1}$ to 1 $g \cdot L^{-1}$. The Pb(II) removal efficiency of the mudstone was as high as 85% when the amount of mudstone was 1 $g \cdot L^{-1}$, and it had reached the equilibrium at this time. Although the Pb(II) adsorption efficiency of the mudstone exhibited a tendency toward equilibrium with increasing mudstone dosage, when the addition of mudstone was small, the specific surface area and the number of adsorption sites on the mudstone were limited, and the adsorption sites were fully utilized, thus reaching adsorption saturation quickly and resulting in a high adsorption amount. However, the limited number of adsorption sites was not sufficient to adsorb a large amount of the Pb(II) in the solution, so the removal efficiency was low [21]. As the addition of mudstone gradually increased, the specific surface area and the number of adsorption sites and functional groups of the mudstone also increased, which caused the Pb(II) content of the solution to decrease. However, this led to an excess of adsorption sites on the surface of the mudstone, and the phenomenon of

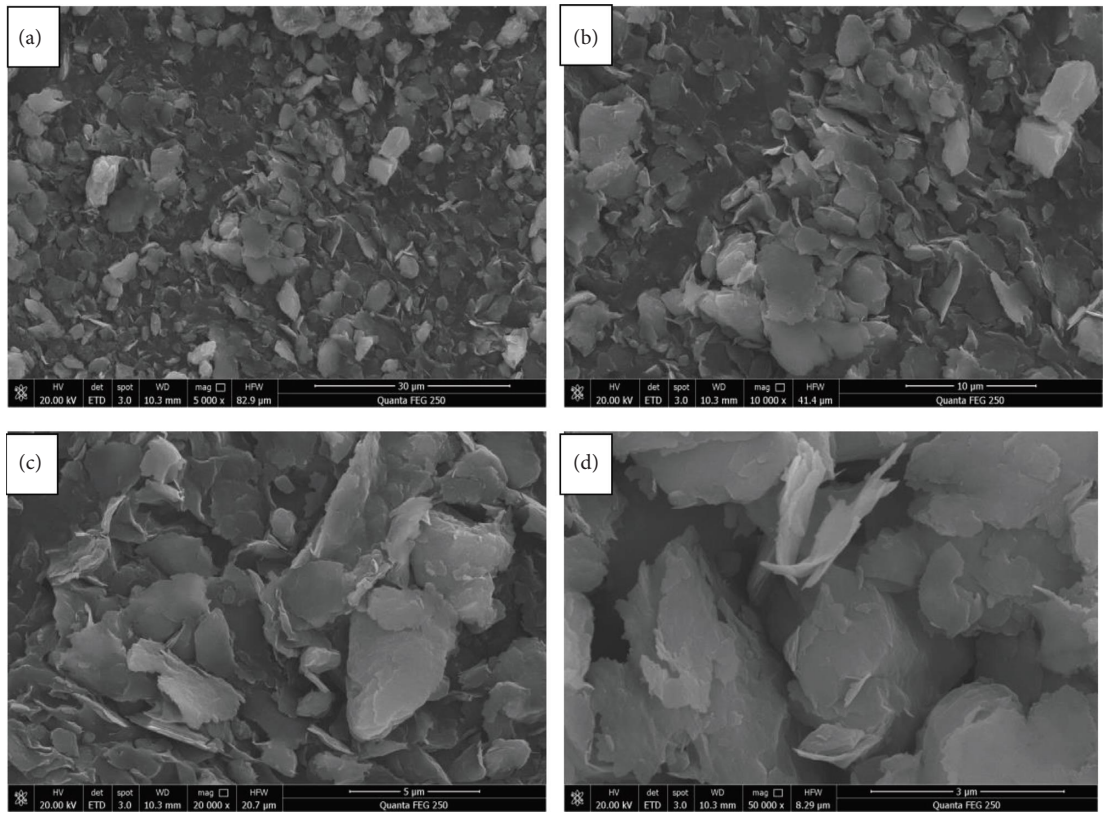

Figure 1: SEM photos of mudstone.

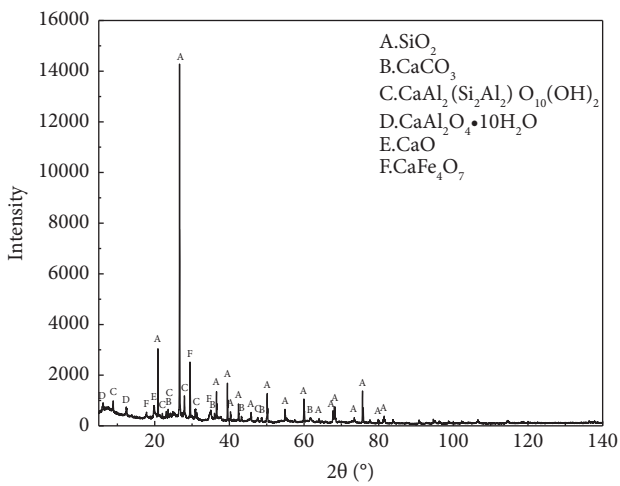

Figure 2: Mudstone X-ray diffraction analysis.

unsaturated utilization of the adsorption sites occurred. Based on the analysis of the results presented in Figure 5, the optimum amount of mudstone addition was $1\,g{\cdot}L^{-1}$ for Pb(II) adsorption by mudstone.

3.2.2. Effect of Solution pH on the Adsorption Effect. According to the above effect of the amount of mudstone addition on the Pb(II) adsorption effect of the mudstone, the amount of mudstone was set as $1\,g{\cdot}L^{-1}$ in the experiment conducted to determine the effect of the solution pH on the adsorption effect. The removal efficiencies were all very low at pH < 3, and the removal efficiencies were significantly higher at pH = 3~6. At pH = 6~8, the curve leveled off and the removal efficiency stabilized near the maximum value, and the removal efficiency was above 85%. Therefore, mudstone is most suitable for Pb(II) removal under weakly acidic or neutral conditions. At pH 6-7, Pb(II) may combine with OH^- to produce $Pb(OH)^+$ and $Pb(OH)_2$ complexes via precipitation, which reduces the unfavorable contact with the oxidized surface [22]. For pH 6-7, the increase in the removal of Pb(II) by the mudstone was the result of the combined effect of physical adsorption and a chemical precipitation reaction; the adsorption amount reached the maximum value, and the adsorption effect gradually stabilized [23]. The mudstone contained Fe and Al oxides with variable charges, and as the pH increased, the variable negative charge in the solution increased, causing the gravitational force on the Pb(II) increase and the electrostatic adsorption of Pb(II) increase. The pH of the solution not only affects the magnitude of the electricity charge on the surface of the clay mineral material and the activity of the adsorption sites, but also the form of the metal ions present in the solution, thus affecting its adsorption properties [24]. Therefore, pH = 6 was determined to be the optimum pH value for Pb(II) adsorption on mudstone.

3.2.3. Effect of Reaction Time on the Adsorption Effect. Based on the effects of the amount of mudstone addition and the pH of the solution on the adsorption effect, the optimum

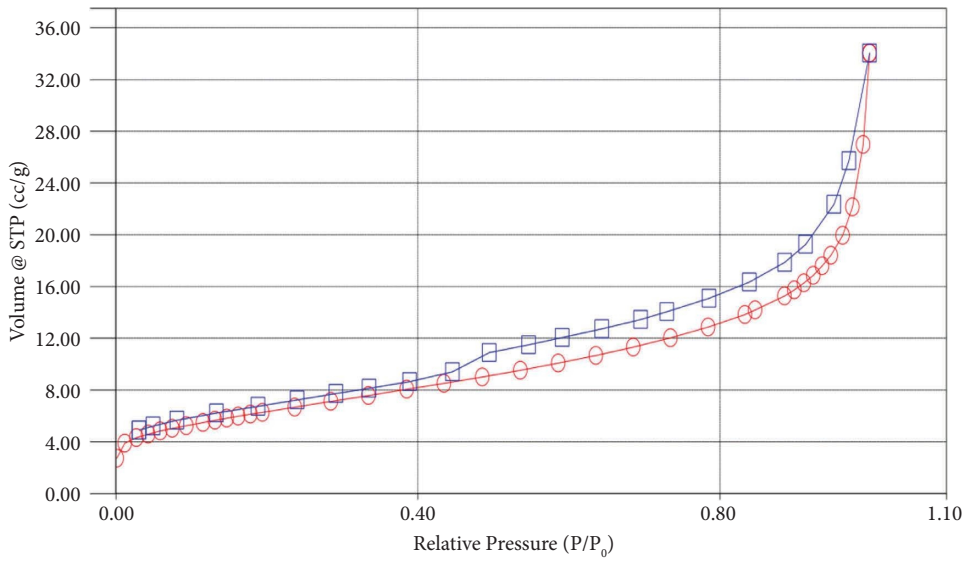

Figure 3: Nitrogen adsorption curve of mudstone.

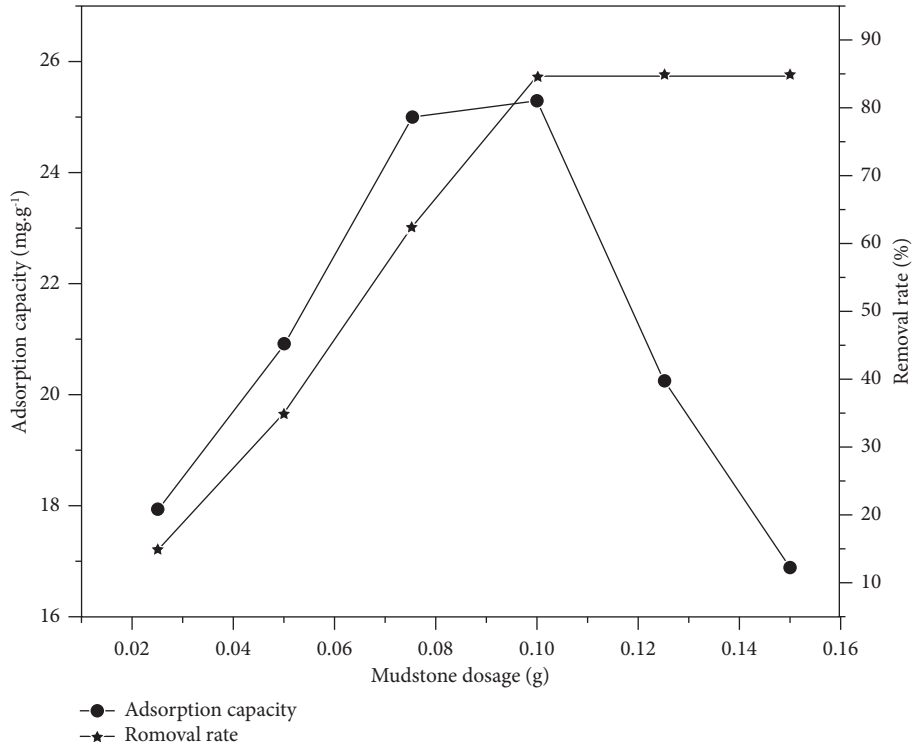

Figure 4: Effect of mudstone dosage on the removal of Pb(II).

amount of mudstone addition and solution pH were set as 1 g·L^{-1} and pH = 6, respectively, in the next set of adsorption experiments. As shown in Figure 6, the adsorption rate of Pb(II) by mudstone was fast, the Pb(II) concentration of the solution decreased rapidly, and the removal efficiency increased. The Pb(II) removal efficiency of the mudstone was nearly 75% in 0–20 min, and the adsorption capacity was nearly 23 mg·g^{-1}. At 60 min, the Pb(II) removal efficiency of the mudstone reached 89%, its Pb(II) adsorption capacity reached 26.7 mg·g^{-1}, and both the removal efficiency and adsorption capacity reached the maximum values. During the reaction, the removal efficiency and adsorption amount did not change significantly as the reaction time increased, and they reached an equilibrium state, indicating that the adsorption of Pb(II) by the mudstone was characterized by rapid adsorption and dynamic equilibrium, which is generally stable and will not be resolved [25]. In summary, in the experiment on the static adsorption of Pb(II) by mudstone, the adsorption time was set to 60 min. The rapid adsorption characteristics enable the mudstone to give full play to the

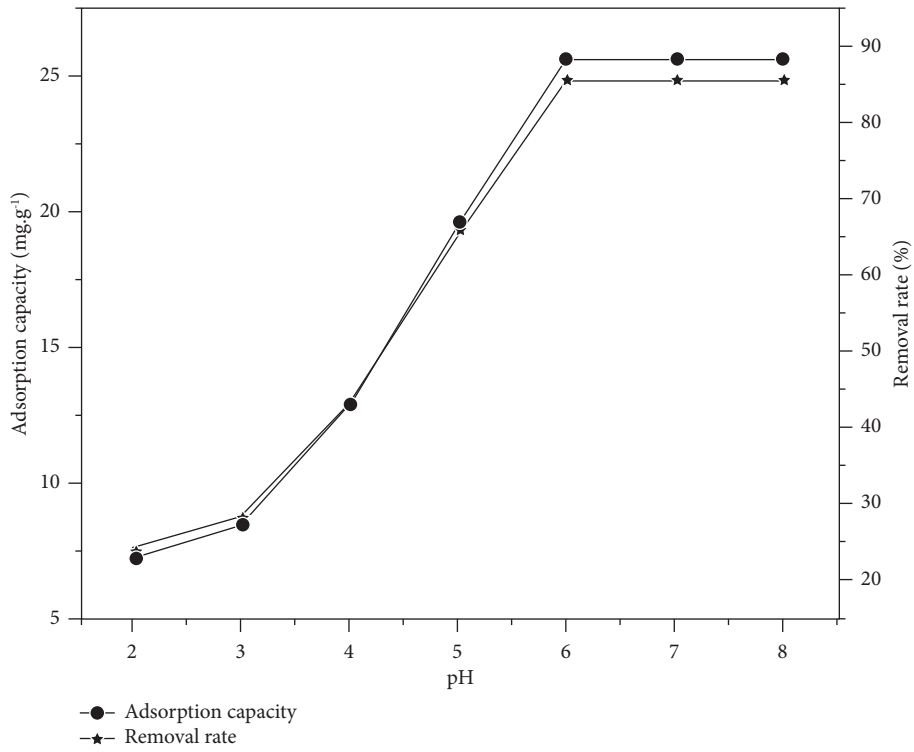

Figure 5: Effect of pH on the removal of Pb(II) by mudstone.

adsorption performance in a short reaction time, which provides a new idea for solving the problem of the emergency treatment of water bodies polluted by heavy metal.

3.2.4. Effect of Pb(II) Ion Content on the Adsorption Effect. The experiments on the effect of different Pb(II) ion contents on the adsorption of Pb(II) were carried out using a mudstone addition of 1 g·L^{-1}, a solution pH of 6, and a reaction time of 90 min. Figure 7 shows the adsorption capacity and removal rate of the mudstone for different Pb(II) contents. It can be seen from Figure 7 that the Pb(II) adsorption capacity of the mudstone increased continuously as the Pb(II) ion content increased, while the removal efficiency exhibited a decreasing trend. On the one hand, the active sites and exchangeable ions on the surface of a certain mass of mudstone material are limited, and when the ionic strength increases to a certain degree, the adsorption sites and functional groups on the surface of the mudstone are reduced. On the other hand, the active sites and exchangeable ions on the surface of a certain mass of mudstone material are limited, and when the ionic strength increases to a certain level, the adsorption sites and functional groups on the surface of mudstone are fully utilized, and the material reaches adsorption saturation, resulting in the excess Pb(II) not being adsorbed, thus reducing the Pb(II) removal rate [26–28]. In addition, the Pb(II) removal efficiency of the mudstone was greater than 80% when the Pb(II) ion content was less than 30 mg·L^{-1}, and it gradually decreased when the Pb(II) ion content was between 30 mg·L^{-1} and 50 mg·L^{-1}, but remained above 75%. Therefore, under the double consideration of the removal rate and adsorption capacity, the mudstone was more effective in removing Pb(II) ions from the solution with a lower Pb(II) ion content, but it also had some value in treating the solution with a high Pb(II) ion content [29, 30].

3.3. Adsorption Isotherm and Adsorption Kinetic Model Analysis

3.3.1. Analysis of the Adsorption Isotherm Model. The adsorption isotherm is the equilibrium state of the adsorption reaction when the reaction proceeds sufficiently at a specific temperature. When the adsorption reaction reaches equilibrium, there is a certain relationship between the ion concentration of the solution and the adsorption capacity of the adsorbent, and this dependence curve is the adsorption isotherm. It is possible to understand the trend of the isotherm under each parameter and to determine the strength of the adsorption performance. The equilibrium time is the time when the adsorption reaction reaches equilibrium, and the adsorption capacity corresponding to this time is the amount of equilibrium adsorption. The experimental results for the Pb(II) adsorption by mudstone from a solution were fitted using the following two models [31].

(1) Langmuir adsorption isotherm model

The adsorption model proposed by Langmuir in 1916 based on the theory of molecular motion is a commonly used equation for adsorption isotherms and has been widely used in the field of adsorption [32]. It is based on the assumption that the adsorption process is a dynamic process and that the

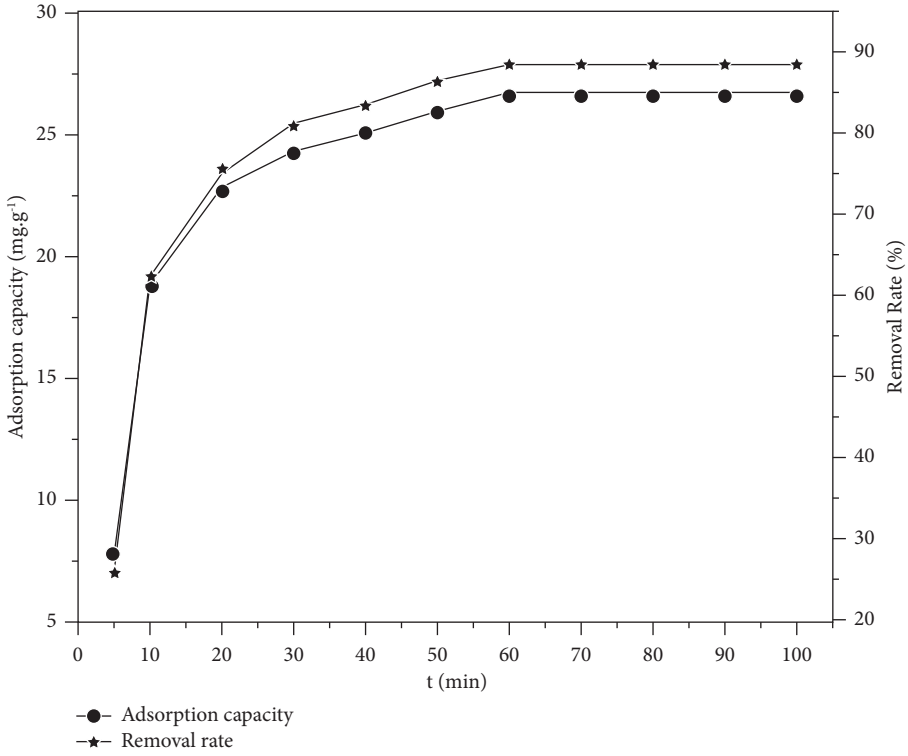

Figure 6: Effect of adsorption reaction time on the adsorption effect.

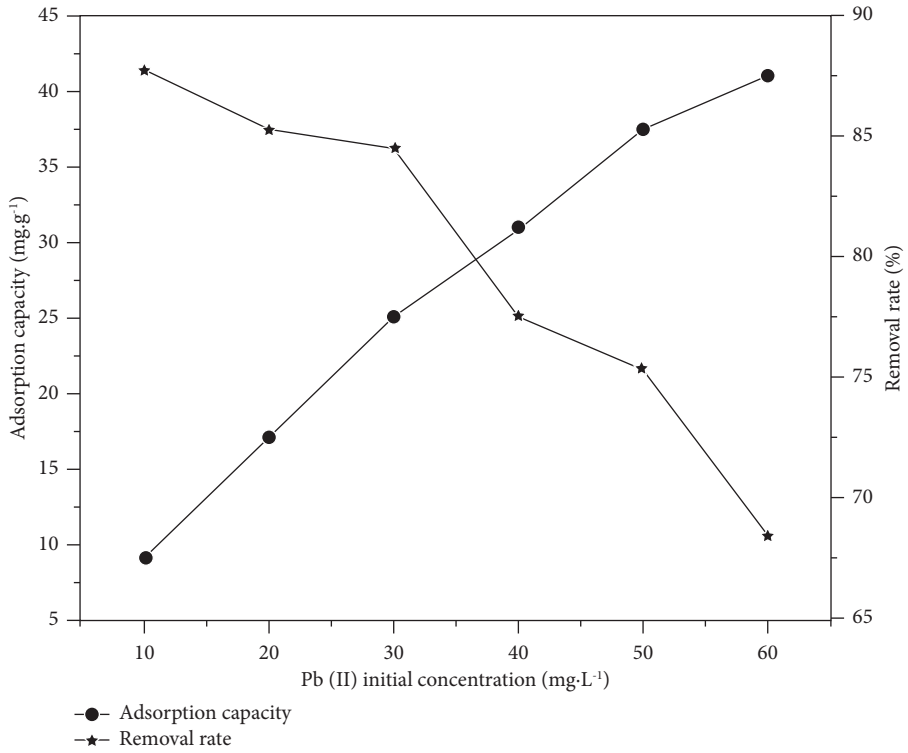

Figure 7: Effect of the initial Pb(II) concentration of the solution on the Pb(II) adsorption of the mudstone.

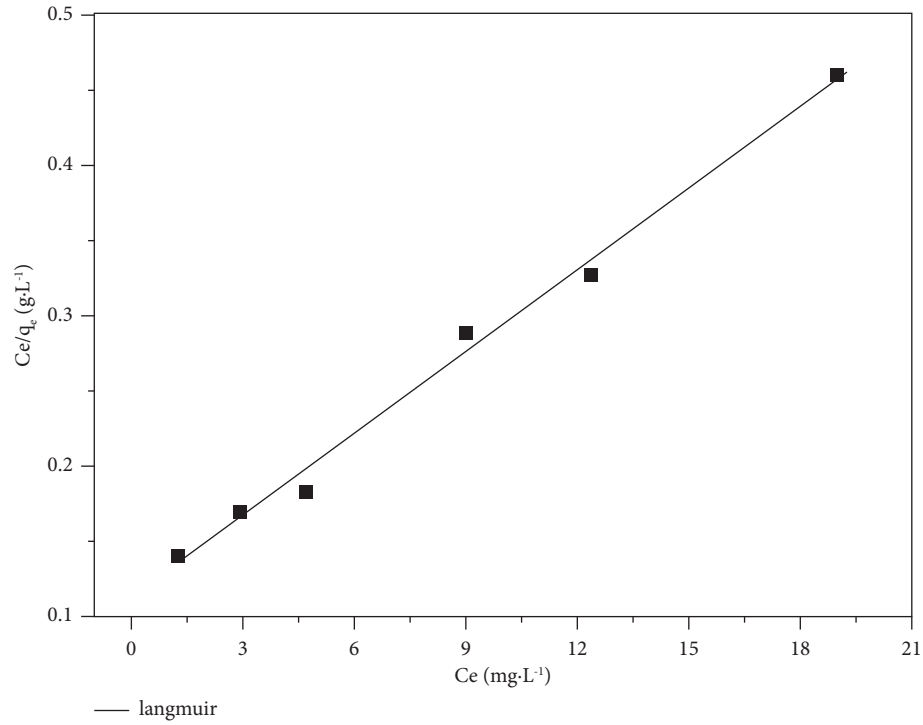

Figure 8: Langmuir fitting model.

desorption rate is the same as the adsorption rate when the adsorption reaction reaches equilibrium [33, 34]. It is applicable to adsorbents with a uniform volume distribution and when the adsorption reaction occurs between single molecular layers. The expression of its adsorption model equation is as follows [35]:

$$\frac{c_e}{q_e} = \frac{c_e}{q_m} + \frac{1}{(b \times q_m)}. \quad (2)$$

Where b is the adsorption equilibrium constant; q_e is the adsorption amount at adsorption equilibrium ($mg \cdot g^{-1}$); q_m is the theoretical saturation adsorption amount ($mg \cdot g^{-1}$); and c_e is the equilibrium concentration of the liquid phase after adsorption equilibrium ($mg \cdot L^{-1}$).

(2) Freundlich adsorption isotherm model

The Freundlich adsorption isotherm assumes that the adsorption process is a nonhomogeneous process, i.e., the adsorption sites on the surface of the adsorbent are irregular and are not independent of each other, but there may be a synergistic effect between the adsorption sites, and it belongs to an empirical equation that is applicable to multicomponent layer adsorption and surface adsorption under nonideal conditions [36]. The Freundlich adsorption isotherm can be used to express different systems of bilayers and reversible adsorption processes by fitting the following equation to the adsorption model [35]:

$$\lg q_e = \lg k + \frac{1}{n} \lg c_e, \quad (3)$$

Where k and n are the adsorption constants; q_e is the adsorption amount at adsorption equilibrium ($mg \cdot g^{-1}$); and c_e is the equilibrium concentration of the liquid phase at adsorption reaction equilibrium ($mg \cdot L^{-1}$).

Based on the results presented in Figures 8 and 9 and Table 2, both adsorption isotherm models can represent the adsorption process of the heavy metal Pb(II) by mudstone, but the correlation coefficient of the Langmuir isotherm model is higher(0.991), and it has a higher degree of linearity. This indicates that the Langmuir isotherm model is more suitable for the adsorption process of the heavy metal Pb(II) by mudstone. The correlation coefficient of the Freundlich adsorption isotherm model is 0.958 (i.e., >0.95), which indicates that the adsorption of the heavy metal Pb(II) by the mudstone occurred in a unimolecular layer structure, while the correlation coefficient of the Freundlich adsorption isotherm model is 0.958> (i.e., >0.95), which indicates that there is also a multimolecular layer reaction in the adsorption of the heavy metal Pb(II) by the mudstone [37]. The maximum adsorption capacity fitted using the Langmuir isotherm model was 54.975 $mg \cdot g^{-1}$. The empirical constant derived from the Freundlich adsorption isotherm model is $n = 1.771$, $1 < 1.771 < 10$, indicating that the adsorption reaction easily proceeds and that the reaction is difficult when $n < 0.5$ [38]. In summary, it can be concluded that the adsorption of the heavy metal Pb(II) by the mudstone is a relatively complex process, and single-molecular-layer

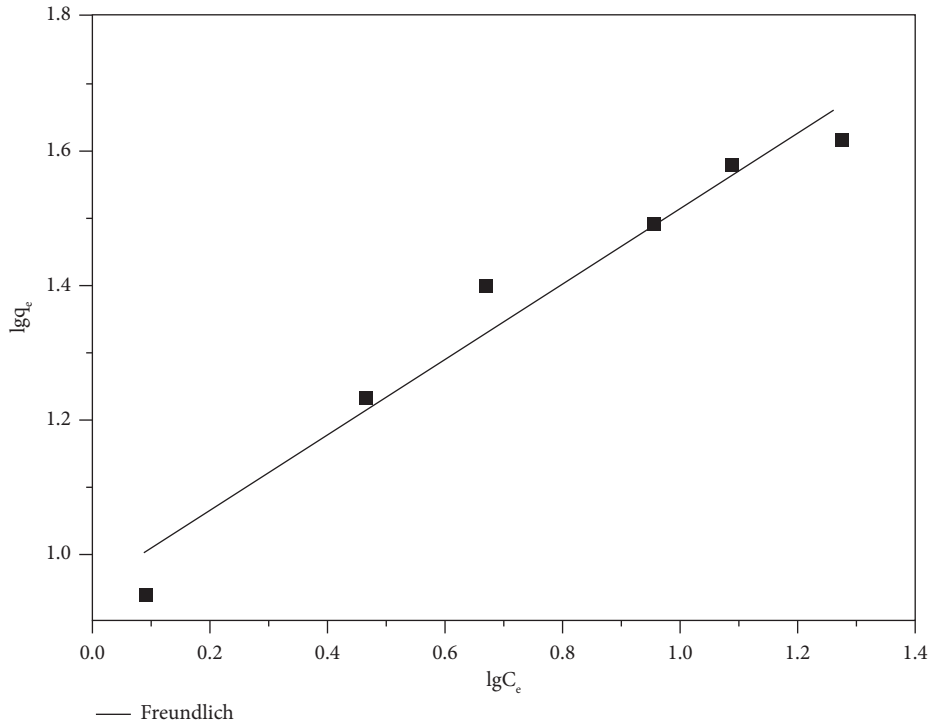

Figure 9: Freundlich fitting model.

Table 2: Parameters of adsorption isotherms.

Models	Langmuir isotherm model			Freundlich isotherm model		
Parameters	R^2	Q_{max} (mg·g^{-1})	B (L·mg^{-})	R^2	K (L·g^{-})	n
Mudstone	0.991	54.975	0.161	0.958	8.900	1.771

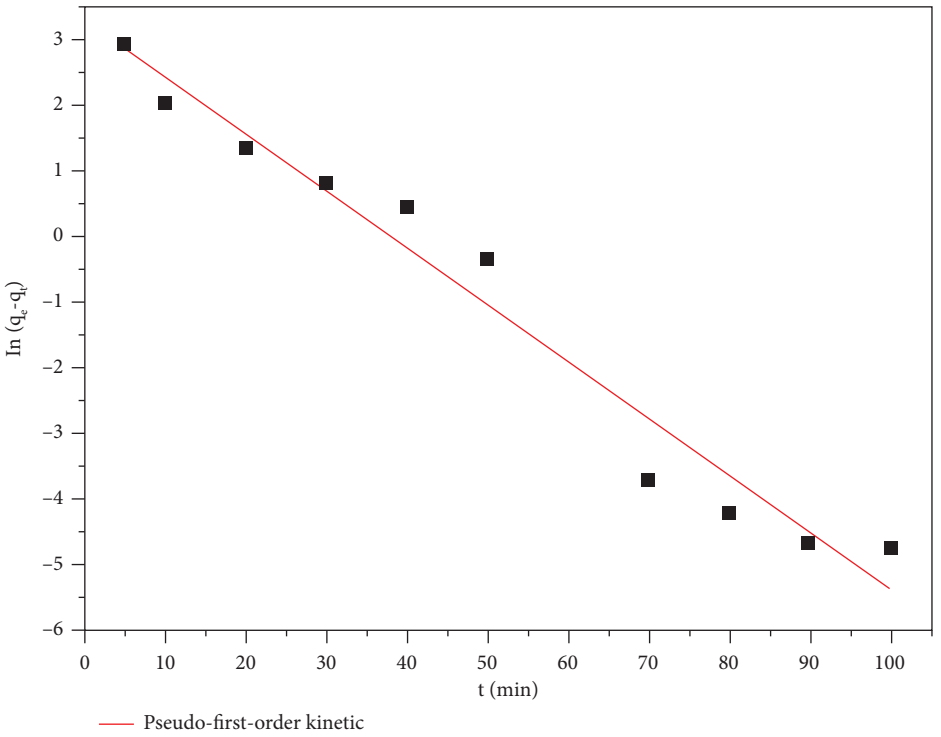

Figure 10: Pseudo-first-order kinetic fitting model.

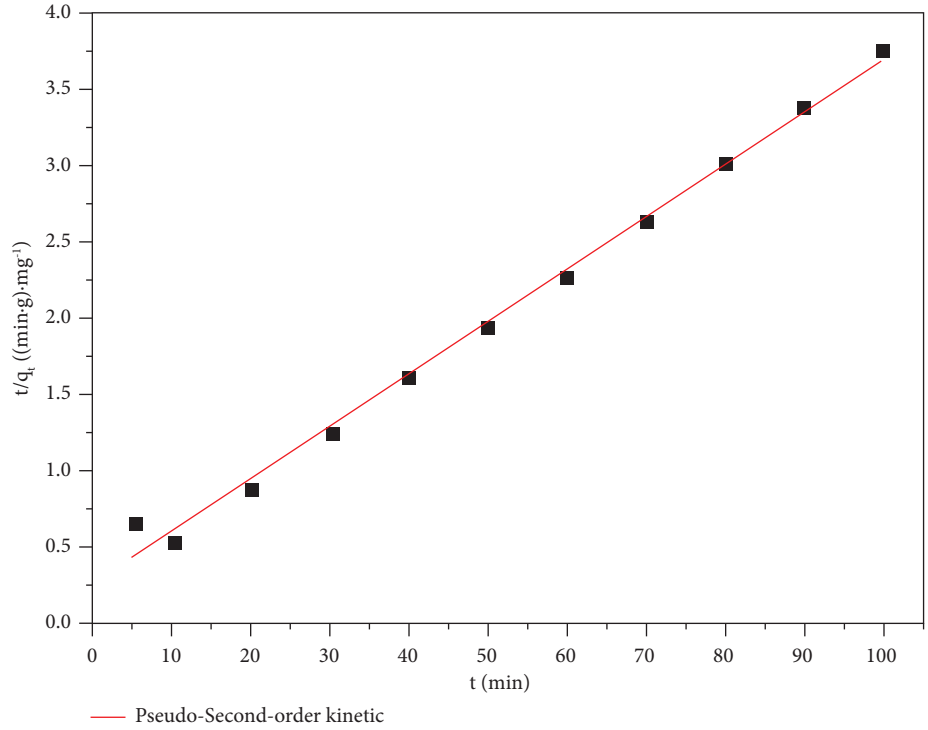

Figure 11: Pseudo-second-order kinetic fitting model.

Table 3: Adsorption kinetics parameters.

Models	Pseudo-first-order kinetic			Pseudo-second-order kinetic		
Parameters	K_1 (min^{-1})	q_e ($mg{\cdot}g^{-1}$)	R^2	K_2 ($mg{\cdot}(g\ min)^{-1}$)	q_e ($mg{\cdot}g^{-}$)	R^2
Mudstone	0.0868	26.875	0.96	0.0046	29.155	0.993

adsorption and multimolecular-layer adsorption coexist and jointly affect the adsorption of the heavy metal Pb(II) by the mudstone.

3.3.2. Adsorption Kinetic Analysis. Adsorption kinetics is the study of the rate, time, and mechanism of adsorption and other characteristics of the reaction. The concentration of the adsorbent and the adsorbent mass can affect the rate of the adsorption reaction, and they are also closely related to the contact time. Usually, the analysis of adsorption kinetics is performed using the pseudo-primary kinetic model and the pseudo-secondary kinetic equation to fit the adsorption process of the studied ions and to predict the equilibrium adsorption capacity [39]. The expressions of the fitted equations are presented shown.

First-order equation [40]:

$$\ln(q_e - q_t) = \ln q_e - k_1 t. \quad (4)$$

Secondary equation [41]:

$$\frac{t}{q_t} = \frac{1}{\left(k_2 q_e^{\ 2}\right)} + \frac{t}{q_e}. \quad (5)$$

In (4) and (5), k_1 is the pseudo-first-order adsorption equilibrium rate constant (min^{-1}), k_2 is the pseudo-second-order adsorption equilibrium rate constant ($mg{\cdot}(g\ min)^{-1}$); q_e is the equilibrium adsorption of lead by the mudstone at adsorption equilibrium ($mg{\cdot}g^{-1}$); and q_t is the adsorption of the heavy metal Pb(II) by the mudstone at time t ($mg{\cdot}g^{-1}$).

Based on the results presented in Figures 10 and 11 and Table 3, we conclude that the adsorption reaction between the mudstone and the heavy metal Pb(II) has a relatively high degree of fitting for both the pseudo-first-order kinetic model and the pseudo-second-order kinetic model, but the R^2 value of the pseudo-second-order kinetic model is larger than that of the pseudo-first-order kinetic model, so the pseudo-second-order kinetic model is more consistent with the adsorption process of the heavy metal Pb(II) in a water body on mudstone. The theoretical adsorption capacity of 29.155 $mg{\cdot}g^{-1}$ obtained from the fitted results is comparable to the adsorption capacity of 26.658 $mg{\cdot}g^{-1}$ obtained from the experiments presented in the previous section, which further indicates that the pseudo-second-order kinetic model is more consistent with the adsorption of Pb(II) by the mudstone.

4. Conclusions

In this study, a mudstone composed of clay mineral material with abundant reserves in China was used as the research object, and the effects of the influencing factors, such as the amount of mudstone addition, solution pH, reaction time, and initial Pb(II) concentration of the solution, on the adsorption of Pb(II) from water bodies by a composite clay mineral material (mudstone) were investigated through static adsorption experiments. The main conclusions of this study are as follows.

The mechanism of using mudstone as a remediation material for lead-contaminated water was analyzed. The main clay minerals contained in the mudstone were $CaCO_3$, SiO_2, $CaAl_2O_4{\cdot}10H_2O$, and $CaFe_4O_7$, among which the silicate minerals were dominant. Its surface structure was rough, and pores and fissures were developed. The clay minerals were abundant, and the cation exchange capacity, specific surface area, large pore size, and rich content of clay minerals indicate that using this mudstone to remediate lead-contaminated water using the adsorption mechanism is feasible. Regarding the factors affecting the adsorption of the Pb(II) in the solution by mudstone, the best Pb(II) adsorption effect of the mudstone in the static adsorption experiments was achieved when the amount of mudstone addition was $1\,g{\cdot}L^{-1}$ and the pH was 6. The best Pb(II) adsorption effect of the mudstone was achieved under these conditions, and the removal efficiency can reached 85.5%. Regarding the adsorption reaction time, the Pb(II) removal efficiency of the mudstone was close to 75% at 30 min, and the Pb(II) adsorption capacity and removal rate of the mudstone were close to the highest value at 60 min, with a removal efficiency of close to 88.8%. After 60 min, the adsorption capacity and removal rate did not change significantly as the reaction time increased, and they tended to become stable. The initial Pb(II) concentration of the solution also affected the adsorption of Pb(II) by the mudstone. The higher the initial concentration was, the higher the adsorption capacity was, and the lower the removal efficiency was. The data obtained from the adsorption experiments on the adsorption of the heavy metal Pb(II) by the mudstone were linearly fitted, and it was concluded that the Langmuir isotherm model was more suitable for describing the adsorption of the heavy metal Pb(II) by the mudstone. In addition, the fitting results indicate that the adsorption of the heavy metal Pb(II) by the mudstone occurred in a single molecular layer structure; while the correlation coefficient of the Freundlich isotherm model was 0.958 (i,e.,> 0.95). This also indicates that the adsorption process of the heavy metal Pb(II) by the mudstone also involved a reaction in multimolecular layers. The R^2 value of the pseudo-secondary kinetic model is larger than that of the pseudo-first-order kinetic model, so the pseudo-secondary kinetic model is more consistent with the adsorption of the heavy metal Pb(II) by the mudstone. This also indicates that the adsorption of the heavy metal Pb(II) by the mudstone was dominated by chemisorption.

Data Availability

No data were used to support this study.

Conflicts of Interest

The authors declare that there are no conflicts of interest.

Acknowledgments

This project was funded by the internal scientific research project of Shaanxi Provincial Land Engineering and Construction Group and the Shaanxi Provincial Innovation Capacity Support Programme (funding numbers: DJNY2021-18 and 2021PT-053).

References

[1] Y. Zhang, *Research on Combined Adsorption Technology of Cadmium Ions in Sewage*, Henan Normal University, Xinxiang, China, 2015.

[2] C. Wang, *Pollution Characteristics of Heavy Metal Contaminated Sediment in Xiawan Port and its Solidification and Stabilization Technology*, Hunan University, Changsha, China, 2013.

[3] S. X. Zhang, "Current status and evaluation of heavy metal pollution in water environment," *China Science and Technology Information*, vol. 11, no. 13, pp. 32–36, 2009.

[4] J. G. Xu, L. Wang, H. Y. Xiao, M. Gao, and J. Li, "Current status of heavy metal pollution in my country's water environment and progress in detection technology," *Journal of Environmental Sciences*, vol. 29, no. 5, pp. 104–108, 2010.

[5] Y. N. Geng, "Research progress on heavy metal pollution in rivers," *Chinese Agricultural Science Bulletin*, vol. 28, no. 11, pp. 262–265, 2012.

[6] S. M. Wang, Y. H. Ma, Z. Liu, F. Han, J. P. Ma, and Q. Li, "Research progress on the characteristics of heavy metal pollution in urban precipitation," *South-to-North Water Transfers and Water Science & Technology*, vol. 13, no. 2, pp. 279–283, 2015.

[7] H. T. Huang, Y. P. Liang, C. C. Wei, H. Lin, and G. L. Mo, "Current status of water heavy metal pollution and its treatment technology," *Light Industry Science and Technology*, vol. 25, no. 5, pp. 99-100, 2009.

[8] P. X. Wu and Z. W. Liao, "Research progress of clay mineral strata," *Journal of Nature*, vol. 22, no. 1, pp. 25–32, 2000.

[9] J. R. Fu, A. J. Zhou, Y. Liu, Y. N. Wu, F. T. Li, and X. J. Wang, "Research progress of urban sewage reclamation technology in China," *Industrial water treatment*, vol. 41, no. 1, pp. 18–24+37, 2021.

[10] Y. Q. Yu and J. M. Cheng, "The 19th meeting of soil environment professional committee of Chinese soil society and the 2nd workshop on soil pollution prevention, control and remediation technology in shandong Province," *Workshop on Agricultural Soil Pollution and Remediation*, 2017.

[11] W. H. Zou, *Study on the Adsorption of Copper and lead Ions by Manganese Oxide Modified Filter Materials*, Hunan University, Changsha, China, 2006.

[12] I. Ali, A. A. Basheer, X. Y. Mbianda et al., "Graphene based adsorbents for remediation of noxious pollutants from

wastewater," *Environment International*, vol. 127, pp. 160–180, 2019.

[13] G. Dobra, S. Garcia-Granda, A. Negre et al., "Silver adsorption on the low temperature activated AluminaGrades. I. Adsorption capacity and kinetics," *Revista de Chimie*, vol. 73, no. 2, pp. 17–32, 2022.

[14] Y. Huang and N. Y. Gao, "Comparative study of fluoride removal performance of modified quartz sand and zeolite filter media," *Environmental Sanitation Engineering*, vol. 3, pp. 128–131, 2003.

[15] Y. Xu, X. F. Liang, L. Peng, Q. R. Zeng, and Y. M. Xu, "Research progress on the passivation remediation of heavy metal contaminated clay minerals in farmland soil," *Shandong Agricultural Sciences*, vol. 49, no. 2, pp. 156–162+167, 2017.

[16] G. J. Song, L. L. Yin, J. R. Wang, L. Wang, and C. H. Sun, "Advances in bentonite modification and its application in wastewater treatment," *Journal of Qingdao University Engineering&Technology Edition*, vol. 4, pp. 35–39, 2004.

[17] D. Xu, X. L. Tan, C. L. Chen, and X. K. Wang, "Removal of Pb(II) from aqueous solution by oxidized multiwalled carbon nanotubes," *Journal of Hazardous Materials*, vol. 154, no. 1-3, pp. 407–416, 2008.

[18] R. Xiao, *Study on the Passivation and Remediation Effect of Purple Mudstone on Cadmium Pollution of gray-brown Alluvial Paddy Soil*, Sichuan Agricultural University, Ya'an, China, 2016.

[19] J. B. Zhao, X. B. He, and T. J. Shao, "Material composition and microstructure of purple soils and purple mudstones in Chongqing area," *Acta Pedologica Sinica*, vol. 49, no. 2, pp. 212–219, 2012.

[20] W. X. Liu, J. L. Li, J. L. Wang, X. B. Chen, and X. Y. Meng, "Adsorption characteristics of modified paulownia leaf adsorbent for lead and cadmium in water," *Journal of Agro-Environment Science*, vol. 33, no. 6, pp. 1226–1232, 2014.

[21] K. Jayaram, I. Y. L. N. Murthy, H. Lalhruaitluanga, and M. N. V. Prasad, "Biosorption of lead from aqueous solution by seed powder of Strychnos potatorum L," *Colloids and Surfaces B: Biointerfaces*, vol. 71, no. 2, pp. 248–254, 2009.

[22] W. Q. Ding, H. Li, X. L. Yang, and J. Y. Liao, "The effect of heavy metal adsorption on the surface charge properties of purple soil," *Journal of Agro-Environment Science*, vol. 3, pp. 711–715, 2006.

[23] K. Q. Li, Y. J. Wang, M. R. Yang, Z. Q. Zhu, and Z. Zheng, "Adsorption kinetics and mechanism of Pb(II) on polyamine functionalized mesoporous carbon," *Environmental Sciences*, vol. 35, no. 8, pp. 3198–3205, 2014.

[24] T. Zhang, L. C. Zheng, H. J. Yu et al., "Solution pH affects single, sequential and binary systems of sulfamethoxazole and cadmium adsorption by self-assembled cellulose: promotion or inhibition?" *Journal of Hazardous Materials*, vol. 402, Article ID 124084, 2021.

[25] J. Zhu, P. Wang, L. W. Luo, T. Y. Wang, and Y. Zhang, "Research status and progress of heavy metal ion adsorption by diatomaceous earth," *Journal of Central South University of Forestry and Technology*, vol. 31, no. 7, pp. 183–189, 2011.

[26] W. Liu, T. Wang, A. G. Borthwick et al., "Adsorption of Pb2+, Cd2+, Cu2+ and Cr3+ onto titanate nanotubes: competition and effect of inorganic ions," *Science of the Total Environment*, vol. 456-457, pp. 171–180, 2013.

[27] D. P. Sounthararajah, P. Loganathan, J. Kandasamy, and S. Vigneswaran, "Adsorptive removal of heavy metals from water using sodium titanate nanofibres loaded onto GAC in fixed-bed columns," *Journal of Hazardous Materials*, vol. 287, pp. 306–316, 2015.

[28] L. N. Nemeş and L. Bulgariu, "Optimization of process parameters for heavy metals biosorption onto mustard waste biomass," *Open Chemistry*, vol. 14, no. 1, pp. 175–187, 2016.

[29] J. Y. Zhao, *Study on the Adsorption Performance and Adsorption Mechanism of Honeycomb Stone for Heavy Metal Ions*, Anhui Jianzhu University, Hefei, China, 2016.

[30] T. R. Yu, G. L. Ji, and C. P. Ding, *Electrochemistry of Variable Charge Soils*, China Science press, Beijing, China, 1996.

[31] Y. Wang, *Preparation of Multi-Level Structures of Iron-Based Compounds and Their Application in the Field of Water Treatment and Lithium Power*, Qingdao University of Science & Technoology, Shandong, China, 2014.

[32] F. Gao, *Screening of media Materials for the Treatment of Uranium Contaminants in Groundwater by PRB and its Effectiveness*, East China University of Technology, Fuzhou, China, 2015.

[33] M. J. Wu, *Study on Adsorption Characteristics of High-Rank Apropelic Coal in Ankang Area*, China University of Geosciences, Wuhan, China, 2012.

[34] D. P. Wu, *Coal Containing Methane Fluid-Solid Coupling Mathematical Model and its Application*, Chongqing University, Chongqing, China, 2014.

[35] U. Kumar and M. Bandyopadhyay, "Sorption of cadmium from aqueous solution using pretreated rice husk," *Bioresource Technology*, vol. 97, no. 1, pp. 104–109, 2006.

[36] C. Shi, *Study on the Removal of Rhodamine B from Water by Low Temperature Plasma with Activated Carbon Fiber*, Hefei University of Technology, Hefei, China, 2013.

[37] D. L. Guerra, C. Airoldi, V. P. Lemos, and R. S. Angélica, "Adsorptive, thermodynamic and kinetic performances of Al/Ti and Al/Zr-pillared clays from the Brazilian Amazon region for zinc cation removal," *Journal of Hazardous Materials*, vol. 155, no. 1-2, pp. 230–242, 2008.

[38] Z. Wang, F. C. Yi, and Y. Feng, "Analysis of the adsorption behavior and mechanism of uranium on wood fiber," *Atomic Energy Science and Technology*, vol. 49, no. 2, pp. 263–272, 2015.

[39] M. K. Aroua, S. P. P. Leong, L. Y. Teo, C. Y. Yin, and W. M. A. W. Daud, "Real-time determination of kinetics of adsorption of lead(II) onto palm shell-based activated carbon using ion selective electrode," *Bioresource Technology*, vol. 99, no. 13, pp. 5786–5792, 2008.

[40] S. Lagergren, "About the theory of so-called adsorption of soluble substances," *Kungl- Svenska Vetenskapsakademiens Handlingar*, vol. 24, no. 4, pp. 1–39, 1898.

[41] Y. S. Ho, "Review of second-order models for adsorption systems," *ChemInform*, vol. 37, no. 48, pp. 681–689, 2006.

Hindawi
Journal of Chemistry
Volume 2022, Article ID 4250299, 25 pages
https://doi.org/10.1155/2022/4250299

Review Article

Adsorption of Heavy Metals in Contaminated Water Using Zeolite Derived from Agro-Wastes and Clays: A Review

Ismael Kithinji Kinoti,[1] **Joanne Ogunah**,[2] **Cyprian Muturia M'Thiruaine**,[1] **and Joseph Mwiti Marangu**[1]

[1]*Physical Sciences, Meru University of Science and Technology, Meru, Kenya*
[2]*Department of Physical Sciences, University of Embu, Embu, Kenya*

Correspondence should be addressed to Joseph Mwiti Marangu; jmarangu2011@gmail.com

Received 23 April 2022; Accepted 12 August 2022; Published 22 September 2022

Academic Editor: Jun Wu

Due to climate change and anthropogenic activities such as agriculture, mining, and urbanization, water contamination has become a very real modern problem. Modern solutions such as activated carbon, reverse osmosis, and ultrafiltration, among others, have been employed in the decontamination of water. These methods are, however, expensive to set up and maintain and therefore have proved a challenge to implement in developing countries. Zeolite materials exhibit excellent structural properties, such as high ion exchange capacity, porosity, and relative surface area, which make them attractive to water decontamination processes. However, conventional zeolites are expensive, and recent research has focused on utilizing low-cost materials such as agro-wastes and clays as raw materials for the synthesis of zeolites. This review aims to discuss the role of low-cost zeolites in their removal of heavy metals and the feasibility of agro-wastes and natural clays in the synthesis of zeolites. Recent research studies based on the synthesis of zeolites from clays and agro-wastes and their application in heavy metal removal have been reviewed and discussed. Agro-wastes such as rice husk ash and sugarcane bagasse ash and layered silicate clays such as kaolinite and smectites are particularly of interest to zeolite synthesis due to their high silica to alumina ratio. Zeolites synthesized through various methods such as hydrothermal, molten salt, and microwave irradiation synthesis have been discussed with their effect on the adsorption of various heavy metals.

1. Introduction

Water utilization for domestic, industrial, or agricultural purposes gives rise to different forms of wastewater [1] in a continuous process due to the never-ending stream of human activities requiring usage of water. According to UN-WWDR [2], over 80% of global wastewater is released to the environment without undergoing proper treatment. This brings about 1.8 billion people at risk of waterborne diseases, owing to contaminated water sources [3]. Dye contaminants resulting from artificial pigments are some of the largest water contaminants in the world. It is estimated that the dye industry discharges approximately 7.5 metric tons to the environment every year [4]. Contaminants such as methylene and celestine blue [5], rhodamine, and crystal violet [6], among others, are known to cause poor light penetration to water bodies, thereby hindering photosynthesis and consequently death to aquatic life. In response to a growing population and economy in most low and lower-middle income countries, exposure to contaminants is only estimated to increase, according to a report by UNEP [7]. With the most agricultural system incorporating modern techniques of farming and especially use of herbicides, they are also becoming a common contaminant in most water systems. Fenuron for instance, a common herbicide used to control growth of weeds, is suspected to be carcinogenic to human beings [8] and highly toxic if ingested in large amounts [9]. It is estimated that only 1% of pesticides and herbicides reach their intended target and the rest finds its way to soil, water systems, and vegetables and other

consumable crops [9]. Heavy metals, on the other hand, are recognized as the most poisonous contaminants with adverse effects to the environment and health in general [10].

Wastewater has been classified as domestic, industrial, or storm wastewater [2]. Domestic wastewater arises from domestic water uses in homes or business premises such as cleaning, laundry, and toilet flushing, among others. Domestic wastewater mainly comprises detergent chemicals, fecal matter and urine, and bleach, among other substances [11]. Industrial wastewater arises from industrial processes such as cooling processes or as byproducts of industrial processes. Industrial wastewater can be highly toxic to the environment depending on the involved industrial process [12]. Storm wastewater is generally water due to natural processes such as rainfall and mainly comprises eroded material and other particular matter depending on where the water has runoff [13]. Urban storm water mainly contains heavy metals and other toxic materials due to runoff from open garages and carwashes, especially in many developing countries, where wastewater treatment plans are not available for such small businesses [14]. In cases where there are treatment systems in place inclusive of municipal wastewater treatment systems, major focus is on the removal of biological and solid pollutants through biological treatments in stabilization [15]. However, toxic elements of the wastewater such as heavy metals are left untreated despite the fact that they pose a major health concern [16]. Many methods have been adopted for the removal of heavy metals from wastewater. Use of nanocomposites of multiwalled carbon nanotubes [17, 18], magnetic composites of Fe_3O_4 [19], and activated carbon [20], among others, have been employed on the small scale. Modern large-scale implementations of water purification systems capable of removing heavy metals is often through reverse osmosis, ultrafiltration, and ion exchange, among others, that are unfortunately not accessible to most low and middle-income countries due to high costs of operation and maintenance [21].

Heavy metals are elements considered to have a relatively high atomic weight or density [22]. These include cadmium, copper, iron, chromium, and lead, among others. Some of these metals in trace amounts are useful in the human body, often taking part in crucial processes such as iron in the formation of hemoglobin [23], copper in the efficient absorption of iron into the body [24], and zinc in the synthesis of proteins in the body [25]. Other heavy metals tend to bioaccumulate in the bloodstream and thus become toxic, often causing adverse effects on the human body. Cadmium, for example, on finding its way to the human body and ultimately to the liver, will cause hepatotoxicity and bioaccumulation in the kidneys in the renal tissues causing nephrotoxicity [26]. In chromium, the oxidized states of Cr (VI) are considered very toxic because of the high solubility in water and mobility. Chromium permissible limits in water are set to 0.1 mg/L according to USEPA [27]. Arsenic is often found in dyes, paints, drugs, and semiconductors, among other sources. It can occur as either arsenite or arsenate in organic or inorganic forms, both of which are harmful to human beings. Chronic toxicity is characterized by keratosis and pigmentation issues [28]. Long-term exposure to arsenic compounds has been associated with neurological issues, diabetes mellitus, and cardiovascular diseases, among others [29]. Arsenic permissible limit is 0.01 mg/L according to WHO in water [30]. Lead contamination occurs from effluents of battery repair or production industries, cosmetic, ammunition, soldering, or old pipes. Children are said to bioabsorb 50% more lead than adults during their development [29]. Due to its ability to be biodeposited into the body, it is reported that 95% of lead once in human body can be deposited as a form of insoluble phosphate in skeletal bones. Acute poisoning of lead has been linked with headaches, loss of appetite, arthritis, and hallucination, among other effects. Chronic effects include mental retardation, psychosis, birth defects, autism, and kidney damage, among others [31]. Allowable limit of lead in drinking water according to WHO is 0.01 mg/L [32]. This article reviews the structure and properties of zeolites derived from agro-based materials and clays, their methods of synthesis, efficiencies for removal of heavy metals in wastewaters, and the challenges or recommendations around the utilization of the derived zeolites.

2. Wastewater Treatment Processes

Wastewater is made up of solids (350–1200 mg/l), dissolved and particulate matter (250–1000 mg/l), microorganisms (up to 109 numbers/ml) and nutrients, heavy metals, and micropollutants [33]. The most problematic pollutants are solids, as they can clog and/or damage the system. The role of wastewater treatment is to convert the influent into a state that can safely be returned back to the water cycle without negatively impacting the environment [1]. To achieve this, physical [9], chemical [34], and biological processes are applied through the stages of treatment discussed. These stages are summarized in Figure 1.

2.1. Preliminary Treatment. This stage involves the removal of grit and large solids that would damage equipment in later stages or be too large to continue the process [36]. At this stage, plastics, pieces or blocks of wood, metals and glass material, as well as surface oil, gravel, and sand due to stormwater are removed using mechanical and physical-chemical methods [35]. The principle of treatment at the preliminary step is based on the particle size of the contaminant; therefore, size exclusion techniques are indispensable. These include use of screens, comminutors, grit-removers, and skimming tanks [37]. Screening devices are made up of wire mesh, parallel bars, grating, perforated plates, etc., to make uniform size openings usable in the removal of floating matter, often referred to as rakings or screenings. It has been found that sanitary sewage (domestic sewage) makes use of an average of 0.0015–0.015 m^3/Ml screenings with an average screen size of 25–100 mm [37]. The screenings are disposed off through incineration, burial, digestion, or composting.

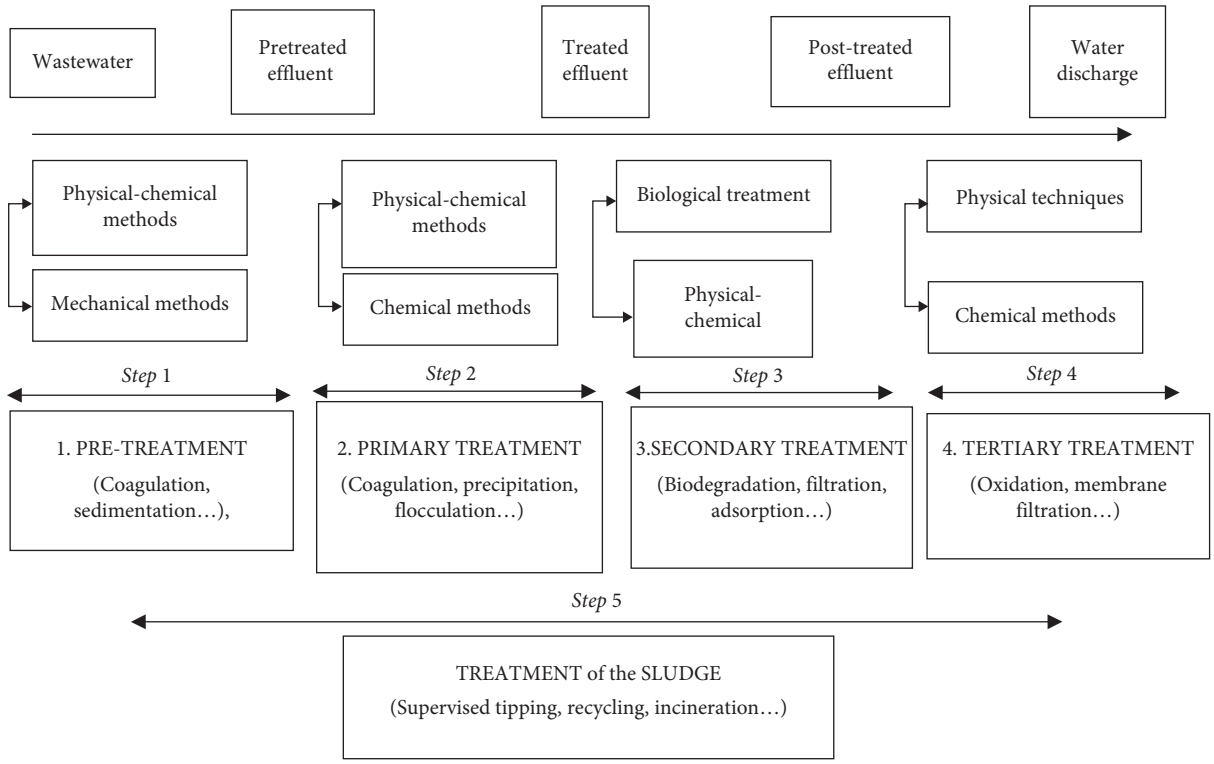

Figure 1: Summary of wastewater treatment processes (adopted from [35]).

2.2. Primary Step. The most prominent method of wastewater treatment at this stage is the physical process, which involves sedimentation by the use of membrane filters that require frequent backwash, which can incur extra costs [38]. However, chemical processes may be employed to induce coagulation and flocculation of suspended materials that will not settle through gravity [39]. By the use of sedimentation and floatation, both inorganic and organic solids are removed from wastewater at this stage. Common contaminants removed at this stage include biochemical oxygen demand, total suspended solids, grease and oils, organic nitrogen, organic phosphorus, and traces of heavy metals. The primary stage manages the removal of 50–70% of the suspended solids and 25–50% of the biochemical oxygen demand [40]. Treatment units that have been applied at this stage include detritus tanks, grit chambers, skimming tanks, screens, and primary sedimentation tanks [41]. The screens at this stage are used in the removal of floating matter with comparatively large particle size. Detritus tanks are used when the flow velocity is low, and they withhold sewage for longer periods (approximately 4 minutes), thereby removing fine settleable particles [41]. In the primary step, chemical precipitation is considered only in special cases where (i) odor becomes a problem; (ii) there is a need to remove phosphorus compounds; (iii) there is industrial waste that is likely to destabilize the biological removal process; and (iv) the strength and flow of the wastewater vary greatly [42].

2.3. Secondary Step. This stage incorporates the use of biological and chemical techniques in the treatment of wastewater from the primary step [43]. Microorganisms are used in the removal of most inorganic and organic contaminants, followed by chemical filtration to remove pathogens [38]. Trickling filters are used to induce the decomposition of organic pollutants in biofilms, a process aided by aerobic or anaerobic microorganisms [38]. About 85% of BOD and TSS are removable at this stage, leaving traces of heavy metals, phosphorus, nitrogen, pathogens, and bacteria for removal at the tertiary stage [44]. Conventional processes applied at this stage include trickling filters, oxidation ponds, activated sludge, and filter pods. Space, initial, and operational costs are factors that determine the choice of an applicable technique in secondary sewage treatment [43]. Often, space is a limiting factor due to the high municipal or local area population and the cost of the land. Therefore, this makes oxidation ponds uneconomical and least adopted in regions where land costs are high [43]. Activated sludge, on the other hand, is widely used since it requires low space, minimizes construction costs, and produces a relatively low odor. This method, however, can be costly to operate owing to energy expenses for the oxygen demand and the air pump operation costs [45]. The trickling filter method offers biological contaminant removal through the salts, rocks, plastics, or stones. These are usually packed in such a way that they allow growth of microorganisms and sewage flow through, in very low velocities, to

ensure ample contact with the microorganisms [46]. The filters have relatively low construction cost, provide a cheap system of oxygen delivery, and can exist with nonelectric systems. However, they are temperature-dependent, can be easily congested, and occupy a larger surface area compared to activated sludge types [43].

2.4. Tertiary Step. This stage involves the disinfection of the water to make it reusable again. In this step, chemical processes like chlorination for removal of residual pathogenic bacteria and more specific adsorbents for the removal of toxic elements like dyes and notorious heavy metals are incorporated [47]. The chlorination process, although often applied due to its effectiveness in disinfection, easy to use, and budget friendly, can be hazardous if used in excess [47]. Chlorinated water is freed from harmful microbes, but for disposal into aquatic ecosystems, it needs to be dechlorinated, as chlorine can form potentially carcinogenic compounds such as mutagen X [48] and trihalomethanes [49] when it reacts with some organic materials. Recently, ultraviolet (UV) light [38] and ozone [47]are being employed for disinfection without alteration of the water quality. In UV treatment, the water effluent is passed through ultraviolet radiation, which alters the genetic structure, thus rendering them sterile and unable to infect wildlife or humans. However, the water needs to have undergone thorough pretreatment before this step since residual organic matter can reduce the UV light effectiveness when they shield the microbes [47]. The downside of UV treatment is the relatively high costs of maintenance of the UV lamps. In ozone treatment, microbes are destroyed on contact with ozone and forms no hazardous byproducts [50]. The use of ozone is convenient since it can be produced as needed onsite and needs no storage; equipment, however, can be expensive to maintain [15]. The final stage in the tertiary step must be filtration, which can be achieved using activated carbon fibers, sand or disc, and drum or bag filters [47]. When it is necessary to reduce a contaminant to a specific micron concentration rating, bag filters are used [51]. Drum filters have woven cloth wrapped over a drum, through which the influent gets into the drum and filtrate out the cloth. Backwash removes contaminants and ensures the continuous functioning of the system [52].

Although these three waste water treatment steps are required for any waste water treatment plant, most of the plants in low- and middle-income countries have reported low efficiencies in the removal of heavy metals.

3. Wastewater Treatment Technologies

3.1. Ion Exchange. Ion exchange has seen great usage in the removal of heavy metals in the water purification process, whereby cations are used to exchange for metal ions in water through physical or chemical processes [53]. An electrostatic field often binds exchangeable ions onto functional groups available on a solid matrix that needs to come into contact with mobile contaminated water to remove the metal ions [54]. Varying experimental conditions affect the affinity of the ion exchange for certain species, thereby separating them from the solution [54]. Ion exchangers often make use of natural zeolites and synthetic resins to remove metal ions [53]. The resins (R) work through hydrogen-based ion exchange where the cation exchanger releases its hydrogen ion (H^+) into the solution to exchange for an ion (X^+) in the solution as follows [54]:

$$\mathrm{R-H} + \mathrm{X}^+ \leftrightarrow \mathrm{R} - X + H^+. \quad (1)$$

Every ion removed from the solution is replaced by another, thus achieving a state of electroneutrality. Several types of ion exchangers including zeolites structured into ion exchangers have been utilized in the removal of heavy metals. Luca [55] comparatively studied the removal of zinc by zeolite ETS-10-based ion exchanger against municipal zeolite A-based ion exchanger and reported higher removal by ETS-10. A different paper by Kumar [56] studied the adsorption of lead (II) ions on a hybrid ion exchanger and reported maximum adsorption capacity 182.7 mg/g ions at 50°C. The adsorption was reported to follow a pseudo-second-order kinetic model for the adsorbed ion. In a similar paper by Ma et al. [57], upon removal of nickel ions using dual-exchanged (Na^+/H^+) chelating resin, metal ion removal was reported to be highly dependent on the pH of the solution and the Na^+ to H^+ ratio. High concentrations of sodium ions led to precipitation of nickel hydroxide, which clogged the ion exchanger. Too much hydrogen ions led to competitive protonation, whose consequence was noted to be reduced nickel ion uptake. The heavy metal ion exchanger method is effective with high metal ion removal efficiency, high selectivity, and rapid adsorption kinetics and is applicable in the whole water treatment range [58]. These advantages have seen its massive utilization in most water purification systems especially in developed countries. The method, however, suffers major challenges such as high operating costs and production of sludge which is expensive to process; resins are easily polluted by organic contaminants, and in the face of heavy pollution, resins spend easily [59].

3.2. Reverse Osmosis. Reverse osmosis (RO) technology makes use of semipermeable membranes (filters) to remove contaminants from water by allowing only water to pass through [60]. With the membrane pore size in the range 0.1–1.0 nm, an applied pressure is necessary to overcome osmotic pressure, thereby requiring high energy to operate [61]. The performance of RO filters is greatly affected by the characteristics of the feed water, such as temperature, salt concentration of the feedwater, and the aforementioned pressure [62]. Generally, a higher feedwater temperature ensures high permeate flow due to increased diffusion rates and lower viscosity associated with higher temperatures. The pressure parameter referred to as net driving pressure (NDP), which is the cumulative sum of all the forces exerted on the RO membrane, is often used to understand the feed pressure [63]. Doubling the NDP hypothetically doubles the flow of the permeate [64]. As water flows through the RO membrane, the TDS concentration on the influent side will

always be higher than that on the effluent side and so will the pressure. A gradient of salt concentration parameter, determined as the difference between influent and effluent TDS of an RO, describes salt rate passage in an RO system. The passage is usually independent of the pressure in the system [62].

In recent years, different studies have been conducted to bring solutions for heavy metal removal using reverse osmosis technology. Thaci and Gashi [65] utilized biowaste materials to design water purification systems, utilizing the material as a guide with reverse osmosis technology to remove contaminants such as lead, zinc, cadmium, cobalt, manganese, and nickel. Others have used spiral bound reverse osmosis membrane [66] and antifouling reverse osmosis membrane using crosslinkers [67], among others.

Reverse osmosis method is very effective in water purification system as it only allows water to pass through by blocking all other ions. It requires simple maintenance, and it is preferred because it does not require chemicals to remove ion contaminants [68]. It is, however, prone to clogging, fouling, and scaling and therefore requires frequent filter change and maintenance [69]. This increases maintenance costs. In addition, reverse osmosis is slow in operation and often not self-sustainable [70].

3.3. Electrodialysis. Electrodialysis is often used as a modification of ion exchange membranes to make them more selective in their contaminant removal or to improve their removal capabilities [61]. Ionic and cationic membranes with embedded electrodialysis stacks are sandwiched by two electrodes. With the application of an electric current, anions and cations pass through the electrodialysis membrane and are retained on the ion exchange membranes, thus creating a divided aqueous solution with concentrate (high content of contaminants) and diluent [71]. Since electrodialysis uses membranes, it is applicable in low TSS wastewater with suspended particle diameter not higher than 10 μm [72]. The larger particle size clogs the membranes. Wastewater needs to contain TDS concentrations of not more than 5000 mg/l for effective removal [73]. Other important factors that affect the functioning of an electrodialysis system include the flow rate of wastewater, its temperature, and composition [74]. The applied voltage and the characteristics of the ion exchange membranes also determined to a large extent the efficiency of the system [74].

Electrodialysis systems can produce very high-quality effluents with relatively low energy consumption, achieving 80–95%water recovery rates [75]. An electrodialysis system consumes approximately 0.49kWh/m^3 at 1000 mg/l of TDS at 75% recovery and 1.75kWh/m^3 at 5000 mg/L of TDS [73]. However, they are selective in their removal and therefore fail to remove colloids and organic matter, often making them uneconomic on their own. Furthermore, electrodialysis systems do not remove neutral toxic components such as bacteria and viruses, requiring posttreatment of the effluent [76]. In addition, electrodialysis operation cost can go above reverse osmosis when influent's TDS concentration exceeds 12,000 ppm [77].

4. Adsorption

Adsorption process has been utilized in water purification systems extensively, making it one of the most used water purification techniques [78]. The adsorption process occurs physically through electrostatic charges or chemically through formation of bonds on the surface or the pores of porous solids in liquid or gaseous media [79]. In this regard, therefore, adsorption can be described as the process, whereby adhesion of atoms, molecules, or ions occurs in response to excess surface energy due to bond deficiency [80]. To efficiently remove contaminants, an adsorbent needs to possess suitable physicochemical characteristics. These include long service life, high adsorption capacity, high selectivity, and low-cost [81]. Surface functional groups, active surface, pore distribution, and pore diameter are important parameters when characterizing adsorbent materials [81].

4.1. Types of Adsorbents. The most common types of commercial adsorbent currently in use include zeolites-based molecular sieves, polymeric adsorbents, activated alumina, activated carbon, silica gel, and carbon-based molecular sieves [82]. Most of the adsorbents like activated carbon and polymeric adsorbents are usually manufactured, while others such as clay occur naturally. Zeolite adsorbents can be synthesized or occur naturally. The structural properties of the adsorbents determine their applications [53, 81, 83–85]. Table 1 summarizes some applications of common adsorbents.

Adsorbents application and type is largely dependent on their specific characteristics. Synthetic adsorbents are currently most sought after due to their customizability at synthesis and their selectivity in adsorption [92–95]. With the world looking for affordable, renewable, and efficient adsorbent solutions, researchers are looking into utilizing agro-wastes and abundant resources like clay for adsorbent purposes.

4.2. Characteristics of Adsorbents. For a material to be effective as an adsorbent for metal ions, it needs to exhibit some characteristics that fall into either physical or chemical characteristic groupings [85]. Physical characteristics include porosity, surface area, density, and particle size. Porosity refers to the total amount of space void available to the material. The more the pores, the higher the adsorption capacity of the material is [96]. Yakout [97] illustrates the increase in mesoporous pore increase in adsorption studies. A similar study by Tang et al. [98] reported higher Pb^{2+} and Cd^{2+} for the activated carbon adsorbent with a higher pore volume, agreeing with this observation. The rate of mass transfer is usually influenced by the external surface area [99]. External mass transfer occurs with the formation of a hydrodynamic layer covering the adsorbent, whereas internal mass transfer occurs through intraparticle diffusion. Efficient adsorption is highly dependent on the internal surface area and is responsible for material pore characterization as microporous, mesoporous, or macroporous. The total volume of pores available to an adsorbent material gives its adsorption capacity [97]. In an adsorptive study by

Table 1: Summary of applications of common adsorbents [83].

Adsorbent	Pore diameter (nm)	Structure	Applications	References
Activated alumina	8.096	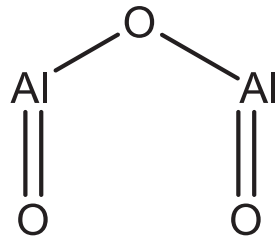	Removing HCl gas from hydrogen Drying gases, transformer oils, and organic solvents Removing fluorine in alkylation processes	[86, 87]
Silica gel	2–11	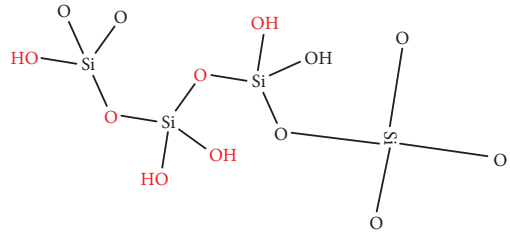	Dew point control for natural gas Act as a desiccant Drying gases, organic solvents, etc.	[81, 88]
Activated carbon	0.54–0.59	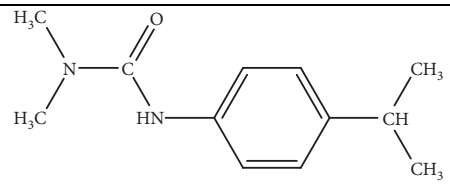	Removing odors Purifying helium Usage in water purification systems	[89, 90]
Zeolites	0.3–0.8	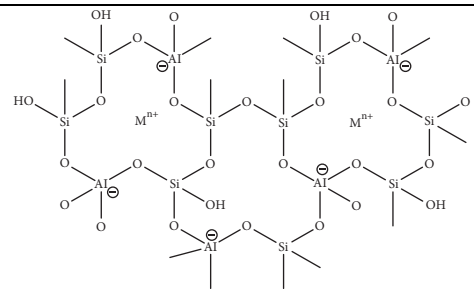	Separation of oxygen from air Purifying hydrogen Recovering carbon dioxide Sweetening of sour gases and liquids	[81, 91]

Ouyang *et al.* [100], the synthesized adsorbent follows pseudo-first-order kinetic model in the adsorption of Pb^{2+}, Cd^{2+}, and Cu^{2+}. This results in the fact that the adsorption process is most likely a physisorption process. This adsorption process follows an external mass transfer phenomenon. In a different study, zeolites synthesized from natural kaolin were used in the adsorption of various metal ions, and the adsorption kinetic study revealed adsorptive energies below 40 kJ/mol, which indicated the physisorption process [101]. Similar findings were reported by Shehata et al. [102].

The chemical characteristics of an adsorbent involve the availability of surface-active functional groups to the material that can interact with contaminants and favorable surface chemistry [103]. Surface chemistry is the determinant of interactions between the adsorbent and the adsorbate, especially adsorption into oxidic sites [96]. In an investigation by Tran et al. [104], studying the effect of modification of the surface chemistry of zeolitic adsorbents on contaminant adsorption, it was reported that the modification of the Na of Y-zeolite improved its cation exchange capacity. Modifying it with surfactants opens the material to a wider range of adsorbates. In a similar study, the authors modified municipal sewage waste incineration fly-ash-based zeolite with Na_2PO_4 and reported 22 times higher adsorption compared to the unmodified zeolite [105]. Similar studies have reported enhanced metal ion adsorption on the modification of surface chemistry of various zeolite-based adsorbents [105–108].

4.3. Adsorbents in Water Treatment. Activated carbon (AC) has been in use for the adsorption of both inorganic and organic contaminants over the years. The selectivity to inorganic or organic compound adsorption depends on the material of origin and the process of activation [109]. Soft carbonaceous materials generally produce large-pored AC that are often applied in removal of organic compounds [110]. Harder materials produce AC with smaller pores often used in the removal of inorganic contaminants [111]. The process of activation can, however, alter the characteristics of the resultant AC [110]. Activated carbon is prepared from carbonaceous compounds such as wood, and agro-wastes achieve a high surface area and porosity for application in

heavy metal adsorption [85]. Activated carbon can be used in various forms ranging granulated form (0.6 – 4 mm granules), powdered form (44 μm), and fibrous structures with low hydrodynamic resistance [112]. Activated carbon has been documented to achieve a high contaminant removal efficiency of more than 94% for contaminant concentration of between 100 and 1600 μg/l with a carbon dose of approximately 1.25 g/l [113]. Activated carbon technology is limited by very high costs of production and use. Researchers circumnavigate this by sourcing cheaper material for the synthesis of activated carbon and/or modifying the surface chemistry of the material [112]. Nejadshafiee and Islami [114] modified activated carbon produced from pistachio shells with Fe_3O_4 nanoparticles and 1,4-butane sultone and reported high adsorption capacities for Pb^{2+} (147.05 mg/g), As^{2+} (151.51 mg/g), and Cd^{2+} (119.04 mg/g). In a similar study, Kyzas et al. [115] investigated the effect of nanobubbles on the adsorption of $Pb^{2+}$by activated carbon based on potato peels and reported almost equal adsorption of the metal ion by the modified carbon compared to the unmodified. However, the adsorption duration was boosted by over 300%, which indicated that the nanobubbles had a catalytic effect on the adsorption process.

Carbon nanotubes (CNTs) have one-dimensional tube-like structures resulting from rolled-up graphene sheets. They can be single-walled (SWCNT) or multiwalled (MWCNT) and contain a high surface area for contaminant adsorption. CNTs offer internal sites, interstitial channels, groove sites, and exterior surfaces as active adsorption sites making them excellent adsorbents [96]. Interactive forces due to carbon on the CNT surface cause challenges of aggregation, difficulty in manipulation, and poor dispersibility. Since the active sites on a CNT are found on defected segments of the structure, like pentagons on a body of hexagon structures, their interaction with other compounds in "raw" form is often limited [116]. They are modified by functionalization to enhance their interactions, using covalent (attached to CNTs skeleton) or noncovalent (functional groups coating the walls of CNTs) functionalized [117]. The process of functionalization is subject to the chemical and physical properties of CNT such as the nature of the CNT surface, particle size, and the chemical composition of the material [118]. In a study to compare adsorption performance of oxidized and double-oxidized MWCNTs, Rodríguez and Leiva [119] reported an increase in adsorption of Cu^{2+} (7.8–14 mg/g), Mn^{2+} (3.7–6.6 mg/g), and Zn^{2+} (2.7–4.0 mg/g). The authors reported that the adsorption followed the Langmuir's adsorption isotherm, which indicated that the adsorption process was a monolayer. The increase in adsorption was an indication of an increment in adsorption sites on the surface of the MWCNT for the double oxidized MWCNT. Other authors have reported similar findings on MWCNT oxidization modifications [120–122]. Polymers such as polydopamine [123] and polyethylenimine [124] have been utilized to functionalize MWCNTs to improve their heavy metal adsorption. High adsorption capacities with polydopamine functionalization have been reported as 318.47 mg/g for Cu^{2+} and 350.87 mg/g for Pb^{2+}.

$$M_{\frac{x}{n}}\left[\,(AlO_2)_x.\left(SiO_2\right)_y\right].w\ (H_2O)$$

Figure 2: General formula of zeolite, adapted from Golbad [127].

Clay and clay-based compounds are other common adsorbents that have been extensively utilized in the removal of heavy metals from wastewater. We have recently published a review article discussing use of clay-based materials in heavy metal removal. The article can be accessed through [125].

4.3.1. Zeolites. Zeolites are crystalline, porous, and hydrated aluminosilicate minerals, characterized by specific molecular pore size [126]. When occurring naturally, they are found in temperatures often below 200°C in basaltic cavities, crystalizing due to hydrothermal alteration or diagenetic processes [126]. Zeolites possess three-dimensional structures that arise from polyhedral $[SiO_4]^{4-}$ and $[AlO_4]^{5-}$ polyhedral (Figure 2). They are capable of both facile and reversible cation exchange, acting as molecular sieves due to their tetrahedral structure, as shown in Figure 2 [128].

M represents a cation, with valence n, whose purpose is to balance negative charges due to aluminium tetrahedral, x and y are the stoichiometric coefficients of alumina and silica, w is the number representing the water molecules. M is often an alkali or an alkali Earth metal.

The crystalline structure gives them fascinating properties, such as shape selectivity, ion exchange, sorption capacity, catalytic activity, and host for advanced materials. The sorptivity of zeolites depends on the opening of the pores and the volume of the voids in the material. The ion exchange of zeolites depends on cation sites nature and how accessible they are for exchange [129].

In heavy metal adsorption studies, natural zeolites such as mordenite, chabazite, and clinoptilolite have been on major focus with performance comparative studies. However, the cation exchange capacity and heavy metal adsorption capacity of natural zeolites are predetermined and therefore limited by natural processes, leaving little room for modification. Synthetic zeolites show flexibility since their topology, pore distribution and size, and cation type in the zeolite framework, and the particle size can be controlled during synthesis [127, 130]. Framework and structure of basic zeolite elements is given in Figure 3.

The arrangement of atoms on the zeolitic molecular structure (Figure 3) gives the lattice a negative charge when Al^{3+} substitutes Si^{4+} in an isomorphous fashion [132]. The zeolite solid achieves electroneutrality through counteractions that reside in hydration water in the voids of the zeolite [131].

The framework of a zeolite describes the connectivity of the tetrahedral arranged atoms to achieve the highest form of symmetry. In describing the framework, a 3-letter code is assigned that is in accordance with the International Zeolite Association (IZA), and the codes are usually derived from the zeolite name, that describes the 'kind of material' [133]. For example, faujasite has the code FAU, and the MFI code represents zeolite Socony Mobil-Five (or ZSM-5). Common

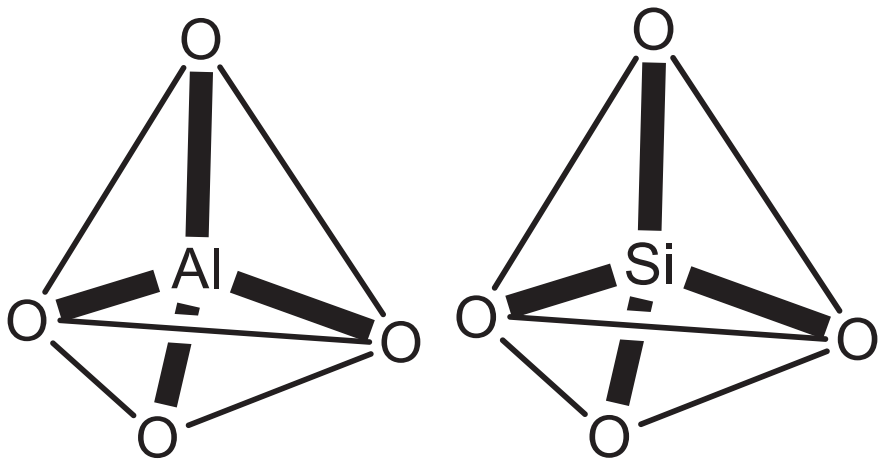

Figure 3: Sketch of the structure of the zeolite and $[AlO_4]^{5-}$ or $[SiO_4]^{4-}$ tetrahedral representation (adapted from [131]).

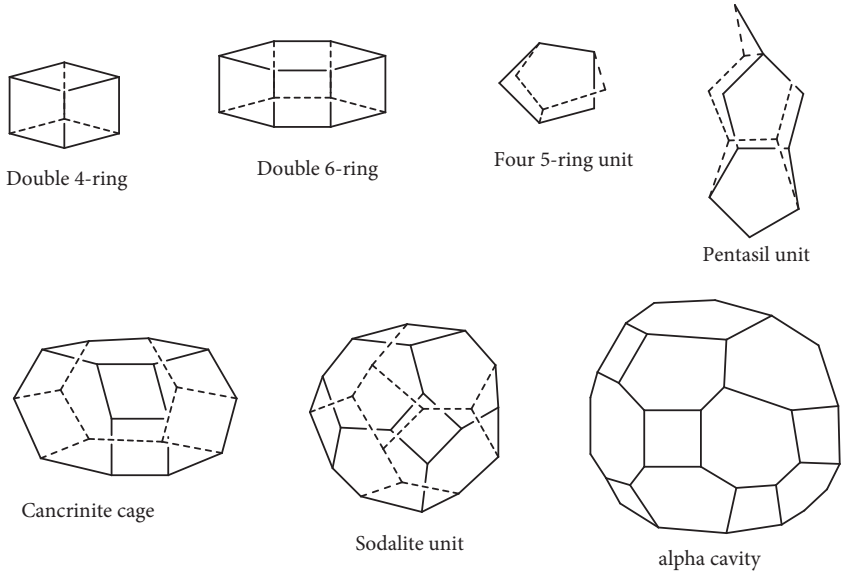

Figure 4: Cavities and subunits common among framework types adapted from [128].

synthetic zeolite types include zeolite A, X, B, Y, and SZM-5, among others. In order to describe a zeolite structure, the framework is described first in terms of the dimensions of the channel system and the opening sizes of the pores. The ring size defining the pore characterizes the pore openings and usually designated the *n*-ring label, whereby *n* stands for the number of O- and T-atoms in a ring. Thus, an 8-ring framework has a pore width of about 0.41 nm and is considered microporous, 10-ring with a pore width and considered mesoporous, and 12-ring with 0.74 nm pore width and considered microporous [127]. A few structural features such as channels, cages, sheets, and chains are shared among zeolite frameworks as shown in Figure 4.

(1) Distribution and Occurrence of Natural Zeolites. Zeolites occur within different types of rocks, of differing ages and in diverse geological environments [134]. They are naturally formed as a result of a solid material reacting with its own pore water. Zeolites have been found to be deposited as cavity fillings in altered volcanic rocks [135]. They have also been found in sedimentary rocks of marine origin, formed as a result of the alteration of volcanic glass [126]. Metamorphic rocks have also been reported to contain zeolites formed under extreme geothermal conditions at great depths [131]. The occurrence of some minerals in the zeolite group is summarized in Table 2.

According to Table 2, it can be seen that most rocks in which zeolites occur are generally volcanic and sedimentary rocks. When they occur in volcanic rocks, they occur as cavity fillings often as vapor or fluid deposition, while in sedimentary rocks, they are often alterations of volcanic glass [142].

(2) Properties of Zeolites. Zeolitic minerals exhibit adverse chemical and physical properties depending on their type. In terms of color, they can be transparent or appear in varying colors. In pure form, zeolites will often appear transparent or colorless and brownish reddish to greenish if they contain impurities [143].

Table 2: Summary of occurrence of some zeolites.

Zeolite mineral	Chemical formula	Occurrence	Reference
Alflarsenite	$NaCa_2Be_3Si_4O_{13}(OH)\cdot 2H_2O$	Syenitic pegmatite (Larvik, Denmark)	[136]
Amicite	$K_2Na_2Al_4Si_4O_{16}\cdot 5H_2O$	Basaltic rock (Howenegg, Germany)	[137]
Analcime	$Na(AlSi_2O_6)\cdot H_2O$	Basalts and phonolites (Catania, Italy)	[138]
Bikitaite	$LiAlSi_2O_6\cdot H_2O$	Lithium-rich pegmatites (Bikita, Zimbabwe)	[139]
Boggsite	$Ca_8Na_3(Si, Al)_{96}O_{192}\cdot 70H_2O$	Porphyritic basalt (Goble Creek, Oregon, USA)	[140]
Brewsterite-Sr	$(Sr, Ba, Ca)[Al_2Si_6O_{16}]\cdot 5H_2O$	Basalts and schists (Strontian, Scotland)	[141]

Most zeolites exhibit density in the range 2–2.3 g/cm^3, although it is not uncommon to observe density values ranging 2.5–2.8 g/cm^3 especially those with abundance of Ba atoms, like Brewsterite. Bulk specific gravity has been documented to range between 0.80 and 0.90 g/cm^3 [144].

Zeolites exhibit massive ion exchange capacities. The cation exchange capacity (CEC) of zeolite minerals is often in the range 200–300 cmol/kg, although it can reach up to 400 cmol/kg. The value of the CEC is dependent upon factors such as the pH, temperature electrolyte concentration in the solution, structural characteristics of the zeolite, dimensions and the shape of new cation, and the anionic charge density in the framework, among others [145].

Zeolites also exhibit a unique property and adsorption selectivity, which is greatly defined by the diverse ions and molecules with varying sizes trapped within the zeolite pores. This parameter is responsible for the novel molecular filtration capabilities of zeolite, which are dependent on the structure of the zeolitic crystal and the separation capacity that is based on polarity, shape, or size, thus making the zeolite a selective adsorbent [144].

The catalytic properties of zeolites arise in response to the distribution of various acidic regions in the crystalline lattice of the zeolite. In addition to this, the size of both the internal cavities that act as reaction chambers and the surface resources have an effect on the catalytic activity of zeolites. Any zeolite is still able to affect reaction selectivity through molecular traffic control, transition state selectivity, or selectivity of the product or the reaction [146].

Other important properties of zeolites include thermal stability that is about 1000°C, structural stability against acid, alkaline and radioactive environments, refractive indices ranging 1.47–1.52, and water adsorption capacity in the range 45–75 ml/100g [143].

Generally, a zeolitic material will be adverse in color depending on impurity levels and show a density in the range of 2–2.8 g/cm^3 with specific gravity values ranging 0.80–0.90 g/cm^3. The material will also portray high CEC values of up to 400 cmol/kg and great selectivity in its ion adsorption [147–149].

5. Synthetic Zeolites

Naturally, zeolites have been formed out of the reaction of volcanic ash and basic lake water in a process lasting thousands of years [150]. Synthetic zeolites are fabricated in a simulated hydrothermal process, temperature, and pressure using synthetic silicates or natural materials [151]. Appropriate equipment, energy, and uncontaminated substrates are required to achieve quality synthetic zeolite. In this regard, it is important to note that the synthesis reactions can incur costs that directly influence the price of the product, in which case would be uneconomic. The recent focus in the field of synthetic zeolites is, therefore, reaction cost reduction [152]. This is achievable by using waste or natural raw materials. High silica natural materials such as diatomite, halloysite, clay minerals, pumice, and volcanic glasses have therefore been in the spotlight for zeolite synthesis [153].

Depending on the silica content, synthetic zeolites are distinguished as low silica (with Si/Al ~ 1–1.5), intermediate silica (with Si/Al = 2.5), and high silica (with Si/Al > 10), a parameter that directly reflects the specific properties of the zeolite [154]. A low Si/Al ratio translates to increased ion exchange capacity for the material and high adsorption capacity towards polar molecules. A high Si/Al ratio translates to high catalytic activity, hydrothermal stability, and increased hydrophobicity [144].

5.1. Synthesis of Zeolites

5.1.1. Factors Affecting Zeolite Synthesis. To achieve high-quality zeolites, years of practical experience have outlined some important factors to consider, namely, the silica to alumina ratio, reactants composition, aging, temperature and time, crystallization, and alkalinity [155]. The composition of the reaction mixture, which incorporates the silica to alumina ratio, the inorganic cations, and OH^- ions, requires close attention to achieve highly customized zeolite compounds [156]. Increasing the Si/Al ratio affects the material's physical properties, while OH^- affects the mobility of the silicates from the solid phase to the solution, thus affecting nucleation times [157]. The inorganic cation has the most important role in balancing the charge of the framework and acts as agents directing the structure, thereby directly affecting the product yield and crystal purity. In the synthesis of hierarchical Y zeolites, Feng et al. [158] studied the effect of NH_4HF_2 etching on the formation of zeolitic crystals with X-ray diffraction (XRD) data showed enhanced peaks for NH_4HF_2-etched zeolite, which demonstrated the effect of reaction mixture composition on zeolite synthesis.

The nature of reactants and the level of their pretreatment is another important factor. Since the synthesis process involves the utilization of both organic and inorganic precursors, inorganic precursors produce more hydroxylated surfaces, as organic precursors incorporate metal ions into

the network [159]. In the synthesis of zeolite W, the researchers used natural zeolite waste. With thermal treatment at 400–900°C, the crystalline zeolite formed remained below 36.5%. However, when they tried alkali fusion treatment at 600°C, a larger amount of Al species was activated and less than 40% of silica species. In this way, more zeolite W crystals were formed [160].

Temperature affects nucleation and rate of crystallization in the synthesis of zeolites. The crystallization rate is usually directly proportional to the temperature change. The nucleation rate, on the other hand, exhibits an inverse proportionality to the temperature change [161]. Zhao et al. [162], in a study to characterize the synthesis of high silica Y zeolites, investigated the effect of precursor pretreatment in the zeolite synthesis with NMR data showing higher zeolite crystal formation for precursors aged at low temperatures.

Reaction time is a factor that is often managed by the crystallization process. The crystallization is adjusted to minimize other phase production, while minimizing the time required to achieve required crystalline phase [163]. In a study investigating the synthesis of zeolite SSZ-13 from coal gangue, the researchers reported gradual increase in synthesis time up to 36 hours [164]. In a similar study, Krachuamram et al. [165] investigated the effect of aging time on crystallites formation and reported an optimum aging time of 3 days for NaX zeolites synthesis.

In summary, the composition of the reaction mixture determines the texture and often the duration of zeolite synthesis. Pretreatment of the precursors can determine the failure or success of zeolite formation. The temperature is often defined by the synthesis method, but plays a role in the nucleation of the zeolite crystals. The reaction time needs to be closely monitored as different zeolites achieve maximum formation within certain time ranges, beyond which crystals degrade.

5.1.2. Methods Applied in the Synthesis of Zeolite. Zeolites are synthesized by heating aluminosilicate raw materials for a period of time that spans hours or days (depending on the type of the raw material and the process conditions) in the presence of high pH solutions [153]. Common methods currently applied in zeolites synthesis include hydrothermal synthesis [166], microwave-assisted synthesis method [167], molten salt [103], activation of alkali fusion activation [168], and synthesis through dialysis [153].

The hydrothermal synthesis method usually simulates the natural conditions through which rocks containing zeolites are formed. Hydrothermal temperatures of 80–350°C are involved in treating aluminosilicate raw materials in an alkaline solution with pH above 8.5 [169]. The reactions that occur (dissolution, gelatinization, condensation, and crystallization) are conducted in an autoclave at elevated pressure [170]. Careful alteration of process parameters gives products with desired properties [153]. Garcia-Villén et al. [166] used the hydrothermal synthesis method to synthesize zeolite using waste from sanitary ware. Researchers used 5M NaOH alkaline solution at temperatures 100, 150, and 200°C for up to 30 days and reported the transformation of quartz and mullite minerals to zeolite. Luo et al. [171] synthesized needle-like zeolites from metakaolin using the same method for utilization in the removal of organic and heavy metal contaminants. Hydrothermal synthesis is a common method in the synthesis of zeolites. It, however, suffers limitations as high cost, especially with the use of high-pressure autoclaves and produces excessive waste, making it environmental unfriendly [172].

Molten salt method for zeolite synthesis was proposed to address the shortcomings of hydrothermal method such as high ratio of solution to solid and low product yields [173]. In the molten salt method, synthesis takes place under molten conditions without the addition of water. The high-silica raw material, a salt, and a convenient alkaline solid are finely ground and melted at convenient temperatures for extended periods of time. They are then cooled, crushed and washed. Common bases used include KOH, NH_4F, and NaOH [174, 175]. Common salts used include $NaNO_3$, KNO3, and NH_4NO_3. This method was often used to synthesize fly ash-based zeolites [176–178]. Since the molten salt method required high temperatures for the synthesis of zeolites, the most serious limitation associated with the method was the high energy consumption rates, often worsened by the duration of synthesis of the material [179]. Recently, authors are using modifications of the method to reduce energy consumption cost through submolten salt (SMS) synthesis. In SMS technology, high-alkaline (above 50%) and high-boiling-point precursors are used to ensure reaction conversion and mass transfer while keeping temperatures low, under ambient pressures [180]. Meng et al. [181] used the SMS method in precursor treatment using 75% alkaline solution and an alkali to ore ratio of 3.5 : 1 at a temperature of 200°C, during the synthesis of zeolite W from potassic rocks. The resulting material achieved an exchange capacity of 156.8mgK^+/g and 30.39mgK^+/g in KCl and simulated sea water solutions, respectively. Similarly, Krisnandi et al. [182] synthesized ZSM-5 zeolite crystals from natural zeolites using the fragmented SMS method. Natural zeolite was pretreated at 250°C in alkaline solution. The resulting material showed the BET surface area of 262 m^2/g, which is typical for a microporous zeolite.

Microwave irradiation is a modern green technique that has been used in the fabrication of zeolites. Different ratios of aluminium to silica sources and structure directors are usually mixed uniformly and irradiated by microwaves in autoclaves [183]. Parameters such as the size and shape of the autoclave, reaction time, and power and temperature of the microwave are adjusted carefully to affect the morphology, as well as the structure, of the zeolite [184]. Majdinasab et al. [185] used the microwave radiation technique in the synthesis of zeolites from pulverized waste glass cullet in comparison with convection heating. The authors reported microwave radiation being more efficient, achieving 60% maximum relative crystallinity of the zeolite. Similarly, Wong et al. [186] successfully synthesized nanocrystalline F-type zeolite using an organic template-free system by using rice husk ash as the silica source under microwave irradiation.

5.1.3. Agro-Waste in Zeolite Synthesis. Rice husk ash (RHA) has been extensively investigated as a potential silica source for the synthesis of zeolites. Many methods have been proposed for the extraction of silica from RHA, including biological treatment, chemical treatment, hydrothermal-baric, and thermal methods at elevated temperatures of 400–700°C [156, 187]. Bohra et al. used RHA alongside aluminium foil as precursors for NaA and NaP zeolite synthesis in two different studies showing a greener approach in the synthesis of zeolites [188]. Most researchers have focused on RHA as an agro-waste source of silica as seen in works of Mallapur et al. [189]; Bohra et al. [190]; Alaba et al. [191]; and Min et al. [156]; among others.

Sugarcane bagasse fly ash (BFA) has also been utilized as a low-cost precursor for zeolite synthesis. BFA is a rich source of alumina, and silica minerals needed to achieve high CEC zeolitic materials. Oliveira et al. [192] synthesized calcined sugarcane BFA and zeolite NaA using the hydrothermal synthesis method for application in the removal of copper ions from wastewater.

Several other agrochemicals that have been utilized in the synthesis of zeolites are summarized in Table 3.

5.1.4. Clays in Zeolite Synthesis. Kaolin-based zeolites have been synthesized in an effort to achieve affordable zeolitic products. Kaolin clay mineral, illustrated in Figure 5, consists of silica tetrahedral joined to alumina octahedral in the ratio of 1 : 1 through shared oxygen atoms. Kaolin-based zeolites will often have Ca, Mg, Fe, Ti, etc., contaminants originating from natural kaolin, which may affect the properties of the final product [199]. Kaolin is often calcined to temperatures ranging from 550 to 950°C to achieve reactive metakaolin for utilization in the synthesis [163].

Fortunately, kaolinite is not the only type of clay mineral utilized in the synthesis of zeolites. Ltaief et al. [200] synthesized faujasite zeolite from Tunisian illitic clay exhibiting hierarchical porosity. Researchers used the molten salt synthesis method using NaOH in muffled furnace. Zeolite crystallization occurred at 60°C in 24 hours. The resultant material was used in adsorption of various heavy metal ions, and removal capacities were reported to be 126 mg/g (Cu^{2+}), 125 mg/g (Co^{2+}), and 98 mg/g (Cr^{3+}). These findings were higher than the commercial faujasite adsorption capacities for the respective metal ions as 120 mg/g, 118 mg/g, and 91 mg/g. This study illustrated a low-cost zeolite material with better efficiency in heavy metal adsorption.

A study by Medina-Rodríguez et al. [201] used Ecuadorian clay to synthesize zeolite X through alkaline fusion and hydrothermal treatment. Sodium aluminate and NaOH were used to fine-tune the properties of the zeolite at synthesis. The resulting zeolite X was reported to have a specific surface area of 376 m^2/g, which was 30 times higher compared to clay (12 m^2/g). The zeolite was used in the removal of Pb^{2+} and achieved an adsorption capacity of 24 mg/g, much higher compared to that of clay (13 mg/g).

Moneim and Ahmed [202] synthesized low silica NaX-Faujasite zeolite from different types of Egyptian clays (kaolinite, smectite-kaolinite, and smectite-rich clays) using a combination of hydrothermal synthesis and alkali fusion methods. Crystallization conditions were 100° Cand 48 hours for smectite-kaolinite clay and 72–96 hours for the kaolinite and smectite-rich clays. The authors reported that the smectite-kaolinite clay had better crystallization rates compared to the rest. Zeolite was applied to remove Cr^{3+}, Ni^{2+}, and Mn^{2+}, and the percentage removal was reported to be 100%, 80%, and 75%, respectively.

Gaidoumi et al. [203] reported the successful synthesis of zeolite HS by using natural pyrophyllite clay as raw material. The clay was treated with alkaline, and the resultant material is characterized by X-ray fluorescence and Fourier transform infrared, among other techniques. The authors reported that the resultant zeolite was nearly pure. Aghaei et al. [204] alkali-fused the same clay to synthesize zeolite Y and reported improved acidity and textural properties compared to commercial zeolite Y. Foroughi et al. [205] combined illite, pyrophyllite and kaolinite clays to synthesize zeolite A through fusion technique and reported mesoporous zeolite structure which contained a surface area of about 59.6 m^2/g and an average pore size of 8 nm.

Joseph et al. [206] synthesized multiple zeolites using vermiculate-kaolinite clay through the alkaline fusion method. The clay mixture achieved the synthesis of faujasite-based zeolite without pretreatment. On thermal activation, the clay was able to produce gismondine zeolite GIS-NaP1. When it was pretreated by acid leaching, the clay produced mixed-phase quartz and Na-P1 zeolites.

6. Characterization of Zeolites

6.1. Scanning Electron Microscopy (SEM) and Energy Dispersive Spectroscopy (EDS). Scanning electron microscopy technique is used to analyze surface morphology and topology of zeolitic materials by focusing a beam of low energy electrons on the sample. Interactions of the beam and the material led to emission of electrons and photons that are detected and take part in the formation of SEM image [207]. EDS is useful in the chemical analysis of materials. It is typically equipped with SEM and makes use of X-rays to identify the chemicals present in a sample [208]. Studies in which SEM analysis has been utilized in zeolite characterization are summarized in Table 4.

6.2. Brunauer–Emmett–Teller (BET) Analysis. BET analysis is an important analytical technique in the characterization of zeolites as it gives data regarding adsorption mechanism of the material. By using probing gases, the BET theory seeks to provide information on the specific surface area of multilayer pore systems to understand the adsorptive characteristics of a material [213]. Nitrogen is a common probe gas, although others can be used, as long as they do not chemically react with the surface of the material analyzed [214]. Previous studies whereby BET analysis has been utilized in zeolite characterization are summarized in Table 5.

Table 3: Other wastes in the synthesis of zeolites.

Waste material	Zeolite formed	Synthesis method	Product yield (%)	Reference
Coal combustion fly ash	Analcime, faujasite, gismondine	Hydrothermal treatment	70–80	[193]
Municipal solid waste fly ash and waste bottle powder	Perlialite, zeolite A and Y	Fusion hydrothermal	—	[194]
Volcanic ash	Na-mordenite	Hydrothermal synthesis	80	[195]
Municipal solid waste	Clinoptilolite	Hydrothermal conversion	69	[196]
Blenod fly ash	Na-X faujasite	Hydrothermal conversion	20–25	[197]
Paper sludge ash	Na-PI zeolite	Hydrothermal synthesis	—	[198]

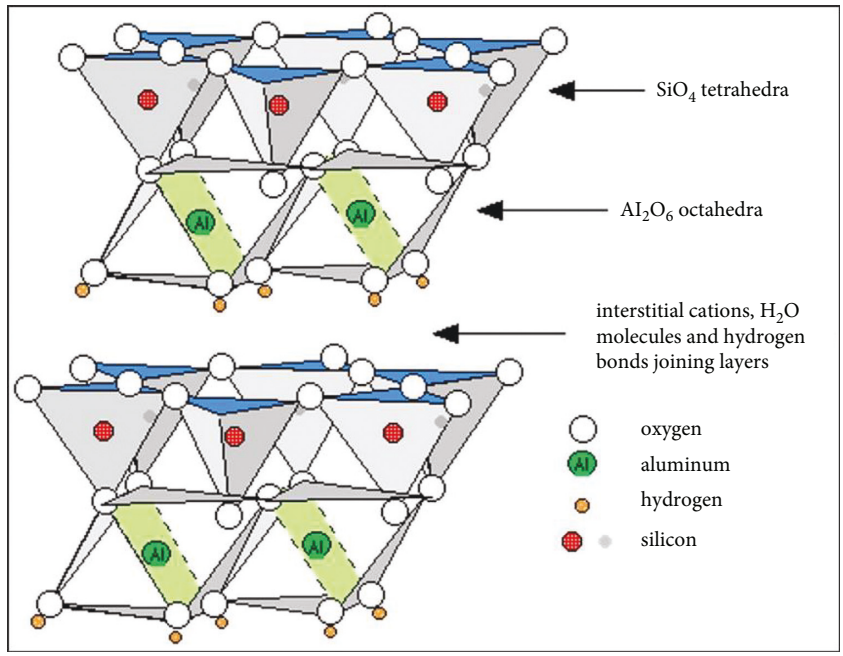

Figure 5: Structure of kaolinite (adapted from [199]).

6.3. X-Ray Diffraction (XRD). XRD technique is extensively used in the analysis of crystalline compounds, more so in the characterization of zeolite compounds. Data resulting from XRD gives insight into the texture, phase, grain size in average, crystal defects, and strain, among others. This is usually possible through the interference of X-ray beams by lattice planes available in a sample [219]. Crystalline samples are identifiable by referencing a standard database for XRD patterns [220]. Previous studies in which XRD analysis has been used in zeolite characterization are summarized in Table 6.

6.4. Fourier Transform Infrared (FTIR) Spectroscopy. FTIR spectroscopy identifies materials by analyzing the vibrations depicted by chemical bonds within a material's molecular structure [222]. Different chemical structures absorb infrared radiation at different wavelengths giving rise to a peak and therefore identification [223]. The chemical environment is important for understanding the functional groups in the material [224]. FTIR analysis is necessary to understand how effective the zeolite is in the removal of heavy metals. FTIR spectroscopy is able to analyze mid-IR region between 5000 and 400 cm^{-1} and near-IR region between 10,000 and 4000 cm^{-1} [225]. Several studies have utilized FTIR analysis in zeolite characterization with different chemical groups as summarized in Table 7.

6.5. Thermogravimetric Analysis (TGA). TGA's sole purpose is identification of a material's thermal stability and percentage of volatile compounds in its structural composition, usually through monitoring the change in the material's weight as heating occurs in a predetermined rate [230]. In zeolite studies, TGA is useful in analysis of a zeolite's amount of pore water. Ezzeddine et al. [231], in a study to utilize zeolite NaX in heavy metal adsorption, used the TGA technique to investigate the water content and absence of the

Table 4: Summary of SEM analysis of zeolites.

Zeolite	Raw material	Synthesis method	Observations	References
FAU-type zeolite	Coal fly ash	Alkaline fusion + hydrothermal treatment	High water content and longer ageing time resulted to better defined zeolite	[209]
K-ZFA Zeolite	Coal fly ash	Hydrothermal alkaline treatment	The material showed low degree agglomeration	[210]
Zeolite A	Natural Sudanese montmorillonite clay	Alkali fusion	Uniform particle morphology. Small particle size in the range 3.72–8.61 μm	[211]
Magnetic NaA Zeolite	Natural kaolin	Hydrothermal treatment	Crystals with the same cubic morphology and almost same diameter (2 μm)	[71]
Cancrinite	Natural Tunisian clay	High pressure hydrothermal treatment	Symmetric hexagonal needlelike shapes	[212]

organic template used during synthesis. Authors reported about 26% water loss between 25 and 900°C. Similarly, in a study conducted by Oliveira et al. [192], weight loss was initially observed up to 200°C and attributed to water loss. Additional weight loss was observed between 350 and 580°C and attributed to elimination of carbon and other organic residues. Other works utilizing TGA analysis have been summarized in Table 8.

7. Adsorption Studies

7.1. Adsorption Isotherm Models. Adsorption isotherms show the relationship between the quantity of the solute that has been adsorbed and the solute's concentration in the liquid phase [131]. Understanding this relationship is important to examine the performance of zeolites in heavy metal adsorption. Different models have been proposed and used over the years to understand this behavior. Some of these methods are discussed.

The Langmuir adsorption isotherm is modeled with the assumption that the maximum adsorption corresponds to saturation of the monolayer adsorbate surface. This implies that all sites of adsorption are identical, and the adsorption energy is constant. The Langmuir isotherm is therefore described by the linear equation [234].

$$\frac{C_e}{q_e} = \frac{1}{Q_0 b} + \frac{C_0}{Q_0}, \tag{2}$$

where q_e represents the quantity of adsorbed metal ion in (mg/g), C_e as the residual ion concentration at equilibrium, and Q_0 and b, Langmuir's constants for sorption capacity and energy, respectively. b should vary with temperature since it is a representation of the enthalpy of adsorption [131].

The Freundlich isotherm is structured with the assumption that surface adsorption energies are irregular, implying heterogenous nature of adsorption [235]. This model can therefore be described by

$$q_e = K_f C_e^{1/n}, \tag{3}$$

where q_e represents solute's adsorption per unit mass of the adsorbent at equilibrium in mg/g, C_e is residual ion concentration in the liquid phase at equilibrium, and K_f is the Freundlich constants determined by the conditions of the experiment [131]. The equation can be rewritten in linear form as

$$\log Q_e = \log K_f + \frac{1}{n}\log C_e. \tag{4}$$

When the value of $1/n$ falls below 1, this is an indication that the adsorption is heterogenous. Values near or equal to 1 indicate a material exhibiting somewhat homogeneous binding sites in relation to its porosity [236]. The utilization of these models in the adsorption analysis of some zeolites has been summarized in Table 9.

Lesser common isotherm models in zeolite metal ion adsorption studies such as Dubinin–Radushkevich (D-R) and Temkin isotherm models exist. D-R isotherm assumes filling of pores in the adsorption process in a multilayer character, involving van der Waals forces [234]. This model is often applied in the expression of Gaussian energy of adsorption distribution upon heterogenous adsorptive surface [243]. It is, however, unrealistic at low pressures since under such conditions, it does not follow Henry's laws. It is therefore most suitable for intermediate adsorbate concentrations [244]. Its best application in metal ion adsorption is differentiation between physical or chemical adsorption mechanism of adsorbates. D-R is described as follows [30]:

$$\ln Q_e = \ln Q_m - \beta \mathrm{E}^2, \tag{5}$$

$$E = \mathrm{RT}\ln\left(1 + \frac{1}{C_e}\right), \tag{6}$$

$$E = \frac{1}{\sqrt{2B}}, \tag{7}$$

where e is Polanyi's constant, β is D-R constant, R is the gas constant, T is the absolute temperature in Kelvin, and E is the mean adsorption energy.

Temkin adsorption isotherm considers the indirect effect multiple adsorbents might have on each other (adsorbent/adsorbent interaction), upon the process of adsorption. This isotherm is governed by the assumption that the adsorption heat (ΔH_{ab}) of all interacting species decreases with increase

Table 5: Summary of BET analysis of zeolites.

Zeolite	Synthesis method	Observations	References
Zeolite A	Hydrothermal synthesis	An increase in pore size was observed compared to fly ash	[215]
Zeolite NaA	Hydrothermal synthesis	Mean surface area found to be 46.6 m^2/g	[216]
Clinoptililite	Ultrasonic-assisted preconcentration	Material identified as nanoporous	[217]
Zeolite X	Hydrothermal synthesis	Pore volume observed to be 0.22 cm^3/g and 260 m^2/g BET surface area	[218]

Table 6: Summary of the XRD analysis of zeolites.

Zeolite	Synthesis method	Observations	References
Clinoptililite	Ultrasonic-assisted preconcentration	Pore closure reduces peak intensity on modification	[217]
Zeolite X	Hydrothermal synthesis	Rietveld calculations shown 75% zeolite content	[218]
Zeolite A	Hydrothermal synthesis	Rietveld calculations shown 70% zeolite content	[218]
Zeolite ZSM-5	Hydrothermal treatment	The increase in nucleation period favored the formation of zeolite crystal	[221]

Table 7: Summary of FTIR analysis of zeolites.

Zeolite	Synthesis method	Observations		References
		Wavelength (cm^{-1})	Group or Reason	
Needle-like nanozeolite	Hydrothermal synthesis	3400 1640	O-H stretch Zeolitic water influence	[171]
Hydroxy-sodalite/ cancrinite	Hydrothermal alkali activation	1400–400 (disappear) 4000–3500 (disappear)	Si-O, Si-O-Al vibrations -OH vibrations	[226]
ZIF-8	Solvothermal synthesis	421 692 755 1100–1310 1577	Zn-N Co-N CN C = N C = C	[227]
NaP zeolite	One step hydrothermal synthesis	1008 and 735 690 600 435	Si-O or Al-O assymetric stretching Symmetric stretching of Si-O or Al-O symmetric stretching Double ring in NaP Si-O or Al-O bending	[228]
Phillipsite zeolite	Hydrothermal synthesis	439.19 607.47 693.06 1026.96 1638.92 3435.81	O-Si-O Si-C Mn-O Assymetric Si-O-Al H-O-H or C = C Si-OH	[229]

in surface coverage. This model is therefore only valid for intermediate adsorbate concentrations [234]. It is given by

$$Q_e = \frac{\mathrm{RT}}{b} \ln K_t + \frac{\mathrm{RT}}{b} \ln C_e, \tag{8}$$

where b (j/mol) and Kt (L/g) represent Temkin constants, calculated from the slope and intercept of the plot of Q_e versus ln Ce, respectively [244].

Most zeolite-based adsorption isotherms follow Langmuir model according to Table 9. This translates that the metal ion adsorption is a monolayer adsorption, according to the high R^2 values. The few that follow Freundlich isotherm model such as Cu and Cd adsorption by fly-ash synthesized zeolite X [239] imply a multilayer adsorption criterion.

7.2. Adsorption Kinetics. The pseudo-first-order (PFO) model, first described by Lagergren, is described by the linearized equation [245].

$$\ln (q_e - q_t) = \ln q_e - k_1 t, \tag{9}$$

where q_t is adsorbed adsorbate at time t in mg/g, q_e is adsorption at equilibrium in mg/g, and k_1 is rate constant per minute. To determine the value of k_1, a plot of $\ln (q_e - q_t)$ against t is drawn.

Table 8: Summary of the TGA analysis of zeolites.

Zeolite	Observations (%)			References
	Percentage loss (%)	Temperature	Interpretation	
Faujasite-type zeolite	1.43	110°C	Surface water loss	[232]
	3.73	200°C	Internal water desorption	
Nanoclinoptilolite	2	—	Surfactant adsorption into sample	[233]
Nax-zeolite	26	200°C	Physisorbed water molecules	[231]
Needle-like nanozeolite	14	100–175°	Zeolitic water	[171]

Table 9: Summary of adsorption isotherms on synthetic zeolites derived from agro-wastes and clay.

Zeolite	Raw materials	Metal ion	Langmuir model		Freundlich model		References
			q_e (mg/g)	R^2	K_f (mg/g)	R^2	
Zeolite X	Ecuadorian clay	Pb^{2+}	131.6	0.994	31.33	0.977	[201]
Zeolite NaA	Bagasse ash	Ca^{2+}	555.54	0.987	2.24	0.9986	[237]
ZSM-5	Chlorite clay	As^{5+}	411.41	0.9907	74.63	0.9043	[238]
		Pb^{2+}	546.25	0.9921	653.15	0.7300	
Zeolite X	Coal fly ash	Ni^{2+}	1.136	0.8348	0.22	0.5669	[239]
		Cd^{2+}	1.795	0.5600	0.23	0.8077	
		Cu^{2+}	3.209	0.9890	1.65	0.9954	
NaA zeolite	Oil shale ash	Cu^{2+}	156.74	0.998	87.07	0.979	[240]
		Ni^{2+}	53.02	0.996	27.42	0.984	
		Pb^{2+}	224.72	0.978	91.34	0.938	
		Cd^{2+}	118.34	0.993	62.91	0.768	
Linde F (K) zeolite	Fly ash	Cu^{2+}	59.9	0.9763	66.8	0.0691	[241]
		Cd^{2+}	118.6	0.9567	1.42	0.7002	
		Pb^{2+}	476.1	0.9864	248.5	0.8149	
Zeolite 4A	Recycled coal fly ash	Co^{2+}	13.72	0.998	6.66	0.959	[242]
		Cr^{3+}	41.61	0.998	28.47	0.850	
		Cu^{2+}	50.45	1.000	37.11	0.974	
		Zn^{2+}	8.96	0.997	6.27	0.834	
		Ni^{2+}	30.80	0.945	18.47	0.623	

The pseudo-second-order (PSO) model has the assumption that solute adsorption is proportional to active sites on the adsorbent. Therefore, the rate of reaction is dependent on solute amount on the surface of the adsorbent. The PSO equation is illustrated as follows:

$$\frac{t}{q_t} = \frac{1}{k_2 q_e^2} + \frac{t}{q_e}, \tag{10}$$

where k_2 is a PSO rate constant. Applications of these modes in adsorption studies for synthetic zeolites are summarized in Table 10.

Other lesser common kinetic models in the adsorptive studies of metal ions in zeolite materials include intraparticle diffusion and Elovich models. Intraparticle diffusion model is common for a process whereby there is an increase in the rate of adsorption with increase in temperature, common in chemical adsorption processes. This model is illustrated by

$$Q = K_p \sqrt{t} + C, \tag{11}$$

where K_p and C are intraparticle diffusion constants. A plot of Q versus $\sqrt{t}$ is used in estimation of the diffusion process. If the plot is observed as a straight line, the adsorption is predicted to involve at least two stages of intraparticle diffusion. This model can also be used to predict the thickness of the interface between the adsorbate and adsorbent [30].

Elovich model, given in equations(12) and (13) [30], is generally applicable to heterogenous-based chemisorption process, and the rate of desorption is negligible. This model is often used in the prediction of surface diffusion and mass and the activation or deactivation energy of an adsorbent [251].

$$Q = \frac{1}{\beta}\ln\left(t + \frac{1}{\alpha\beta}\right) - \frac{1}{\beta}\ln(\alpha\beta). \tag{12}$$

If $t \gg 1/\alpha\beta$, then

$$Q = \frac{1}{\beta}\ln(\alpha\beta) + \frac{1}{\beta}\ln(t), \tag{13}$$

where β and α are Elovich constants estimated from the plot of Q versus ln (t).

7.3. Thermodynamics of Adsorption. An adsorption process is largely affected by the temperature of the reaction medium. Thermodynamic studies are used focused on studying the behavior of the adsorbent efficiency at different temperatures by analyzing Gibb's free energy, enthalpy, and entropy of the reaction. The formulae used for this analysis are [53]

Table 10: Summary of adsorption kinetics on synthetic zeolites.

Zeolite	Raw material	Metal ion	Pseudo-first order		Pseudo-second order		References
			q_e	R^2	q_e	R^2	
ZSM-11	Rice husk ash	Pb^{2+}	1.4754	0.8503	3.3367	0.6912	[246]
		Zn^{2+}	1.0859	0.9929	1.7050	0.9662	
Zeolite A	Rice hush and aluminium cans	Co^{2+}	65.28	0.9418	89.30	0.9529	[247]
		Cu^{2+}	65.23	0.9286	94.57	0.9565	
Faujasite		Co^{2+}	62.14	0.9518	83.06	0.9566	
		Cu^{2+}	67.16	0.9268	92.03	0.9451	
Merlinoite	Sugarcane bagasse ash and kaolin	Pb^{2+}	127.17	0.8430	250.0	0.9999	[248]
Linde F (K)	Fly ash	Cu^{2+}	3.2319	0.8271	21.598	0.9983	[249]
		Cd^{2+}	1.6945	0.9867	22.221	0.9998	
		Pb^{2+}	2.098	0.9337	49.751	0.9982	
		Ni^{2+}	1.9823	0.8561	12.821	0.9998	
Zeolite NaP	Aluminium and fumed silica wastes	Ni^{2+}	45.15	0.8841	45.15	0.9846	[250]
		Cu^{2+}	66.75	0.8858	66.75	0.9934	

Table 11: Summary of adsorption thermodynamics on synthetic zeolites.

Zeolite	Raw material	Metal ion	T (K)	ΔG^0 (kJ/mol)	ΔH^0 (kJ/mol)	ΔS^0 (kJ/mol)	References
Zeolite Na-P1	Coal fly ash	Cr^{3+}	298	164	23	−85	[252]
			308	165			
			318	166			
Zeolite X	Raw municipal bio-slag	Cs^+	288	14.482	20.53	0.021	[253]
			298	14.272			
			308	14.062			
11Å-tobermorite	Coal fly ash	Cu^{2+}	298.15	4.368	−1.090	−9.047	[254]
			318.15	4.906			
			338.15	5.439			
		Pb^{2+}	298.15	4.342	−2.760	−5.277	
			318.15	4.923			
			338.15	5.683			
Zeolite Y	Fly ash	Cu^{2+}	301.15	−7.67	14.14	72.43	[255] bohr
			318.15	−8.90			
			338.15	−10.35			
		Ni^{2+}	301.15	−7.48	16.94	81.08	
			318.15	−8.86			
			338.15	−10.48			

$$K_d = \frac{C_A}{C_B}, \tag{14}$$

$$\Delta G^0 = -\mathrm{RT} \ln K_d, \tag{15}$$

$$\ln K_d = \frac{\Delta S^0}{R} - \frac{\Delta H^0}{RT}, \tag{16}$$

where K_d is the constant of thermodynamic equilibrium, R is gas constant, T is the absolute temperature, and C_A and C_B are the concentrations of the adsorbate on the adsorbent and residual concentration at equilibrium, respectively [53].

An endothermic adsorption is given by a positive enthalpy value. A negative Gibb's free energy value implies thermodynamically spontaneous and sustainable at diverse temperatures. A positive entropy value gives an insight that there is randomness at the liquid-solid interface in the adsorption [53]. Thermodynamic studies on various synthetic zeolites are summarized in Table 11.

From Table 11, it can be inferred that the majority of zeolites give a positive Gibb's free energy value. This implies that, for the most studies summarized, the adsorption of the heavy metals is not thermodynamically spontaneous and therefore not diverse over a large range of temperatures. Zeolite Y, however, synthesized by Liu et al. [255] differed and gave negative Gibbs free energy for both copper (II) and nickel (II) ions adsorption. This implies that the adsorption is feasible over a range of temperatures and therefore sustainable. Zeolites Na-P1 [252], X [253], and Y [256] give positive enthalpy values. This implies endothermic adsorption process (physisorption). The negative enthalpy of 11Å-tobermorite [254] zeolite implies an exothermic adsorption process, which implies a chemisorption process in

the metal ions adsorption. Zeolite X and Y give positive entropy values, while 11Å-tobermorite and Na-P1 give negative values for the metal adsorption processes. A positive entropy value implies increased randomness at the solid-liquid interface, and thus, high metal ion adsorption is expected in such systems.

8. Conclusions

Although several methods exist for removal of heavy metals from wastewaters, heavy metals in waters still pose a global health concern. We therefore conclude the following:

(1) Most low- and middle-income countries have low uptake of existing methods of heavy metal removal from waste waters such as ion exchange, reverse osmosis, and electrodialysis due to high costs of installation, operation, and maintenance.

(2) Low-cost zeolites are efficient heavy metal adsorbents and allow modification to simultaneously remove both organic and inorganic water contaminants.

(3) Utilization of agro-wastes in the synthesis of zeolites for the removal of heavy metals is biased towards rice husk ash and bagasse ash. Other kinds of agro-wastes have not been explored.

(4) Hydrothermal synthesis of zeolites remains to be the most dominant method of zeolite synthesis even though other greener methods exist.

(5) Clay minerals have seen tremendous utilization in the synthesis of zeolites due to high silica to alumina ratios. Kaolin is especially a favorite among researchers, due to the formation of metakaolin, which is highly reactive and rich in aluminosilicates.

9. Areas of Future Research

Based on the reviewed works herein, the authors recommend following potential areas of future research:

(1) Cost-benefit analysis of clay and agro-waste zeolite application in heavy metal removal from waste waters

(2) Mechanism of removal of heavy metals and other contaminants by zeolites from contaminated water

(3) Incorporation of zeolites into other structures to form composite materials for water decontamination

(4) Impact of interfering elements on the removal of heavy metals by zeolites

(5) Criteria for eligibility of an agro-waste material as a raw material for zeolite synthesis

(6) Influence of synthesis methods on the cost, structure, application, and reproducibility of zeolites

(7) Influence of raw material source, type, and environment on the structure of synthesized zeolite

(8) Acceptability, adoption, and utilization of green chemistry methods of synthesis of zeolites, in developing countries

(9) Optimization of thermodynamic models for the analysis of all processes in zeolite heavy metal adsorption

Data Availability

Data cited are included in the cited articles.

Conflicts of Interest

The authors declare no conflicts of interest in the publication of this article.

Acknowledgments

The authors of this work acknowledge every author of the works cited hereof and thank them for their contribution to the compilation of this review. The authors acknowledge Meru University of Science and Technology Library for providing access to scholarly repositories for articles cited in this work.

References

[1] J. A. Nathanson, "Watewater treatment," 2021, https://www.britannica.com/technology/wastewater-treatment.

[2] WWDR. UN, "Wastewater, the untapped resource," 2017, http://www.unesco.org/new/en/natural-sciences/environment/water/wwap/wwdr/2017-wastewater-the-untapped-resource/.

[3] WHO, "People globally do not have access to safe drinking water—UNICEF," 2021, https://www.who.int/news/item/18-06-2019-1-in-3-people-globally-do-not-have-access-to-safe-drinking-water-unicef-who.

[4] K. Maheshwari, M. Agrawal, and A. B. Gupta, *Dye Pollution in Water and Wastewater*, Springer, Berlin, Germany, 2021.

[5] S. M. Wabaidur, M. A. Khan, M. R. Siddiqui et al., "Oxygenated functionalities enriched MWCNTs decorated with silica coated spinel ferrite – a nanocomposite for potentially rapid and efficient de-colorization of aquatic environment," *Journal of Molecular Liquids*, vol. 317, p. 113916, 2020.

[6] E. R. Kenawy, A. A. Ghfar, S. M. Wabaidur et al., "Cetyltrimethylammonium bromide intercalated and branched polyhydroxystyrene functionalized montmorillonite clay to sequester cationic dyes," *Journal of Environmental Management*, vol. 219, pp. 285–293, 2018.

[7] UNEP, "A snapshot of the world' s water quality: towards a global assessment," 2016, https://uneplive.unep.org/media/docs/assessments/unep_wwqa_report_web.pdf.

[8] A. Székács, "Herbicide mode of action," *In R. Mesnage & J. G. Zaller (Eds.), Herbicides*, Elsevier, Amsterdam, Netherlands, pp. 41–86, 2021.

[9] I. Ali, O. M. L. Alharbi, Z. A. ALOthman, A. M. Al-Mohaimeed, and A. Alwarthan, "Modeling of fenuron pesticide adsorption on CNTs for mechanistic insight and removal in water," *Environmental Research*, vol. 170, pp. 389–397, 2019.

[10] R. Sharma, P. R. Agrawal, R. Kumar, G. Gupta, and Ittishree, "Current scenario of heavy metal contamination in water," *In A. Ahamad, S. I. Siddiqui, & P. Singh (Eds.) Contamination of Water*, 1st edn, Elsevier, Amsterdam, Netherlands, pp. 49–64, 2021.

[11] D. Mara, "What is domestic wastewater and why treat it?" in *Domestic Wastewater Treatment in Developing Countries*, pp. 18–24, Routledge, London, UK, 2013.

[12] T. S. Anirudhan and P. S. Suchithra, "Heavy metals uptake from aqueous solutions and industrial wastewaters by humic acid-immobilized polymer/bentonite composite: kinetics and equilibrium modeling," *Chemical Engineering Journal*, vol. 156, no. 1, pp. 146–156, 2010.

[13] J. D. Edwards, "Characterizing your wastewater," *Industrial Wastewater Treatment*, 1st edn, CRC Press, Boca Raton, FL, USA, pp. 9–31, 2020.

[14] T. M. Mungai and J. Wang, "Heavy metal pollution in suburban topsoil of nyeri, kapsabet, voi, ngong and juja towns, in Kenya," *SN Applied Sciences*, vol. 9, no. 9, pp. 960–1011, 2019.

[15] C. Ohm, "Treating water pollution. water pollution," 2018, https://www.water-pollution.org.uk/treating-water-pollution/.

[16] G. K. Kinuthia, V. Ngure, D. Beti, R. Lugalia, A. Wangila, and L. Kamau, "Levels of heavy metals in wastewater and soil samples from open drainage channels in Nairobi, Kenya: community health implication," *Scientific Reports*, vol. 10, no. 1, pp. 8434–8513, 2020.

[17] M. Jamshidian, B. Sadeghalvad, I. Ghasemi, H. Ebrahimi, and I. Rezaeian, "Fabrication of polyethersulfone/functionalized MWCNTs nanocomposite and investigation its efficiency as an adsorbent of Pb (II) ions," *Arabian Journal for Science and Engineering*, vol. 46, no. 7, pp. 6259–6273, 2020.

[18] A. Mittal, M. Naushad, G. Sharma, Z. A. Alothman, S. M. Wabaidur, and M. Alam, "Fabrication of MWCNTs/ThO2 nanocomposite and its adsorption behavior for the removal of Pb (II) metal from aqueous medium," *Desalination and Water Treatment*, vol. 57, no. 46, pp. 21863–21869, 2015.

[19] A. A. Alqadami, M. Naushad, Z. A. ALOthman, M. Alsuhybani, and M. Algamdi, "Excellent adsorptive performance of a new nanocomposite for removal of toxic Pb (II) from aqueous environment: adsorption mechanism and modeling analysis," *Journal of Hazardous Materials*, vol. 389, Article ID 121896, 2020.

[20] R. Guillossou, J. le Roux, R. Mailler et al., "Organic micropollutants in a large wastewater treatment plant: what are the benefits of an advanced treatment by activated carbon adsorption in comparison to conventional treatment?" *Chemosphere*, vol. 218, pp. 1050–1060, 2019.

[21] J. Carmody, "Water treatment in developing countries | office of sustainability - student blog," 2020, https://usfblogs.usfca.edu/sustainability/2020/04/17/water-treatment-in-developing-countries/.

[22] LennTech, "Heavy metals," 2017, https://www.lenntech.com/processes/heavy/heavy-metals/heavy-metals.htm.

[23] G. van de Walle, "Iron deficiency anemia symptoms," 2022, https://www.healthline.com/nutrition/iron-deficiency-signs-symptoms.

[24] S. Y. Morris and E. Klein, "Copper and nutrition: why It's good for you. nutrition," 2021, https://www.healthline.com/health/heavy-metal-good-for-you-copper.

[25] J. Kubala, "Zinc: benefits, deficiency, food sources and side effects. nutrition," 2018, https://www.healthline.com/nutrition/zinc.

[26] M. Jaishankar, T. Tseten, N. Anbalagan, B. B. Mathew, and K. N. Beeregowda, "Toxicity, mechanism and health effects of some heavy metals," *Interdisciplinary Toxicology*, vol. 7, no. 2, pp. 60–72, 2014.

[27] A. Puri and M. Kumar, "A review of permissible limits of drinking water," *Indian Journal of Occupational and Environmental Medicine*, vol. 16, no. 1, pp. 40–44, 2012.

[28] Z. Fu and S. Xi, "The effects of heavy metals on human metabolism," *Toxicology Mechanisms and Methods*, vol. 30, no. 3, pp. 167–176, 2020.

[29] G. Georgiou, "Effects of heavy metals on human health. health effects of heavy metals," 2022, https://www.detoxmetals.com/effects-of-heavy-metals-on-human-health/?v=518f4a738816.

[30] E. I. Ugwu, A. Othmani, and C. C. Nnaji, "A review on zeolites as cost-effective adsorbents for removal of heavy metals from aqueous environment," *International journal of Environmental Science and Technology*, vol. 19, no. 8, pp. 8061–8084, 2021.

[31] N. R. Jyothi, "Heavy metal sources and their effects on human health," 2020, https://www.intechopen.com/chapters/74650.

[32] K. G. Bhattacharyya and S. S. Gupta, "Adsorptive accumulation of Cd (II), Co (II), Cu (II), Pb (II) and Ni (II) ions from water onto Kaolinite: influence of acid activation," *Adsorption Science and Technology*, vol. 27, no. 1, pp. 47–68, 2009.

[33] C. Warwick, A. Guerreiro, and A. Soares, "Sensing and analysis of soluble phosphates in environmental samples: a review," *Biosensors and Bioelectronics*, vol. 41, no. 1, pp. 1–11, 2013.

[34] M. Naushad, G. Sharma, and Z. A. Alothman, "Photodegradation of toxic dye using Gum Arabic-crosslinked-poly (acrylamide)/Ni (OH)2/FeOOH nanocomposites hydrogel," *Journal of Cleaner Production*, vol. 241, Article ID 118263, 2019.

[35] G. Crini and E. Lichtfouse, "Advantages and disadvantages of techniques used for wastewater treatment," *Environmental Chemistry Letters*, vol. 17, no. 1, pp. 145–155, 2019.

[36] R. M. Abdullah, H. Ali, and M. Mohammed, "Characteristics of erbil wastewater," 2020, https://www.researchgate.net/profile/Hiwa-Ali-2/publication/342004577_characteristics_of_erbil_wastewater/links/5ede1c8892851cf13868fc48/characteristics-of-erbil-wastewater.pdf.

[37] V. Gautam, "Preliminary treatment of sewage: 4 appurtenances. waste management," 2016, https://www.engineeringenotes.com/waste-management/sewage/preliminary-treatment-of-sewage-4-appurtenances-waste-management/39922.

[38] D. Alving, R. Arnold, J. Hunsicker et al., "Sustainable greywater filtration on a residential scale," 2019, https://drum.lib.umd.edu/handle/1903/24766.

[39] H. Bridle, K. Jacobsson, and A. C. Schultz, "Sample Processing," *Waterborne Pathogens: Detection Methods and Applications*, pp. 67–114, 2013.

[40] A. Sonune and R. Ghate, "Developments in wastewater treatment methods," *Desalination*, vol. 167, pp. 55–63, 2004.

[41] M. Sautya, "Primary treatment process of sewage. civil engineering," 2018, https://civilnoteppt.com/primary-treatment-process-of-sewage/.

[42] J. P. Guyer, "Introduction to primary wastewater treatment," *CED Engineering*, vol. 12, 2011.

[43] R. E. Hall, "Secondary wastewater treatment apparatus. appropedia," 2009, https://www.appropedia.org/Secondary_wastewater_treatment.

[44] M. L. Davis and S. J. Masten, *Principles of Environmental Engineering and Science*, McGraw-Hill Companies, New York, NY, USA, 2004.
[45] E. Massi, "Anaerobic digestion," *Fuel Cells in the Waste-to-Energy Chain*, vol. 45, pp. 47–63, 2012.
[46] M. L. Sikosana, K. Sikhwivhilu, R. Moutloali, and D. M. Madyira, "Municipal wastewater treatment technologies: a review," *Procedia Manufacturing*, vol. 35, pp. 1018–1024, 2019.
[47] T. Frankel, "What is tertiary wastewater treatment, and how does it work? smart ideas for water," 2020, https://www.ssiaeration.com/what-is-tertiary-wastewater-treatment/.
[48] T. A. McDonald and H. Komulainen, "Carcinogenicity of the chlorination disinfection by-product MX," *Journal of Environmental Science and Health, Part C*, vol. 23, no. 2, pp. 163–214, 2005.
[49] CDC, "Disinfection by-products," 2016, https://www.cdc.gov/healthywater/global/household-water-treatment/chlorination-byproducts.html?CDC_AA_refVal=https%3A%2F%2Fwww.cdc.gov%2Fsafewater%2Fchlorination-byproducts.html.
[50] K. Ikehata and Y. Li, "Ozone-based processes," *Advanced Oxidation Processes for Waste Water Treatment*, pp. 115–134, 2018.
[51] J. Väänänen, *Microsieving in Municipal Wastewater Treatment: Chemically Enhanced Primary and Tertiary Treatment*, Department of Chemical Engineering, Lund University, Lund, Sweden, 2017.
[52] B. M. Wilén, M. Cimbritz, T. Pettersson, and A. Mattsson, "Large scale tertiary filtration – results and experiences from the discfilter plant at the Rya WWTP in Sweden," *Water Practice and Technology*, vol. 11, no. 3, pp. 547–555, 2016.
[53] R. Chakraborty, A. Asthana, A. K. Singh, B. Jain, and A. B. H. Susan, "Adsorption of heavy metal ions by various low-cost adsorbents: a review," *International Journal of Environmental Analytical Chemistry*, vol. 102, no. 2, pp. 342–379, 2022.
[54] C. Cobzaru and V. Inglezakis, "Ion exchange," *Progress in Filtration and Separation*, pp. 425–498, Academic Press, Cambridge, MA, USA, 2015.
[55] P. de Luca, I. Bernaudo, R. Elliani, A. Tagarelli, J. BNagy, and A. Macario, "Industrial waste treatment by ETS-10 ion exchanger material," *Materials*, vol. 11, p. 2316, 2018.
[56] V. Kumar and V Kumar, "Adsorption kinetics and isotherms for the removal of rhodamine B dye and Pb+ 2 ions from aqueous solutions by a hybrid ion-exchanger," *Arabian Journal of Chemistry*, vol. 12, no. 3, pp. 316–329, 2019.
[57] A. Ma, A. Abushaikha, S. J. Allen, and G. McKay, "Ion exchange homogeneous surface diffusion modelling by binary site resin for the removal of nickel ions from wastewater in fixed beds," *Chemical Engineering Journal*, vol. 358, pp. 1–10, 2019.
[58] H. Esmaeili and R. Foroutan, "Investigation into ion exchange and adsorption methods for removing heavy metals from aqueous solutions," *International Journal of Biology, Pharmacy and Allied Sciences*, vol. 4, no. 12, pp. 626–629, 2015.
[59] N. K. Soliman and A. F. Moustafa, "Industrial solid waste for heavy metals adsorption features and challenges; a review," *Journal of Materials Research and Technology*, vol. 9, no. 5, pp. 10235–10253, 2020.
[60] Z. F. Pan and L. An, "Removal of heavy metal from wastewater using ion exchange membranes," in *Applications of Ion Exchange Materials in the Environment*, 1st edn, Springer, Cham, Switzerlaand, pp. 25–46, 2019.
[61] C. F. Carolin, P. S. Kumar, A. Saravanan, G. J. Joshiba, and M. Naushad, "Efficient techniques for the removal of toxic heavy metals from aquatic environment: a review," *Journal of Environmental Chemical Engineering*, vol. 5, no. 3, pp. 2782–2799, 2017.
[62] D. Bonta, "Factors that impact reverse osmosis filter performance," 2019, https://www.wqpmag.com/factors-impact-reverse-osmosis-filter-performance.
[63] M. Sarai Atab, A. J. Smallbone, and A. P. Roskilly, "An operational and economic study of a reverse osmosis desalination system for potable water and land irrigation," *Desalination*, vol. 397, pp. 174–184, 2016.
[64] J. Hanford, "Zero Waste: A Look at the Future of Reverse Osmosis. Water Quality Products," 2003, https://www.wqpmag.com/zero-waste-look-future-reverse-osmosis.
[65] B. S. Thaçi and S. T. Gashi, "Reverse osmosis removal of heavy metals from wastewater effluents using biowaste materials pretreatment," *Polish Journal of Environmental Studies*, vol. 28, no. 1, pp. 337–341, 2018.
[66] A. Karunakaran, A. Chaturvedi, J. Ali, R. Singh, S. Agarwal, and M. C. Garg, "Response surface methodology-based modeling and optimization of chromium removal using spiral-wound reverse-osmosis membrane setup," *International journal of Environmental Science and Technology*, vol. 19, no. 7, pp. 5999–6010, 2021.
[67] A. R. Kavaiya and H. D. Raval, "Highly selective and antifouling reverse osmosis membrane by crosslinkers induced surface modification," *Environmental Technology*, vol. 43, 2021.
[68] A. A. Alsarayreh, M. A. Al-Obaidi, R. Patel, and I. M. Mujtaba, "Scope and limitations of modelling, simulation, and optimisation of a spiral wound reverse osmosis process-basedwater desalination," *Processes*, vol. 8, no. 5, p. 573, 2020.
[69] I. Shahonya, F. Nangolo, M. Erinosho, and E. Angula, "Scaling and fouling of reverse osmosis (RO) membrane: technical review," *Advances in Material Science and Engineering Lecture Notes in Mechanical Engineering*, Springer, Berlin, Germany, 2021.
[70] Vedantu, "Reverse Osmosis—Principle, Advantages, Disadvantages and Applications," 2018, https://www.vedantu.com/chemistry/reverse-osmosis.
[71] H. Liu, S. Peng, L. Shu, T. Chen, T. Bao, and R. L. Frost, "Magnetic zeolite NaA: synthesis, characterization based on metakaolin and its application for the removal of Cu2+, Pb2+," *Chemosphere*, vol. 91, no. 11, pp. 1539–1546, 2013.
[72] S. U. D. Khan, S. U. D. Khan, S. N. Danish, J. Orfi, U. A. Rana, and S. Haider, "Nuclear energy powered seawater desalination," *Renewable Energy Powered Desalination Handbook*, pp. 225–264, Butterworth-Heinemann, Oxford, UK, 2018.
[73] R. Singh, "Desalination and on-site energy for groundwater treatment in developing countries using fuel cells," *Emerging Membrane Technology for Sustainable Water Treatment*, pp. 135–162, Elsevier, Amsterdam, Netherlands, 2016.
[74] L. Karimi and A. Ghassemi, "How operational parameters and membrane characteristics affect the performance of electrodialysis reversal desalination systems: the state of the art," *Journal of Membrane Science and Research*, vol. 2, no. 3, pp. 111–117, 2016.
[75] D. Zarzo, "Beneficial uses and valorization of reverse osmosis brines," *Emerging Technologies for Sustainable Desalination*

Handbook, pp. 365–397, Butterworth-Heinemann, Oxford, UK, 2018.

[76] B. V. Salas, "Desalination: trends and technologies," in *Desalination, Trends and Technologies*, M. Schorr, Ed., Taylor & Francis, Oxford, UK, 9th edition, 2012.

[77] S.-C. Chua, M. H. Isa, and Y.-C. Ho, "Electrodialysis (ED) A review on the fundamental concept, advantages, limitations and future trend," *Platform: Journal of Science and Technology*, vol. 3, no. 2, pp. 14–22, 2020.

[78] M. A. Al-Ghouti and D. A. Da'ana, "Guidelines for the use and interpretation of adsorption isotherm models: a review," *Journal of Hazardous Materials*, vol. 393, Article ID 122383, 2020.

[79] A. A. Alqadami, M. A. Khan, M. R. Siddiqui, and Z. A. Alothman, "Development of citric anhydride anchored mesoporous MOF through post synthesis modification to sequester potentially toxic lead (II) from water," *Microporous and Mesoporous Materials*, vol. 261, pp. 198–206, 2018.

[80] M. J. Thyfault, "Removal of iron, zinc, and copper from waters impacted by acid mine drainage using natural zeolite," Open Access Theses & Dissertations, University of Texas, Austin, TX, USA, 2016.

[81] P. Pourhakkak, M. Taghizadeh, A. Taghizadeh, and M. Ghaedi, "Adsorbent," *Interface Science and Technology*, vol. 33, pp. 71–210, 2021.

[82] A. Gupta, V. Sharma, K. Sharma et al., "A review of adsorbents for heavy metal decontamination: growing approach to wastewater treatment," *Materials*, vol. 14, no. 16, p. 4702, 2021.

[83] Benoni, "What are the main types of adsorbents? adsorbent knowledge," 2018, https://www.benonitechs.com/post/what-are-the-main-types-of-adsorbents-how-about-their-typical-applications.

[84] G. Crini, E. Lichtfouse, L. D. Wilson, and N. Morin-Crini, "Conventional and non-conventional adsorbents for wastewater treatment," *Environmental Chemistry Letters*, vol. 17, no. 1, pp. 195–213, 2019.

[85] S. Dubey, D. Gusain, Y. Chandra Sharma, and F. Bux, "Adsorbents," *Batch Adsorption Process of Metals and Anions for Remediation of Contaminated Water*, CRC Press, Boca Raton, FL, USA, 2021.

[86] S. Azarfar, F. Noorbakhsh, M. Salmani, S. Ansari, R. Soleymani, and S. Sadighi, "Experimental study and characterization of activated alumina adsorbent," in *Proceedings of the Iran International Aluminum Conference (IIAC2016)*, pp. 2–7, Tehran, Iran, May, 2016.

[87] R. Prins, "On the structure of γ-Al2O3," *Journal of Catalysis*, vol. 392, pp. 336–346, 2020.

[88] T. A. Hamza, A. H. Sherif, and E. A. Abdalla, "A novel approach to reinforce provisional material using silica gel powder," *Stomatological Disease and Science*, vol. 1, no. 1, 2017.

[89] A. Larasati, G. D. Fowler, and N. J. D. Graham, "Chemical regeneration of granular activated carbon: preliminary evaluation of alternative regenerant solutions," *Environmental Sciences: Water Research & Technology*, vol. 6, no. 8, pp. 2043–2056, 2020.

[90] G. Sethia and A. Sayari, "Activated carbon with optimum pore size distribution for hydrogen storage," *Carbon*, vol. 99, pp. 289–294, 2016.

[91] P. Baile, E. Fernández, L. Vidal, and A. Canals, "Zeolites and zeolite-based materials in extraction and microextraction techniques," *Analyst*, vol. 144, no. 2, pp. 366–387, 2019.

[92] K. He, Y. Chen, Z. Tang, and Y. Hu, "Removal of heavy metal ions from aqueous solution by zeolite synthesized from fly ash," *Environmental Science and Pollution Research*, vol. 23, no. 3, pp. 2778–2788, 2015.

[93] M. Hong, L. Yu, Y. Wang et al., "Heavy metal adsorption with zeolites: the role of hierarchical pore architecture," *Chemical Engineering Journal*, vol. 359, pp. 363–372, 2019.

[94] P. J. Reeve and H. J. Fallowfield, "Natural and surfactant modified zeolites: a review of their applications for water remediation with a focus on surfactant desorption and toxicity towards microorganisms," *Journal of Environmental Management*, vol. 205, pp. 253–261, 2018.

[95] Z. Yuna, "Review of the natural, modified, and synthetic zeolites for heavy metals removal from wastewater," *Environmental Engineering Science*, vol. 33, no. 7, pp. 443–454, 2016.

[96] D. Gusain, F. Bux, and (Faizel), *Batch Adsorption Process of Metals and Anions for Remediation of Contaminated Water*, vol. 1, 1st edition, 2021.

[97] S. M. Yakout, "Effect of porosity and surface chemistry on the adsorption-desorption of uranium (VI) from aqueous solution and groundwater," *Journal of Radioanalytical and Nuclear Chemistry*, vol. 308, no. 2, pp. 555–565, 2016.

[98] C. Tang, Y. Shu, R. Zhang et al., "Comparison of the removal and adsorption mechanisms of cadmium and lead from aqueous solution by activated carbons prepared from Typha angustifolia and Salix matsudana," *RSC Advances*, vol. 7, no. 26, pp. 16092–16103, 2017.

[99] K. F. S. Richard, A. E. B. Torres, D. A. S. Maia et al., "Assessing mass transfer rates in porous adsorbents using gas adsorption microcalorimetry," *Chemical Engineering Science*, vol. 229, Article ID 115983, 2021.

[100] D. Ouyang, Y. Zhuo, L. Hu, Q. Zeng, Y. Hu, and Z. He, "Research on the adsorption behavior of heavy metal ions by porous material prepared with silicate tailings," *Minerals*, vol. 9, no. 5, p. 291, 2019.

[101] H. S. Ibrahim, T. S. Jamil, and E. Z. Hegazy, "Application of zeolite prepared from Egyptian kaolin for the removal of heavy metals: II. Isotherm models," *Journal of Hazardous Materials*, vol. 182, no. 1–3, pp. 842–847, 2010.

[102] M. F. Shehata, S. El-Shafey, N. S. Ammar, and A. M. El-Shamy, "Reduction of Cu+2 and Ni+2 ions from wastewater using mesoporous adsorbent: Effect of treated wastewater on corrosion behavior of steel pipelines," *Egyptian Journal of Chemistry*, vol. 62, no. 9, pp. 1587–1602, 2019.

[103] G. Li, C. Foo, X. Yi et al., "Induced active sites by adsorbate in zeotype materials," *Journal of the American Chemical Society*, vol. 143, no. 23, pp. 8761–8771, 2021.

[104] H. N. Tran, P. van Viet, and H. P. Chao, "Surfactant modified zeolite as amphiphilic and dual-electronic adsorbent for removal of cationic and oxyanionic metal ions and organic compounds," *Ecotoxicology and Environmental Safety*, vol. 147, pp. 55–63, 2018.

[105] Q. Qiu, X. Jiang, G. Lv et al., "Adsorption of heavy metal ions using zeolite materials of municipal solid waste incineration fly ash modified by microwave-assisted hydrothermal treatment," *Powder Technology*, vol. 335, pp. 156–163, 2018.

[106] M. Kragović, M. Stojmenović, J. Petrović et al., "Influence of alginate encapsulation on point of zero charge (pHpzc) and thermodynamic properties of the natural and Fe (III) - modified zeolite," *Procedia Manufacturing*, vol. 32, pp. 286–293, 2019.

[107] M. Qiu and C. He, "Efficient removal of heavy metal ions by forward osmosis membrane with a polydopamine modified

zeolitic imidazolate framework incorporated selective layer," *Journal of Hazardous Materials*, vol. 367, pp. 339–347, 2019.

[108] K. O. Sulaiman, M. Sajid, and K. Alhooshani, "Application of porous membrane bag enclosed alkaline treated Y-Zeolite for removal of heavy metal ions from water," *Microchemical Journal*, vol. 152, Article ID 104289, 2020.

[109] A. A. M. Daifullah, B. S. Girgis, and H. M. H. Gad, "A study of the factors affecting the removal of humic acid by activated carbon prepared from biomass material," *Colloids and Surfaces A: Physicochemical and Engineering Aspects*, vol. 235, no. 1–3, pp. 1–10, 2004.

[110] A. C. Lua, "A detailed study of pyrolysis conditions on the production of steam-activated carbon derived from oil-palm shell and its application in phenol adsorption," *Biomass Conversion and Biorefinery*, vol. 10, no. 2, pp. 523–533, 2019.

[111] B. R. Müller, "Effect of particle size and surface area on the adsorption of albumin-bonded bilirubin on activated carbon," *Carbon*, vol. 48, no. 12, pp. 3607–3615, 2010.

[112] R. Soni, S. Bhardwaj, and D. P. Shukla, "Various water-treatment technologies for inorganic contaminants: current status and future aspects," *In P. Devi, P. Singh, & S. K. Kansal (Eds.) Inorganic Pollutants in Water*, 1st edn, Elsevier, Amsterdam, Netherlands, pp. 273–295, 2020.

[113] A. Chavoshani, M. Hashemi, M. M. Amin, and S. C. Ameta, "Introduction," *Micropollutants and Challenges: Emerging in the Aquatic Environments and Treatment Processes*, Elsevier, Amsterdam, Netherlands, 2020.

[114] V. Nejadshafiee and M. R. Islami, "Adsorption capacity of heavy metal ions using sultone-modified magnetic activated carbon as a bio-adsorbent," *Materials Science and Engineering: C*, vol. 101, pp. 42–52, 2019.

[115] G. Z. Kyzas, G. Bomis, R. I. Kosheleva et al., "Nanobubbles effect on heavy metal ions adsorption by activated carbon," *Chemical Engineering Journal*, vol. 356, pp. 91–97, 2019.

[116] M. Abbasi, "Synthesis and characterization of magnetic nanocomposite of chitosan/SiO2/carbon nanotubes and its application for dyes removal," *Journal of Cleaner Production*, vol. 145, pp. 105–113, 2017.

[117] J. Xu, Z. Cao, Y. Zhang et al., "A review of functionalized carbon nanotubes and graphene for heavy metal adsorption from water: preparation, application, and mechanism," *Chemosphere*, vol. 195, pp. 351–364, 2018.

[118] S. S. Fiyadh, M. A. AlSaadi, W. Z. Jaafar et al., "Review on heavy metal adsorption processes by carbon nanotubes," *Journal of Cleaner Production*, vol. 230, pp. 783–793, 2019.

[119] C. Rodríguez and E. Leiva, "Enhanced heavy metal removal from acid mine drainage wastewater using double-oxidized multiwalled carbon nanotubes," *Molecules 2020*, vol. 25, no. 1, p. 111, 2019.

[120] T. C. Egbosiuba and A. S. Abdulkareem, "Highly efficient as-synthesized and oxidized multi-walled carbon nanotubes for copper (II) and zinc (II) ion adsorption in a batch and fixed-bed process," *Journal of Materials Research and Technology*, vol. 15, pp. 2848–2872, 2021.

[121] M. Solic, S. Maletic, M. K. Isakovski et al., "Removing low levels of Cd (II) and Pb (II) by adsorption on two types of oxidized multiwalled carbon nanotubes," *Journal of Environmental Chemical Engineering*, vol. 9, no. 4, Article ID 105402, 2021.

[122] M. Šolic, S. Maletic, M. Kragulj Isakovski et al., "Comparing the adsorption performance of multiwalled carbon nanotubes oxidized by varying degrees for removal of low levels of copper, nickel and chromium (VI) from aqueous solutions," *Water (Switzerland)*, vol. 12, no. 3, pp. 723–818, 2020.

[123] W. Zhan, L. Gao, X. Fu, S. H. Siyal, G. Sui, and X. Yang, "Green synthesis of amino-functionalized carbon nanotube-graphene hybrid aerogels for high performance heavy metal ions removal," *Applied Surface Science*, vol. 467, pp. 1122–1133, 2019.

[124] S. Deng, X. Liu, J. Liao, H. Lin, and F. Liu, "PEI modified multiwalled carbon nanotube as a novel additive in PAN nanofiber membrane for enhanced removal of heavy metal ions," *Chemical Engineering Journal*, vol. 375, 2019.

[125] I. K. Kinoti, E. M. Karanja, E. W. Nthiga, C. M. M'thiruaine, and J. M. Marangu, "Review of clay-based nanocomposites as adsorbents for the removal of heavy metals," *Journal of Chemistry*, vol. 2022, Article ID 7504626, 25 pages, 2022.

[126] W. S. Wise, "Minerals zeolites," in *Reference Module in Earth Systems and Environmental Sciences*Elsevier, Amsterdam, Netherlands, 2013.

[127] S. Golbad, "Synthesis and characterization of microporous and mesoporous zeolites from flyash for heavy metal removal from wastewater," University of Wisconsin-Milwaukee, Milwaukee, WI, USA, Master of Science, 2016.

[128] F. R. Ribeiro, "Zeolites: science and technology," *Springer Science & Business Media*, vol. 80, 2012.

[129] S. Mitchell, A. B. Pinar, J. Kenvin, P. Crivelli, J. Kärger, and J. Pérez-Ramírez, "Structural analysis of hierarchically organized zeolites," *Nature Communications*, vol. 6, pp. 8633–8714, 2015.

[130] N. Koshy and D. N. Singh, "Fly ash zeolites for water treatment applications," *Journal of Environmental Chemical Engineering*, vol. 4, no. 2, pp. 1460–1472, 2016.

[131] A. M. Salih, "The purification of industrial wastewater to remove heavy metals and investigation into the use of zeolite as a remediation tool," in *Doctoral Dissertation*University of Wolverhampton, Wolverhampton, UK, 2018.

[132] Y. Wang, C. Wang, L. Wang, L. Wang, and F. S. Xiao, "Zeolite fixed metal nanoparticles: new perspective in catalysis," *Accounts of Chemical Research*, vol. 54, no. 11, pp. 2579–2590, 2021.

[133] S. Tajik, H. Beitollahi, F. G. Nejad et al., "Recent electrochemical applications of metal–organic framework-based materials," *Crystal Growth & Design*, vol. 20, no. 10, pp. 7034–7064, 2020.

[134] J. Behin, E. Ghadamnan, and H. Kazemian, "Recent advances in the science and technology of natural zeolites in Iran," *Clay Minerals*, vol. 54, no. 2, pp. 131–144, 2019.

[135] K. Margeta and A. Farkaš, "Introductory chapter: zeolites - from discovery to new applications on the global market," in *Zeolites - New Challenges*, pp. 1026–1056, Intechopen, London, UK, 2020.

[136] J. D. Grice, G. Raade, and M. A. Cooper, "Alflarsenite: structure and relationship to other Be-Si and zeolite framework structures," *The Canadian Mineralogist*, vol. 48, no. 2, pp. 255–266, 2010.

[137] A. Alberti, G. Vezzalini, and IUCr, "The crystal structure of amicite, a zeolite," *Acta Crystallographica Section B Structural Crystallography and Crystal Chemistry*, vol. 35, no. 12, pp. 2866–2869, 1979.

[138] A. Yu. Likhacheva, S. v. Rashchenko, and Yu. v. Seryotkin, "The deformation mechanism of a pressure-induced phase transition in dehydrated analcime," *Mineralogical Magazine*, vol. 76, no. 1, pp. 129–142, 2012.

[139] L. N. Warr, "Ima–cnmnc approved mineral symbols," *Mineralogical Magazine*, vol. 85, no. 3, pp. 291–330, 2021.

[140] D. G. Howard, R. W. Tschernich, J. v Smith, and G. L. Klein, "Boggsite, a new high-silica zeolite from goble, columbia

county, Oregon," *American Mineralogist*, vol. 75, no. 9–10, pp. 1200–1204, 1990.

[141] M. Akizuki, Y. Kudoh, and T. Kuribayashi, "Crystal structures of the {011}, {610}, and {010} growth sectors in brewsterite," *American Mineralogist*, vol. 81, no. 11–12, pp. 1501–1506, 1996.

[142] A. Augustyn, "Silicate mineral," 2020, https://www.britannica.com/science/silicate-mineral.

[143] C. J. Rhodes, "Properties and applications of zeolites," *Science Progress*, vol. 93, no. 3, pp. 223–284, 2010.

[144] S. M. Auerbach, K. A. Carrado, and P. K. Dutta, *Handbook of Zeolite Science and Technology*, CRC Press, Boca Raton, FL, USA, 2003.

[145] H. S. Sherry, "The ion-exchange properties of zeolites. I. Univalent ion exchange in synthetic faujasite," *Journal of Physical Chemistry*, vol. 70, no. 4, pp. 1158–1168, 2002.

[146] S. H. Lee, D. K. Lee, C. H. Shin et al., "Synthesis, characterization, and catalytic properties of zeolites IM-5 and NU-88," *Journal of Catalysis*, vol. 215, no. 1, pp. 151–170, 2003.

[147] L. H. Chen, M. H. Sun, Z. Wang, W. Yang, Z. Xie, and B. L. Su, "Hierarchically structured zeolites: from design to application," *Chemical Reviews*, vol. 120, no. 20, pp. 11194–11294, 2020.

[148] E. Kianfar, "Nanozeolites: synthesized, properties, applications," *Journal of Sol-Gel Science and Technology*, vol. 91, no. 2, pp. 415–429, 2019.

[149] J. Xu, Q. Wang, and F. Deng, "Metal active sites and their catalytic functions in zeolites: insights from solid-state NMR spectroscopy," *Accounts of Chemical Research*, vol. 52, no. 8, pp. 2179–2189, 2019.

[150] E. Cherian, G. Kalavathy, T. J. Joshi, M. G. Lydia Phoebe, and B. Gurunathan, "Importance of nanocatalyst and its role in biofuel production," *Biofuels and Bioenergy*, pp. 171–182, Elsevier, Amsterdam, Netherlands, 2022.

[151] S. Prodinger and M. A. Derewinski, "Synthetic zeolites and their characterization," *Nanoporous Materials for Molecule Separation and Conversion*, pp. 65–88, Elsevier, Amsterdam, Netherlands, 2020.

[152] A. Khaleque, M. M. Alam, M. Hoque et al., "Zeolite synthesis from low-cost materials and environmental applications: a review," *Environmental Advances*, vol. 2, Article ID 100019, 2020.

[153] M. Król, "Natural vs. Synthetic zeolites," *Crystals*, vol. 10, no. 7, p. 622, 2020.

[154] E. Sarti, T. Chenet, L. Pasti, A. Cavazzini, E. Rodeghero, and A. Martucci, "Effect of silica alumina ratio and thermal treatment of beta zeolites on the adsorption of toluene from aqueous solutions," *Minerals*, vol. 7, no. 2, p. 22, 2017.

[155] S. Shandong, "Factors affecting the synthesis of zeolite molecular sieves," 2021, https://www.sunhighrising.com/info/factors-affecting-the-synthesis-of-zeolite-60384086.html.

[156] H. S. Min, N. Ahmad Nizam, A. Osumanu Haruna Professor, and P. Adeniyi Alaba, *Zeolites: Synthesis, Characterisation & Practice*, P. Nagar, Ed., Ideal International E-Publication, Indore, India, 2017.

[157] I. Petrov and T. Michalev, "Synthesis of zeolite A: a review," *Proceedings—Chemical Technologies*, vol. 51, 2012.

[158] A. Feng, Y. Yu, L. Mi, Y. Cao, Y. Yu, and L. Song, "Synthesis and characterization of hierarchical Y zeolites using NH4HF2 as dealumination agent," *Microporous and Mesoporous Materials*, vol. 280, pp. 211–218, 2019.

[159] D. Georgiev, B. Bogdanov, K. Angelova, I. Markovska, and Y. Hristov, "Synthetic zeolites- structure, classification, current trends in zeolite synthesis review," 2009, https://www.researchgate.net/publication/322211658.

[160] Z. Zijun, G. Effeney, G. J. Millar, and M. Stephen, "Synthesis and cation exchange capacity of zeolite W from ultra-fine natural zeolite waste," *Environmental Technology & Innovation*, vol. 23, Article ID 101595, 2021.

[161] D. Georgiev, B. Bogdanov, I. Markovska, and Y. Hristov, "A study on the synthesis and structure of zeolite NaX," *Journal of Chemical Technology and Metallurgy*, vol. 48, no. 2, pp. 168–173, 2013.

[162] Y. Zhao, Z. Liu, W. Li et al., "Synthesis, characterization, and catalytic performance of high-silica Y zeolites with different crystallite size," *Microporous and Mesoporous Materials*, vol. 167, pp. 102–108, 2013.

[163] D. Georgiev, B. Bogdanov, Y. Hristov, and I. Markovska, "Synthesis of NaA zeolite from natural kaolinite," *Oxidation Communications*, vol. 34, no. 4, pp. 812–819, 2011.

[164] J. Han, X. Jin, C. Song et al., "Rapid synthesis and NH 3 -SCR activity of SSZ-13 zeolite via coal gangue," *Green Chemistry*, vol. 22, no. 1, pp. 219–229, 2020.

[165] S. Krachuamram, K. C. Chanapattharapol, and N. Kamonsutthipaijit, "Synthesis and characterization of NaX-type zeolites prepared by different silica and alumina sources and their CO2 adsorption properties," *Microporous and Mesoporous Materials*, vol. 310, Article ID 110632, 2021.

[166] F. García-Villén, E. Flores-Ruíz, C. Verdugo-Escamilla, and F. J. Huertas, "Hydrothermal synthesis of zeolites using sanitary ware waste as a raw material," *Applied Clay Science*, vol. 160, pp. 238–248, 2018.

[167] Y. Li, R. Zhao, Y. Pang, X. Qiu, and D. Yang, "Microwave-assisted synthesis of high carboxyl content of lignin for enhancing adsorption of lead," *Colloids and Surfaces A: Physicochemical and Engineering Aspects*, vol. 553, pp. 187–194, 2018.

[168] W. M. Xie, F. P. Zhou, X. L. Bi et al., "Accelerated crystallization of magnetic 4A-zeolite synthesized from red mud for application in removal of mixed heavy metal ions," *Journal of Hazardous Materials*, vol. 358, pp. 441–449, 2018.

[169] Z. Tauanov, D. Shah, V. Inglezakis, and P. K. Jamwal, "Hydrothermal synthesis of zeolite production from coal fly ash: a heuristic approach and its optimization for system identification of conversion," *Journal of Cleaner Production*, vol. 182, pp. 616–623, 2018a.

[170] Y. Kobayashi, F. Ogata, T. Nakamura, and N. Kawasaki, "Synthesis of novel zeolites produced from fly ash by hydrothermal treatment in alkaline solution and its evaluation as an adsorbent for heavy metal removal," *Journal of Environmental Chemical Engineering*, vol. 8, no. 2, Article ID 103687, 2020.

[171] H. Luo, W. W. Law, Y. Wu, W. Zhu, and E. H. Yang, "Hydrothermal synthesis of needle-like nanocrystalline zeolites from metakaolin and their applications for efficient removal of organic pollutants and heavy metals," *Microporous and Mesoporous Materials*, vol. 272, pp. 8–15, 2018.

[172] G. Yao, J. Lei, X. Zhang, Z. Sun, and S. Zheng, "One-step hydrothermal synthesis of zeolite X powder from natural low-grade diatomite," *Materials*, vol. 11, no. 6, p. 906, 2018.

[173] J. Che, X. Yao, J. Kong et al., "Molten-salt synthesis and spectral characteristics of perovskite KCa2Nb3O10:Sm3+ phosphors," *Journal of Luminescence*, vol. 244, Article ID 118665, 2022.

[174] M. Maharana and S. Sen, *Fly-Ash Derived Zeolite as a Versatile Novel Material in Civil Engineering: An Overview*, Springer, Berlin, Germany, 2021.

[175] H. Susanto, N. A. C. Imani, N. R. Aslamiyah, T. Istirokhatun, and M. H. Robbani, "The effect of an ultrasound radiation on the synthesis of 4A zeolite from fly ash," *IOP Conference Series: Materials Science and Engineering*, vol. 367, no. 1, Article ID 012026, 2018.

[176] K. Ojha, N. C. Pradhan, and A. N. Samanta, "Zeolite from fly ash: synthesis and characterization," *Bulletin of Materials Science*, vol. 27, no. 6, pp. 555–564, 2004.

[177] M. Park, C. L. Choi, W. T. Lim, M. C. Kim, J. Choi, and N. H. Heo, "Molten-salt method for the synthesis of zeolitic materials: I. Zeolite formation in alkaline molten-salt system," *Microporous and Mesoporous Materials*, vol. 37, no. 1–2, pp. 81–89, 2000.

[178] X. Querol, N. Moreno, J. Umaña et al., "Synthesis of zeolites from coal fly ash: an overview," *International Journal of Coal Geology*, vol. 50, no. 1–4, pp. 413–423, 2002.

[179] Q. Miao, B. Zhao, S. Liu, J. Guo, Y. Tong, and J. Cao, "Decomposition of the potassic rocks by sub-molten salt method and synthesis of low silica X zeolite," *Asia-Pacific Journal of Chemical Engineering*, vol. 11, no. 4, pp. 558–566, 2016.

[180] J. Yang, T. Li, X. Bao, Y. Yue, and H. Liu, "Mesoporogen-free synthesis of hierarchical sodalite as a solid base catalyst from sub-molten salt-activated aluminosilicate," *Particuology*, vol. 48, pp. 48–54, 2020.

[181] Y. Meng, B. Zhao, H. Zhang, X. Liu, and J. Cao, "Synthesis of zeolite W from potassic rocks activated by KOH sub-molten salt method," *Crystal Research and Technology*, vol. 53, no. 6, Article ID 1700216, 2018.

[182] Y. K. Krisnandi, I. Mahmuda, D. U. C. Rahayu, and R. Sihombing, "Synthesis and characterization of ZSM-5 zeolite from dealuminated and fragmentated bayat-klaten natural zeolite," *Journal of Physics: Conference Series*, vol. 1095, no. 1, Article ID 012044, 2018.

[183] Y. H. Hsiao, T. Y. Ho, Y. H. Shen, and D. Ray, "Synthesis of analcime from sericite and pyrophyllite by microwave-assisted hydrothermal processes," *Applied Clay Science*, vol. 143, pp. 378–386, 2017.

[184] X. Zeng, X. Hu, H. Song et al., "Microwave synthesis of zeolites and their related applications," *Microporous and Mesoporous Materials*, vol. 323, Article ID 111262, 2021.

[185] A. R. Majdinasab, P. K. Manna, Y. Wroczynskyj et al., "Cost-effective zeolite synthesis from waste glass cullet using energy efficient microwave radiation," *Materials Chemistry and Physics*, vol. 221, pp. 272–287, 2019.

[186] S. F. Wong, K. Deekamwong, J. Wittakayun et al., "Nanocrystalline K-F zeolite from rice husk silica as an eco-friendly solid base catalyst for the synthesis of jasminaldehyde under microwave irradiation," *Sains Malaysiana*, vol. 47, no. 2, pp. 337–345, 2018.

[187] N. Soltani, A. Bahrami, M. I. Pech-Canul, and L. A. González, "Review on the physicochemical treatments of rice husk for production of advanced materials," *Chemical Engineering Journal*, vol. 264, pp. 899–935, 2015.

[188] S. Bohra, D. Kundu, and M. K. Naskar, "One-pot synthesis of NaA and NaP zeolite powders using agro-waste material and other low cost organic-free precursors," *Ceramics International*, vol. 40, no. 1, pp. 1229–1234, 2014.

[189] V. P. Mallapur and J. U. K. Oubagaranadin, "A brief review on the synthesis of zeolites from hazardous wastes," *Transactions of the Indian Ceramic Society*, vol. 76, no. 1, pp. 1–13, 2017.

[190] S. Bohra, K. P. Dey, D. Kundu, and M. K. Naskar, "Synthesis of zeolite T powders by direct dissolution of rice husk ash: an agro-waste material," *Journal of Materials Science*, vol. 48, no. 22, pp. 7893–7901, 2013.

[191] P. Alaba, O. B. Ayodele, W. M. Ashri, and W. Daud, "Overview of the synthesis of nanozeolite from agro-waste," 2017, https://www.researchgate.net/profile/Peter-Alaba/publication/320676597_Synthesis_of_hierarchical_mesoporous_zeolite/links/5a19a1ce0f7e9be37f9a533b/Synthesis-of-hierarchical-mesoporous-zeolite.pdf#page=30.

[192] J. A. Oliveira, F. A. Cunha, and L. A. M. Ruotolo, "Synthesis of zeolite from sugarcane bagasse fly ash and its application as a low-cost adsorbent to remove heavy metals," *Journal of Cleaner Production*, vol. 229, pp. 956–963, 2019.

[193] O. B. Kotova, I. N. Shabalin, D. A. Shushkov, and L. S. Kocheva, "Hydrothermal synthesis of zeolites from coal fly ash," *Advances in Applied Ceramics*, vol. 115, no. 3, pp. 1–6, 2015.

[194] L. Deng, Q. Xu, and H. Wu, "Synthesis of zeolite-like material by hydrothermal and fusion methods using municipal solid waste fly ash," *Procedia Environmental Sciences*, vol. 31, pp. 662–667, 2016.

[195] M. Esaifan, M. Hourani, H. Khoury, H. Rahier, and J. Wastiels, "Synthesis of hydroxysodalite zeolite by alkali-activation of basalt powder rich in calc-plagioclase," *Advanced Powder Technology*, vol. 28, no. 2, pp. 473–480, 2017.

[196] Y. W. Chiang, K. Ghyselbrecht, R. M. Santos, B. Meesschaert, and J. A. Martens, "Synthesis of zeolitic-type adsorbent material from municipal solid waste incinerator bottom ash and its application in heavy metal adsorption," *Catalysis Today*, vol. 190, no. 1, pp. 23–30, 2012.

[197] M. Gross, M. Soulard, P. Caullet, J. Patarin, and I. Saude, "Synthesis of faujasite from coal fly ashes under smooth temperature and pressure conditions: a cost saving process," *Microporous and Mesoporous Materials*, vol. 104, no. 1–3, pp. 67–76, 2007.

[198] T. Wajima, T. Shimizu, and Y. Ikegami, "Synthesis of zeolites from paper sludge ash and their ability to simultaneously remove NH4+ and PO4 3–," *Journal of Environmental Science and Health, Part A*, vol. 42, no. 3, pp. 345–350, 2007.

[199] S. C. Aboudi Mana, M. M. Hanafiah, and A. J. K. Chowdhury, "Environmental characteristics of clay and clay-based minerals," *Geology, Ecology, and Landscapes*, vol. 1, no. 3, pp. 155–161, 2017.

[200] O. O. Ltaief, S. Siffert, S. Fourmentin, and M. Benzina, "Synthesis of Faujasite type zeolite from low grade Tunisian clay for the removal of heavy metals from aqueous waste by batch process: kinetic and equilibrium study," *Comptes Rendus Chimie*, vol. 18, no. 10, pp. 1123–1133, 2015.

[201] D. F. Medina, D. M. San Martin, C. M. López et al., "Removal of Pb (II) in aqueous solutions using synthesized zeolite X from Ecuadorian clay," *Ingeniería e Investigación*, vol. 41, no. 2, Article ID e89671, 2021.

[202] M. A. Moneim and E. A. Ahmed, "Synthesis of faujasite from Egyptian clays: characterizations and removal of heavy metals," *Geomaterials*, vol. 05, no. 02, pp. 68–76, 2015.

[203] A. Gaidoumi, A. Chaouni Benabdallah, B. el Bali, and A. Kherbeche, "Synthesis and characterization of zeolite HS using natural pyrophyllite as new clay source," *Arabian Journal for Science and Engineering*, vol. 43, no. 1, pp. 191–197, 2017.

[204] E. Aghaei, M. Ebrahiminejad, R. Khoshbin et al., "Synthesis of mesoporous Y zeolite from pyrophyllite as Si and Al source used in gasoline and gasoil production from heavy oil," *Fuel and Combustion*, vol. 13, no. 1, pp. 50–66, 2020.

[205] M. Foroughi, A. Salem, and S. Salem, "Potential of fusion technique in production of mesoporous zeolite A powder from poor kaolin through modification by boehmite: effect of clay mineralogy on particle morphology," *Advanced Powder Technology*, vol. 32, no. 7, pp. 2423–2432, 2021.

[206] I. v. Joseph, L. Tosheva, G. Miller, and A. M. Doyle, "FAU-type zeolite synthesis from clays and its use for the simultaneous adsorption of five divalent metals from aqueous solutions," *Materials 2021*, vol. 14, no. 13, p. 3738, 2021.

[207] M. Omidi, A. Fatehinya, M. Farahani et al., "Characterization of biomaterials," *Biomaterials for Oral and Dental Tissue Engineering*, vol. 97–115, pp. 97–115, 2017.

[208] S. Nasrazadani and S. Hassani, "Modern analytical techniques in failure analysis of aerospace, chemical, and oil and gas industries," *Handbook of Materials Failure Analysis with Case Studies from the Oil and Gas Industry*, pp. 39–54, Butterworth-Heinemann, Oxford, UK, 2016.

[209] I. v. Joseph, L. Tosheva, and A. M. Doyle, "Simultaneous removal of Cd (II), Co (II), Cu (II), Pb (II), and Zn (II) ions from aqueous solutions via adsorption on FAU-type zeolites prepared from coal fly ash," *Journal of Environmental Chemical Engineering*, vol. 8, no. 4, Article ID 103895, 2020.

[210] Z. Tauanov, P. E. Tsakiridis, S. v. Mikhalovsky, and V. J. Inglezakis, "Synthetic coal fly ash-derived zeolites doped with silver nanoparticles for mercury (II) removal from water," *Journal of Environmental Management*, vol. 224, pp. 164–171, 2018b.

[211] M. A. Ismail, M. A. Z. Eltayeb, and S. A. A. Maged, "Synthesis of zeolite A from Sudanese montmorillonite clay to remove nickel and copper ions from aqueous solutions," *IJCBS*, vol. 4, pp. 46–56, 2013.

[212] V. Wernert, O. Schaef, L. Aloui et al., "Cancrinite synthesis from natural kaolinite by high pressure hydrothermal method: application to the removal of Cd2+ and Pb2+ from water," *Microporous and Mesoporous Materials*, vol. 301, Article ID 110209, 2020.

[213] P. Labs, "Bet specific surface area—particle techology labs," 2011, https://www.particletechlabs.com/analytical-testing/gas-adsorption-and-porosimetry/bet-specific-surface-area.

[214] M. Nasrollahzadeh, M. Atarod, M. Sajjadi, S. M. Sajadi, and Z. Issaabadi, "Plant-mediated green synthesis of nanostructures: mechanisms, characterization, and applications," *Interface Science and Technology*, vol. 28, pp. 199–322, 2019.

[215] W. Feng, Z. Wan, J. Daniels et al., "Synthesis of high quality zeolites from coal fly ash: mobility of hazardous elements and environmental applications," *Journal of Cleaner Production*, vol. 202, pp. 390–400, 2018.

[216] G. K. R. Angaru, Y. L. Choi, L. P. Lingamdinne et al., "Facile synthesis of economical feasible fly ash–based zeolite–supported nano zerovalent iron and nickel bimetallic composite for the potential removal of heavy metals from industrial effluents," *Chemosphere*, vol. 267, Article ID 128889, 2021.

[217] T. Amiri-Yazani, R. Zare-Dorabei, M. Rabbani, and A. Mollahosseini, "Highly efficient ultrasonic-assisted preconcentration and simultaneous determination of trace amounts of Pb (II) and Cd (II) ions using modified magnetic natural clinoptilolite zeolite: response surface methodology," *Microchemical Journal*, vol. 146, pp. 498–508, 2019.

[218] D. Czarna, P. Baran, P. Kunecki, R. Panek, R. Żmuda, and M. Wdowin, "Synthetic zeolites as potential sorbents of mercury from wastewater occurring during wet FGD processes of flue gas," *Journal of Cleaner Production*, vol. 172, pp. 2636–2645, 2018.

[219] P. S. Nayak and B. K. Singh, "Instrumental characterization of clay by XRF, XRD and FTIR," *Bulletin of Materials Science*, vol. 30, no. 3, pp. 235–238, 2007.

[220] R. Kohli and K. Mittal, "Methods for assessing surface cleanliness," *Developments in Surface Contamination and Cleaning*, vol. 12, pp. 23–105, 2019.

[221] N. Goyal, S. Barman, and V. K. Bulasara, "Efficient removal of bisphenol S from aqueous solution by synthesized nanozeolite secony mobil-5," *Microporous and Mesoporous Materials*, vol. 259, pp. 184–194, 2018.

[222] M. A. Khan, A. A. Alqadami, S. M. Wabaidur et al., "Oil industry waste based non-magnetic and magnetic hydrochar to sequester potentially toxic post-transition metal ions from water," *Journal of Hazardous Materials*, vol. 400, Article ID 123247, 2020.

[223] M. Rani, Keshu, and U. Shanker, "Green nanomaterials: an overview," *Green Functionalized Nanomaterials for Environmental Applications*, pp. 43–80, Elsevier, Amsterdam, Netherlands, 2022.

[224] N. Birkner, "How an FTIR spectrometer operates," 2011, https://chem.libretexts.org/Bookshelves/Physical_and_Theoretical_Chemistry_Textbook_Maps/Supplemental_Modules_%20(Physical_and_Theoretical_Chemistry)/Spectroscopy/Vibrational_Spectroscopy/Infrared_Spectroscopy/How_an_FTIR_Spectrometer_Operates.

[225] K. Song, "Interphase characterization in rubber nanocomposites," *Progress in Rubber Nano-composites*, pp. 115–152, Elsevier, Amsterdam, Netherlands, 2017.

[226] M. Esaifan, L. N. Warr, G. Grathoff et al., "Synthesis of hydroxy-sodalite/cancrinite zeolites from calcite-bearing kaolin for the removal of heavy metal ions in aqueous media," *Minerals*, vol. 9, no. 8, p. 484, 2019.

[227] K. Ahmad, H. ur R. Shah, M. Ashfaq et al., "Effect of metal atom in zeolitic imidazolate frameworks (ZIF-8 & 67) for removal of Pb2+ & Hg2+ from water," *Food and Chemical Toxicology*, vol. 149, Article ID 112008, 2021.

[228] X. Pu, L. Yao, L. Yang, W. Jiang, and X. Jiang, "Utilization of industrial waste lithium-silicon-powder for the fabrication of novel nap zeolite for aqueous Cu (II) removal," *Journal of Cleaner Production*, vol. 265, Article ID 121822, 2020.

[229] W. Patcharin, K. Sriamporn, and A. Kanokkan, "Utilization biomass from bagasse ash for phillipsite zeolite synthesis," *Advanced Materials Research*, vol. 383–390, pp. 4038–4042, 2011.

[230] K. R. Rajisha, B. Deepa, L. A. Pothan, and S. Thomas, "Thermomechanical and spectroscopic characterization of natural fibre composites," *Interface Engineering of Natural Fibre Composites for Maximum Performance*, pp. 241–274, Woodhead Publishing, Sawston, UK, 2011.

[231] Z. Ezzeddine, I. Batonneau-Gener, Y. Pouilloux, H. Hamad, and Z. Saad, "Synthetic nax zeolite as a very efficient heavy metals sorbent in batch and dynamic conditions," *Colloids and Interfaces*, vol. 2, no. 2, p. 22, 2018.

[232] D. P. De-La-Vega, C. González, C. A. Escalante et al., "Uso de zeolita faujasita para adsorción de iones en aguas residuales municipales," *Tecnología y Ciencias Del Agua*, vol. 9, no. 4, pp. 184–208, 2018.

[233] M. R. Mirbaloochzehi, A. Rezvani, A. Samimi, and M. Shayesteh, "Application of a novel surfactant-modified natural nano-zeolite for removal of heavy metals from drinking water," *Advanced Journal of Chemistry-Section A*, vol. 2020, no. 5, pp. 612–620, 2020.

[234] D. Ao, A. P. Olalekan, and A. M. Olatunya, "Langmuir, Freundlich, Temkin and Dubinin–radushkevich Isotherms:

studies of equilibrium sorption of $Zn2^{+}$ unto phosphoric acid modified rice husk," *IOSR Journal of Applied Chemistry*, vol. 3, no. 1, pp. 38–45, 2012.

[235] Z. A. Alothman, A. H. Bahkali, M. A. Khiyami et al., "Low cost biosorbents from fungi for heavy metals removal from wastewater," *Separation Science and Technology*, vol. 55, no. 10, p. 1766, Article ID 1608242, 2019.

[236] S. K. Papageorgiou, F. K. Katsaros, E. P. Kouvelos, J. W. Nolan, H. le Deit, and N. K. Kanellopoulos, "Heavy metal sorption by calcium alginate beads from Laminaria digitata," *Journal of Hazardous Materials*, vol. 137, no. 3, pp. 1765–1772, 2006.

[237] M. Tadesse, "Synthesis and characterization of zeolite a using bagasse ash, as biosilica source for water hardness removal," 2018, http://213.55.101.23/handle/123456789/949.

[238] M. Shamsayei, Y. Yamini, and H. Asiabi, "Synthesis and characterization of layered double hydroxide decorated zeolite as the efficient sorbent for removal of toxic metal ions," *Environmental Progress & Sustainable Energy*, vol. 41, no. 1, Article ID e13727, 2022.

[239] V. K. Jha, M. Nagae, M. Matsuda, and M. Miyake, "Zeolite formation from coal fly ash and heavy metal ion removal characteristics of thus-obtained Zeolite X in multi-metal systems," *Journal of Environmental Management*, vol. 90, no. 8, pp. 2507–2514, 2009.

[240] W. w. Bao, H. f. Zou, S. c. Gan, X. c. Xu, G. j. Ji, and Ky Zheng, "Adsorption of heavy metal ions from aqueous solutions by zeolite based on oil shale ash: kinetic and equilibrium studies," *Chemical Research in Chinese Universities*, vol. 29, no. 1, pp. 126–131, 2013.

[241] X. Zhang, T. Cheng, C. Chen et al., "Synthesis of a novel magnetic nano-zeolite and its application as an efficient heavy metal adsorbent," *Materials Research Express*, vol. 7, no. 8, Article ID 085007, 2020.

[242] K. S. Hui, C. Y. H. Chao, and S. C. Kot, "Removal of mixed heavy metal ions in wastewater by zeolite 4A and residual products from recycled coal fly ash," *Journal of Hazardous Materials*, vol. 127, no. 1–3, pp. 89–101, 2005.

[243] N. Ayawei, A. N. Ebelegi, and D. Wankasi, "Modelling and interpretation of adsorption isotherms," *Journal of Chemistry*, vol. 2017, Article ID 3039817, 11 pages, 2017.

[244] A. A. Inyinbor, F. A. Adekola, and G. A. Olatunji, "Kinetics, isotherms and thermodynamic modeling of liquid phase adsorption of Rhodamine B dye onto Raphia hookerie fruit epicarp," *Water Resources and Industry*, vol. 15, pp. 14–27, 2016.

[245] G. W. Kajjumba, S. Emik, A. Öngen, H. Kurtulus Özcan, and S. Aydın, "Modelling of adsorption kinetic processes—errors, theory and application," in *Advanced Sorption Process Applications*IntechOpen, London, UK, 2019.

[246] M. A. Anang, R. Zugle, and B. Sefa-Ntiri, "Assessing the adsorptive and photodegradative efficiencies of ZSM-11 synthesized from rice husk ash," *Journal of Chemistry*, vol. 2020, Article ID 6094126, 13 pages, 2020.

[247] E. A. Abdelrahman, Y. G. Abou El-Reash, H. M. Youssef, Y. H. Kotp, and R. M. Hegazey, "Utilization of rice husk and waste aluminum cans for the synthesis of some nanosized zeolite, zeolite/zeolite, and geopolymer/zeolite products for the efficient removal of Co (II), Cu (II), and Zn (II) ions from aqueous media," *Journal of Hazardous Materials*, vol. 401, Article ID 123813, 2021.

[248] T. Chuenpratoom, K. Hemavibool, K. Rermthong, and S. Nanan, "Removal of lead by merlinoite prepared from sugarcane bagasse ash and kaolin: synthesis, isotherm, kinetic, and thermodynamic studies," *Molecules 2021*, vol. 26, p. 7550, 2021.

[249] T. Cheng, C. Chen, R. Tang, C.-H. Han, and Y. Tian, "Competitive adsorption of Cu, Ni, Pb, and Cd from aqueous solution onto fly ash-based linde F (K) zeolite," *Journal of Chemical & Engineering Data*, vol. 37, no. 1, 2018.

[250] R. M. Abdel-Hameed, E. Abdel-Aal, F. Farghaly et al., "Exploitation of industrial solid wastes for preparing zeolite as a value-added product and its kinetics as adsorbent for heavy metal ions," *Physicochemical Problems of Mineral Processing*, vol. 57, no. 1, pp. 87–99, 2020.

[251] A. Saravanan, P. S. Kumar, P. R. Yaashikaa, S. Karishma, S. Jeevanantham, and S. Swetha, "Mixed biosorbent of agro waste and bacterial biomass for the separation of Pb (II) ions from water system," *Chemosphere*, vol. 277, Article ID 130236, 2021.

[252] Z. Ghasemi, I. Sourinejad, H. Kazemian, M. Hadavifar, S. Rohani, and H. Younesi, "Kinetics and thermodynamic studies of Cr (VI) adsorption using environmental friendly multifunctional zeolites synthesized from coal fly ash under mild conditions," *Chemical Engineering Communications*, vol. 207, no. 6, pp. 808–825, 2020.

[253] S. Khandaker, Y. Toyohara, G. C. Saha, M. R. Awual, and T. Kuba, "Development of synthetic zeolites from bio-slag for cesium adsorption: kinetic, isotherm and thermodynamic studies," *Journal of Water Process Engineering*, vol. 33, Article ID 101055, 2020.

[254] J. Yang, H. Sun, T. Peng, L. Zeng, and X. Zhou, "Mild hydrothermal synthesis of 11Å-TA from alumina extracted coal fly ash and its application in water adsorption of heavy metal ions (Cu (II) and Pb (II))," *International Journal of Environmental Research and Public Health 2022*, vol. 19, 2022.

[255] L. Liu, X. B. Luo, L. Ding, and S. L. Luo, "Application of nanotechnology in the removal of heavy metal from water," *Nanomaterials for the Removal of Pollutants and Resource Reutilization*, pp. 83–147, Elsevier, Amsterdam, Netherlands, 2019.

[256] X. Liu, G. Wang, Q. Luo, X. Li, and Z. Wang, "The thermodynamics and kinetics for the removal of copper and nickel ions by the zeolite Y synthesized from fly ash," *Materials Research Express*, vol. 6, no. 2, p. 025001, 2018.

Hindawi
Journal of Chemistry
Volume 2022, Article ID 2828860, 12 pages
https://doi.org/10.1155/2022/2828860

Research Article

Kinetic and Isotherm Studies of the Adsorption Phenacetin onto Two Copper Porous Coordination Compounds: Nonlinear Regression Analysis

Djoumbissie Alvine Loris,[1] Tchuifon Tchuifon Donald Raoul,[1,2] Atemkeng Donlifack Cyrille,[1] Kuete Tiotsop Idris-Hermann,[1] Doungmo Giscard,[3] Tayo Djampouo Alain Clovis,[1] Anagho Solomon Gabche,[1] and Ngoune Jean[1]

[1]*Research Unit of Noxious Chemistry and Environmental Engineering, Department of Chemistry, Faculty of Science, University of Dschang, Dschang, Cameroon*
[2]*Laboratory of Energy,Materials,Modeling and Method, Department of Process Engineering, National Higher Polytechnic School of Douala, University of Douala, Douala, Cameroon*
[3]*Institute of Inorganic Chemistry, Christian-Albrechts University of Kiel, Kiel, Germany*

Correspondence should be addressed to Tchuifon Tchuifon Donald Raoul; tchuifondonald@yahoo.fr and Ngoune Jean; jeangoune@yahoo.com

Received 30 May 2022; Revised 6 July 2022; Accepted 29 July 2022; Published 30 August 2022

Academic Editor: Jun Wu

Two coordination compounds, copper (II) fumarate (CuFum) and copper (II) tartrate (CuTart), synthesized from copper (II) with fumaric acid and tartaric acid as ligands and using the slow evaporation method have been applied to study the adsorption of phenacetin in aqueous solution. These compounds were characterized by elemental analysis, IR-FT spectroscopy, and X-ray powder diffraction. The melting points of the synthesized coordination compounds were found to be above 350°C. The influence of parameters such as the initial pH, the contact time, and the initial concentration on the adsorption of phenacetin in an aqueous solution has been studied. The studies showed that adsorption equilibrium was reached after 80 minutes for both coordination compounds; the adsorption capacity increased with increasing phenacetin concentration, and the maximum adsorption capacity was obtained in the acidic medium at pH 4. The adsorbed amount of phenacetin on copper (II) fumarate (CuFum) was 25.158 mg/g while that on copper (II) tartrate (CuTart) was 25.906 mg/g. Nonlinear regression analysis showed the best fit for the Freundlich model isotherm for CuTart with R^2 of 0.963 and a Chi-square test (χ^2) of 0.529 while for the CuFum material, it is the Redlich-Peterson model with R^2 of 0.975 and Chi-square test (χ^2) of 0.263. The kinetic study shows that the pseudo-second-order model better describes the adsorption of the two materials. The results show that physisorption and chemisorption participate in the adsorption of phenacetin and that these materials can be used for the elimination of phenacetin in solution.

1. Introduction

Phenacetin, also known by the designations pethoxyacetanilide, aceto-4-phenetidine acetophenetidin, N-acetyl-p-phenetidine, and acetophenetidine, is a non-opioid antipyretic and analgesic. It can be isolated from Bursera grandifolia, a herbal remedy with antipyretic properties [1]. The antipyretic effect was observed by its action on the brain via a decrease in the temperature set point [2]. Phenacetin is also used principally as an analgesic for the treatment of fever and related complications [1, 3]. The analgesic effects were observed through its activities on the sensory tracts of the spinal cord. However, the long-term and chronic consumption of phenacetin led to several toxicological complications ranging from nephrotoxicity to carcinogenicity [4]. The carcinogenicity was observed in the urinary tract and renal pelvis [5]. As

a result of these severe complications, phenacetin and drugs containing phenacetin were withdrawn from the market by the order of the U.S. Food and Drug Administration in 1983 [6].

Due to its low cost, phenacetin is still being used for research into the physical and refractive properties of crystals [7]. Conventional methods are being used to remove pharmaceutical compounds from wastewater; some examples of which are chlorination, oxidation, biological treatment, electrochemical treatment, and adsorption. However, the adsorption method has many advantages over the others, such as easy operation, high efficiency, and no risk of highly toxic sub-products [8]. The most used adsorbents for the removal of pharmaceutical compounds from aqueous solution are activated carbons [9–11] clay minerals [12], polymeric resins [13], and other adsorbents, such as molecular polymers [14], mesoporous materials [15], and metal-organic frameworks [16]. Despite all these, it is still of interest to study modified adsorbents or new adsorbents that may be more efficient at removing pharmaceutical compounds from water than conventional ones.

Metal-organic frameworks (MOFs) are a new class of adsorbent materials, with high porosity and high specific area that is formed by metal ions linked to organic ligand bridges, to generate coordination compounds that extend into space in all dimensions. These materials allow a more flexible design of chemical functionality and easy modification, which makes them more promising materials for the adsorption of pharmaceutical compounds. Among the MOFs, a porous Cu-based MOF based on a pentacarboxylate ligand 2,5-bis(3,5-dicarboxyphenyl)-benzoic acid (H_5L), namely, $[(CH_3)_2NH_2]\{[Cu_2(L)\cdot(H_2O)_2]\cdot x$ solvent$\}n$, has been used as a sorbent to remove diclofenac sodium and chlorpromazine hydrochloride from the aqueous solution [17]. These compounds exhibit excellent gas adsorption capacities taking advantage of large permanent porosity and excellent diclofenac adsorption in an aqueous solution.

In this work, we used copper (II) fumarate and copper (II) tartrate as novel adsorbents. These adsorbents have never been used for the adsorption of any pollutants. Hence, this work aimed to evaluate the adsorption properties of these complexes for the removal of phenacetin from an aqueous solution. Isotherms studies were carried out, and the experimental data were analyzed using the two-parameter non-linear regression kinetics, and two and three-parameter non-linear isotherm models.

2. Materials and Methods

2.1. Phenacetin. Phenacetin with a purity of 98% was purchased from Aldrich. The stock solution was prepared by dissolving 250 mg of phenacetin in 100 mL of hot distilled water (75°C). Working solutions of concentration varying between 20–50 mg/L were freshly prepared by diluting the stock solution. NaOH (0.10 M) and HCl (0.10 M) were used to adjust the pH value of the phenacetin solutions. Distilled water was used throughout this study.

2.2. Adsorbents. Copper (II) fumarate (CuFum) was synthesized hydrothermally as follows: In a 50 mL round-bottomed flask containing about 20 mL of distilled water, were introduced fumaric acid, $C_4H_4O_4$ (196.07 mg; 1.23 mmol) and sodium hydroxide, NaOH (80 mg; 2 mmol) which dissolved instantly under magnetic stirring. To the colorless solution obtained was added copper (II) nitrate trihydrate, $Cu(NO_3)_2.3H_2O$ (384.7 mg, 1.23 mmol). The resulting solution was kept under continuous stirring for 24 hours. At the end of this time, a blue precipitate was formed which was collected by filtration. Subsequently, the blue powder obtained (396.4 mg) was washed with distilled water and dried at room temperature. The yield from this synthesis was 60%. The balanced equation of this reaction is as follows:

$$Cu(No_3)_2.3H_2O + C_4H_4O_4 + 2NaOH \xrightarrow{H_2O/RT} [Cu(OH_2)_3(O_4C_4H_2)] + 2NaNo_3 + 2H_2O. \quad (1)$$

Copper (II) tartrate (CuTart) was prepared according to the method described by Al-Dajani et al. [18] as follows: In a round-bottomed flask containing about 20 mL of distilled water, tartaric acid was introduced, $C_4H_6O_6$ (150 mg, 1 mmol) and sodium hydroxide, NaOH (80 mg, 2 mmol) which gradually dissolved under magnetic stirring. To the colorless solution obtained was added copper (II) chloride dihydrate, $Cu(Cl)_2.2H_2O$ (170.5 mg, 1 mmol). A pale green precipitate was gradually formed upon magnetic stirring for over 24 hours. The mixture was filtered and the residue dried at room temperature. A green powder (174 mg) was obtained, with a yield of 44%. The balanced equation for this reaction is as follows:

$$CuCl_2.2H_2O + C_4H_6O_6 + 2NaOH \xrightarrow{H_2O/RT} [Cu(OH_2)_3(O_6C_4H_4)] + 2NaCl + 2H_2O. \quad (2)$$

2.3. Samples Characterization. Elemental analysis was performed using a Euro Vector CHNS-O element analyzer. FT-IR spectra were recorded using a Perkin-Elmer FT-IR 100 spectrophotometer. The melting point of the compound was obtained using an SMP3 Stuart Scientific melting point apparatus, while the UV-vis spectrophotometer model

GENESYS 10S was employed to record the electronic spectra of the investigated compounds. Powder X-rays diffraction was performed using STOE Stadi-p X-ray powder diffractometer with Cu Kα1 radiation ($\lambda = 1.54056$ Å; Ge monochromator; flat samples) in transmission geometry.

2.4. Adsorption. Adsorption experiments were carried out by mechanical agitation at room temperature. For each run, 25 mL of phenacetin solution of a known initial concentration between 20 and 50 mg/L was treated with 35 mg of the two compounds. After agitation, the solution was filtered, and the filtrate was analyzed to obtain the concentration of the residual phenacetin by using the UV/Vis spectrophotometer (GENESYS 10S). Similar measurements were carried out by varying the pH of the solution and contact time. The amount (Q_t) of phenacetin adsorbed was calculated using the following expression:

$$Q_t = \frac{(C_o - C_t)V}{m}, \tag{3}$$

where C_o is the initial concentration of the phenacetin, C_t is the concentration at time t, V is the volume of the solution, and Q_t is the quantity of phenacetin adsorbed at time t while m is the mass of the absorbent.

2.4.1. Effect of Initial pH. To determine the effect of pH, the adsorption of phenacetin by each adsorbent was investigated over a pH range of 2 to 10 at ambient temperature. For each adsorbent, 35 mg was treated with 25 mL of an aqueous solution of 40 mg/L of phenacetin. The initial pH of the solution was adjusted by adding HCl or NaOH solution at a concentration of 0.01 mol/L.

2.4.2. Effect of Contact Time. To determine the effect of agitation time on the adsorption process, 35 mg of adsorbent was agitated in a 25 mL solution of phenacetin with an initial concentration of 40 mg/L for different contact times varying between 5 and 120 minutes. After each contact time t, the solution was rapidly filtered and the residual concentration was determined by spectrophotometry. The amount (Q_e) of phenacetin adsorbed was calculated using equation (4).

2.5. Equilibrium Isotherms. To study the equilibrium of the adsorption of phenacetin onto each adsorbent, data from the equilibrium experiments were analyzed using non-linear equilibrium models of two- to three parameters.

Langmuir isotherm: the Langmuir isotherm is often used for the equilibrium adsorption of solutes from solutions. It is expressed as [19]:

$$Q_e = \frac{Q_m K C_e}{1 + K C_e}, \tag{4}$$

where Q_e is the adsorption capacity at the equilibrium concentration (mg/g); C_e is the equilibrium concentration of adsorbate in solution (mg/L), while Q_m is the maximum adsorption capacity (mg/g) and K is the Langmuir constant (L/m).

Freundlich isotherm: the Freundlich isotherm is an empirical equation employed to describe multilayer adsorption. This model predicts that the pharmaceutical concentration on the adsorbent will increase with the increase in the adsorbate concentration in the solution. The model equation is given as [20]:

$$Qe = K_f C_e^{1/n}, \tag{5}$$

where K_f (L/mg) is the Frendlich isotherm constant and $1/n$ is the heterogeneity factor which can vary between 0 and 1.

Elovich isotherm: the Elovich isotherm is an equation employed to describe monolayer adsorption. This model predicts that chemical bonds are formed between adsorbents and adsorbates. The model equation is given as [21]:

$$\frac{Q_e}{Q_m} = K_E C_e \exp\left(-\frac{Q_e}{Q_m}\right). \tag{6}$$

Here, K_E is the Elovich constant.

Temkin isotherm: the Temkin isotherm assumes that the decrease in the heat of adsorption is linear and the adsorption is characterized by a uniform distribution of binding energies. It is expressed by the following equation [22]:

$$Q_e = \frac{RT}{b} \ln(AC_e), \tag{7}$$

where $b = RT/B$ is related to the heat of adsorption (J/mol), R is the gas constant (8.314 J/mol·K), T is the absolute temperature (K), and A is the Temkin equilibrium constant (L/g) corresponding to the maximum binding energy.

Redlich-Peterson isotherm: the Redlich-Peterson is an empirical isotherm that incorporates three parameters. It may be used to represent adsorption equilibrium over a wide concentration range. It combines some elements from both the Langmuir and Frendlich equations, and consequently, it can be employed either in heterogeneous or homogenous systems [23]. It can be described as follow:

$$Q_e = \frac{A_{RP} C_e}{1 + B_{RP} C_e^{\beta}}, \tag{8}$$

where A_{RP} (L/g) and B_{RP} (L/mg) are Redlisch–Peterson isotherm constants, β is an exponent which lies between 0 and 1.

Langmuir-Freundlich isotherm: the Langmuir-Freundlich isotherm includes the knowledge of adsorption on heterogeneous surfaces. It describes the distribution of adsorption energy onto the heterogeneous surface of the adsorbent [24]. It can be described as follow:

$$Qe = \frac{Q_m K_{LF} Ce^{\beta}}{1 + K_{LF} Ce^{\beta}}, \tag{9}$$

where Q_e is the equilibrium adsorbed quantity (mg/g); C_e is the equilibrium adsorbate concentration (mg/L); β is the heterogeneity parameter and it has values between 0 and 1 and K_{LF} is the equilibrium constant of the Langmuir-Freundlich equation (L^{β}/mg^{β}) for a heterogeneous solid.

2.6. Kinetic Models. Four different kinetic models were considered for this study: pseudo-first order, pseudo-second order, Elovich, and intra-particle diffusion.

Pseudo-first-order model: the pseudo-first-order kinetic model describes an adsorption process base on multilayer adsorption. Its equation is generally expressed as follows:

$$Q_t = Q_e\left[1 - \exp\left(-K_1\right)t\right], \tag{10}$$

where Q_e and Q_t are the adsorption capacities at equilibrium and at time t, respectively (in mg/g) and K_1 is the rate constant for the pseudo-first-order adsorption (L/mg.min)

Pseudo-second-order model: the pseudo-second-order kinetic model was initially proposed as a second order rate equation for the removal of heavy metals from water using natural zeolites and it was based on the strong bond between adsorbent and adsorbate [25].

$$Q_t = \frac{Q_e^2 K_2 t}{1 + Q_e K_e t}, \tag{11}$$

where K_2 is the rate constant for the pseudo-second-order adsorption (L/mg.min).

Elovich model: the Elovich empirical equation model was firstly for the adsorption of carbon monoxide onto manganese dioxide [26]. However, this equation is now generally known as the Elovich equation and has been extensively applied to chemisorption data. This equation can be expressed mathematically as follows:

$$Q_t = \frac{\ln\left(\alpha\beta\right)}{\beta} + \frac{\ln\ t}{\beta}, \tag{12}$$

where α (mg/g.min) represents the initial rate of adsorption and β (mg/g.min) the desorption rate constant.

Intra-particular diffusion model: the intraparticle diffusion model developed by Weber and Morris is presented as follows [19, 20]:

$$Q_t = K_{id}t^{1/2} + C, \tag{13}$$

where C (mg/g) is a constant associated with the thickness of the boundary layer and its higher value corresponds to a greater effect on the limiting boundary layer. K_{id} (mg/g.min$^{-1/2}$) is the rate constant of the intra-particle diffusion model.

2.7. Error Functions. In this study, non-linear regression was applied using the Microsoft Excel Solver function from Excel Microsoft 2013 for fitting the curve. The best fit for experimental data was determined from the coefficient of determination (R^2), residual root mean square error (RMSE), Chi-square test (χ^2), Sum Square of Errors (SSE), and Average Relative Error (ARE). The expressions of the error functions are given as follows:

$$\chi^2 = \sum_{i=1}^{N} \frac{\left(Q_{e,\ \exp} - Q_{e,\mathrm{cal}}\right)^2}{Q_{e,\mathrm{cal}}}, \tag{14}$$

$$\mathrm{RMSE} = \sqrt{\frac{1}{n-2}\sum_{i=1}^{N}\left(Q_{e,\ \exp} - Q_{e,\mathrm{cal}}\right)^2}, \tag{15}$$

$$\mathrm{SCE} = \sum_{i=1}^{N}\left(Q_{e,\ \exp} - Q_{e,\mathrm{cal}}\right)_i^2, \tag{16}$$

$$\mathrm{ARE} = \frac{100}{N}\sum_{i=1}^{N}\left|\frac{Q_{e,i,\mathrm{cal}} - Q_{e,i,\ \exp}}{Q_{e,i,\ \exp}}\right|, \tag{17}$$

$$R^2 = \frac{\sum_{i=1}^{N}\left(Q_{e,cal} - Q_{e\ \exp}\right)^2}{\sum_{i=1}^{N}\left(Q_{e,cal} - Q_{e\ \exp}\right)^2 + \left(Q_{e,cal} - Q_{e\ \exp}\right)^2}, \tag{18}$$

where $Q_{e,\exp}$ and $Q_{e,\mathrm{cal}}$ (mg/g) are the equilibrium capacity of adsorption obtained from the experiment and by calculating from the model, respectively, and N is the number of data points.

3. Results and Discussions

3.1. Characterization of Copper (II) Carboxylate

3.1.1. Copper (II) Fumarate (CuFum). The synthesized copper (II) fumarate was a blue powder that was found to be insoluble in toluene, distilled water, ethanol, acetone, and acetonitrile. It was soluble in DMSO and its boiling point was as high as 350°C.

(1) Infrared Spectroscopy. The IR spectrum of the copper (II) fumarate (Figure 1) shows the presence of organic ligands used in the synthesis through the typical vibrations of carboxylic groups.

In the analysis region, the complex shows a low-intensity peak around 3566.78 cm^{-1} corresponding to the O-H group, which could indicate that this compound contains water molecules. This frequency is slightly lower than 3600 cm^{-1}, indicating that these water molecules may be linked to the central metal or engaged in interactions with its surroundings. This spectrum also exhibits a broad band with a maximum centered around 2895.62 cm^{-1}; which is characteristic of aliphatic C-H vibrations of elongation. This band, expected around 3000 cm^{-1} is slightly shifted towards low frequencies. The bands observed at 1395.41 cm^{-1} and 1533.41 cm^{-1} could correspond respectively to asymmetric vibration of COO^- and symmetric vibration of COO^- in the fumarate, with a difference of 138.01 cm^{-1} which reflects a bridging coordination mode of this grouping [27, 28]. The absence of any band around ≈1710 cm^{-1} indicates the total deprotonation of all carboxylate groups in the complex [29]. The band at 1214.78 cm^{-1} can be assigned to the C-O group of the fumarate. The band observed

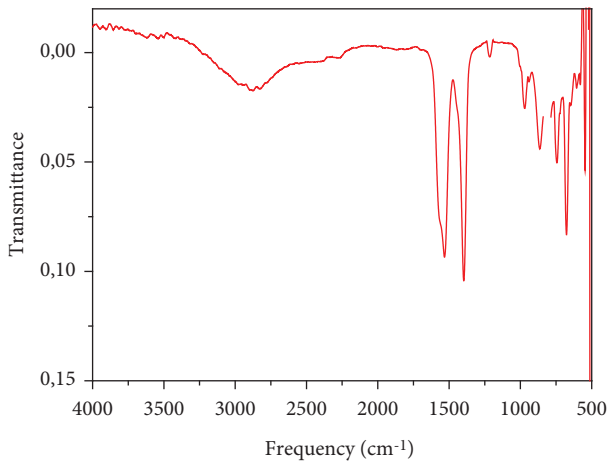

Figure 1: Infrared spectrum of copper (II) fumarate.

in the interval 998.97–989.84 cm^{-1} represents the valence vibrations, that are characteristic of the C=C deformation group. Finally, the absorption bands between 691.92 and 579.38 cm^{-1} are the characteristic frequencies of the Cu-O bond. From the attributions from the IR spectrum, it can be said that the product formed is a copper complex based on the fumarate ligand.

(2) Elemental Analysis. The experimental results obtained from the elemental analysis of the synthesized compound and the relative theoretical values are presented in Table 1 below.

The comparison of the percentages of the different elements (C and H) obtained experimentally and theoretically, as well as infrared spectroscopy permitted us to propose the empirical formula $[Cu(O_4C_4H_2)_2(H_2O)_4]$ for the compound. The analysis we were able to have was about (C,H,N), but the result shows us that the compound contained only C and H with is in accordance since the reactant used does not contain Nitrogen.

Figure 2 below shows the XRD of the adsorbent copper (II) fumarate obtained between 5 to80°.

(3) Powder X-ray Diffraction. This diffractogram shows sharp Bragg peaks of good intensity indicating that the material has high crystallinity.

From the empirical formula proposed by elemental analysis, and the functional group shown by Infrared spectroscopy, the following structure was proposed for the compound.

3.1.2. Copper.(II) Tartrate (CuTart). The results of the UV-Vis spectroscopy, IR spectroscopy, and powder XRD of the synthesized copper(II) tartrate are similar to those obtained from the literature [30]. The structure proposed from the analyses is the following:

3.2. Adsorption Study

3.2.1. Effect of Initial pH. The effect of initial pH on the adsorption of phenacetin by the two porous coordination compounds was studied by varying the initial pH of the

Table 1: Composition of analyzed elements for $[Cu(O_4C_4H_2)_2(H_2O)_4]$.

	% C	% H
Experimental values	25.623	4.331
Theoretical values	26.27	3.86

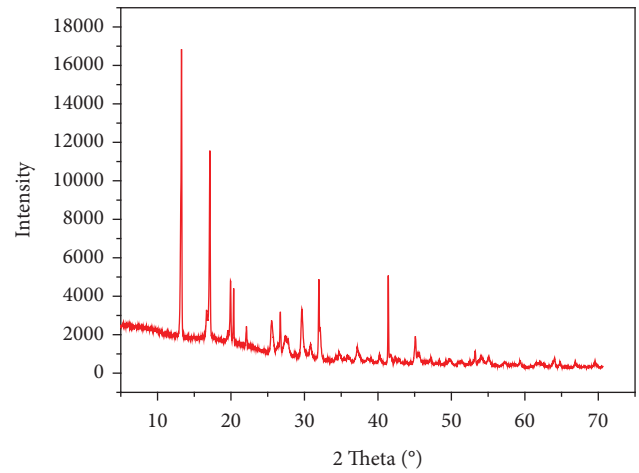

Figure 2: Powder X-rays diffraction of copper (II) fumarate.

phenacetin solution. The result is shown in Figure 3. According to this figure, the removal of phenacetin from an aqueous solution is highly dependent on the pH of the solution. Figure 4 shows that the adsorption is maximum at pH 4 with 17.928 mg/g and 19.631 mg/g adsorbed for copper (II) fumarate and copper (II) tartrate, respectively. The decrease in the amount of phenacetin adsorbed at pH greater than 4 can be explained by repulsive electrostatic interactions between an adsorbent and the adsorbate. The amount of phenacetin adsorbed by copper (II) tartrate is greater than that for copper (II) fumarate. This could be explained by the presence in copper (II) tartrate of hydroxide groups which are absent in copper (II) fumarate.

3.2.2. Effect of Contact Time. The time of agitation is a very significant parameter in the adsorption process because it determines the time necessary to reach equilibrium adsorption. The adsorption of phenacetin from an aqueous solution of an initial concentration of 40 mg/L and pH 4 was carried out on 35 mg of each carboxylate at the rotational speed of 150 rpm. The result obtained for the increasing stirring times is shown in Figure 5 which gives the amount of phenacetin adsorbed (Q_t) as a function of time.

Figure 5 shows that the adsorption takes place in three phases. The first rapid phase occurs during the first 20 minutes and the second phase takes place a little more slowly, stopping at equilibrium which is 80 min for the metal carboxylates. The rapidity of the first phase can be explained by a large number of sites available at the start of the adsorption process. This availability favors their occupation by the molecules of phenacetin. The same trend was observed by Gadipelly et al. [16] during the adsorption of ciprofloxacin onto MOF-5 (zinc (II) benzene dicarboxylate). As the

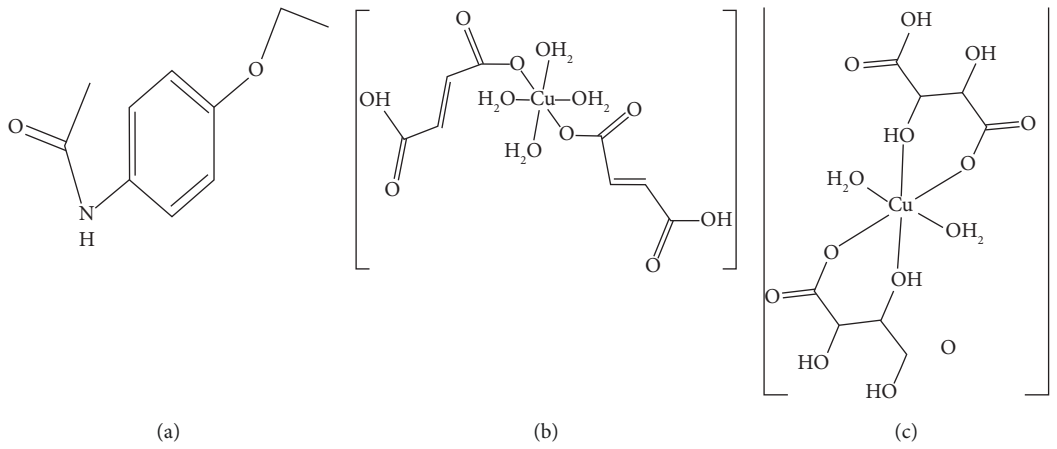

Figure 3: Structure of phenacetin (a), copper (II) fumarate (CuFum) (b) and copper (II) tartrate (CuTart) (c).

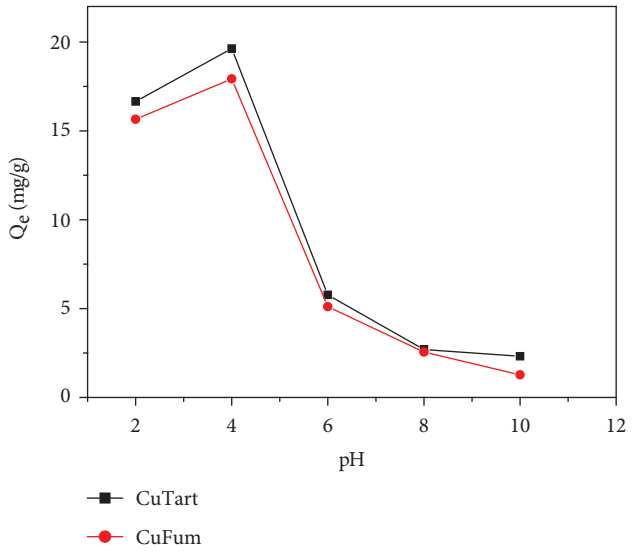

Figure 4: The effect of pH on the adsorption of phenacetin onto CuTart and CuFum.

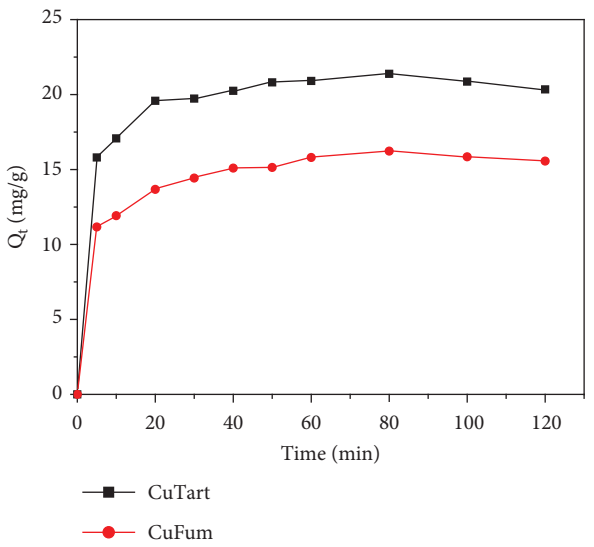

Figure 5: Effect of contact time on the adsorption of phenacetin onto CuTart and CuFum.

adsorption continues, the number of available sites decreases and the adsorbent becomes saturated. The amount of phenacetin adsorbed during this phase can be attributed to the π-π interactions between the organic compounds and adsorbents. The adsorption capacity of copper (II) tartrate is 21.381 mg/g while that of copper (II) fumarate is 16.225 mg/g.

3.2.3. Effect of Initial Concentration. The effect of initial concentration on the adsorption of phenacetin was investigated and the results are shown in Figure 6 below.

The increasing adsorption capacities of the porous coordination compounds with the increase in the concentration of phenacetin may be due to π-π interactions between the organic compounds and adsorbents. The π-π interactions in most cases are responsible for the mechanism of adsorption of aromatic compounds [31]. This result can also be explained by saying that, increasing the initial concentration of phenacetin leads to an increase in the driving force of mass transfer and hence an increase in the rate at which phenacetin molecules pass from solution to the particle surface [32]. The quantity of phenacetin adsorption onto all samples of porous coordination compounds did not show a plateau, suggesting that there was no monolayer formation on the surfaces of the adsorbents. The increase in adsorption capacity with an increase in initial concentration indicates that the porous coordination compounds have a high potential for the removal of phenacetin from their solutions.

3.3. Isotherm Study. In general, the adsorption isotherm indicates how the molecules are distributed between the liquid and solid phase when the adsorption processes attain equilibrium. This part aims at finding the models that can accurately describe the data obtained from the experiments of the adsorption of phenacetin onto copper (II) fumarate and copper (II) tartrate. Three models of two-parameter isotherms and two models of three-parameter isotherms were studied. The non-linear plots of these isotherms are given in Figures 7 and 8.

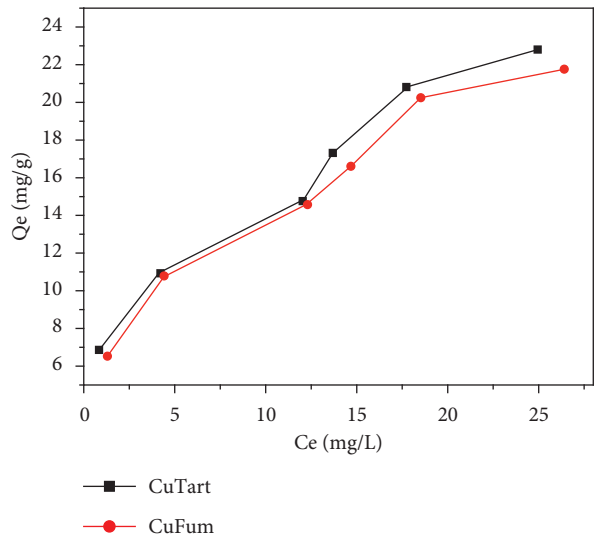

Figure 6: Effect of initial concentration on the adsorption of phenacetin onto CuTart and CuFum.

The analysis in Table 2 shows that among the two-parameter isotherms studied, the Freundlich model is the one that best describes the metal carboxylate adsorption phenomenon. This is due to its coefficient of determination which tends toward 1 and the values of the error functions which are lower than those obtained by the other models. The validation of the Freundlich model allows us to say that it is a multilayer adsorption on a heterogeneous surface for the two adsorbents, and the interactions between the adsorbent's surface and the adsorbate play a significant role in the adsorption process [33]. The value of $1/n$ less than 1 in the Freundlich model shows that there is an affinity between the surface of the materials and the adsorbate solution. These values support the hypothesis that the surfaces of the different materials are heterogeneous [33]. The change in adsorption energy ΔQ obtained from the Temkin model is positive regardless of the material, which means that the adsorption process is exothermic.

By still using Table 3, and considering the three-parameter isotherms, it can be deduced that based on the low error values and the high values of the coefficient of determination, the best representation of the experimental adsorption data is given by the Redlich-Peterson model. This implies that the adsorption of the phenacetin by the different materials takes place on heterogeneous surfaces. Its heterogeneity parameter between 0 and 1 shows that the model for the adsorption of phenacetin by the adsorbents cannot be reduced to the Langmuir isotherm.

This confirms the hypothesis of the two-parameter isotherm, according to which the Freundlich model is that which best describes the adsorption process. The distribution of residues between [−2; 2], around the x-axis shows that the Freundlich and Redlich-Peterson models are more suitable for describing the adsorption process. The asymmetry at the level of the distribution of residuals around the x-axis suggests that the basic model hypothesis is not followed during the adsorption process.where A_{RP} and B_{RP} are models constants of Redlich-Peterson; β is heterogeneity parameter; A is Temkin model constant; $K_{L,}$ Langmuir constant, $K_{LF,}$ Langmuir-Freundlich constant and K_F, Freundlich constant.

3.4. Batch Studies. Pseudo-first order, pseudo-second order, intra-particle diffusion, and Elovich kinetic models were used to investigate and describe the adsorption mechanism. These kinetic models have been presented in non-linear forms (Figure 9) and their calculated parameters are shown in Table 3 below.

The pseudo-first-order model is based on multilayer adsorption on the surface of each adsorbent material. This type of adsorption is based on van der Waal-type interactions between the phenacetin and the copper MOFs. These interactions thus highlight physical adsorption between the adsorbate and the adsorbent. The low values of the error functions of the pseudo-first-order model as well as the coefficient of determination R^2 which tends toward 1 suggest that this model best describes the adsorption of phenacetin by copper (II) fumarate. Also, the pseudo-second-order model highlights π-π interaction between the phenacetin and copper (II) fumarate. These interactions, which are of a chemical nature imply that there is monolayer adsorption. The low values of the error functions of the pseudo-second-order model as well as the coefficient of determination R^2 which tends towards unity plead in favor of this model for the adsorption of phenacetin by copper (II) tartrate. The equilibrium adsorbed amounts, which are close to the experimental amounts in the case of this model suggest that the adsorption of phenacetin by the adsorbents depends on π-π interactions. The Elovich model assumes that the solid surfaces are energetically heterogeneous.

The comparison of the adsorbed quantity of phenacetin from this present work with those obtained from literature are shown in Table 4 below.

By comparing the adsorbed quantities of phenacetin by copper (II) fumarate (25.158 mg/g) and by copper (II) tartrate

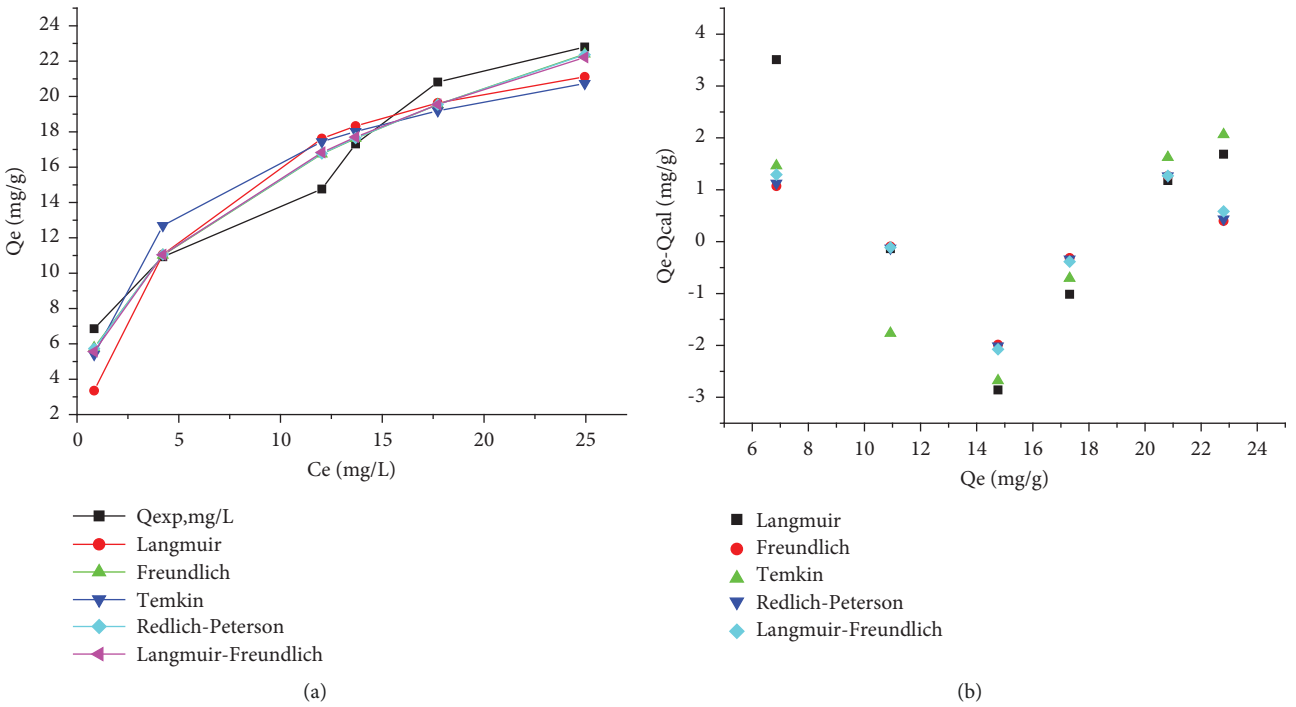

Figure 7: Non-linear isotherm (a) and residual (b) plot for copper(II) tartrate (CuTart).

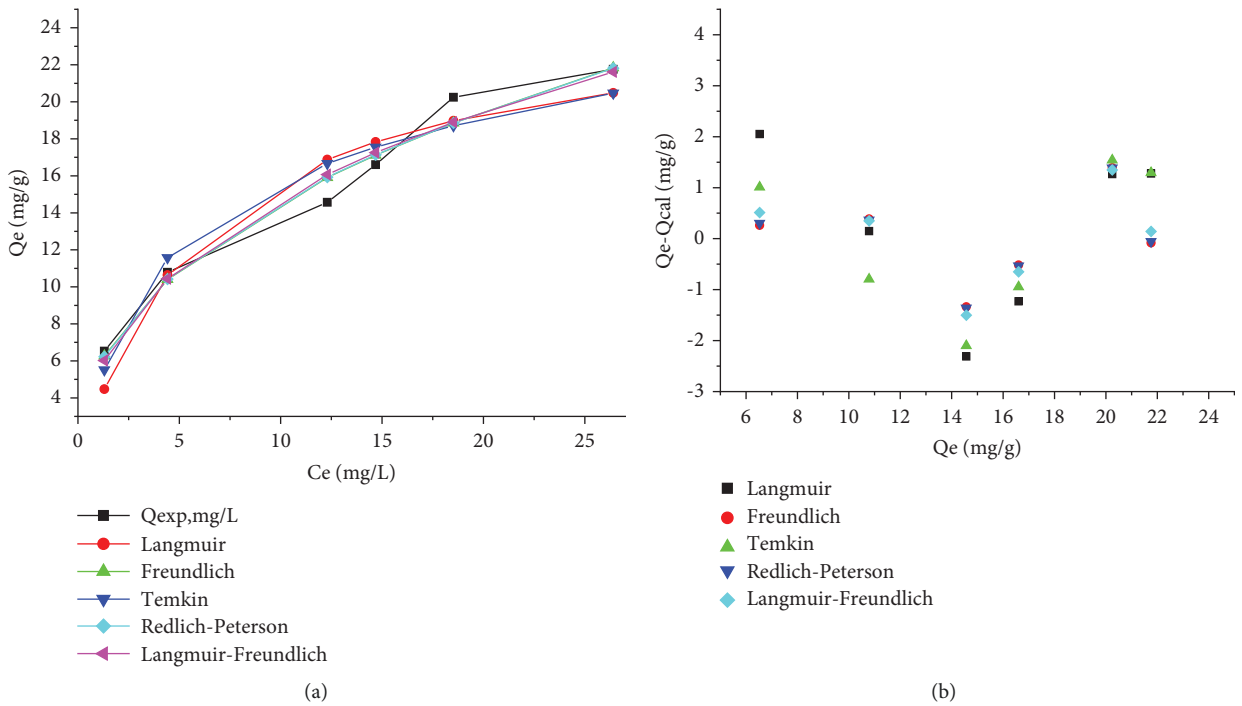

Figure 8: Non-linear isotherm (a) and residual (b) plot for copper(II) fumarate (CuFum).

Table 2: Adsorption of phenacetin: non-linear fitting analysis for two and three parameter isotherms.

N°	Models	Constants	Values	R^2	SSE	χ^2	ARE	RMSE
CuTart								
1.	Langmuir	Q_m (mg/g) K_L (L/mg)	25.906 0.176	0.899	25.75	4.398	15.109	2.537
2.	Freundlich	$1/n$ K_F (L/g)	0.399 6.204	0.963	6.963	0.529	6.594	1.319
3.	Temkin	ΔQ (kJ/mol) A (L/mg)	547.466 3.920	0.890	19.828	1.424	12.763	2.228
4.	Redlich-peterson	A_{RP} (L.mg^2/g) B_{RP} β	163.981 25.620 0.609	0.962	7.238	0.561	6.850	1.345
5.	Langmuir-freundlich	Q_m (mg/g) K_{LF} (L^{β}.mg$^{-\beta}$) β	118.358 0.001 0.455	0.959	8.081	0.662	7.466	1.421
CuFum								
6.	Langmuir	Q_m (mg/g) K_L (L/mg)	25.158 0.166	0.929	14.33	1.509	11.370	1.893
7.	Freundlich	$1/n$ K_F(L/g)	0.415 5.611	0.933	4.215	0.256	4.521	1.026
8.	Temkin	ΔQ (kJ/mol) A (L/mg)	498.459 2.326	0.933	11.001	0.764	9.417	1.658
9.	Redlich-peterson	A_{RP} (L.mg^2/g) B_{RP} β	130.178 22.449 0.593	0.975	4.293	0.263	4.618	1.036
10.	Langmuir-freundlich	Q_m (mg/g) K_{LF} (L^{β}.mg$^{-\beta}$) β	8366 0.004 0.500	0.971	4.897	0.317	5.437	1.106

Table 3: Kinetic data obtained by non-linear fitting analysis.

N°	Models	Constants	Values	R^2	SSE	χ^2	ARE	RMSE
CuTart								
1.	Pseudo-first order	Q_e (mg/g) K_1 (1/min)	20.389 0.257	0.809	6.715	0.363	3.606	0.918
2.	Pseudo-second order	Q_e (mg/g) K_2 (g/min.mg)	21.293 0.024	0.940	1.798	0.095	1.862	0.474
3.	Elovich	α (mg/g.min) β (g/mg)	7389.66 0.609	0.854	4.320	0.217	3.049	0.735
4.	Intraparticle diffusion model	K_p (mg/g.min$^{0.5}$) C (mg/g)	0.521 16.213	0.679	9.513	0.491	4.72	1.090
CuFum								
1.	Pseudo-first order	Q_e (mg/g) K_1 (1/min)	66.202 0.017	0.986	0.298	0.023	1.056	0.193
2.	Pseudo-second order	Q_e (mg/g) K_2 (g/min.mg)	16.114 0.022	0.925	2.114	1.637	2.854	0.514
3.	Elovich	α (mg/g.min) β (g/mg)	348.238 0.618	0.931	1.818	0.120	2.488	0.476
4.	Intraparticle diffusion model	K_p (mg/g.min$^{0.5}$) C (mg/g)	0.540 10.894	0.809	5.122	0.353	4.716	0.800

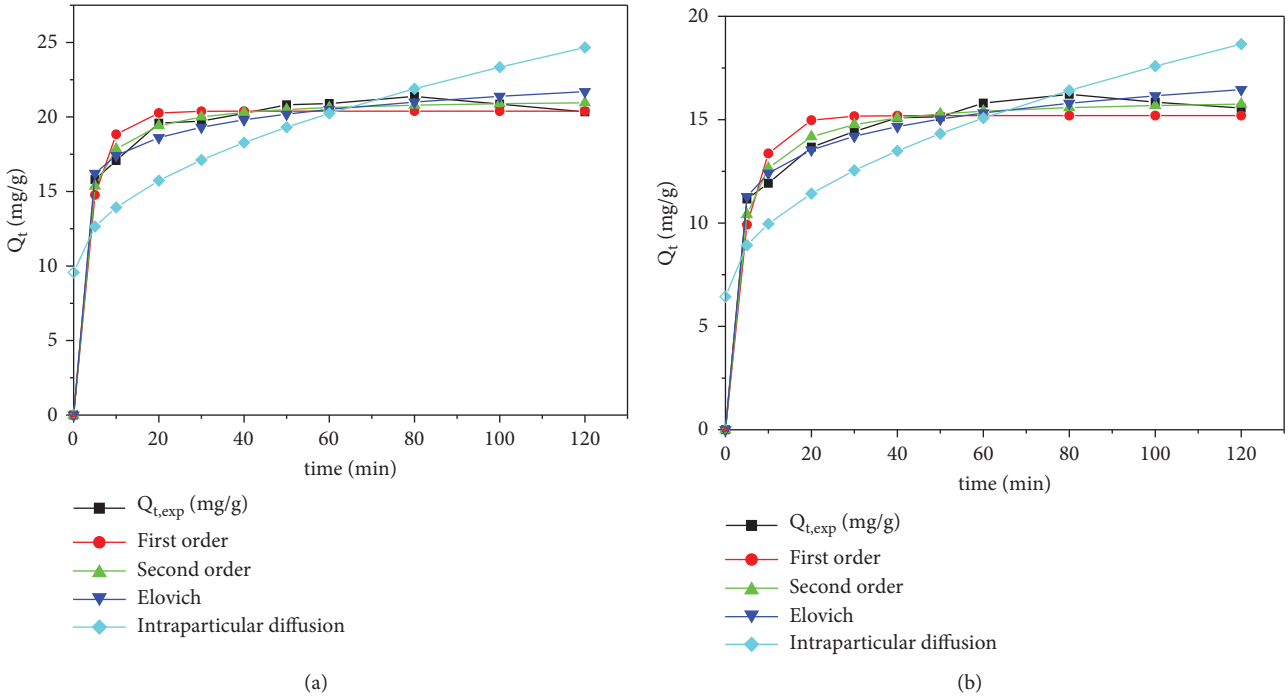

Figure 9: Non-linear kinetic adsorption plot onto CuTart (a) and CuFum (b).

Table 4: Comparison of adsorption capacity of phenacetin.

Adsorbents	Quantity of phenacetin adsorbed	References
BP1M	13.18 mg/g	[34]
P1M	7.40 mg/g	[34]
B1M	4.11 mg/g	[34]
CuFum	25.158 mg/g	Present work
CuTart	25.906 mg/g	Present work

(25.906 mg/g) and that adsorbed by activated carbons BP1M (13.18 mg/g), P1M (7.40 mg/g) and B1M (4.11 mg/g) [34], the adsorbed quantities obtained from this work is greater than those obtained in the literature. These coordination compounds are potentials adsorbent of phenacetin.

4. Conclusion

In this work, two porous coordination compounds, CuFum and CuTart have been used for the adsorption of phenacetin in an aqueous solution. These compounds were characterized using elemental analysis, IR spectroscopy, thermogravimetric analysis, and powder XRD. The different results obtained enabled us to propose the chemical formulas and then to deduce the structures of the two coordination compounds. Batch adsorption studies showed that increasing the initial concentration of phenacetin enhances the interaction between it and the coordination compounds, resulting in an increase in adsorption capacity. According to the different error functions and coefficients of determination, the kinetic studies show that the adsorption data best fitted by the pseudo-second-order model is more appropriate to describe the adsorption of phenacetin by CuTart, while for CuFum the pseudo-first-order model is the most appropriate. This indicates that the adsorption of phenacetin on CuTart may be due to chemical interactions while for CuFum it may be due to physical interactions. Isotherm models confirmed that the system is heterogeneous and the adsorption is physical in nature. This study shows that these coordination polymers are suitable for the adsorption of pharmaceutical compounds.

Data Availability

The data used to support the findings of the study can be obtained from the corresponding author upon request.

Conflicts of Interest

The authors have declared no conflicts of interest regarding the publication of this study.

Acknowledgments

This work was the result of the thesis work of the student (now Dr. Alvine Djoumbissie).

References

[1] F. Velázquez, R. Manríquez, L. Maya, L. Barrientos, and F. López-Dellamary, "Phenacetin isolated from *Bursera grandifolia*, a herbal remedy with antipyretic properties," *Natural Product Communications*, vol. 4, no. 11, 2009.

[2] E. M. Glenn, B. J. Bowman, and N. A. Rohloff, "Anti inflammatory and PG inhibitory effects of phenacetin and acetaminophen," *Agents and Actions*, vol. 7, no. 5-6, pp. 513–516, 1977.

[3] L. P. Seegers, P. Z. Jager, and J. Noordwijk, "The anti-inflammatory, analgesic and antipyretic activities of non-

narcotic analgesic drug mixtures in rats," *Archives Internationales de Pharmacodynamie et de Therapie*, vol. 251, pp. 237–254, 1981.

[4] Y. Nagata and A. Masuda, "Bladder tumor associated with phenacetin abuse: a case report and a review of the literature," *Tokai Journal of Experimental & Clinical Medicine*, vol. 32, pp. 86–89, 2007.

[5] K. Grimland, "Phenacetin and renal damage at a Swedish factory," *Acta Medica Scandinavica*, vol. 174, pp. 3–26, 1998.

[6] P. M. Ronco and A. Flahault, "Drug-induced end stage renal disease," *New England Journal of Medicine*, vol. 331, no. 25, pp. 1711-1712, 1994.

[7] O. A. Kolawole and A. B. Benjamin, "Theoretical investigation on biological activity of phenacetin and its derivatives via DFT and docking approach," *Chemical Science International Journal*, vol. 25, no. 3, pp. 1–7, 2019.

[8] E. K. Putra, R. Pranowo, J. Sunarso, N. Indraswati, and S. Ismadji, "Performance of activated carbon and bentonite for adsorption of amoxicillin from wastewater: mechanisms, isotherms and kinetics," *Water Research*, vol. 43, no. 9, pp. 2419–2430, 2009.

[9] G. N. Ndifor-Angwafor, A. Bopda, D. R. T. Tchuifon, C. S. Ngakou, T. Kuete I-H, and S. G. Anagho, "Removal of paracetamol from aqueous solution by adsorption onto activated carbon prepared from rice husk," *Journal of Chemical and Pharmaceutical Research*, vol. 9, pp. 56–68, 2017.

[10] A. Macías-García, J. García-Sanz-Calcedo, J. P. Carrasco-Amador, and R. Segura-Cruz, "Adsorption of paracetamol in hospital wastewater through activated carbon filters," *Sustainability*, vol. 11, no. 9, pp. 2672–2711, 2019.

[11] D. T. Nguyen, H. N. Tran, R.-S. Juang et al., "Adsorption process and mechanism of acetaminophen onto commercial activated carbon," *Journal of Environmental Chemical Engineering*, vol. 8, no. 6, Article ID 104408, 2020.

[12] G. Corbin, E. Vulliet, B. Lanson, A. Rimola, and P. Mignon, "Adsorption of pharmaceuticals onto smectite clay minerals: a combined experimental and theoretical study," *Minerals*, vol. 11, pp. 62–12, 2021.

[13] R. Coimbra, C. Escapa, M. Otero, and M. Otero, "Adsorption separation of analgesic pharmaceuticals from ultrapure and waste water: batch studies using a polymeric resin and an activated carbon," *Polymers*, vol. 10, no. 9, pp. 958–1015, 2018.

[14] S. h. Lee, O. H. Lin, and R. a. Doong, "Design of size-tunable molecularly imprinted polymer for selective adsorption of acetaminophen," *Clean Technologies and Environmental Policy*, vol. 19, no. 1, pp. 243–250, 2016.

[15] K. Jedynak, B. Szczepanik, N. Rędzia, P. Słomkiewicz, A. Kolbus, and P. Rogala, "Ordered mesoporous carbons for adsorption of paracetamol and non-steroidal anti-inflammatory drugs: ibuprofen and Naproxen from aqueous solutions," *Water*, vol. 11, no. 5, pp. 1099–1120, 2019.

[16] C. R. Gadipelly, K. V. Marathe, and V. K. Rathod, "Effective adsorption of ciprofloxacin hydrochloride from aqueous solutions using metal-organic framework," *Separation Science and Technology*, vol. 53, no. 17, pp. 2826–2832, 2018.

[17] Z. Luo, S. Fan, J. Liu et al., "A 3D stable metal–organic framework for highly efficient adsorption and removal of drug contaminants from water," *Polymers*, vol. 10, no. 2, pp. 209–223, 2018.

[18] M. T. M. Al-Dajani, H. H. Abdallah, N. Mohamed, M. Hemamalini, and H.-K. Fun, "Diaquabis (hydrogentartrato) copper (II) dehydrate," *Acta Crystallographica Section E, Structure Reports*, vol. 66, pp. 774-775, 2010.

[19] N. V. O. Sousa, V. C. Tecia, S. B. Honorato et al., "Coconut bagasse treated by thiourea/ammonia solution for cadmium removal: kinetics and adsorption equilibrium," *Biotechnology Resource*, vol. 7, pp. 1504–1524, 2012.

[20] H. M. F. Freundlich, "Over the adsorption in solution," *Zeitschrift fur Physikalische Chemie*, vol. 57A, pp. 385–470, 1906.

[21] E. W. Shin and R. M. Rowell, "Cadmium ion sorption onto lignocellulosic biosorbent modified by sulfonation: the origin of sorption capacity improvement," *Chemosphere*, vol. 60, no. 8, pp. 1054–1061, 2005.

[22] S. Rangabhashiyam, N. Anu, M. Giri Nandagopal, and N. Selvaraju, "Relevance of isotherm models in biosorption of pollutants by agricultural by products," *Journal of Environmental Chemical Engineering*, vol. 2, no. 1, pp. 2398–2414, 2014.

[23] O. Redlich and D. L. Peterson, "A useful adsorption isotherm," *Journal of Physical Chemistry*, vol. 63, no. 6, p. 1024, 1959.

[24] Y. S. Ho and G. McKay, "Pseudo-second order model for sorption processes," *Process Biochemistry*, vol. 34, no. 5, pp. 451–465, 1999.

[25] S. H. Chien and W. R. Clayton, "Application of elovich equation to the kinetics of phosphate release and sorption in soils," *Soil Science Society of America Journal*, vol. 44, no. 2, pp. 265–268, 1980.

[26] R. L. Tseng, F. C. Wu, and R. S. Juang, "Liquid phase adsorption of dyes and phenols using pinewood-based activated carbons," *Carbon*, vol. 41, no. 3, pp. 487–495, 2003.

[27] G. B. Deacon and R. J. Phillips, "Relationships between the carbon-oxygen stretching frequencies of carboxylato complexes and the type of carboxylate coordination," *Coordination Chemistry Reviews*, vol. 33, no. 3, pp. 227–250, 1980.

[28] K. Mészáros Szécsényi, V. M. Leovac, Ž. K. Jaćimović et al., "Transitionmetal complexes withpyrazole-based ligands part 8 characterization and thermal decomposition of zinc (II) complexes with di- and trisubstitutedpyrazoles," *Journal of Thermal Analysis and Calorimetry*, vol. 63, no. 3, pp. 723–732, 2001.

[29] K. Nakamoto, *Infrared and Raman Spectra of Inorganic and Coordination Compounds Part B: Applications in Coordination, Organometallic, and Bioinorganic CHEMISTRY*, John Wiley & Sons, Hoboken, New Jersey, USA, 2009.

[30] S. Ariponnammal and R. Velvizhi, "Structural, spectroscopic, and magnetic studies on copper tartrate crystals," *Zeitschrift für Naturforschung A*, vol. 74, no. 9, pp. 813–819, 2019.

[31] T. D. R. Tchuifon, S. G. Anagho, G. N. Nche, and J. M. Ketcha, "Adsorption of salicylic and sulfosalicylic acid onto powdered activated carbon prepared from rice and coffee husks," *International Journal of Current Engineering and Technology*, vol. 5, pp. 1641–1652, 2015.

[32] S. Chowdhury and P. Saha, "Sea shell powder as a new adsorbent to remove basic green 4 (malachite Green) from aqueous solutions: equilibrium, kinetic and thermodynamic studies," *Chemical Engineering Journal*, vol. 164, no. 1, pp. 168–177, 2010.

[33] I. H. T. Kuete, D. R. T. Tchuifon, G. N. Ndifor-Angwafor, A. T. Kamdem, and S. G. Anagho, "Kinetic, isotherm and thermodynamic studies of the adsorption of thymol blue onto powdered activated carbons from garcinia cola nut shells impregnated with H_3PO_4 and KOH: non-linear regression Analysis," *Journal of Encapsulation and Adsorption Sciences*, vol. 10, no. 01, pp. 1–27, 2020.

[34] C. Ngakou, H. M. Ngomo, and S. G. Anagho, "Batch equilibrium and effects of ionic strength on kinetic study of adsorption of phenacetin from aqueous solution using activated carbon derived from a mixture of Ayous sawdust and cucurbitaceae peelings," *Current Journal of Applied Science and Technology*, vol. 26, no. 2, pp. 1–24, 2018.

Hindawi
Journal of Chemistry
Volume 2022, Article ID 2857700, 12 pages
https://doi.org/10.1155/2022/2857700

Research Article

Characteristics of Water Pollution and Evaluation of Water Quality in Subsidence Water Bodies in Huainan Coal Mining Areas, China

Xinyue Deng[1,2] and Guangzhou Chen[1,2,3]

[1]*Anhui Key Laboratory of Water Pollution Control and Waste Water Recycling, Hefei 230601, Anhui, China*
[2]*Anhui Key Laboratory of Environmental Pollution Control and Waste Resource Utilization, Hefei 230601, Anhui, China*
[3]*Anhui Research Academy of Ecological Civilization, Hefei 230601, Anhui, China*

Correspondence should be addressed to Guangzhou Chen; chgzh5@163.com

Received 22 April 2022; Accepted 8 June 2022; Published 15 July 2022

Academic Editor: Jun Wu

The subsidence water bodies in coal mining areas are vulnerable to being polluted by the surrounding mining production wastewater, domestic sewage, and agricultural return flow. Therefore, it is important to grasp the water quality condition of the above water bodies. A total of 16 surface water samples from 7 different subsidence water bodies in the Huainan mining area were collected and focused on the selection of 22 water quality indicators for water pollution characteristics analysis. The result of correlation analysis showed that Cr and Zn came from the same source of pollution. Three principal factors were selected by factor analysis, which could explain 82.294% of the total variance. Principal factor 1 indicated a mixture of pollution related to nitrogen and phosphorus nutrients, organic pollutants, and heavy metals; principal factor 2 showed heavy metal pollution; and principal factor 3 presented the pollution from heavy metals and cations. Results of cluster analysis showed that the water quality status of 16 sampling points could be divided into 4 clusters. The results of the heavy metal pollution index method showed that the heavy metal pollution was most serious in sample 9 (S9), S15, and S16, and the main elements of pollution were Ni, Fe, and Mn. Single-factor evaluation, comprehensive pollution index, the universal exponential formula of logarithmic power function, and membership degree method were used to evaluate the five important water quality indicators, namely total nitrogen, ammonia nitrogen, total phosphorus, dissolved oxygen, and chemical oxygen demand. The results showed that the total nitrogen pollution in the study area was more serious, most of the sites exceed class V standards of the surface water, S14 and S16 were heavily polluted. Based on the comparison of the different methods, the surface water quality in the study area can be reflected more comprehensively.

1. Introduction

In China, the proportion of coal in total energy consumption has been reduced from 70.7% (1978) to 56.8% (2020) [1], but the consumption of coal still occupies a large proportion. Long-term mining activities result in surface subsidence, which has caused irreversible impacts on the geological environment of coal mining areas [2]. The area of subsidence water bodies is expanding and has become a special kind of surface water body [3]. At present, the coal mining subsidence area is about 7262.17 hm^2 and more than 70% is subsidence water bodies [4]. They are easily polluted and the ecological environment is easily damaged. Therefore, it is important to choose a scientific method to assess the water quality of subsidence water bodies to realize the sustainable development of mining areas.

In the 1980s, the environmental problems caused by the subsidence of coal mining areas in Huainan were noticed [5]. Early studies evaluated the water ecological environment states by employing the frequently used water quality indicators (transparency, total phosphorus, total nitrogen, permanganate index, etc.), conducted water resources investigation and research on eutrophication characteristics in the subsidence areas, and analyzed the functional uses of the water body [6, 7].

Pei et al. used the comprehensive nutrition state index method to assess the eutrophication state of the subsidence water bodies of Yangzhuang village in Panji, and the result

was mild-moderate eutrophication [8]. Qu et al. concluded that the nitrogen to phosphorus ratio (N:P = 25–117) of the subsidence water bodies was high with obvious seasonal variation, and the N:P was lower in the growing season than in other seasons [9]. Subsequently, heavy metal contamination of the water bodies raised concerns. Wang et al. determined Cd, Cu, Pb, and Zn in different tissues of crucian carp, and concluded that the aquatic ecosystem was not contaminated by them, the metal concentrations were lower than the regulations for cultured fish [10]. In risk assessment, Chen et al. evaluated the health risk of heavy metals (Cu, Ni, Pb, Cd, Co, Cr, As, Hg, etc.) in the subsidence water bodies based on the Monte Carlo method; the results showed that the total carcinogenic risk values for two exposure pathways of Cr, Ni, and As were greater than the maximum acceptable level, and the highest carcinogenic risk was found in the water body of Xinji'er mine [11].

In recent years, various water quality evaluation methods have been put forward, it is helpful to identify the pollutant characteristics and clarify the water quality objectives. Liu et al. selected four evaluation methods, including single-factor evaluation, comprehensive pollution index, graded evaluation, and comprehensive water quality identification index method to compare, and concluded that the evaluation results of the comprehensive water quality identification index were reliable and applicable to the water quality evaluation of coal mine subsidence water bodies [12]. In the evaluation process of groundwater quality in Urumqi city, Wang et al. calculated the weight of water quality indexes by the fuzzy synthesis evaluation coupled grey relational analysis (GRA-fuzzy), and concluded that it was better than the single-factor evaluation and Nemero synthesis index evaluation method [13]. Liu and Zheng thought that the modified comprehensive water quality identification index (WQI) method not only overcame the shortcomings of single-factor evaluation but also took into account the impact of multiple indicators [14]. In addition, there were other water quality evaluation methods, such as the fuzzy comprehensive evaluation method [15], T-S fuzzy neural network method [16], and grey correlation analysis method [17].

The above studies have achieved some results, but the selection of subsidence water bodies was not comprehensive enough, and usually only the several typical water bodies were analyzed [18, 19]. In addition, the single evaluation method, that was frequently used, was not conducive to the mutual verification and comparison between evaluation results. Therefore, to understand the pollution situation of Huainan subsidence water bodies more scientifically and reasonably, a more comprehensive water quality evaluation was needed.

The research objectives of this article were (1) to analyze water pollution characteristics of subsidence water bodies based on water quality monitoring data to understand the pollution status of subsidence water bodies; (2) to use the factor analysis model to identify pollution sources; and (3) to provide a scientific basis for water resources development and pollution prevention by comparing four water quality evaluation results.

2. Materials and Methods

2.1. Study Area and Locations of the Samples. Huainan mining area is located on both sides of the Huai River in northern Anhui Province, and spans the cities of Huainan and Fuyang, with an area of about 3200 km^2. The advantageous geographical location and convenient transportation provide convenient conditions for the mining and transportation of coal resources [20]. The prospective coal reserve reaches 44.4 billion tons, and the proven reserve reaches 15.3 billion tons [21]. Due to the ground subsidence caused by coal mining, the cumulative area of the subsidence area was about 316.81 km^2 by the end of 2019 [22]. With the continuous mining of coal, the subsidence area is increasing and the area of subsidence water bodies is expanding. According to the spatial distribution of subsidence water bodies, 7 subsidence water bodies were selected, 16 sampling points were set up, and the specific points were shown in Figure 1 (Due to the short distance, some points may be blocked). In addition to the consideration of physical and chemical parameters and nutrient indexes (pH, total hardness, ammonia nitrogen, NO_3^-, TN, and TP), oxygen-consuming organic matter index (DO, COD, and TOC), cations and anions (K^+, Na^+, Mg^{2+}, Cl^-, and F^-), this study selected 8 heavy metal indexes (Cu, Zn, Cr, As, Pb, Ni, Fe, and Mn) that were more concerned in subsidence water bodies to evaluate the water quality of the study area, and a total of 22 indexes were selected.

2.2. Collection of Water Samples and Test. The water samples from the subsidence water bodies were collected on February 18–19, 2021. Standard water sampling bottles were used to hold the water samples, and the collected samples were pretreated according to different measurement indexes by selecting the corresponding pretreatment methods. Then they were stored away from light and transported to the laboratory for testing. At each sampling point, pH, water temperature, and dissolved oxygen (DO) were measured on-site using an HQ40D portable multi-parameter water quality analyzer. Chemical oxygen demand (COD), total organic carbon (TOC), total nitrogen (TN), total phosphorus (TP), ammonia nitrogen, nitrate ion (NO_3^-), total hardness, K^+, Na^+, Mg^{2+}, F^-, Cl^-, Cu, Zn, Cr, As, Pb, Ni, Fe, and Mn were brought back to the professional testing institution for testing. The testing standards of the water quality indexes involved in this article were shown in the supplementary materials (Section 2.2).

2.3. Water Quality Assessment Methods

2.3.1. Single-Factor Evaluation Method. The single-factor evaluation method determines the comprehensive water quality category according to the category of the single index with the worst water quality among all the water quality indexes involved in the evaluation [23]. The selected indicators (COD, TN, TP, ammonia nitrogen, and DO) were compared with Environmental quality standards for surface water (GB3838-2002) [24], and the thresholds for the five

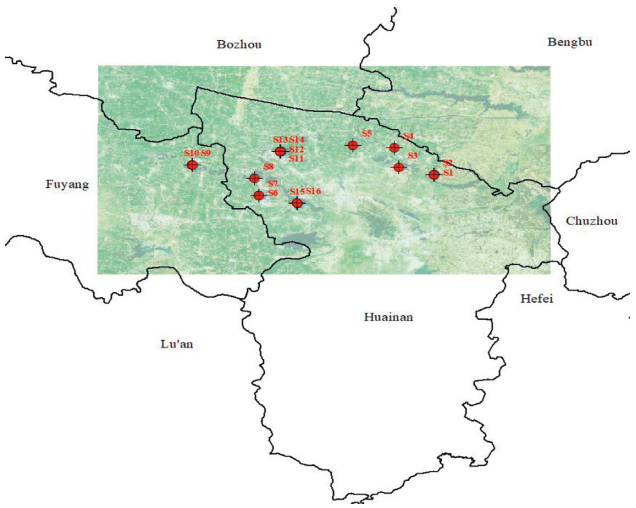

FIGURE 1: Sampling points located in the coal mining subsidence water area of Huainan, China.

levels of standards were shown in Table S1 (supplementary Table 1). In this study, the class V standard was selected as the reference standard and calculated by equation (1):

$$P_i = \frac{C_i}{C_0}, \tag{1}$$

where C_i is i^{th} pollutant concentration value (mg/L), C_0 is i^{th} pollutant evaluation standards (mg/L), and P_i is i^{th} pollutant pollution index.

2.3.2. Comprehensive Pollution Index Method. The comprehensive pollution index method assumes that the contribution of each factor to water quality is basically the same, and calculates the arithmetic mean of the sum of the standard indices of each factor. The method can determine the degree of pollution of the study water bodies [25], which is calculated by equation (2):

$$P = \frac{1}{m}\sum_{i=1}^{m} P_i, \tag{2}$$

where P_i is the pollution index of pollutant i.

The comprehensive pollution index corresponding to the classification of water quality is as follows [26]: $P \le 0.25$, clean; $0.25 < P \le 0.4$, relatively clean; $0.4 < P \le 0.5$, light pollution; $0.5 < P \le 0.99$, medium pollution; and $P \ge 1$, heavy pollution.

2.3.3. Universal Exponential Formula of Logarithmic Power Function. The Environmental Quality Standard for Surface Water (GB3838-2002) divides the water quality evaluation criteria into five levels, and the concentration limits of the environmental quality level 5 standards for some indicators were shown in Table S2. After optimizing the parameters, the universal exponential formula of the logarithmic power function was as follows [27]:

$$\mathrm{WQI}_j = 0.0466 * \left(\ln x_j\right)^{2.1029}, \tag{3}$$

where x_j is the "normative value" of the indicator j listed in Table S2, calculated by equation (4):

$$x_j = \begin{cases} \left(\dfrac{c_{j0}}{c_j}\right)^2, & c_j \le c_{j0}, \text{For the DO,} \\ \left(\dfrac{c_j}{c_{j0}}\right)^2, & c_j \ge c_{j0}, \text{For the CODcr, dissolved iron,} \\ \left(\dfrac{c_j}{c_{j0}}\right)^{1/2}, & c_j \ge c_{j0}, \text{For Zn, Hg, petroleum, } \textit{Escherichia coli}\text{, volatile phenols, CN,} \\ \dfrac{c_j}{c_{j0}}, & c_j \ge c_{j0}, \text{For the remaining 12 indicators in the original table,} \\ 1, & c_j > c_{j0}, \text{For the DO,} \\ 1, & c_j < c_{j0}, \text{Other indexes except dissolved oxygen.} \end{cases} \tag{4}$$

The formula for the composite index of the m indicator is as follows:

$$\mathrm{WQI} = \sum_{j=1}^{m} W_j * \mathrm{WQI}_j, \tag{5}$$

where W_j is the normalized weight of index j.

2.3.4. Membership Degree Method. The membership degree method refers to a pollution indicator that belongs to a certain category of standard degree, in the same category, the greater affiliation of water quality is worse, and the smaller affiliation of water quality is better [28], can be calculated by equation (6):

$$y = \frac{x - x_0}{x_1 - x_0}, \tag{6}$$

where y is the membership degree corresponding to the type of water quality specified in x_1, x is the measured value (mg/L) and x_0 and x_1 are the standard values of two adjacent levels of x ($x_0 < x < x_1$).

2.3.5. Heavy Metal Pollution Index (HPI). The heavy metal pollution index method is a method for comprehensive evaluation of water quality pollution caused by various heavy metals in water bodies based on the weighted arithmetic mean method that can be calculated by equations (7)–(9) [29-31]:

$$W_i = \frac{k}{S_i}, \tag{7}$$

$$Q_i = \frac{100C_i}{S_i}, \tag{8}$$

$$\mathrm{HPI} = \frac{\sum_{i=1}^{n}(Q_i W_i)}{\sum_{i=1}^{n} W_i}, \tag{9}$$

where S_i is the standard value of the concentration of heavy metal i in the water body (μg/L); k is the proportionality constant, taken as 1; C_i is the measured concentration of heavy metal i in the water body (μg/L); Q_i is the quality level evaluation of heavy metal i; HPI is the heavy metal pollution index; n is the number of heavy metal elements involved in the evaluation; W_i is the weight of heavy metal i, which is regarded as an inversely proportional value to S_i in the model.

Generally, the critical pollution index of the HPI value is set at 100 [32]. However, Edet and Offiong divided the degree of heavy metal pollution into three levels (high, medium, and low): when HPI > 30, the degree of pollution is high; when $15 \le \mathrm{HPI} \le 30$, the degree of pollution is moderate; and when HPI < 15, the degree of pollution is low [33].

2.4. Statistical Analysis Methods. IBM SPSS 23.0 software was used for statistical analysis of the data, including Pearson correlation analysis, one-way ANOVA, factor analysis, and cluster analysis.

3. Results and Discussion

3.1. Characteristics of Water Quality Factors

3.1.1. Physical and Chemical Parameters and Nutrient Indexes. The physicochemical parameters and nutrient indicators measured in this study included pH, total hardness, ammonia nitrogen, NO_3^-, TN, and TP. The pH of 16 sampling sites ranged from 7.25–8.84, which belonged to medium alkaline water bodies (pH = 6–10) [34], and met the pH standard limits (6–9) in the Environmental Quality Standards for Surface Water (GB3838-2002), and most of the sampling sites could also meet the requirements of the pH value of the Water Quality Standard for Fisheries (GB11607-89; pH = 6.5–8.5) [35] and the total hardness ranged from 155 to 260 mg/L with an average value of 199 mg/L. Moreover, the content of ammonia nitrogen ranged from 0.338 to 1.060 mg/L, and all of them reached the water quality standard of surface water category IV (1.5 mg/L). The content of NO_3^- ranged from 0.016 to 5.640 mg/L and all sampling sites reached the standard limit (10 mg/L). The content of TN and TP at each sampling point was shown in Figure 2. As seen in Figure 2(a), the content of TN ranged from 1.87 to 5.46 mg/L and exceeded the surface water class V standard (2.0 mg/L) at all sites except for S15. In the end, the content of TP ranged from 0.06 to 0.74 mg/L in Figure 2(b), except for S8, S14, and S16 which exceeded the surface water class V standard (0.4 mg/L), and all other sampling points could meet the class V standard of surface water. Overall, the total nitrogen index exceeded the standard more seriously.

3.1.2. Oxygen Consuming Organic Matter Index. The content of DO and COD at each sampling point was shown in Figure 3. DO is an important indicator of the self-purification ability of water bodies. Generally speaking, the higher the dissolved oxygen in water, the better the water quality. However, due to the overgrowth of algae, DO may be oversaturated [20], which can have adverse effects on fish. The content of DO in the study area ranged from 7.15 to 15.29 mg/L (water temperature was 11.2–15.6°C), and the average content of DO was 10.6 mg/L, which could meet the surface water class I standard (7.5 mg/L) except for sampling site S1. COD indicator can represent the pollution degree of water bodies by organic matter to a certain extent. The greater the COD, the more serious the pollution of water bodies by organic matter. The content of COD measured in this study ranged from 16 to 49 mg/L, with an average value of 30.56 mg/L. Except for S14 and S16, which exceeded the surface water class V standard (40 mg/L), the other sampling sites met the standard. TOC is an indicator of organic content directly expressed as the amount of carbon in the water sample, and the higher the TOC value, the higher the organic content in the water. The content of TOC measured in the study area ranged from 0.8 to 12.1 mg/L, with an average value of 8.31 mg/L.

3.1.3. Heavy Metal Index. Heavy metal pollutants have the characteristics of easy accumulation, difficult decomposition, and strong toxicity [36, 37]. Heavy metals entering the water environment will cause serious and lasting environmental pollution to rivers and lakes, and enrich the environment through the food chain in organisms step by step [38], which will also be harmful to humans. In this study, the contents of eight heavy metals, including Cu, Zn, Cr, As, Pb, Ni, Fe, and Mn, were detected to study the heavy metal pollution in subsidence water bodies. The contents of Cu, Cr, and Pb were 0.97–2.46 μg/L, 0.12–1.08 μg/L, and 0.18–1.19 μg/L, respectively,

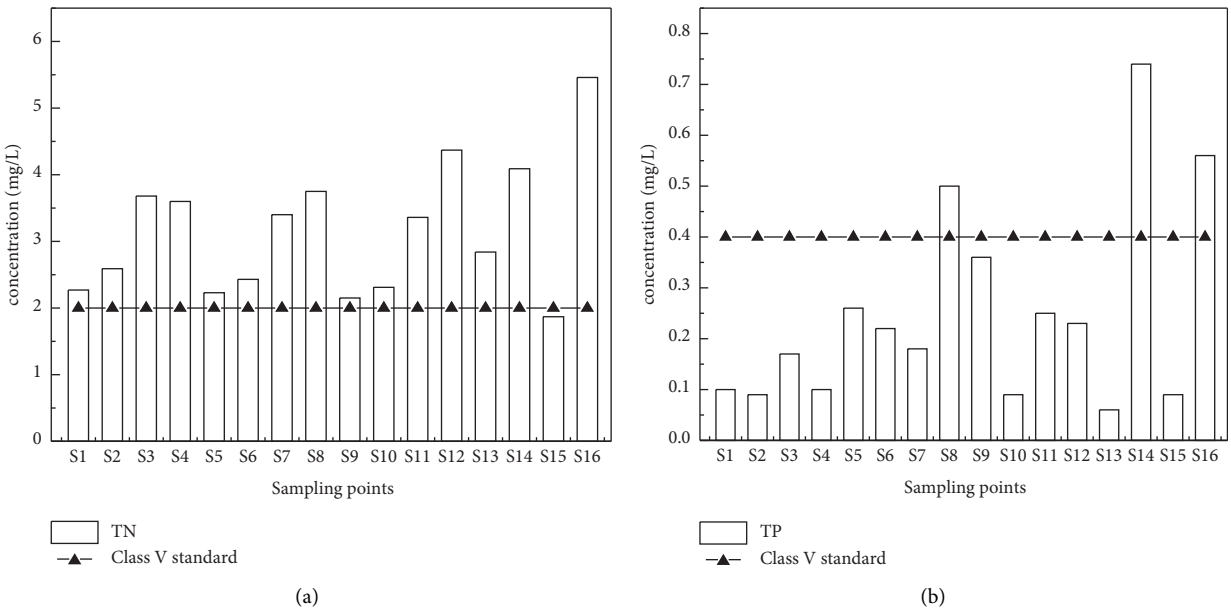

Figure 2: The content of TN (a) and TP (b) at each sampling point in the Huainan coal mining subsidence water bodies.

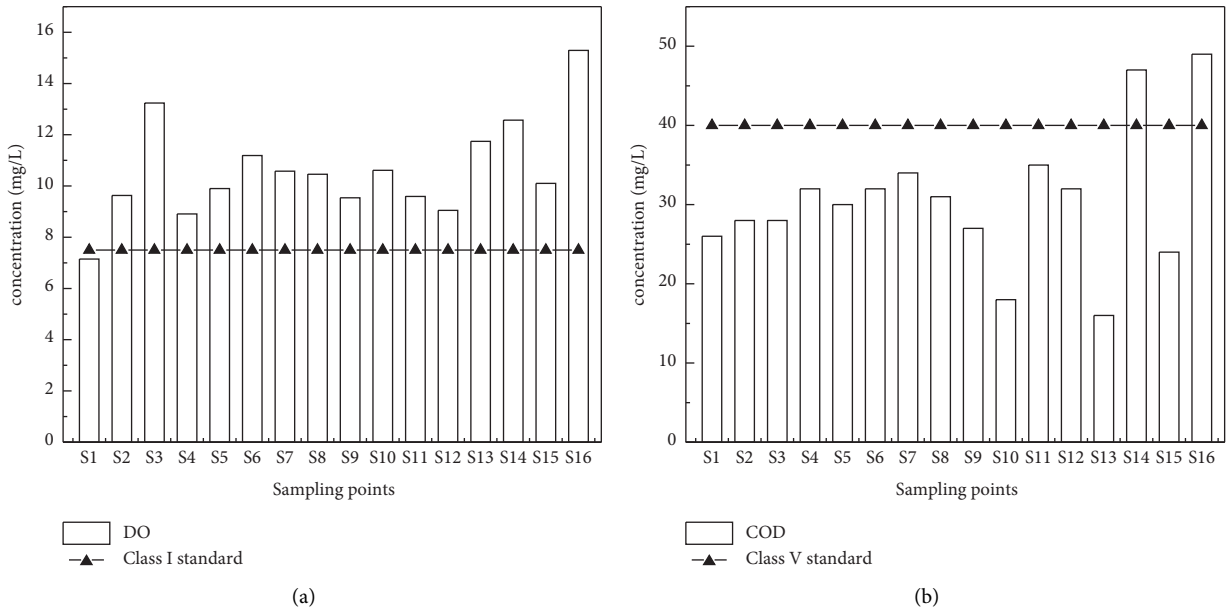

Figure 3: The content of DO (a) and COD (b) at each sampling point in the Huainan coal mining subsidence water bodies.

and all sites reached the surface water class I standard (10 μg/L). The contents of Zn and As were 3.93–17.4 μg/L and 2.14–14.6 μg/L, respectively, and all sampling sites reached the standard of surface water class I (50 μg/L). The content of Ni was 1.12–6.99 μg/L, all of which were lower than the standard limit of specific items for centralized surface water sources of living drinking water (20 μg/L).

The pollution of Fe and Mn was more serious. The content of Fe and Mn was shown in Figure 4. The content of Fe was 34.9–666 μg/L, except for S9 and S10, the rest of the sampling points were lower than the standard limit value of the supplementary project of the centralized surface water source of drinking water (300 μg/L), and the content of Fe at S9 reached 666 μg/L that seriously exceeded the standard. The content of Mn was 18.5–120 μg/L. Except at S4 and S11, the rest of the sites were lower than the standard limit value of the supplementary project of a centralized surface water source for drinking water (100 μg/L). In summary, the concentration of Cu, Zn, Cr, As, Pb, and Ni in the study area was low, but the pollution caused by heavy metal Fe from the Xieqiao coal mine (S9–S10) was more serious.

3.1.4. Other Pollution Indicators. In addition to physico-chemical indicators, nutrients, oxygen-consuming organic matter indicators, and heavy metal indicators, K^+, Na^+, Mg^{2+},

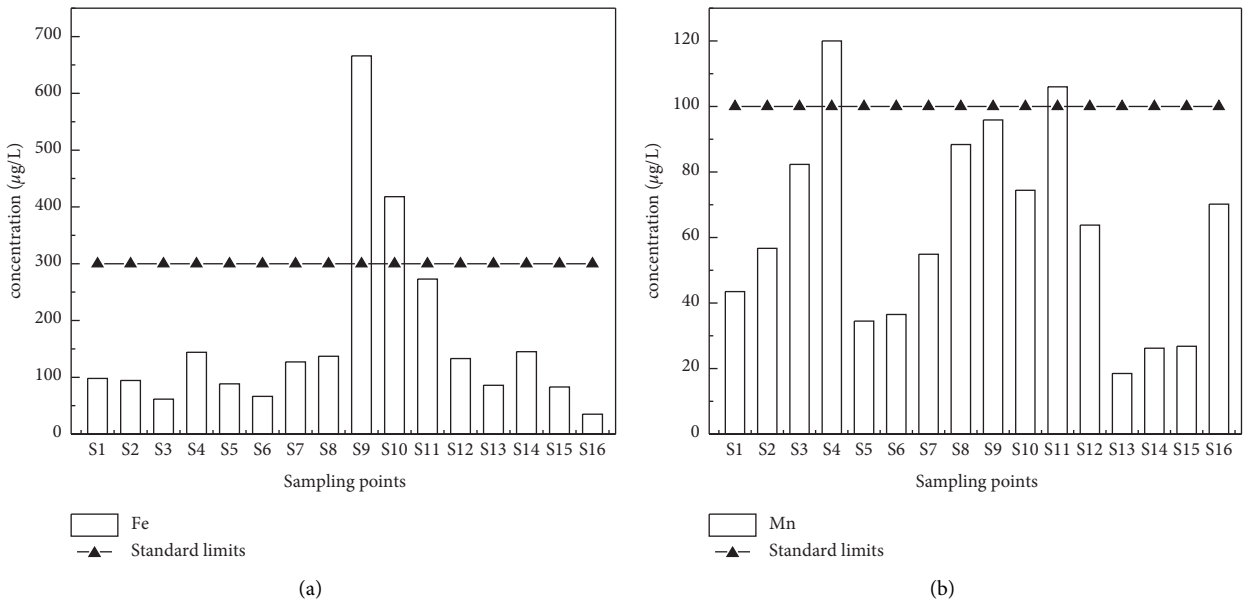

Figure 4: The content of Fe (a) and Mn (b) at each sampling point in the Huainan coal mining subsidence water bodies. (The standard limits of Fe and Mn in the figure refer to the standard limits of supplementary items of centralized surface water sources for drinking water.)

Cl^-, and F^- were also detected in this study. Among them, the pollution of $Cl^-$and F^- was more serious. The content of Cl^- and F^- was shown in Figure 5. Chlorine (Cl) is one of the common elements in coal. During coal combustion, Cl in coal is released in the form of hydrogen chloride or granular Cl [39]. The content of Cl^- in each sampling site ranged from 78.3 to 341 mg/L, among which the Cl^- in S1, S2, S4, S5, S9, S10, and S13 was lower than 100 mg/L. As shown in Figure 5(a), except for S15 and S16, the content of Cl^- at all sampling sites was less than the standard limit (250 mg/L), but the content of Cl^- greater than 50 mg/L is generally considered to be contaminated [20], and it can be seen that the monitoring area has been contaminated by Cl^-, especially S15 and S16 of Xinji'er mine. The concentration of F^- was between 1.10 and 5.45 mg/L. As can be seen in Figure 5(b), only five locations (S4, S7, S9, S10, and S16), reached the surface water class V standard (1.5 mg/L), while the other sampling sites exceeded the standard, among them the Guqiao coal mine (S11–S14) was more seriously polluted. F is an essential trace element for the human body, but it can lead to serious bone diseases if the specific limit value is exceeded [40]. Industrial and civil coal burning, coal gangue, slime, and other solid wastes may lead to fluorine pollution, which belongs to coal fluorine pollution [41].

Based on the above detection results, the pollution of TN in the subsidence water bodies of the study area was serious for all the sample points. At S14 (Guqiao mine) and S16 (Xinji'er mine east), the concentration of TP exceeded the standard and the concentration of COD was high. The content of F^- exceeded the standard at S14, and the content of Fe exceeded the standard seriously at S9 (Xieqiao mine).

3.2. Correlation Analysis. Pearson correlation analysis was performed on 20 water quality indicators (data of Fe and Cl^- that did not satisfy the normal distribution were removed). As seen from the results of the correlation analysis conducted between heavy metals in Figure 6(a), it can be concluded that Pb and Cu have a significant correlation ($P < 0.05$); in addition, there were significant correlations between Cr and Zn ($P < 0.01$) and Cr and Pb ($P < 0.05$). It indicated that Cr and Zn may be contaminated from the same source.

Pearson correlation analysis results of heavy metals with physicochemical properties were showed in Figure 6(b). It revealed that NO_3^- showed a significant positive correlation with Pb and Mn at the 0.05 level. Moreover, heavy metal showed a significant correlation with physicochemical indexes TN, TP, DO, COD, pH, Na^+, and F^-. And they showed an extremely significant positive correlation with TN, TP, and COD at the 0.01 level. Ni was significantly correlated with Na^+, K^+, and ammonia nitrogen, among them Ni showed an extremely significant positive correlation with Na^+ and K^+ at the 0.01 level.

3.3. One-Way ANOVA. To investigate whether there is variability in pollutant concentrations between water bodies with different subsidence times, the 16 sampling sites were divided into three categories according to the age of the subsidence water bodies as older water bodies (S1, S2, S3, S6, S7), middle water bodies (S5, S9, S10, S15, S16), and newer water bodies (S4, S8, S11, S12, S13, S14). After the homogeneity of variance test (Table S3), the one-way ANOVA between different subsidence ages of water bodies was performed for each water quality evaluation index that met the conditions. The results were shown in Table S4, from which it could be concluded that there were significant differences ($P < 0.05$) in Mg^{2+}, F^-, and ammonia nitrogen. Further analysis by multiple comparisons showed that Mg^{2+} differed significantly between medium and new water bodies, F^- differed significantly between new and old

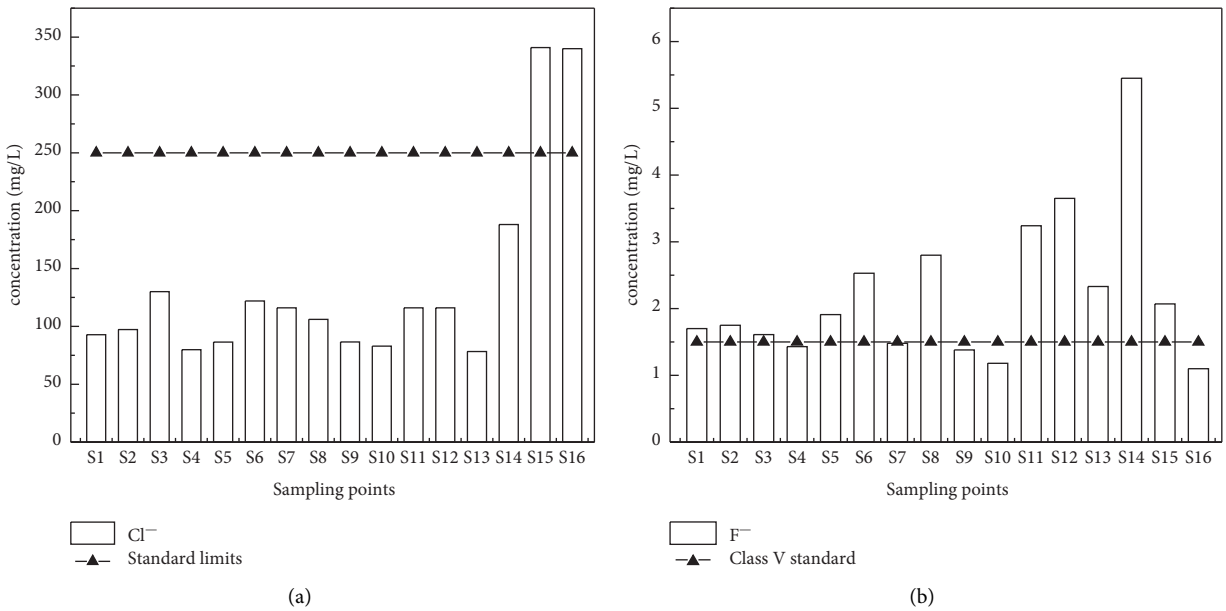

Figure 5: The content of Cl^- (a) and F^- (b) at each sampling point in the Huainan coal mining subsidence water bodies. (The standard limits of Cl^- in the figure refer to the standard limits of supplementary items of centralized surface water sources for drinking water).

water bodies, new and medium water bodies, and ammonia nitrogen differed significantly between old and medium water bodies.

3.4. Identification of Pollution Sources in Subsidence Water Bodies. The data were tested to decide whether they conformed to normal distribution by the one-sample Kolmogorov–Smirnov method. When the distribution of the variables did not conform to the normal distribution, the data needed to be logarithmically transformed, and the data that still did not obey the normal distribution after transformation should be excluded. The article used the KMO to verify the feasibility of the selected water quality factors for factor analysis, and the KMO test value of 0.695 ($P < 0.05$), which was greater than 0.6, so it met the analysis requirements. This article finally selected TN, COD, TP, As, Ni, Na, Cu, Pb, and Cr as the water quality factors for factor analysis.

As seen in Table 1, the first three factors were extracted according to the standard with an eigenvalue greater than 1. The three factors explained 35.511%, 24.868%, and 21.915% of the total variance, respectively, and the cumulative explained 82.294% of the total variance.

To make the obtained principal factors easier to interpret, the rotated factor loading matrix was analyzed. The factor loadings reflected the correlation degree between the main factors and the variables, detailed information was in Table S5. When the factor loadings were greater than 0.75, it indicated a strong correlation, 0.5–0.75 indicated moderate correlation, and 0.3–0.5 indicated weak correlation [42].

The variables with the high factor loadings greater than 0.75 were selected as the main correlation factors. Principal factor 1 mainly reflected TN, TP, COD, and As; principal factor 2 mainly reflected Cu, Pb, and Cr; and principal factor 3 mainly reflected Ni and Na^+. The three principal factors were strongly correlated with their respective main variables. Figure 7 was the three-dimensional graph of factor loadings, through the factor loadings graph, it was conducive to the intuitive display of the relationship between water quality variables.

The meaning of each principal factor was explained as follows: the contribution of the principal factor 1 was the largest, which had the greatest influence. The principal factor 1 was related to nitrogen and phosphorus nutrients, organic pollutants, and heavy metal pollutants, which were mixed pollution. Nitrogen and phosphorus fertilizers in agricultural production in the surrounding areas were used to improve the yield, but it also brought negative effects causing nitrogen and phosphorus loss to pollute the environment of surrounding water bodies. Especially during the rainy period, nitrogen and phosphorus flowed into the subsidence water bodies with surface water led to the increase of nitrogen and phosphorus nutrients [43]. The principal factor 2 was closely related to heavy metal pollution, which might come from coal gangue leaching, and the leaching water contains some toxic heavy metal elements [20]. The principal factor 3 was influenced by both heavy metals and cations.

The results of the factor scores were shown in Table S6. The higher the factor score, the more serious the sampling site was affected by this pollution. Among all sampling sites, S16 and S14 were the two most seriously polluted by TN, COD, TP, and As. S9 and S11 were subjected to the most

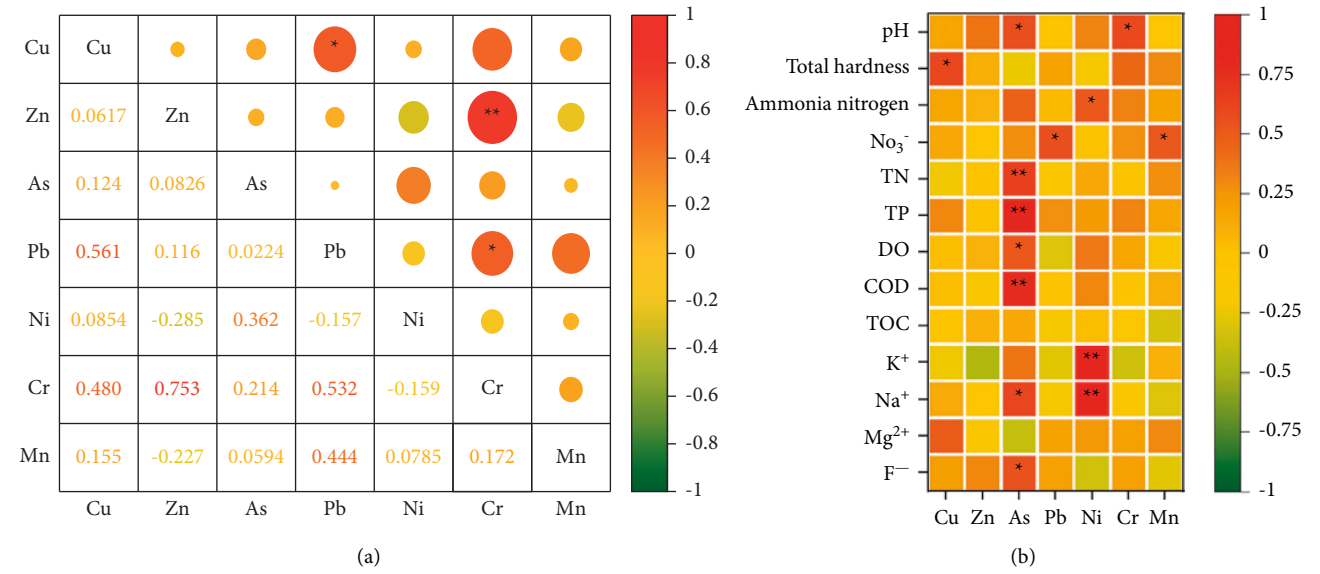

Figure 6: Heat map of correlation coefficient of heavy metal content in subsidence water bodies (a); heat map of correlation coefficients between heavy metals and other water quality parameters in subsidence water bodies (b).

Table 1: Characteristic value and variance contribution of factor analysis of water quality indicators.

Factors	Characteristic value	Variance contribution rate/%	Cumulative variance contribution rate/%
1	3.196	35.511	35.511
2	2.238	24.868	60.379
3	1.972	21.915	82.294

Extraction method: a principal component analysis.

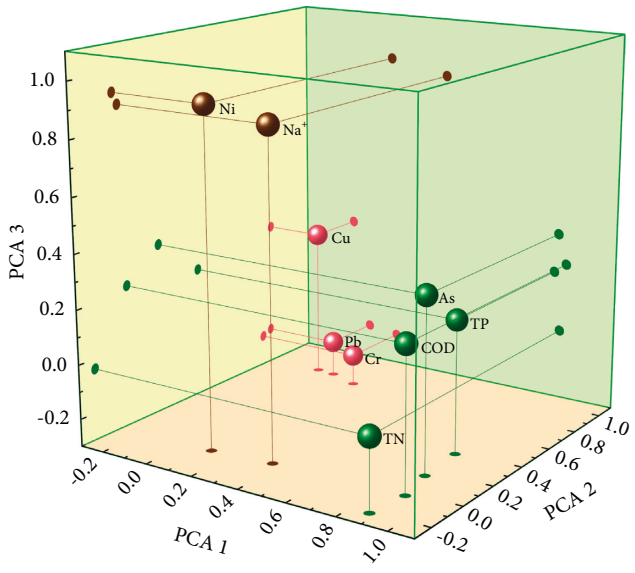

Figure 7: Three-dimensional diagram of the component plot.

serious pollution of Cu, Pb, and Cr. S15 and S16 were subjected to the most serious pollution of Ni and Na^+. The composite factor scores of S14 and S16 were higher, and it indicated that the water quality pollution was more serious in these two sampling points.

3.5. Cluster Analysis. Hierarchical clustering of sampling sites was performed based on factor scores. Using the factor scores of sampling points and the spectrum diagram for analysis was shown in Figure S1 (supplementary Figure 1), they were divided into four clusters, cluster 1 had nine sites, with a low integrated score and a better water quality situation relative to other sites. Cluster 2 has five sites, mainly affected by the main factor 1 and main factor 2, indicating that these five monitoring sites polluted by heavy metals, organic pollutants, nitrogen, and phosphorus nutrients were mainly affected by the surrounding mining production, the comprehensive score was high, and the water quality situation was poor. Cluster 3 and cluster 4 have only one component, factor score 3 for the S15 sampling point of cluster 3 was very high and polluted by the heavy metals and cations of the dual impact. For cluster 4, factor score 1 of the S16 sampling point was very high and had a high comprehensive score, indicating that the comprehensive pollution of the S16 place was serious, water quality was poor, and the former evaluation was consistent with it.

3.6. Evaluation of Surface Water Quality in Coal Mining Subsidence Area

3.6.1. Evaluation Results of the Single-Factor Evaluation Method. Five water quality indicators, namely TN, ammonia nitrogen, TP, DO, and COD, were selected to evaluate

the water quality of surface water in the Huainan coal mining subsidence area by the single-factor evaluation method. Class V standard in the Environmental Quality Standards for Surface Water (GB3838-2002) was used for the analysis, only S15 reached the surface water V standard, and the rest of the sites exceeded the class V standard. The reasons for exceeding the standard for most of the sampling sites were due to excess of TN concentrations, the specific results were shown in Table S7. Among them, TN and TP exceeded the standard at S8, TN, TP, and COD exceeded the standard at S14 and S16, and only TN exceeded the standard at the remaining sampling points.

3.6.2. Evaluation Results of the Comprehensive Pollution Index Evaluation Method. The integrated pollution index of each sampling point was 0.445–1.282, the specific results were shown in Table S7. The composite pollution index of each point was S10 < S15 < S13 < S1 < S2 < S6 < S5 < S9 < S3 < S4 < S7 < S11 < S12 < S8 < S14 < S16, and the composite pollution index of S10, S15, S13, and S1 were between 0.4 and 0.5, which were light pollution; S2, S6, S5, S9, S3, S4, S7, S11, S12, and S8 had a combined pollution index between 0.5 and 0.99, which were medium pollution; S14 and S16 were greater than 1, which were heavy pollution. Figure 8 showed the average contribution rate of various pollutants at each sampling point in the comprehensive pollution index method, which could be seen that TN has the greatest influence on the water quality situation in the study area, followed by COD.

3.6.3. Evaluation Results of the Universal Exponential Formula of Logarithmic Power Function. The five indexes TN, ammonia nitrogen, TP, DO, and COD were selected to evaluate the surface water by using the universal exponential formula of the logarithmic power function. Equations (3)–(5) were used to calculate the water quality integrated index (WQI) of 16 sampling points, the evaluation results were shown in Table S8. For S14 and S16, the comprehensive pollution index evaluation results were heavy pollution, and the evaluation results of the universal exponential formula of logarithmic power function were class V standard, both indicated that these two sites were serious pollution compared with other sites. At S1, S10, S13, and S15, the comprehensive pollution index evaluation results were light pollution, and the evaluation results of the universal exponential formula of logarithmic power function were class III standard, so it indicated that the pollution level of these four sampling sites was relatively light.

3.6.4. Evaluation Results of the Membership Degree Method. The five indicators of TN, ammonia nitrogen, TP, DO, and COD were selected to evaluate the water quality of the subsidence water bodies by using the membership degree method. The affiliation degree of each index indicated the degree of this measured value belongs to the standard level, the larger the value, the heavier the pollution, the specific results were shown in Table S9. For example, the affiliation

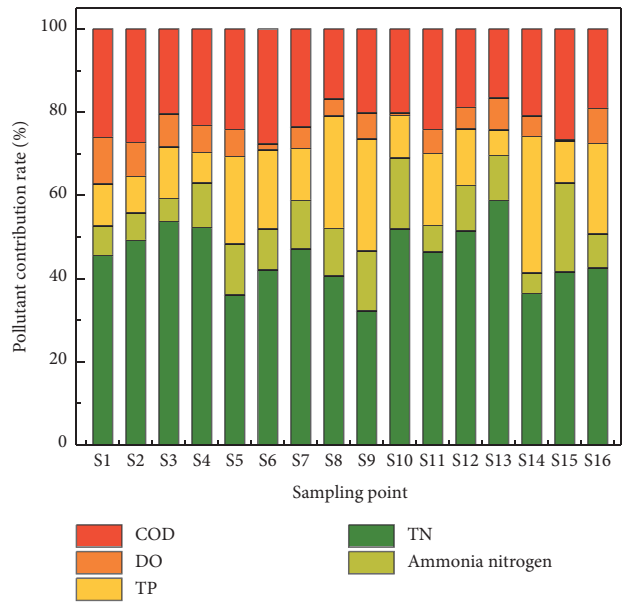

Figure 8: The contribution rate of pollutants at each sampling point for the comprehensive pollution index method.

degree of ammonia nitrogen at S9 was 0.924, which meant that the ammonia nitrogen concentration was close to the upper limit of surface water class III standard. From the evaluation results, it could be seen that the TN pollution was serious, which was consistent with the results of the single-factor evaluation method and the comprehensive pollution index evaluation method. For S8 and S16, except for the evaluation results of DO were class I standard, the other evaluation results were class IV and V standards. The water quality situation at the above two locations was poor. The concentrations of COD at S2, S3, S5, and S9 belong to the surface water IV standard; their affiliation was higher, belonging to the class IV standard,but the pollution was close to the lower limit of V water.

3.6.5. A Comparison of the Four Methods. The single-factor evaluation method is simple to calculate and intuitively reflects the exceedance of a single water quality index, but it is difficult to ensure the scientificity and reasonableness to determine whether the water quality of the study area meets the standard only by the worst water quality index. In the process of using the single-factor evaluation method, most of the sites in this study area were evaluated as poor class V only because TN exceeded the class V standard.

The comprehensive pollution index method considers the degree of comprehensive influence of multiple indicators on water quality pollution and quantifies the water quality situation. The universal exponential formula of the logarithmic power function continuously describes the water quality situation with specific index values, and the evaluation results can visually reflect the different degrees of pollution belonging to a certain level [26]. Overall, the two evaluation results were similar in this study, but the comprehensive pollution index method cannot determine a

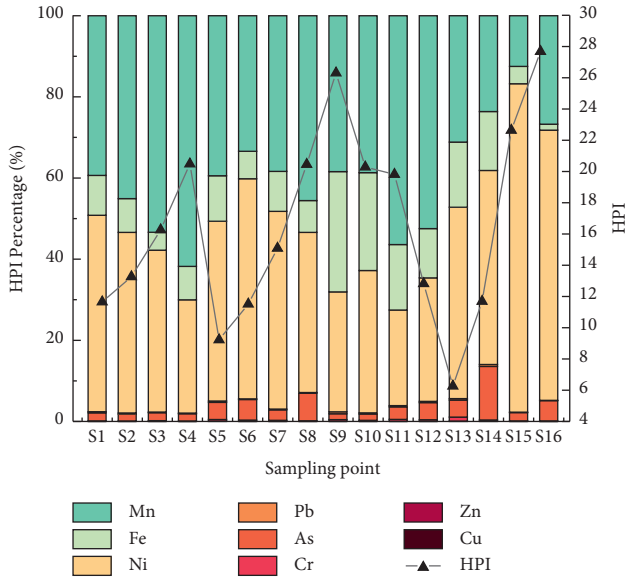

Figure 9: Changes of HPI at different sampling points of the subsidence water bodies and proportion of HPI of different heavy metals.

specific water quality category, and the evaluation results of the universal exponential formula of logarithmic power function were more refined.

The membership degree method could evaluate the specific differences for the same water quality indicator at different sampling points, and be quantitatively compared, the method was better than the single-factor evaluation method and the comprehensive pollution index method [44], but the degree of comprehensive impact of water quality pollution for multiple indicators was not comprehensive consideration.

In the light of the analysis of a single indicator, the membership degree method could give reliable evaluation results and could clearly distinguish the degree of pollution of similar water bodies. Compared with the single-factor evaluation method, its result was more reliable. Evaluation results of the universal exponential formula of logarithmic power function could visually reflect the different levels of pollution belonging to a certain level. Compared with the evaluation results, the comprehensive pollution index method was more reliable.

3.7. Evaluation Results of the Heavy Metal Pollution Index Method. The heavy metal pollution index method (HPI) was used to evaluate the heavy metal pollution in the subsidence water bodies, and the HPI variation of different sampling points and the percentage of various heavy metal HPI were obtained, as shown in Figure 9. The HPI of the sampling points ranged from 6.26 to 27.68, and the HPI of the seven sampling points S1, S2, S5, S6, S12, S13, and S14 were all within 15, which were lightly polluted; the HPI values of the remaining sampling points (S3, S4, S7, S8, S9, S10, S11, S15, and S16) were in the range of 15–30, which were moderately polluted, and there were no heavy pollution points. The overall degree of heavy metal pollution at each sampling point was S13 < S5 < S6 < S1 < S14 < S12 < S2 < S7 < S3 < S11 < S10 < S8 < S4 < S15 < S9 < S16, and the main factors causing heavy metal pollution were Ni, Fe, and Mn. Meanwhile, it could also be seen from Figure 9 that S9, S15, and S16 had the most serious heavy metal pollution.

3.8. Discussion. In the study area, the concentration of TN exceeded 2 mg/L at most sampling points and exceeded the class V standard of the surface water. In the previous study [45], it was also found that the concentration of TN in Huainan coal mining subsidence water bodies was high with an average value of 3.04 mg/L. Among them, the Panyi mine and Guqiao coal mine were also monitored, and the content of TN was 4.07 and 2.77 mg/L, respectively. Fertilization of farmland and aquaculture in the study area may lead to nitrogen runoff into water bodies. Therefore, the subsequent management of Huainan subsidence water bodies needed to pay attention to the impact of agricultural surface source pollution and aquaculture on the subsidence water bodies.

In this study, seven typical subsidence water bodies were selected. Because the scope of each collapsed area is very large, not enough samples were taken. So it would affect the representativeness of water quality. Every water quality evaluation method had its advantages and disadvantages. So, the characteristics of water quality indicators should be fully considered to select the appropriate evaluation methods. By comparing the results of different evaluation methods, more scientific and reasonable evaluation results could be obtained.

4. Conclusions

(1) For all the sample points, the pollution of TN in the subsidence water bodies of the study area was serious. In sampling point S14 (Guqiao coal mine) and S16 (east Xinji'er mine), the concentration of TP exceeded the standard and the concentration of COD was high. The content of F^- exceeded the standard at S14, and the content of Fe exceeded the standard seriously at S9 (Xieqiao mine).

(2) The correlation analysis of water quality indicators showed that the heavy metals Cr and Zn have significantly strong correlation ($P < 0.01$), and the pollution sources of Cr and Zn might be the same. The heavy metal As showed significantly strong positive correlations with TN, TP, and COD ($P < 0.01$). One-way ANOVA showed that Mg^{2+}, F^-, and ammonia nitrogen were significantly different in different water bodies with different subsidence times.

(3) By factor analysis, three principal factors were selected. Principal factor 1 represented mixed pollution related to nitrogen and phosphorus nutrients, organic pollutants, and heavy metal pollutants; principal factor 2 was closely related to heavy metal pollution; and principal factor 3 was influenced by

both heavy metals and cations. The 16 sampling points were divided into 4 clusters according to the score of three main factors. The comprehensive score of S16 of cluster 4 was high, and the water quality was bad.

(4) The single-factor evaluation result showed that using the class V standard as the target standard, only S15 reached the standard, all other sampling points exceeded the class V standard, and most of the sampling points exceeded the standard because of the content of TN. The evaluation results of the comprehensive pollution index method showed that the comprehensive pollution index at S14 and S16 was greater than 1, which was heavy pollution. For S14 and S16 sites, the evaluation result of the universal exponential formula of logarithmic power function was class V, which showed that these two sites were seriously polluted compared with other sites. According to the evaluation results of the membership degree method, it could be seen that the pollution of TN was serious and the water quality at S16 was bad, which was consistent with the previous evaluation results.

(5) The heavy metal pollution was most serious at S9, S15, and S16 in the study area, and the main factors causing heavy metal pollution were Ni, Fe, and Mn.

Data Availability

The data used to support the findings of this study are available from the corresponding author upon request.

Conflicts of Interest

The authors declare that there are no conflicts of interest regarding the publication of this article.

Acknowledgments

The work was funded by the National Natural Science Foundations of China (Grant Nos. 41471422 and 51878004) and Top Notch Talents Program of Universities in Anhui Province (Grant No. 2019gxbjZD24).

Supplementary Materials

Table S1: Threshold values of the five grades for DO, COD, ammonia nitrogen, TN, and TP under Environmental Quality Standard for Surface Water (mg/L). Table S2: c_{jk} specification value, x_{jk}, and logarithm lnx_{jk} of surface water environmental quality classification standard. Table S3: Homogeneity of variance test. Table S4: one-way ANOVA and multiple comparisons. Table S5: Rotated component matrix. Table S6: Factor scores. Table S7: Evaluation results of the single-factor evaluation and the comprehensive pollution index evaluation method. Table S8: Comprehensive evaluation index and grade evaluation of water quality at each sampling point. Table S9: Water quality membership evaluation results. Figure S1: cluster dendrogram. (*Supplementary Materials*)

References

[1] NBSC (National Bureau of statistics of China), *China Statistical Yearbook*, China Statistics Press, Beijing, China, 2021.

[2] Z. Q. Wang, "Analysis and prevention of mined-out collapse in coal mine: an example from Changguang Coal Mine in Guangde County, China," *West-China Exploration Engineering*, vol. 32, no. 9, pp. 4–6, 2020.

[3] J. S. Liu, *Analysis on Surface Water Quality and Environmental Influencing Factors in Panji Mining Area of Huainan City*, Anhui University of Science and Technology, Huainan, China, 2009.

[4] G. C. He, H. Liu, and H. R. Gui, "Environment evaluation on typical water area resulting from coal-mine subsidence in Huainan," *Journal of China Coal Society*, vol. 30, no. 6, pp. 754–758, 2005.

[5] Y. Yang, "Preliminary study on the environmental impact of coal development in Panxie Mining Area of Huainan," *Coal Engineering*, vol. 18, no. 5, pp. 35–37, 1986.

[6] Z. H. Wang, H. R. Gui, and Z. X. Luo, "The aquatic environment for excavate coal subside seeper area in Huainan," *Coal Geology & Exploration*, vol. 33, no. 2, pp. 38–41, 2005.

[7] G. C. He, X. M. Song, and H. Liu, "Investigation and evaluation of the current environmental situation of the watershed in the coal mining collapse zone of huainan city," *Mining Safety & Environmental Protection*, vol. 32, no. 6, pp. 43–45+48, 2005.

[8] W. M. Pei, S. C. Dong, S. P. Yao, C. Xu, and Y. C. Chen, "Eutrophication evaluation of water-accumulating mining-induced collapsed area in Huainan Panji using CCD images from HJ-1 satellite," *Coal Geology & Exploration*, vol. 41, no. 5, pp. 49–55, 2013.

[9] X. J. Qun, Q. T. Yi, Y. B. Hu et al., "Nutrient spatiotemporal distribution and eutrophication process in subsidence waters of Huainan and Huaibei mining areas, China," *Chinese Journal of Applied Ecology*, vol. 24, no. 11, pp. 3249–3258, 2013.

[10] X. Wang, Z. Chu, F. Zha, S. Liu, G. Liu, and Z. Dong, "Determination of heavy metals in water and tissues of crucian carp (*Carassius auratus* gibelio) collected from subsidence pools in huainan coal fields (China)," *Analytical Letters*, vol. 48, no. 5, pp. 861–877, 2015.

[11] G. Z. Chen, X. M. Wang, R. W. Wang, and G. J. Liu, "Health risk assessment of potentially harmful elements in subsidence water bodies using a Monte Carlo approach: an example from the Huainan coal mining area, China," *Ecotoxicology and Environmental Safety*, vol. 171, pp. 737–745, 2019.

[12] J. Liu, Q. T. Yi, and J. P. Yan, "Coal mining subsided area water pollution features and assessment in suixi-xiaoxian mining area, huaibei coalfield," *Coal Geology of China*, vol. 30, no. 5, pp. 53–71, 2018.

[13] D. D. Wang, C. D. Yang, and L. M. Shao, "The spatiotemporal evolution of hydrochemical characteristics and groundwater quality assessment in Urumqi, Northwest China," *Arabian Journal of Geosciences*, vol. 14, no. 3, 2021.

[14] Y. L. Liu and Y. A. Zheng, "Water quality assessment and spatial-temporal variation analysis in yellow river basin," *Environmental Sciences*, vol. 43, no. 3, pp. 1332–1345, 2022.

[15] N. Adimalla, "Groundwater quality delineation based on fuzzy comprehensive assessment method (FCAM): a case study," *Arabian Journal of Geosciences*, vol. 13, no. 23, 2020.

[16] W. Ye, W. Song, C. F. Cui, and J. H. Wen, "Water quality evaluation method based on a T-S fuzzy neural network—application in water environment trend analysis of taihu lake basin," *Water*, vol. 13, no. 21, 2021.

[17] Y. R. Zhao, Y. Q. Liu, M. K. Huang, L. W. Chai, and X. F. Cao, Y. Huang, Study on the selecting optimization of marine water environment monitoring stations around the Hong Kong-Zhuhai-Macao bridge," *Environmental Engineering*, vol. 36, no. 7, pp. 149–154, 2018.

[18] J. Chen, S. C. Dong, H. W. Yi, Y. L. Ren, and S. P. Yao, "Health risk assessment of water environment of coal mining subsidence area in Panyi coal mine of Huainan," *Coal Geology & Exploration*, vol. 45, no. 4, pp. 118–125, 2017.

[19] L. Zhang, Q. T. Yi, H. Li, X. Xu, and X. M. Wang, "Water quality and water environmental capacity for the small subsidence lakes in the Huainan and Huaibei coal mine areas, Anhui Province," *Chinese Journal of Ecology*, vol. 34, no. 4, pp. 1121–1128, 2015.

[20] J. Huang, *Source Apportionment of Subsidence Water Pollution of Panji Mine and Xieqiao Mine in Huainan*, Anhui University of Science and Technology, Huainan, China, 2012.

[21] Y. J. Geng, S. C. Peng, X. H. Wang, and R. Z. Li, "Comprehensive evaluation of eco-environment in huainan coal mining area," *Journal of Anhui Agricultural Sciences*, vol. 44, no. 17, pp. 73–82, 2016.

[22] Y. L. Cai, "Exploring the characteristics of coal mining ground collapse and management measures in Huainan mining area," *West-China Exploration Engineering*, vol. 31, no. 2, pp. 15–17, 2019.

[23] Z. L. Xu and H. L. Yin, *Comprehensive Water Quality Analysis and Evaluation in Urban Water Environment Management*, China Water & Power Press, Beijing, China, 2012.

[24] State Environmental Protection Administration of China, *Environmental Quality Standards for Surface water (GB3838-2002)*, China Environmental Press, Beijing, China, 2002.

[25] W. J. Lu and T. Zhang, "Comparison and analysis of several appraisal methods for river water quality," *Environmental Science and Management*, vol. 34, no. 4, pp. 174–176, 2009.

[26] J. Guo, C. M. Wang, D. Z. Huang, L. Q. Li, and H. Lian, "Pollution characterization and water quality assessment of Dongting Lake," *Environmental Chemistry*, vol. 38, no. 1, pp. 152–160, 2019.

[27] J. Y. Wang, W. S. Wang, and Z. Y. Li, "Exponential universal formula of power function in logarithm form for ground water quality assessment," *Advanced Engineering Sciences*, vol. 43, no. 3, pp. 12–17, 2011.

[28] G. F. Li, "Evaluating the water pollution of Changjiang River Huangshi section by the controlling measure method," *Environmental Monitoring in China*, vol. 12, no. 5, pp. 55–57, 1996.

[29] H. Zuo, X. L. Ma, Y. Z. Chen, and Y. Liu, "Studied on distribution and heavy metal pollution index of heavy metals in water from upper reaches of the yellow river, China," *Spectroscopy and Spectral Analysis*, vol. 36, no. 9, pp. 3047–3052, 2016.

[30] S. Chidambaram, M. Bala Krishna Prasad, M. V. Prasanna, R. Manivannan, and P. Anandhan, "Evaluation of metal pollution in groundwater in the industrialized environs in and around dindigul, tamilnadu, India," *Water Quality, Exposure, and Health*, vol. 7, no. 3, pp. 307–317, 2015.

[31] S. Venkatramanan, S. Y. Chung, T. H. Kim, M. V. Prasanna, and S. Y. Hamm, "Assessment and distribution of metals contamination in groundwater: a case study of busan city, korea," *Water Quality, Exposure, and Health*, vol. 7, no. 2, pp. 219–255, 2015.

[32] R. Singh, A. S. Venkatesh, T. H. Syed, A. G. S. Reddy, M. Kumar, and R. M. Kurakalva, "Assessment of potentially toxic trace elements contamination in groundwater resources of the coal mining area of the Korba Coalfield, Central India," *Environmental Earth Sciences*, vol. 76, no. 16, 2017.

[33] A. E. Edet and O. E. Offiong, "Evaluation of water quality pollution indices for heavy metal contamination monitoring. A study case from Akpabuyo-Odukpani area, Lower Cross River Basin (southeastern Nigeria)," *Geojournal*, vol. 57, no. 4, pp. 295–304, 2002.

[34] Z. H. Wang, *Studying on the Aquatic Entironment of Phytoplankton in Excavating Coal Subsidence Pool in Mine: A Case Study of Xie-Er Mine Subsidence Pool in Huainan*, Anhui University of Science and Technology, Huainan, China, 2005.

[35] State Environmental Protection Administration of China, *Water Quality Standard for Fisheries (GB11607-89)*, Standards Press of China, Beijing, China, 1990.

[36] S. Dwivedi, S. Mishra, and R. D. Tripathi, "Ganga water pollution: a potential health threat to inhabitants of Ganga basin," *Environment International*, vol. 117, pp. 327–338, 2018.

[37] N. Saha, M. S. Rahman, M. B. Ahmed, J. L. Zhou, H. H. Ngo, and W. Guo, "Industrial metal pollution in water and probabilistic assessment of human health risk," *Journal of Environmental Management*, vol. 185, pp. 70–78, 2017.

[38] X. L. Gao and C. T. A. Chen, "Heavy metal pollution status in surface sediments of the coastal Bohai Bay," *Water Research*, vol. 46, no. 6, pp. 1901–1911, 2012.

[39] C. N. Da, H. Wang, B. Xu et al., "The migration and release characteristics of chlorine during coal combustion in coal-fired power plants," *Environmental Chemistry*, vol. 39, no. 10, pp. 2833–2839, 2020.

[40] P. Z. Duan, X. P. Jia, X. K. Hou, R. Xia, Y. Guo, and X. Zhang, "Characterization and adsorption properties of magnetic Al-mof composite for fluoride," *Research of Environmental Sciences*, vol. 34, no. 5, pp. 1139–1147, 2021.

[41] X. P. Hong and H. D. Liang, "Analysis on the status que and causes of fluorine and acid pollution around coal-rich areas in China," *Journal of Mining Science and Technology*, vol. 5, no. 1, pp. 1–11, 2020.

[42] Y. Tang, Y. M. Lu, and S. Wu, "Spatio-temporal distribution and source ldentification of water pollutants in minjiang river basin," *Journal of Yangtze River Scientific Research Institute*, vol. 36, no. 8, pp. 30–35+48, 2019.

[43] J. Huang, L. M. Gao, and S. P. Li, "Source apportionment of subsidence water pollution in coal mining areas," *Environmental Monitoring in China*, vol. 29, no. 6, pp. 66–69, 2013.

[44] Y. M. Ning, F. N. Yin, and X. B. Li, "Water quality evaluation of Huangshi section of the Yangtze River based on the comprehensive pollution index method and the grey relational analysis," *Journal of Hubei Normal University (Natural Science)*, vol. 40, no. 3, pp. 39–46, 2020.

[45] X. Liu, H. Cheng, L. Zheng et al., "Distribution characteristics and environmental significance of nitrogen and phosphorus in the Huainan coal mining subsidence area," *Journal of University of Science and Technology of China*, vol. 44, no. 11, pp. 926–932, 2014.

Hindawi
Journal of Chemistry
Volume 2022, Article ID 5867768, 11 pages
https://doi.org/10.1155/2022/5867768

Research Article

The Combined Application of Surface Floating Wetlands and Bottom Anaerobic to Remediate AMD-Contaminated Lakes

Tianling Fu,[1] **Yonggui Wu**,[1] **Hu Wang**,[2] **Kaiju Chen**,[1] **Yan Zeng**,[1] **Zhongzheng Wen**,[1] **Zhengyan Ran**,[1] **and Li He**[1]

[1]*Guizhou University, Guiyang 550025, China*
[2]*Guizhou Chuyang Ecological Environmental Protection Technology Co.,Ltd., Guiyang 550025, China*

Correspondence should be addressed to Tianling Fu; yfhb31@126.com

Received 12 April 2022; Accepted 9 June 2022; Published 27 June 2022

Academic Editor: Jun Wu

Acid mine drainage (AMD) causes environmental pollution that affects many countries with historic or current mining industries. The eco-remediation system (RW) which combined surface floating wetlands and bottom anaerobic sediments (SFW-BAS) was selected for AMD-contaminated lakes (AMDW). Meanwhile, AMDW and nature aquatic ecosystems (NW) were set as the control groups, respectively. The parameters, including pH, Eh, Fe, Mn, SO_4^{2-}, and the degradation rate of the native dominant plant litter were investigated to assess the effects of remediation. The results showed that the average of pH, Eh, and EC, was 2.73, 484.08 mv, and 2395.33 $\mu s \cdot cm^{-1}$, respectively. The average content of SO_4^{2-}, Fe, Mn, Cu, Zn, and Pb was 2190 $mg \cdot L^{-1}$, 40.2 $mg \cdot L^{-1}$, 4.6 $mg \cdot L^{-1}$, 249.2 $\mu g \cdot L^{-1}$, 1563 $\mu g \cdot L^{-1}$, and 112.9 $\mu g \cdot L^{-1}$, respectively. The degradation rate of plant litters in AMDW ranged from 14.5% to 22.6%. However, RW ultimately improved the water quality and the degradation of litters. RW has a good effect on buffering the acidity, ranging from 3.96 to 7.41. The pH of RW (6.14) is close to that of NW (7.41). The average content of SO_4^{2-}, Fe, Mn, Cu, Zn, and Pb was 2071 $mg \cdot L^{-1}$, 3.4 $mg \cdot L^{-1}$, 2.4 $mg \cdot L^{-1}$, 85.3 $\mu g \cdot L^{-1}$, 607.4 $\mu g \cdot L^{-1}$, and 47.8 $\mu g \cdot L^{-1}$, respectively, which showed good pollutant removal performance. The degradation rate of plant litters in RW ranged from 27.8% to 32.6%. Therefore, RW can be used to remediate AMDW.

1. Introduction

Upon exposure to water and oxygen and as a result of the activities of indigenous microbial populations, iron pyrite (FeS_2) and other sulphide minerals can be oxidized to form acidic and sulphate-rich drainage, which is a consequence of the mining and processing of metal ores and coals [1–3]. The oxidation of pyritic mining waste is a self-perpetuating corrosive process that has generated acid mine drainage (AMD) effluent for centuries or longer [4]. AMD is characterized by a low pH and high levels of sulphate and toxic metallic ions [2]. It is an important environmental issue since it can degrade the waterways in and around mine districts [5]. Both the terrestrial and aquatic ecosystems and processes may be disturbed [6, 7]. In aquatic ecosystems, it can be observed as a severe disturbance or even destruction of the water quality and the functions, habitats, biological communities, and species composition of these ecosystems. Studies have shown that AMD could significantly decrease the water quality [8, 9] and the activity of the invertebrates, aquatic plants, or zoobenthos [10]. Additionally, it may also affect the degradation of plant litter in the streams [11].

Therefore, there have been numerous studies devoted to reducing AMD formation or to treating these waste waters [6, 12]. However, few studies are designed to evaluate the techniques for ecological restoration of AMD-contaminated land or water. The optimized strategies are aimed to suppress the formation of AMD by treating the acid-producing rock directly and stopping/retarding the production of acidity at the source. These techniques include the use of alkaline amendments (e.g., limestone, hydrated lime, fly ash, and waste phosphate rock) [13, 14], covering the tailings with a layer of sediment or organic material (e.g., sewage sludge, manure mixture, and olive pomace) [15], coating

technologies (e.g., solid-phase phosphates, phospholipids, and lipids) [16], the use of bactericides (e.g., sodium dodecyl sulphate, benzoic acid, and sodium benzoate), or the use of natural organic acids (e.g., fulvic acids, tannic acids, oxalic acid, and humic acids) [17]. Since large quantities of AMD are produced in the wider environment, the traditional methods could not meet the requirements. The current abiotic and bioremediative strategies for the remediation of AMD have been considered "active" and "passive" processes. The active treatment process involves abiotic remediation strategies (the addition of a chemical-neutralizing agent, e.g., limestone, hydrated lime, pebble quicklime, soda ash, or caustic soda) [14] and biological systems, such as sulphidogenic bioreactors [18]. In the passive treatment process, the abiotic technologies are mainly anoxic limestone drains (ALD) [19], but the biological remediation strategies have wider choices, such as wetlands [20] or compost bioreactors [18], the reducing and alkalinity-producing system (RAPS) [21], successive alkalinity-producing systems (SAPS), permeable reactive barriers (PRBs) [22], and iron-oxidizing bioreactors. Nevertheless, these strategies are purposed to suppress the formation of the AMD or to treat the production before it enters the environment. It will not work on already polluted water but on the wider environment, where the natural ecological system has been destroyed by the AMD. Surface floating wetlands are easy and cheap to construct and therefore used to treat mine tailings water and polluted rivers [23]. Surface floating wetlands are based on the self-cleaning capability of plants to augment aquatic projects and rapidly remove pollutants from water bodies [23]. Furthermore, there was the potential of activated sludge for the remediation of sulphur-rich wastewaters, owing to its simplicity and low cost [24]. Activated sludge could form suitable microbial community for AMD treatment [24]. If SFW-BAS could be constructed, the removal effects of contaminants from AMDW will increase with easy and low cost.

In this study, there are characterized by an inherently fragile ecosystem and sensitive processes of biogeochemical cycling in the karst regions in southwest China. RW was constructed to remediate AMDW, and RW included floating aerobic wetlands on the surface and anaerobic sediments in the bottom. AMDW and NW were set as the control groups, respectively. The water quality (pH, Eh, EC, Fe, Mn, and SO_4^{2-}) and litter decomposition rate of NW, AMDW, and RW were evaluated to compare to the remediation effect for the contaminated waters. These findings would provide the basic data of AMDW treatment.

2. Materials and Methods

2.1. Study Regions. The study was carried out at the Guizhou province, located in the central karst region of Southwest China, which has a well-developed karst landform [25]. It has a moderate, subtropical, humid monsoon climate, which is characterized by hot and wet summers and mild and humid winters. Karst ecosystems are rich in water and mineral resources and can provide unique habitats for numerous fish and wildlife. Unfortunately, they are inherently fragile, at risk of degradation and vulnerable to the environmental change (e.g., human habitation, mining, and draining the sewage) [26]. Coal resources are extremely abundant in the Guizhou Province, but the sulphur contents in the coal are relatively high, with an average of 2.34% [27]. Because of the long time and large-scale mining activities of the coal and metal mines, large volumes of sulphide waste rock or tailings were discarded in this region. The main iron sulphide minerals are pyrite and marcasite (FeS_2), but others, such as chalcopyrite ($CuFeS_2$), covellite (CuS), galena (PbS), and sphalerite (ZnS), also exist [3, 28].

2.2. Simulated Experiments. The simulation of the microcosm aquatic ecosystems was carried out with six cylindrical tanks, each with a height of 900 mm and an internal diameter of 950 mm. A 15–20 cm layer of sediment from the Huaxi Reservoir and a 60 cm layer of lake water were placed in these tanks. The Huaxi Reservoir is a typical karst lake. The submerged vegetation, including *Vallisneria natans* Hara, *Hydrilla verticillata*, *Ceratophyllum demersum* L, *pondweed,* and *Ottelia acuminate,* was planted in these tanks. These microcosms were incubated in the open air, receiving natural lighting and temperature throughout the year. The cultivation lasted approximately three months, until these microcosms could be self-sustaining, and they were set as the simulation of the natural aquatic ecosystem (NW). Then, four microcosms were treated with the AMD on a regular basis, which were set as the simulation of the AMD-contaminated aquatic ecosystem (AMDW). Approximately two months later, two of the AMDW microcosms were equipped with an SFW-BAS treatment system, which was set as the eco-remediation aquatic ecosystem (RW). The surface floating wetlands consist of plastic foam or an empty bottle made of lightweight material that floats, has basins with holes in the bottom to be beneficial to the roots and for the water to penetrate, has soil or another suitable medium to support the vegetation, and contains vegetation that is a mix of cattail, stick tight, *Lolium perenne*, *Alternanthera philoxeroides,* and another native species. The bottom anaerobic sediments were formed by the original addition of the activated sludge and by constantly obtaining organic substances from the surface floating wetlands. The layout of the system is shown in Figure 1.

RW was successfully built for the remediation of AMDW (Figure 2). RW was in normal operation for 210 d. Plants grew well in the floating aerobic wetlands. There were fluffy anaerobic sediments at the bottom. RW could promote vertical interactions between the aerobic vegetation and anaerobic microorganisms to remediate AMDW.

2.3. Sampling and Analytical Methods. The litter of the native dominant woody species at the local shore, such as *Salix babylonica* and *Broussonetia papyrifera,* and submerged plants, such as *Vallisneria natans* Hara*, Hydrilla verticillata,* and *Ceratophyllum demersum* L, was collected in this study. The above selected litters were thoroughly cleaned by water and air-dried prior to the reuse or storage. Five grams of air-dried leaves were packed into 15 ∗ 30 cm nylon

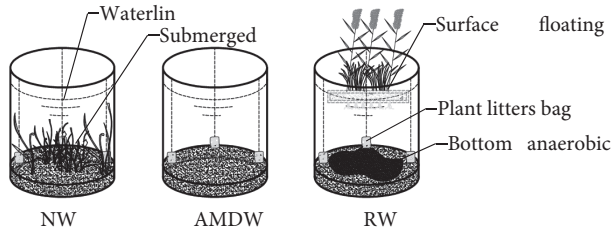

Figure 1: Microcosm experimental setup. NW: simulating the natural aquatic ecosystem; RW: simulating the eco-remediation AMD-contaminated aquatic ecosystem; AMDW: simulating the AMD-contaminated aquatic ecosystem. In the microcosm RW, an eco-remediation system that combines floating aerobic wetlands on the surface with constructed anaerobic sediments in the bottom (SFW-BAS) was employed.

Figure 2: A pilot passive system for the remediation of an AMD-polluted ecosystem.

mesh bags with a mesh size of $2 * 2$ mm. The bags were placed at the bottom of the microcosm and on the surface of the sediments in quintuplicate at the three habitats representing NW, AMDW, and RW. The bags were retrieved 0, 15, 30, 60, 120, and 210 d after they were mounted. The decomposition rate was determined by direct measurements of the weight losses from the litter bags [29]. The mass losses were determined in oven-dried values (48 h, 60°C or until constant weight) after a strict cleaning.

Synchronously, water samples were collected at a depth of 0.2 m. The pH, electrical conductivity (EC), redox potential (Eh), and dissolved oxygen (DO) were determined in the water of the microcosm systems. The pH and EC were detected by a portable pH/EC/TDS instrument (HI 98129, HANNA, Germany). The Eh and DO were recorded by a potentiometer and DO6 probes, respectively. The water samples for the metal analysis were filtered through 0.45 μm membrane filters, acidified with nitric acid to pH <1, and analysed by flame atomic absorption spectroscopy (WFX100 Beijing Ruili, China). The SO_4^{2-} concentrations were determined by the conventional ignition method in gravimetry.

2.4. Data Analysis. All data were analysed with SPSS 13.0. The differences in each evaluation index at different times were compared with a single-factor analysis of variance (ANOVA), and those in different microcosms were compared with two-factor ANOVA. Moreover, Duncan's multiple range was used to treat the average significant difference among the multiple comparisons.

3. Results

3.1. Effects of Remediation on pH, EC, Eh, and DO. The water in the microcosm NW was crystal clear, the submerged

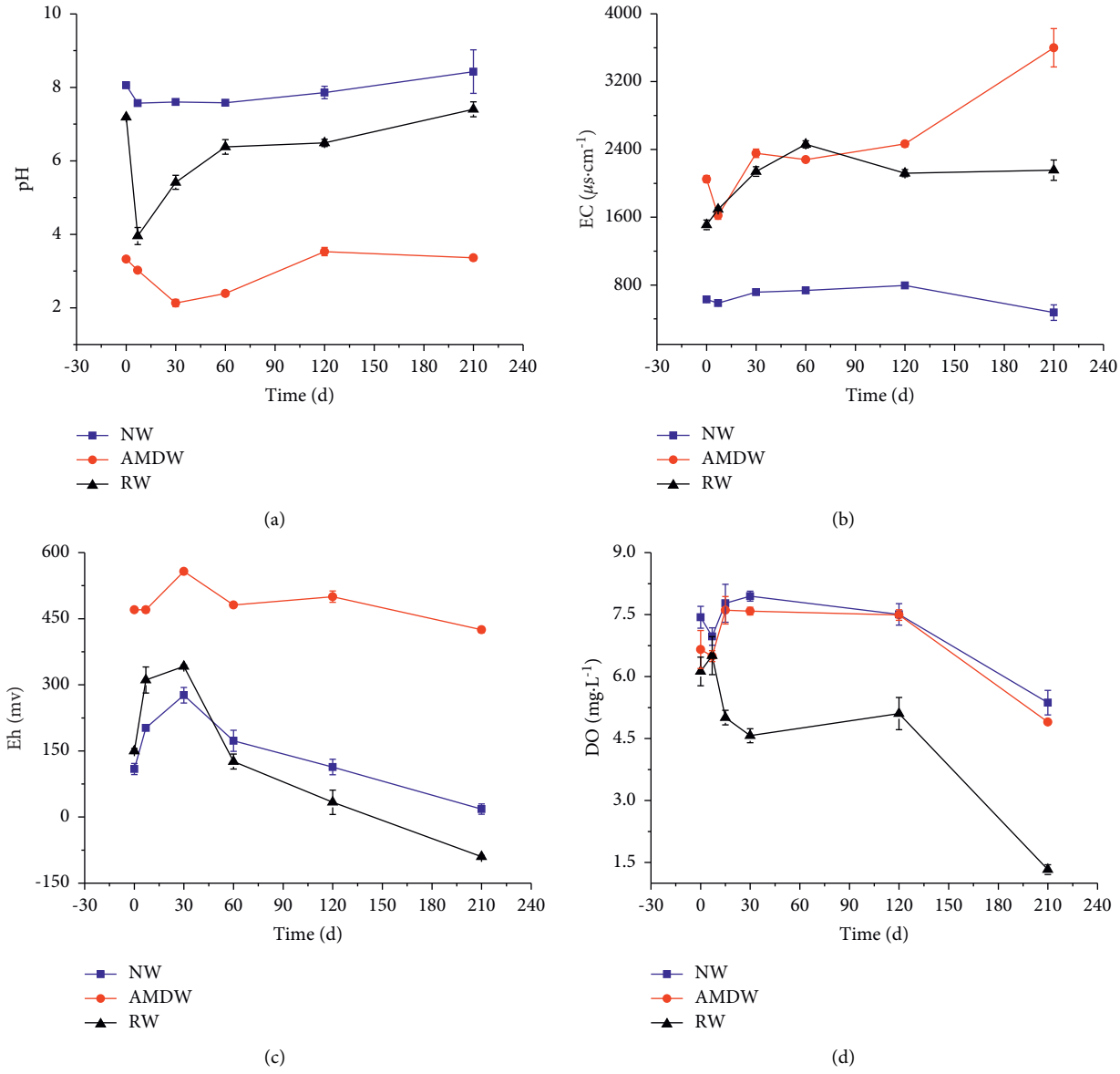

Figure 3: The temporal variation of pH, EC, Eh, and DO in NW, RW, and AMDW.

plants (*Vallisneria natans* Hara, *Ceratophyllum demersum* L, *Hydrilla verticillata*, *Potamogeton distinctus,* and *Ottelia acuminata*) were growing well, and fish and shrimps were shuttling back and forth in the microcosms. The pH ranged from 6.45 to 8.06 (with a mean of 7.46), and the DO varied from 5.4 to 8.1 mg·L^{-1} (with a mean of 7.26 mg·L^{-1}) (Figures 3(a) and 3(d)). The ECs were relatively low, with a range of 310 to 810 μs·cm^{-1} (Figure 3(b)), and the Eh varied from 150 to −100 mV during the experiment time (Figure 3(c)). These indexes agreed well with those of the natural waters. The Fe, Mn, Cu, Zn, and SO_4^{2-} concentrations remained at a very low level during the period of observation (Figure 4), which can meet class III of the environmental quality standards for surface water (GB3838-2002, China).

In the microcosms AMDW, the water colour changed to dark red, and the bottoms and walls became coated with a layer of ochre particles. All the submerged vegetation, filamentous algae, fish, and shrimps disappeared. The average of the pH was 2.73, with the lowest value being 1.38 (Figure 3(a)), and the water presented an obvious acidification with a high salinity (1200–3750 μs·cm^{-1}; Figure 3(b)) and Eh (420–690 mv; Figure 3(c)). Simultaneously, the concentrations of the contaminated ions and sulphate in the AMDW were continuously increasing, with values dozens or hundreds of times higher than those in NW (Figure 4), which presented a typical AMD contamination [3].

Compared to the microcosm AMDW, RW had good performance in raising the pH to neutral (Figure 3(a)), buffering the strong oxidizing nature (Figure 3(c)) and reducing the metal levels to environmentally permissible limits (Table 1; Figure 4; GB3838-2002, China). The average of pH in RW was 6.14, ranging from 3.96 to 7.41. The pH of RW (6.14) is close to that of NW (7.41), indicating that RW had

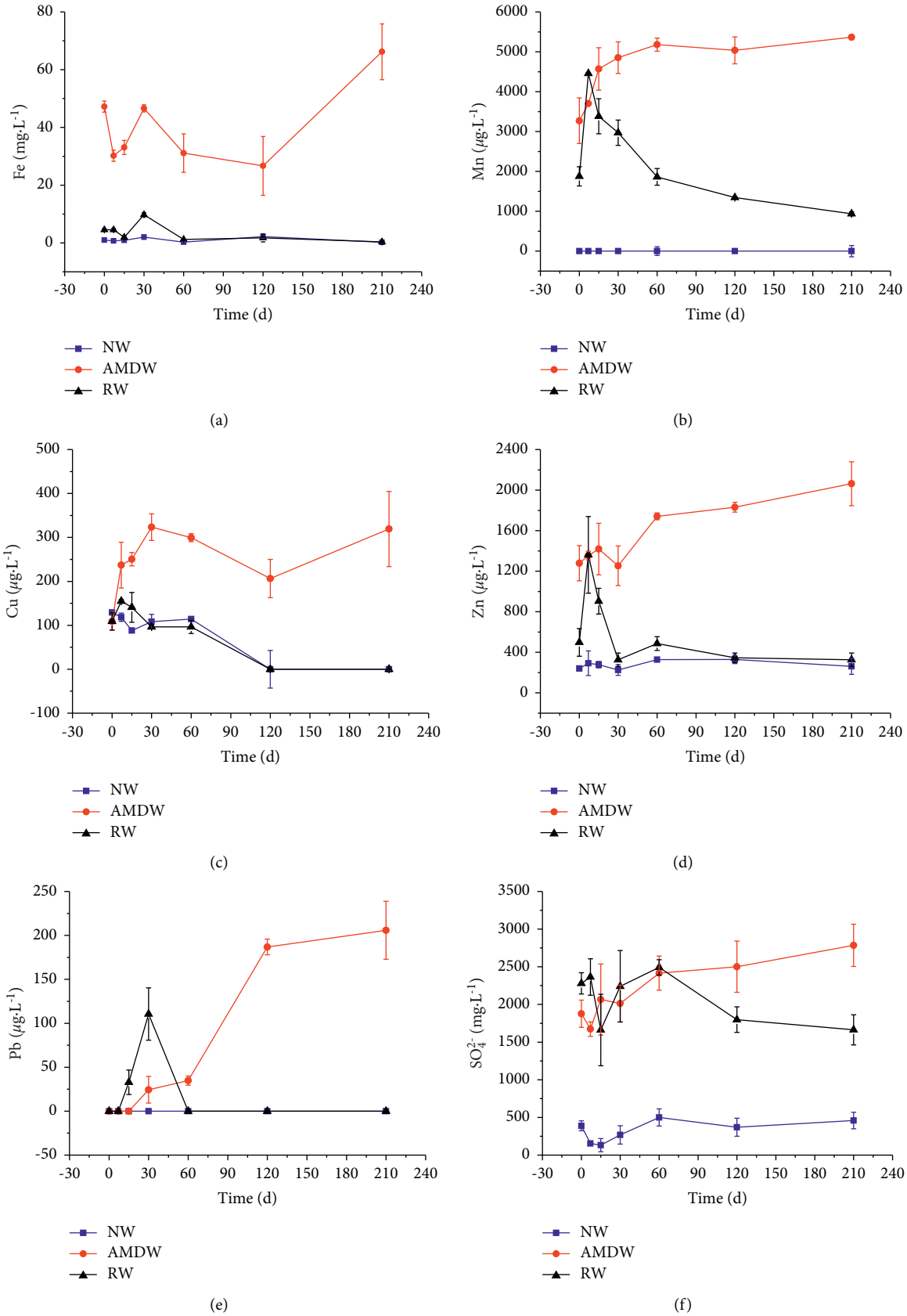

Figure 4: Concentration variation of Fe, Mn, Cu, Zn, Pb, and SO_4^{2-} in NW, RW, and AMDW.

Table 1: The Duncan multiple comparison of the typical pollution ions among NW, RW, and AMDW.

	Fe ($mg{\cdot}L^{-1}$)	Mn ($mg{\cdot}L^{-1}$)	Cu ($\mu g{\cdot}L^{-1}$)	Zn ($\mu g{\cdot}L^{-1}$)	Pb ($\mu g{\cdot}L^{-1}$)	SO_4^{2-} ($mg{\cdot}L^{-1}$)
NW	1.1 ± 0.8 A^1a^2	0.0 ± 0.0 * Aa	79.7 ± 55.8Aa	279.4 ± 40.4Aa	0.0 ± 0.0 * Aa	324 ± 144Aa
RW	3.4 ± 3.2Aa	2.4 ± 1.2Bb	85.3 ± 62.3Aa	607.4 ± 389Aa	47.8 ± 56.7Aa	2071 ± 352Bb
AMDW	40.2 ± 14.0Bb	4.6 ± 0.8Cc	249.2 ± 76Bb	1563 ± 315Bb	112.9 ± 96.7Aa	2190 ± 390Bb
F	48.478	41.108	17.009	31.6	2.651	70.95
p	0.00001	0.00001	0.0003	0.00001	0.1111	0.00001

A^1 is p value <1%; a^2 is p value <5%. *The value is less than IDLs (instrument detection limit).

good effects on buffering the acidity of AMDW. The microcosm RW also ensured regular growth and activity for the microorganisms and benthonic animals (porous texture, well-agglomerated microbes could be seen in the bottom of the system, and there was a large amount of *chironormus larva* in the water). However, these microorganisms and benthonic animals consumed the DO intensively resulted in anaerobic conditions and maintained a higher salinity than in NW (Figures 3(d) and 3(b)).

3.2. Effects of Remediation on Fe, Mn, Cu, Zn, Pb, and SO_4^{2-}. Compared to the microcosm AMDW, the ecological remediation significantly reduced the concentrations of harmful ions such as Mn, Cu, Zn, and Pb (Table 1 and Figure 4), which have a trend of decreasing with time (Figure 4). Except for Mn, the other metals meet class III of the environmental quality standards for surface water. For SO_4^{2-}, remarkable reduction occurred from 120 to 210 d (at the surface of the constructed sediments, Eh: from −90 mV to −255 mV) [8]. Compared to the control microcosms (AMDW), the sulphate concentrations decreased dramatically from 2500 to 1700 $mg{\cdot}L^{-1}$ (Figure 4(f); Table 1) due to the high rates of sulphur removal [30]. However, the effect was limited. Despite its sharp decline, it remains at a high level with a value of over 1600 $mg{\cdot}L^{-1}$ after 210 d, which was significantly higher than those in the blank microcosms (NW) (<500 $mg{\cdot}L^{-1}$).

3.3. Effects of Remediation of Degradation of the Litters. The AMD significantly decreased the degradation rates of the plants growing on the bank or submerged plants compared with NW (Figure 5) and affected the normal ecosystem function of the waters. Under NW conditions, the highest values of the degradation rates of the litters were observed (25–35%), and the rates continuously increased and then became constant with time. After 210 d, the degradation rates of *Salix babylonica* and *Broussonetia papyrifera* were 58.1% (Figure 5(a)) and 52.6% (Figure 5(b)), respectively, and those of *Ceratophyllum demersum* L, *Vallisneria natans* Hara, and *Hydrilla verticillata* were 54.8% (Figure 5(c)), 44.6% (Figure 5(d)), and 54.1% (Figure 5(e)), respectively. The degradation rates in AMDW were notably lower than those in NW at the same time (Figure 5), and there are significant differences (Table 2). Additionally, the degradation rates of the above ordered litters after 210 d were only 36.58%, 35.09%, 20.7%, 30.5%, and 25.1%, respectively.

The degradation trend in RW was consistent with that of NW. RW remediation significantly improved the degradation rate of the litters and became more similar to that of NW over time, which was preferable for the ecosystem function (Figure 5). The rates after 210 d were 44.7%, 46.6%, 49.4%, 43.4%, and 54.3%, respectively, and there were no significant differences in *Salix babylonica Ceratophyllum demersum* L, *Vallisneria natans* Hara, and *Hydrilla verticillata* compared with NW (Table 2). However, the rates still had large variations within NW (Figure 5), which indicated that it will be hard to recover the ecosystem once it is destroyed.

4. Discussion

In this study, we developed a pilot passive system for the remediation of an AMD-polluted ecosystem. This system combined both the floating aerobic wetlands on the surface and constructed anaerobic sediments at the bottom, which can promote vertical interactions between the aerobic vegetation and anaerobic microorganisms (Figure 6). On the lake's surface, the floating aerobic wetlands are partially installed, and the associated oxidation and hydrolysis reactions can eventually result in the precipitation of dissolved metals [31]. In addition, to some extent, the filtering, uptake, adsorption and exchange by plants, soil, and other biological materials could remove the metals and other ions [3, 32]. At the lake's bottom, the constructed anaerobic sediments can promote the anaerobic bacterial activity, which ultimately results in a series of reduction reactions and the subsequent precipitation of metal sulphides and generation of alkalinity [12, 33]. The low-cost natural products and wastes such as straw, wood chips and saw dust, spent mushroom compost, mixed manure, and potatoes [34, 35] were used as organic substrates in the AMD treatment systems to create reducing conditions. In this study, we used residual sludge from the municipal wastewater treatment plant as the first organic substances. The sewage sludge contains abundant and easily degradable organic matter, nitrogen, and phosphorus, which can quickly create anaerobic environments for the microbial consortia within the sediments in the pilot experiments. When RW is stable, the organic substrates could continuously be obtained from the surface wetland. Overall, this remediation system involves two parts of the surface and the bottom, providing a combination of aerobic and anaerobic environments and their interactions. The surface floating wetlands provide an ongoing supply of organic substances to the bottom (like acid reduction using microbiology (ARUM) by Kalin [36], which continuously provides nutrients for the reducing bacteria to establish and maintain reductive conditions in the sediment and ameliorate the lake's pH. Within

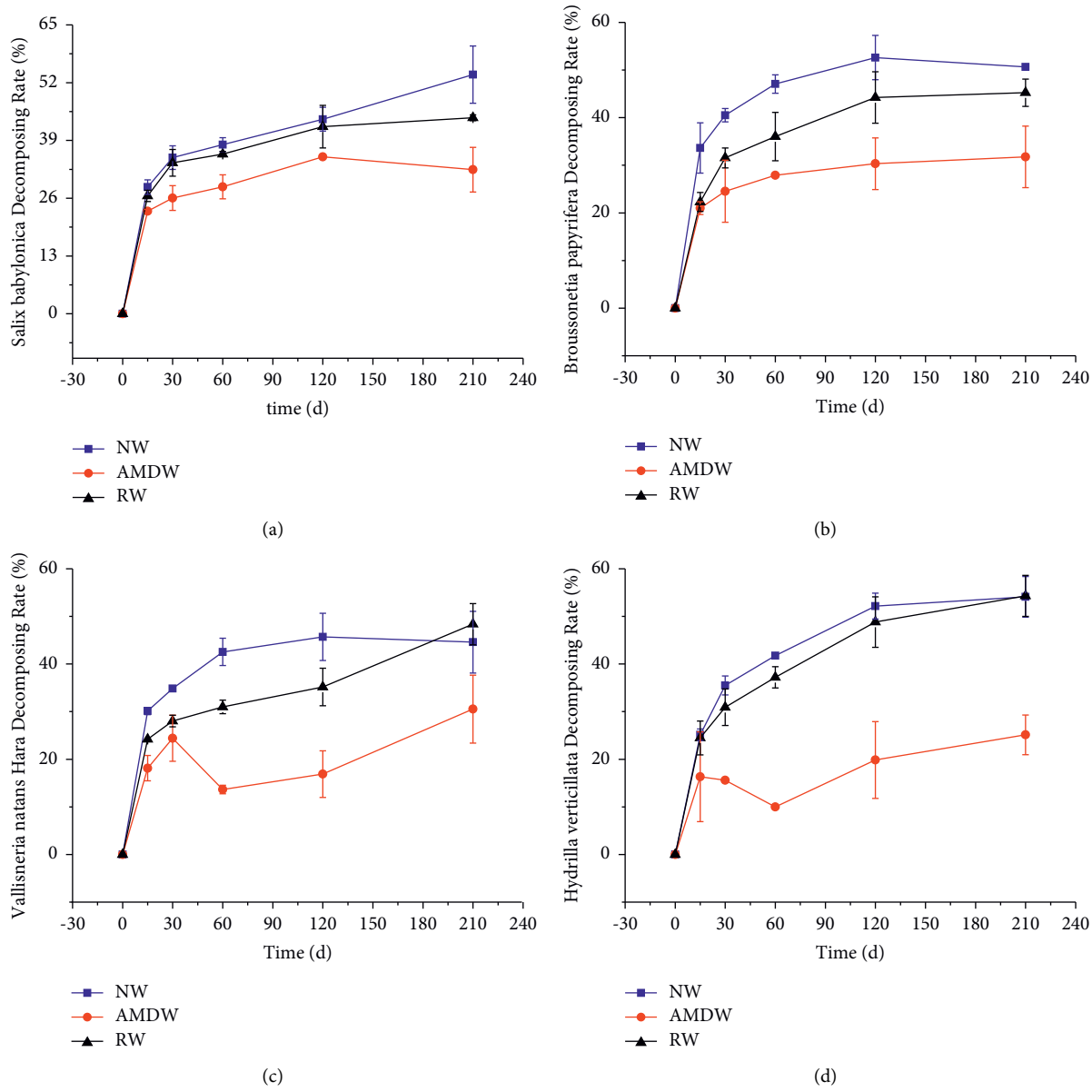

Figure 5: Continued.

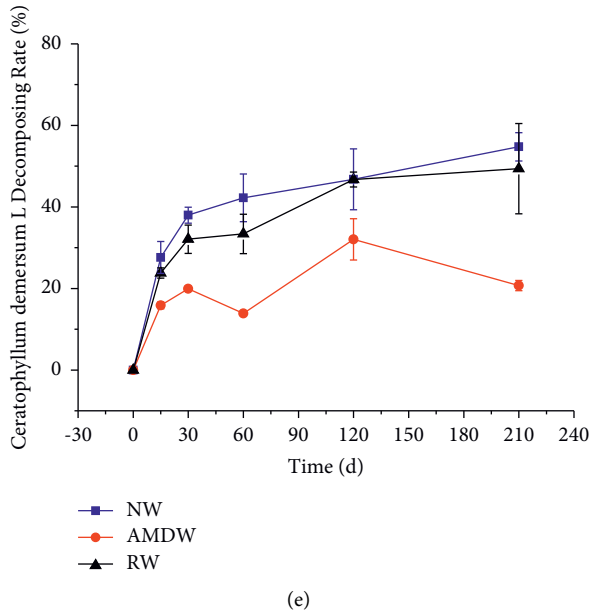

Figure 5: The degradation trend of the five plant litters in NW, AMDW, or RW. *Salix babylonica* and *Broussonetia papyrifera* are native dominant woody species at the local shore; *Vallisneria natans* Hara, *Hydrilla verticillata*, and *Ceratophyllum demersum* L are native dominant submerged plants in the Huaxi Reservoir.

Table 2: The Duncan multiple comparison of the litter decomposition rate among NW, RW, and AMDW (%).

	Salix babylonica	*Broussonetia papyrifera*	*Ceratophyllum demersum* L	*Vallisneria natans* Hara	*Hydrilla verticillata*
NW	33.2 ± 18.4 A^1a^2	37.4 ± 19.6 Aa	34.9 ± 19.3 Aa	33.0 ± 17.2 Aa	34.8 ± 20.1 Aa
RW	30.4 ± 16.2 ABa	29.9 ± 16.9 ABb	30.9 ± 18.0 Aa	27.8 ± 16.0 ABa	32.6 ± 19.4 Aa
AMDW	24.2 ± 12.7 Bb	22.6 ± 11.7 Bc	17.1 ± 10.5 Bb	17.3 ± 10.4 Bb	14.5 ± 8.7 Bb
F	9.762	17.067	12.274	9.985	13.331
p	0.0045	0.0006	0.002	0.0041	0.0015

A^1 b^2: A^1 is p value <1%; b^2 is p value <5%.

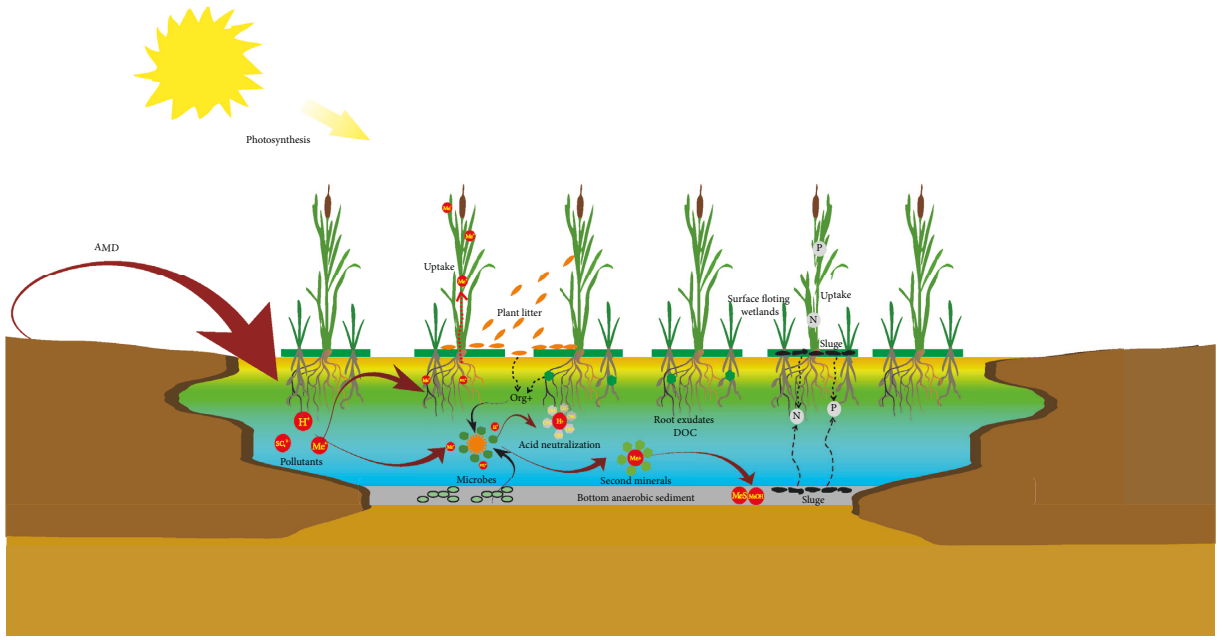

Figure 6: The possible remediated strategy of RW for AMD-contaminated lakes.

the bottom constructed sediments, the decomposition of the additive sewage sludge or organic substances from the surface wetlands is always occurring. These processes can form inorganic C, N, and P, which will diffuse to the surface waters for the surface wetland plants to grow and remove metals by the adsorption or exchange from the water column.

Effectively buffering the acidity in these systems is a crucial issue in this study. The generation of alkalinity to buffer the acidity in acidic aquatic ecosystems is a remediation process that occurs spontaneously in nature [37]. The primary production of the photosynthetic organisms (e.g., phytoplankton, periphytic algae, or moss) is associated with natural alkalinity-generating processes in acidic systems [12, 33]. However, consuming acidity by biological reduction in the sediments or under anaerobic conditions plays an important role [33, 38]. In most aquatic ecosystems, the bottom sediments are under anoxic conditions. Under these anaerobic conditions, the nitrate reduction (denitrification), manganese reduction, iron reduction, and sulphate reduction would occur in an orderly fashion [33]. These reduction reactions are mediated by the indigenous microorganisms in anoxic environments where the appropriate electron acceptors (NO_3^-, Mn^{4+}, Fe^{3+}, and SO_4^{2-}) and electron donors (usually organic substances) are present. These processes consume hydrogen ions (H^+), which leads to an increase in the pH [12, 33].

For those alkalinity-generating processes, RW effectively increased the pH of the waters in the lakes (Figure 3(a)), which promoted the precipitation of metals. Therefore, most metal ions with low K_{sp}, such as Fe, Mn, Cu, and Zn, could form soluble hydroxides or carbonates [39, 40]. The main metal ions, such as Fe and Al, formed hydroxide colloids, which can be adsorbed into organic compounds and several kinds of ions, and then coprecipitated [41, 42]. When these series of reactions progresses, the precipitation of oxides, hydroxides, and other organic particulates can result in the movement of these metals from the water column into the sediments [43]. The bottom constructed sediments will create anaerobic environments. Under these conditions, the anaerobic and sulphate-reducing bacteria can use the sulphate to oxidize the organic matter and release bicarbonate and hydrogen sulphide [44]. Then, the produced hydrogen sulphide readily reacts with the dissolved metals to form insoluble metal sulphides that subsequently precipitate. Ultimately, the elimination of most of the above ions (Figure 4) results in a gradual decline in EC (Figure 3(b)).

The plants on the banks and those that are submerged are more important to the biological component in aquatic ecosystem [45]. The decomposition of these litters plays a vital role in the normal circulation of materials, energy flow, and the health and stability of the aquatic ecosystem [29]. It is of great significance to employ litter degradation as an indicator for evaluating the effects of contamination and eco-remediation. The organic matter will be converted into inorganic matter by a large number of microbes and benthonic animal communities in NW for the continuous degradation of the litter [46], in which the microbes are active, breed normally, and have a better degradation effect (Figure 4) due to the neutral pH and the absence of harmful substances. However, in AMDW, not only are the activity of the aquatic organisms and the richness and quantity of the microbes and benthonic animals markedly inhibited due to the low pH (2.73); high salinity; high concentrations of Fe, Mn, Cu, Zn, Pb and other toxic elements; and the rust-like suspended particles [33], but the degradation rates of the litters are also decreased. AMD pollution could cause long-term impairment to the waterways and biodiversity, which has serious human health and ecological implications [47].

5. Conclusions

The ecological remediation conducted in this study had good effects on buffering the acidity and removing metals and sulphate, which ultimately improved the water quality and the degradation of litters. However, there are large differences between the NW and RW in the anaerobic situation, primarily in terms of increasing the organic matter. The eco-technological remediation technology may be used as a pretreatment stage for the lake's water column. More studies are needed to develop a real and a sustainable remediation system in AMDW.

Data Availability

The main table and figure data used to support the findings of this study are included within the article.

Conflicts of Interest

The authors declare that they have no conflicts of interest.

Authors' Contributions

Kaiju Chen, Yan Zeng, Zhongzheng Wen, Zhengyan Ran, and Li He worked on conceptualization, investigation, and data curation. Tianling Fu and Hu Wang worked on writing the original draft, review and editing, and visualization. Tianling Fu supervised, reviewed, and edited the manuscript and took part in project administration. Yonggui Wu worked on supervision.

Acknowledgments

This work was supported by the Guizhou Province Science and Technology Agency Fund, China ([2020]3Y006 and [2020]4Y030).

References

[1] J. Plaza-Cazón, L. Benítez, J. Murray, P. Kirschbaum, and E. Donati, "Influence of extremophiles on the generation of acid mine drainage at the abandoned pan de azúcar mine (Argentina)," *Microorganisms*, vol. 9, no. 2, p. 281, 2021.

[2] X. Guo, S. Fu, J. Di, Y. Dong, and G. Jiang, "Study on the treatment of acid mine drainage containing fe2+ and mn2+ using modified spontaneous combustion gangue," *Journal of Renewable Materials*, vol. 9, no. 3, pp. 541–555, 2021.

[3] A. Akcil and S. Koldas, "Acid mine drainage (AMD): causes, treatment and case studies," *Journal of Cleaner Production*, vol. 14, no. 12-13, pp. 1139–1145, 2006.

[4] G. Naidu, S. Ryu, R. Thiruvenkatachari, Y. Choi, S. Jeong, and S. Vigneswaran, "A critical review on remediation, reuse, and resource recovery from acid mine drainage," *Environmental Pollution*, vol. 247, pp. 1110–1124, 2019.

[5] Y. Sato, T. Hamai, T. Hori et al., "Optimal start-up conditions for the efficient treatment of acid mine drainage using sulfate-reducing bioreactors based on physicochemical and microbiome analyses," *Journal of Hazardous Materials*, vol. 423, Article ID 127089, 2022.

[6] J. Skousen, C. E. Zipper, A. Rose et al., "Review of passive systems for acid mine drainage treatment," *Mine Water and the Environment*, vol. 36, no. 1, pp. 133–153, 2017.

[7] T. M. Valente and C. Leal Gomes, "Occurrence, properties and pollution potential of environmental minerals in acid mine drainage," *Science of the Total Environment*, vol. 407, no. 3, pp. 1135–1152, 2009.

[8] H. Tang, J. Z. Luo, L. W. Zheng et al., "Characteristics of pores in coals exposed to acid mine drainage," *Energy Reports*, vol. 7, pp. 8772–8783, 2021.

[9] D. Chen, Y. P. Chen, and Y. Lin, "Heavy rainfall events following the dry season elevate metal contamination in Mining-Impacted rivers: a case study of wenyu river, qinling, China," *Archives of Environmental Contamination and Toxicology*, vol. 81, no. 2, pp. 335–345, 2021.

[10] D. M. DeNicola and M. G. Stapleton, "Using macroinvertebrates to assess ecological integrity of streams remediated for acid mine drainage," *Restoration Ecology*, vol. 24, no. 5, pp. 656–667, 2016.

[11] K. S. Johnson, P. C. Thompson, L. Gromen, and J. Bowman, "Use of leaf litter breakdown and macroinvertebrates to evaluate gradient of recovery in an acid mine impacted stream remediated with an active alkaline doser," *Environmental Monitoring and Assessment*, vol. 186, no. 7, pp. 4111–4127, 2014.

[12] D. B. Johnson and K. B. Hallberg, "Acid mine drainage remediation options: a review," *Science of the Total Environment*, vol. 338, no. 1-2, pp. 3–14, 2005.

[13] S. Shirin, A. Jamal, C. Emmanouil, and A. K. Yadav, "Assessment of characteristics of acid mine drainage treated with fly ash," *Applied Sciences*, vol. 11, no. 9, p. 3910, 2021.

[14] V. Rey, C. A. Ríos, L. Y. Vargas, and T. M. Valente, "Use of natural zeolite-rich tuff and siliceous sand for mine water treatment from abandoned gold mine tailings," *Journal of Geochemical Exploration*, vol. 220, Article ID 106660, 2021.

[15] B. A. Firpo, J. Weiler, and I. A. H. Schneider, "Technosol made from coal waste as a strategy to plant growth and environmental control," *Energy Geoscience*, vol. 2, no. 2, pp. 160–166, 2021.

[16] D. M. Kargbo, G. Atallah, and S. Chatterjee, "Inhibition of pyrite oxidation by a phospholipid in the presence of silicate," *Environmental Science and Technology*, vol. 38, no. 12, pp. 3432–3441, 2004.

[17] K. Sasaki, M. Tsunekawa, S. Tanaka, and H. Konno, "Suppression of microbially mediated dissolution of pyrite by originally isolated fulvic acids and related compounds," *Colloids and Surfaces A: Physicochemical and Engineering Aspects*, vol. 119, no. 2-3, pp. 241–253, 1996.

[18] L. Zhang, Y. Y. Qiu, Y. Zhou, G. H. Chen, M. C. M. van Loosdrecht, and F. Jiang, "Elemental sulfur as electron donor and/or acceptor: mechanisms, applications and perspectives for biological water and wastewater treatment," *Water Research*, vol. 202, Article ID 117373, 2021.

[19] C. A. Cravotta, "Abandoned mine drainage in the swatara creek basin, southern anthracite coalfield, Pennsylvania, USA: 2. performance of treatment systems," *Mine Water and the Environment*, vol. 29, no. 3, pp. 200–216, 2010.

[20] A. Pat-Espadas, R. Loredo Portales, L. Amabilis-Sosa, G. Gómez, and G. Vidal, "Review of constructed wetlands for acid mine drainage treatment," *Water*, vol. 10, no. 11, p. 1685, 2018.

[21] P. L. Younger, A. Jayaweera, A. Elliot et al., "Passive treatment of acidic mine waters in subsurface-flow systems: exploring RAPS and permeable reactive barriers," *Land Contamination and Reclamation*, vol. 11, no. 2, pp. 127–135, 2003.

[22] S. G. Benner, D. W. Blowes, and C. J. Ptacek, "A full-scale porous reactive wall for prevention of acid mine drainage," *Groundwater Monitoring & Remediation*, vol. 17, no. 4, pp. 99–107, 1997.

[23] R. Sharma, J. Vymazal, and P. Malaviya, "Application of floating treatment wetlands for stormwater runoff: a critical review of the recent developments with emphasis on heavy metals and nutrient removal," *Science of the Total Environment*, vol. 777, Article ID 146044, 2021.

[24] J. E. Burgess and R. M. Stuetz, "Activated sludge for the treatment of sulphur-rich wastewaters," *Minerals Engineering*, vol. 15, no. 11, pp. 839–846, 2002.

[25] X. Cao, P. Wu, and Z. Cao, "Element geochemical characteristics of a soil profile developed on dolostone in central Guizhou, southern China: implications for parent materials," *Acta Geochimica*, vol. 35, no. 4, pp. 445–462, 2016.

[26] J. Ma, Z. Quan, Y. Sun, J. Du, and B. Liu, "Excess sulfur and Fe elements drive changes in soil and vegetation at abandoned coal gangues, Guizhou China," *Scientific Reports*, vol. 10, no. 1, Article ID 10456, 2020.

[27] G. Hao, F. Yun, L. Zhanyuan, Y. Sen, and Z. Song, "Study on the property and reuse of coal gangue in Liupanshui, Guizhou Province, China," *International Journal of Mining, Reclamation and Environment*, vol. 27, no. 5, pp. 366–373, 2013.

[28] L. Pan, X. Guan, B. Liu et al., "Pollution characteristics, distribution and ecological risk of potentially toxic elements in soils from an abandoned coal mine area in southwestern China," *Minerals*, vol. 11, no. 3, p. 330, 2021.

[29] R. Aerts, "Climate, leaf litter chemistry and leaf litter decomposition in terrestrial ecosystems: a triangular relationship," *Oikos*, vol. 79, no. 3, p. 439, 1997.

[30] M. Kalin, J. Cairns, and R. McCready, "Ecological engineering methods for acid mine drainage treatment of coal wastes," *Resources, Conservation and Recycling*, vol. 5, no. 2-3, pp. 265–275, 1991.

[31] J. Opitz, M. Alte, M. Bauer, and S. Peiffer, "The role of macrophytes in constructed surface-flow wetlands for mine water treatment: a review," *Mine Water and the Environment*, vol. 40, no. 3, pp. 587–605, 2021.

[32] P. Rajasulochana and V. Preethy, "Comparison on efficiency of various techniques in treatment of waste and sewage water – a comprehensive review," *Resource-Efficient Technologies*, vol. 2, no. 4, pp. 175–184, 2016.

[33] M. Kalin, A. Fyson, and W. N. Wheeler, "The chemistry of conventional and alternative treatment systems for the neutralization of acid mine drainage," *Science of the Total Environment*, vol. 366, no. 2-3, pp. 395–408, 2006.

[34] W. Y. Chia, K. W. Chew, C. F. Le et al., "Sustainable utilization of biowaste compost for renewable energy and soil

amendments," *Environmental Pollution*, vol. 267, Article ID 115662, 2020.

[35] A. Grasserová, A. Hanč, P. Innemanová, and T. Cajthaml, "Composting and vermicomposting used to break down and remove pollutants from organic waste: a mini review," *European Journal of Environmental Sciences*, vol. 10, no. 1, pp. 9–14, 2020.

[36] M. Kalin and W. Caetano Chaves, "Acid reduction using microbiology: treating AMD effluent emerging from an abandoned mine portal," *Hydrometallurgy*, vol. 71, no. 1-2, pp. 217–225, 2003.

[37] P. A. Siver, R. Ricard, R. Goodwin, and A. E. Giblin, "Estimating historical in-lake alkalinity generation from sulfate reduction and its relationship to lake chemistry as inferred from algal microfossils," *Journal of Paleolimnology*, vol. 29, no. 2, pp. 179–197, 2003.

[38] O. Totsche, R. Pöthig, W. Uhlmann, H. Büttcher, and C. E. Steinberg, "Buffering mechanisms in acidic mining lakes–a model-based analysis," *Aquatic Geochemistry*, vol. 9, no. 4, pp. 343–359, 2003.

[39] H. B. Bradl, "Adsorption of heavy metal ions on soils and soils constituents," *Journal of Colloid and Interface Science*, vol. 277, no. 1, pp. 1–18, 2004.

[40] J. f. Peng, Y. h. Song, P. Yuan, X. y. Cui, and G. l. Qiu, "The remediation of heavy metals contaminated sediment," *Journal of Hazardous Materials*, vol. 161, no. 2-3, pp. 633–640, 2009.

[41] B. J. Alloway, "Soil processes and the behaviour of metals," *Heavy metals in soils*, vol. 13, pp. 11–37, 1995.

[42] A. Pohl, "Removal of heavy metal ions from water and wastewaters by sulfur-containing precipitation agents," *Water, Air, & Soil Pollution*, vol. 231, no. 10, p. 503, 2020.

[43] M. Kalin, W. N. Wheeler, and G. Meinrath, "The removal of uranium from mining waste water using algal/microbial biomass," *Journal of Environmental Radioactivity*, vol. 78, no. 2, pp. 151–177, 2005.

[44] L. Shawar, I. Halevy, W. Said-Ahmad et al., "Dynamics of pyrite formation and organic matter sulfurization in organic-rich carbonate sediments," *Geochimica et Cosmochimica Acta*, vol. 241, pp. 219–239, 2018.

[45] A. B. G. Janssen, S. Hilt, S. Kosten, J. J. M. Klein, H. W. Paerl, and D. B. Van de Waal, "Shifting states, shifting services: linking regime shifts to changes in ecosystem services of shallow lakes," *Freshwater Biology*, vol. 66, no. 1, pp. 1–12, 2021.

[46] M. A. Graça, "The role of invertebrates on leaf litter decomposition in streams–a review," *International Review of Hydrobiology*, vol. 86, no. 4-5, pp. 383–393, 2001.

[47] S. E. Crawford, M. Brinkmann, J. D. Ouellet et al., "Remobilization of pollutants during extreme flood events poses severe risks to human and environmental health," *Journal of Hazardous Materials*, vol. 421, Article ID 126691, 2022.

Hindawi
Journal of Chemistry
Volume 2022, Article ID 4282992, 9 pages
https://doi.org/10.1155/2022/4282992

Research Article

Contamination and Ecological Risk Assessment of Heavy Metals in Surface Sediments of Huangshui River, Northwest China

Liwei Chen,[1] **Qi Wei**,[2] **Guangsu Xu**,[1] **Meng Wei**,[1] **and Hao Chen**[1]

[1]*School of Resources and Environmental Engineering, Ludong University, Yantai 264025, China*
[2]*Xining Sewage Treatment Ltd., Xining 810007, China*

Correspondence should be addressed to Liwei Chen; chenliwei@sina.com

Received 31 March 2022; Revised 13 May 2022; Accepted 6 June 2022; Published 24 June 2022

Academic Editor: Xia He

In the Xining area of Huangshui River, China, the concentrations of globally alarming toxic heavy metals such as chromium (Cr), arsenic (As), lead (Pb), cadmium (Cd), and zinc (Zn) in the surface sediments were measured to determine the ecological risks to the riverine ecosystem. Overall, the concentrations of heavy metals in the surface sediments were relatively high. The results indicated that the concentrations of Pb/Zn/Cr were lower than 120/250/200 $mg{\cdot}kg^{-1}$ which was the risk screening value of each heavy metal for soil contamination of agricultural land (GB15618-2018). The concentrations of As/Cd were higher than 120/3.0 $mg{\cdot}kg^{-1}$ which was the risk intervention value of As/Cd for soil contamination of agricultural land (GB15618-2018). Their values were arranged in the following decreasing order: As (151.23–818.55 $mg{\cdot}kg^{-1}$) > Cr (44.18–201.70 $mg{\cdot}kg^{-1}$) > Pb (29.10–121.95 $mg{\cdot}kg^{-1}$) > Zn (1.45–86.18 $mg{\cdot}kg^{-1}$) > Cd (4.36–6.21 $mg{\cdot}kg^{-1}$). The concentrations of As, Cr Pb, and Cd greatly exceeded the background contents of elements in Qinghai soils. While Zn was lower than background. The contamination factor (CF), the geoaccumulation index (I_{geo}), and the potential ecological risk index (RI) of As, Cr, Cd, and Pb followed the descending order of Cd > As > Pb > Cr > Zn. The order of the enrichment factor (EF) was as follows: As > Cd > Pb > Cr > Zn. The contamination level of heavy metals implied that the condition is frightening and probably severely affecting the aquatic ecology. Cd and As were the main contributing elements to the ecological risk of the sediments in the Xining area of the Huangshui River, which should be mainly studied and prevented.

1. Introduction

River serves a set of economic, cultural, and ecological functions such as transportation, ecotourism, aquaculture, agriculture, ecological habitat, and ecological defense impacts. However, human activities have a significant negative impact on the river shore regions and aquatic resources. The input of many bioaccumulative and persistent pollutants from anthropogenic activities might cause serious ecosystem issues [1–3]. Many rivers have been continuously threatened by various contaminants [4, 5]. In a consequence of their nonbiodegradation, biomagnification, and toxicity, heavy metals are considered as one of the world's most hazardous contaminants in the riverine aquatic environment [2, 6, 7]. In fact, different studies were performed on heavy metal accumulation in subsurface sediment and in many biochemical cycles [8–10].

Huangshui River is one of the most important rivers in the northeastern part of Qinghai Province. The water quality and quantity of Huangshui River is the research focus of many scholars. The research on the Huangshui River water body mostly focuses on the water quality of the river and the spatial and temporal distribution of pollutants [11–14]. Li et al. studied the impact of Huangshui River water quality on benthic fauna during the process of urbanization and analyzed the impact of water quality on the ecological environment from the perspective of biological habitats [15, 16].

There are few studies on the Huangshui River sediments. Chen and Huang studied the macroelement geochemical characteristics of the Huangshui River sediments from Huangyuan to Ledu and analyzed the relationship between chemical weathering index and regional natural climatic conditions [17, 18]. Zeng studied the overall situation of

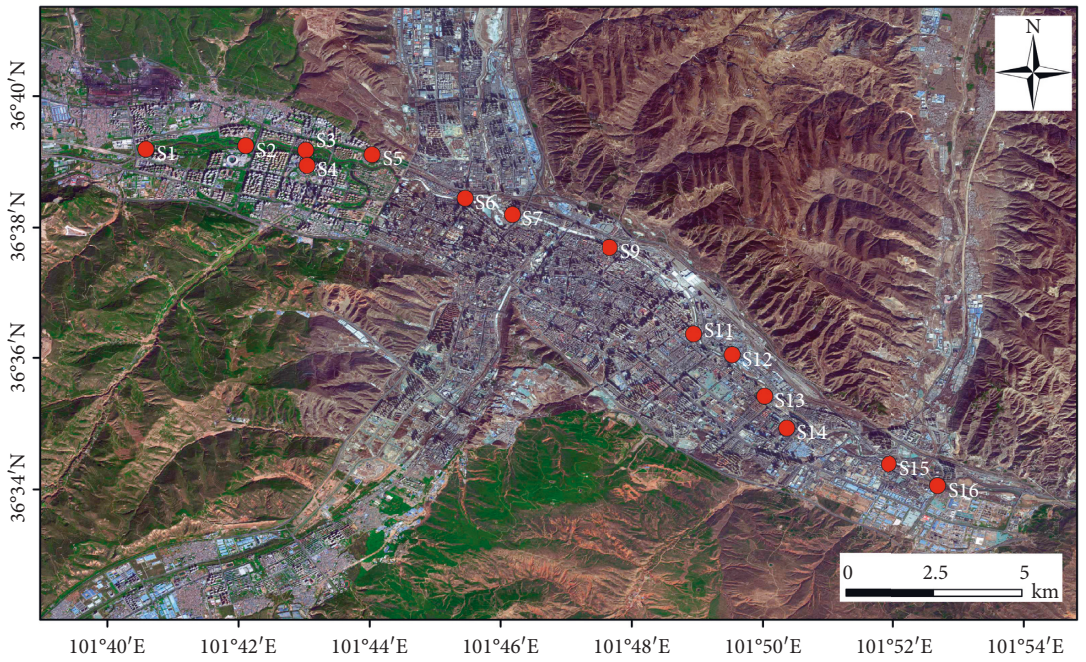

Figure 1: Sampling sites of Huangshui River.

heavy metal pollution along the Huangshui River by measuring the heavy metal content in the surface sediments and river water and the surface soil of the Huangshui River in Xining [19]. Few relevant studies have been conducted in the region; the studies that have been conducted have focused on a few areas. These indicated that the research on heavy metals in river sediments is not well studied.

Unlike some organic pollutants that can be partly degraded, many of the heavy metals accumulated in sediments for a long period pose severe toxicity risks. In addition, when water environmental conditions change, they will be released into water again, causing secondary pollution of water [20]. River sediment is the source and sink of heavy metals and other pollutants in the water environment. It is complex and essential for the ecosystem health, which deserves more investigations. The study fully considered the occurrence, spatial distribution, pollution status, and ecological risk of heavy metals in river sediments. It could reveal the migration and transformation of heavy metals between river water and sediments [21], help people better understand the change of the characteristics of heavy metals in the water environment, and provide a basic understanding of heavy metal pollution control in rivers.

2. Materials and Methods

2.1. Study Sites and Samples. Huangshui River is a tributary of the upper reaches of the Yellow River. It originates from Baohutu Mountain in Haiyan County, Qinghai Province, northwest of China. It has a wide valley and pleasant climate, giving birth to the plateau civilization for thousands of years. The narrow Huangshui River valley is home to nearly 60% of the population, 52% of the cultivated land, and more than 70% of the industrial and mining enterprises in Qinghai Province. Therefore, Huangshui River is called the "Mother River" of Qinghai Province. It is one of the main sources of the Yellow River. Some areas are 2000–4000 m above the sea level. The climate of the Huangshui River basin has the continental characteristics of plateau drought and semi-drought, and the average annual temperature is 2.8–7.9°C, the precipitation is 360–540 mm, and evaporation is 1100–1800 mm. The precipitation from May to September accounts for 81–88% of the annual precipitation.

Based on the characters of land form and intersection of the main stream and tributaries, Xining area of Huangshui River basin was investigated. To collect the inshore sediment samples, 16 sampling points were selected using the global positioning system (GPS) at 1.4 km interval going upstream to downstream (Figure 1) in 2018. The name of sampling stations was marked S1–S16 (Table 1).

Due to the actual terrain conditions, sampling point S8 was too deep to get the sample. Sampling point S10 was in the underground river of the Xining railway station area. No samples were collected. So, a total of 14 sediment samples were collected.

About 1 kg of surface sediments (at a depth of 0–10 cm) from the Huangshui River were collected at each sampling point with plastic spade, which were stored in clean and sterile polyethylene bags and then carried to the laboratory.

2.2. Sample Pretreatment and Instrumental Analysis. After removing foreign objects (leaves, rocks, snails or shells, and plant roots), sediment samples were dried naturally in the laboratory at room temperature and then were processed for grain size analysis. The sediment sample were passed through a 100-mesh sieve for analysis.

1 g of each sample was digested in 25 mL Teflon crucibles on the electric heating plate in mixed solution of HCl-

Table 1: Description of sampling points in the Huangshui River.

Sample number	Latitude	Longitude	Sampling position
S1	36°39′12″ N	101°40′35″ E	Xining Special Steel Park
S2	36°39′15″ N	101°42′6 E	Haihu Wetland Park
S3	36°39′11″ N	101°43′1″ E	Western Suburb Park
S4	36°38′57″ N	101°43′2″ E	Haihu Middle School
S5	36°39′7″ N	101°44′2″ E	Culture Park
S6	36°38′27″ N	101°45′27″ E	People's Park
S7	36°38′12″ N	101°46′10″ E	Local Police Station of Qilian road
S9	36°′42″ N	101°47′40″ E	Morning Market of Wuyi road
S11	36°36′22″ N	101°48′57″ E	Lianhe Village Mosque
S12	36°36′3″ N	101°49′32″ E	Huangzhong Road
S13	36°35′25″ N	101°50′2″ E	Bridge of Minhe Road
S14	36°34′56″ N	101°50′22″ E	Jingxifeng Wetland Park
S15	36°34′23″ N	101°51′56″ E	Tuanjieqiao Market
S16	36°34′3″ N	101°52′41″ E	Ninghu Wetland Park

HNO_3-HF-$HClO_4$, according to the National Standards of People's Republic of China (HJ 832–2017). The concentrations of As, Cr, Zn, Pb, and Cd in sediments were determined by the atomic absorption spectrophotometer (AAS, TAS-990, Beijing General Analysis).

Three parallel samples were used for all samples to control the relative error of each sediment sample which was less than 10%. Moreover, statistical analysis was performed by SPSS 2019. Origin 2019 was used for data visualization.

2.3. Pollution and Ecological Risk Assessment. The contamination factor (CF), enrichment factor (EF), and geoaccumulation index (I_{geo}) are used to assess the pollution and enrichment levels of heavy metal. Potential ecological risk index (RI) was used as pollution indices to assess ecological risks of heavy metals.

2.3.1. Contamination Factor (CF). The contamination factor (CF) is the ratio of the concentration of heavy metals and the background value in the soil. It was introduced by Hakanson and used to describe the contamination level of a substance [22].

$$\mathrm{CF}_i = \frac{C_i}{B_i}, \tag{1}$$

where CF_i is the contamination factor for pollutant, C_i is the concentration of the heavy metal in the sediment sample ($mg{\cdot}kg^{-1}$), and B_i is the background concentration for this heavy metal (background contents of elements in soils of Qinghai Province, Table 2) ($mg{\cdot}kg^{-1}$).

There are four grades of CF: low degree ($\mathrm{CF}_i < 1$), moderate degree ($1 < \mathrm{CF}_i < 3$), substantial degree ($3 < \mathrm{CF}_i < 6$), and very high degree ($\mathrm{CF}_i > 6$) [23].

2.3.2. Enrichment Factor (EF). The enrichment factor is considered as a normalized method to indicate differential variability of heavy metals in sediments from the anthropogenic and natural metal sources [24]. This involves the standardization of heavy metals in sediment with reference elements such as aluminum (Al), iron (Fe), manganese (Mn), titanium (Ti), selenium (Se), lithium (Li), and cesium (Cs) [25–27]. In this study, Li was been chosen to normalize metal concentration because it basically comes from natural sources. The following equation is used to define the normalized EF of heavy metals:

Table 2: The background concentrations of heavy metals in Qinghai Province.

Heavy metals	Cr	As	Pb	Cd	Zn
Background concentrations ($mg{\cdot}kg^{-1}$)	70.1	14	20.9	0.137	80.3

$$\mathrm{EF}_i = \frac{\left(C_i/[Li]\right)_{\mathrm{sample}}}{\left(B_i/[Li]\right)_{\mathrm{background}}}, \tag{2}$$

where C_i is the concentration of the heavy metal in the sediment sample ($mg{\cdot}kg^{-1}$), and B_i is the background concentration for this heavy metal ($mg{\cdot}kg^{-1}$). Background contents of elements in soils of Qinghai Province were used to calculate. There are five categories of contamination recognized: moderate enrichment ($2 < \mathrm{EF} < 5$), moderately severe enrichment ($5 < \mathrm{EF} < 10$), severe enrichment ($10 < \mathrm{EF} < 25$), very severe enrichment ($25 < \mathrm{EF} < 50$), and extremely high enrichment ($\mathrm{EF} > 50$) [28].

2.3.3. Geoaccumulation Index (I_{geo}). The geoaccumulation index was suggested by Muller [29]. It is a geochemical approach for estimating the enrichment of metal concentrations above background or baseline concentrations. Studies have shown that it is an efficient tool for characterizing the sediment pollution levels.

The geoaccumulation index (I_{geo}) indicates the pollution by heavy metals. It is calculated as follows:

$$I_{\mathrm{geo}} = \log_2 \frac{C_n}{1.5B_n}, \tag{3}$$

where C_n and B_n are the heavy metal concentrations in sample ($mg{\cdot}kg^{-1}$) and its geochemical baseline concentration ($mg{\cdot}kg^{-1}$), respectively. The constant factor 1.5 is introduced to minimize the effect of possible variations in the

Table 3: The concentrations of heavy metals in the sediments of Huangshui River (mg·kg^{-1}).

Site	Cr		As		Pb		Cd		Zn	
	Mean	SD	Mean	SD	Mean	SD	Mean	SD	Mean	SD
S1	63.55	0.40	414.93	0.07	80.05	0.07	6.21	0.11	27.70	0.26
S2	44.18	0.45	151.23	0.14	42.75	0.23	5.74	0.03	6.95	0.07
S3	82.68	0.40	425.83	0.25	91.30	0.15	4.53	0.22	35.78	0.09
S4	77.35	0.42	464.20	0.23	29.10	0.09	4.39	0.13	86.18	0.08
S5	86.03	0.12	498.55	0.22	85.80	0.11	4.50	0.13	17.95	0.03
S6	139.85	0.22	499.38	0.41	89.20	0.14	4.36	0.11	34.23	0.08
S7	198.13	0.56	671.05	0.16	106.25	0.15	4.68	0.23	5.90	0.23
S9	190.90	0.29	788.35	0.54	115.60	0.51	4.71	0.33	5.13	0.11
S11	138.75	0.28	473.48	0.33	94.35	0.77	4.80	0.08	2.78	0.08
S12	200.20	0.22	818.55	0.32	116.00	0.08	4.82	0.12	3.50	0.11
S13	201.70	0.45	718.98	0.15	121.95	0.06	5.10	0.08	5.60	0.25
S14	186.25	0.35	532.78	0.14	88.95	0.38	5.09	0.06	3.00	0.11
S15	157.95	0.02	293.90	0.24	54.50	0.44	4.91	0.07	1.60	0.09
S16	161.25	0.21	362.58	0.28	57.00	0.22	5.15	0.04	1.45	0.10

geochemical background values, which may be attributed to mineralogical variations in the sediments [30]. The geochemical baseline concentrations of heavy metals in study area were referred to background contents of elements in soils of Qinghai Province [31]. Degrees of contamination are typically divided into six classifications based on I_{geo} values [32]. Classification I ($I_{geo} < 0$) represents unpolluted, classification II ($0 \le I_{geo} < 1$) represents unpolluted to moderated polluted, classification III ($1 \le I_{geo} < 2$) represents moderated polluted, classification IV ($2 \le I_{geo} < 3$) represents moderate to heavily polluted, classification V ($3 \le I_{geo} < 4$) represents heavily polluted, classification VI ($4 \le I_{geo} < 5$) represents heavily to extremely polluted, and classification VII ($I_{geo} \ge 5$) represents extremely polluted.

2.3.4. Potential Ecological Risk Index (RI). Ecological risk index (RI) is a sedimentological approach for ecological assessment using a diagnostic tool developed by Hakanson [22]. This method not only pays attention to the amount of heavy metals but also combines the ecological effect with the toxicology. Therefore, it can intuitively show the toxicity of heavy metals and its harm to biology. The calculation of RI is on the basis of the assumption that the sensitivity of the aquatic system depends on its productivity. It can be determined through the following formula:

$$C_f^i = \frac{C^i}{C_n^i},$$
$$E_r^i = T_r^i \times C_f^i, \quad (4)$$
$$\mathrm{RI} = \sum E_r^i,$$

where C_f^i represents the contamination factor, C^i is the concentration of the heavy metal (mg·kg^{-1}), and C_n^i is background values (mg·kg^{-1}). If $E_r^i < 45$, $RI < 150$, it is ranked as low risk; if $45 \le E_r^i < 90$, $150 < RI < 300$, it is moderate potential ecological risk; if $90 \le E_r^i < 180$, $300 < \mathrm{RI} < 600$, it is considerable potential ecological risk; if $180 \le E_r^i < 360$, it is ranked high potential ecological risk; if $E_r^i \ge 360$, $RI > 600$, it may cause a very high risk for environment. T_r^i is the toxic response factors (Cd: 30; Cr: 2; Pb: 5; Zn: 1; As: 10) [33].

3. Results and Discussion

3.1. Concentrations and Spatial Distribution of Heavy Metals. Table 3 provides the concentrations of 5 heavy metals in 14 surface sediments from Xining area of Huangshui River. Among the sampling sites, a broad range of heavy metal concentrations was observed. The spatial distribution of As, Cr, and Pb exhibited the similar trend (Figure 2).

The variation of As concentration was 151.23–818.55 mg·kg^{-1}, with an average of 508.13 mg·kg^{-1}. The concentration of As in all sampling points of sediment was higher than the risk intervention values for soil contamination of agricultural land (GB15618-2018) [34] seriously and generally increased first and then decreased, with a sharp decline at sampling points S2 and S11 (Figure 2(a)). However, the concentration of As was still in a high range, and the pollution of As in the sediments of Huangshui River was very serious.

Cr concentrations varied in the range of 44.18–201.70 mg·kg^{-1}, which were lower than the risk screening values for soil contamination of agricultural land. In the Xining area of Huangshui River, the concentration of Cr in sediment gradually increased. From sampling site S6, it increased significantly and maintained a high concentration level within a certain distance, while at sampling site S11, it decreased significantly (Figure 2(b)). The concentration of Pb varied in the range of 29.10–121.95 mg·kg^{-1}, which was lower than the risk screening values for soil contamination of agricultural land. Its variation trend was basically the same as that of As and Cr. The concentration at sampling site S11 decreased significantly. During sampling site investigation, it was found that there were construction projects in the middle reaches, which may be the cause of lead pollution.

The concentration of Zn was lower than the background value of soil content in Qinghai Province and the risk screening values for soil contamination of agricultural land.

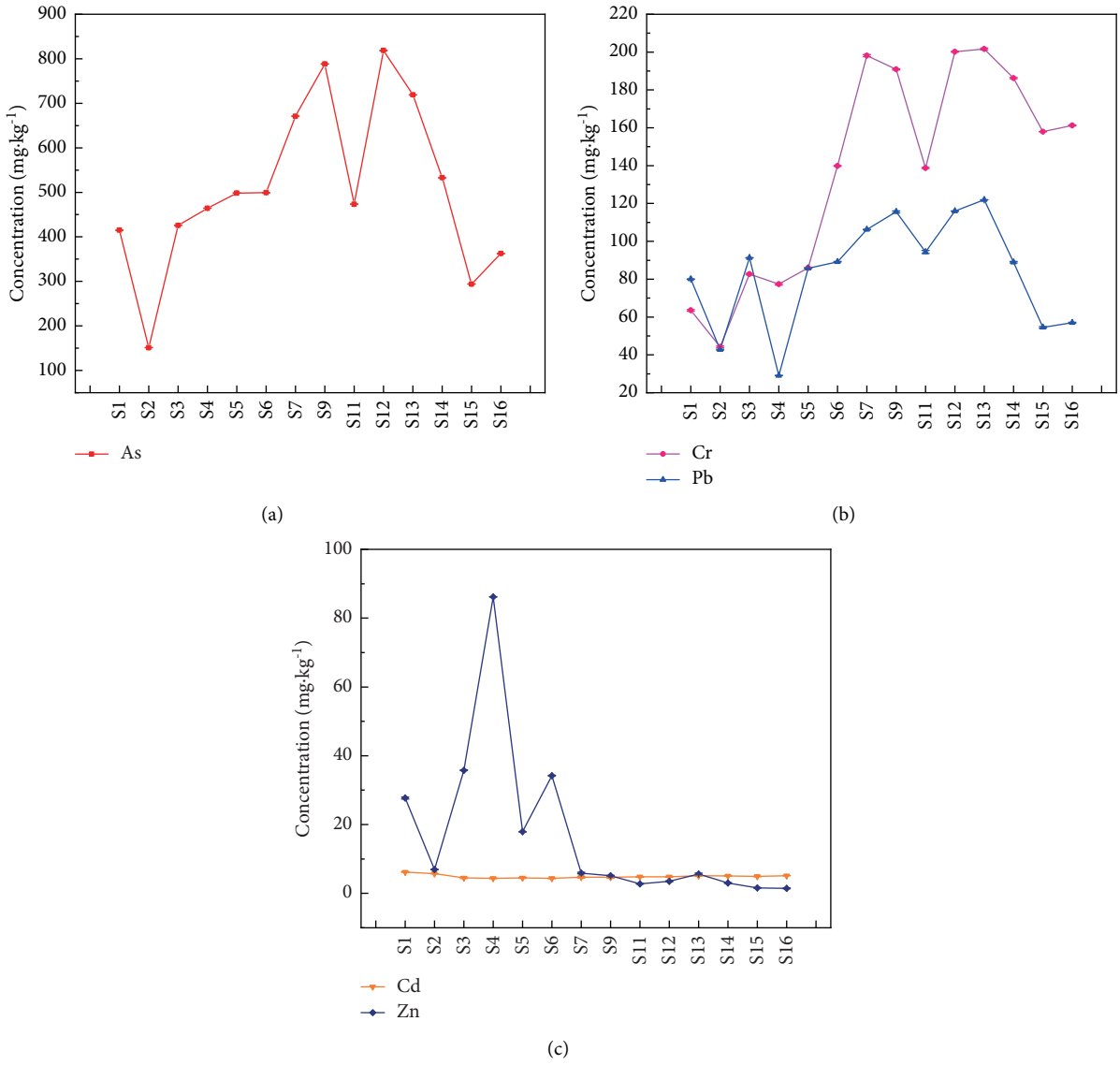

Figure 2: Variation of heavy metals concentrations in the sediments. (a) As; (b) Cr, Pb; (c) Cd, Zn.

Zn exhibited a nonfluctuating pattern with lower values (Figure 2(c)). Therefore, it can be preliminarily judged that there is no Zn pollution in the sediments of Huangshui River. Cd concentration varied from 4.36 mg·kg^{-1} to 6.21 mg·kg^{-1} with the maximum value near S1 which exceeded *t*, the risk intervention values for soil contamination of agricultural land seriously. It indicated that Cd released from Xining Special Steel Co., Ltd. affected the concentration of heavy metals in sediments of Huangshui River.

The concentrations of Cr, Pb, As, and Cd were higher than the corresponding values of soil elements in layer A of Qinghai Province. The order of the heavy metals concentration was as follows: As > Cr > Pb > Zn > Cd.

The concentration and variation trends of Pb and Cd were similar to those of previous studies [14, 18, 19]. But as for As and Cr were quite different. Most of the concentrations of five heavy metals were clearly greater than previous studies. Different sampling sites may be the reasons for such differences. Moreover, the reason for exceeding the standard and background values of heavy metals in sediment is that Xining Special Steel Co., Ltd. in the upstream area expands production scale year by year and the increase of new construction sites along the Huangshui River. The rapid urbanization process and development of transportation result in the accumulation of heavy metals in river sediments [35, 36].

3.2. Assessment of Heavy Metals Pollution in Sediment. The mean contamination factor (CF) values of Cr, As, Pb, Cd, and Zn were 1.97, 36.29, 4.01, 35.97, and 0.02, respectively (Figure 3). The contamination factor value for Zn was low (CF < 1). In contrast, As and Cd showed very high levels of contamination at all locations. Cr showed moderate levels of contamination (except at S1 and S2 which was low

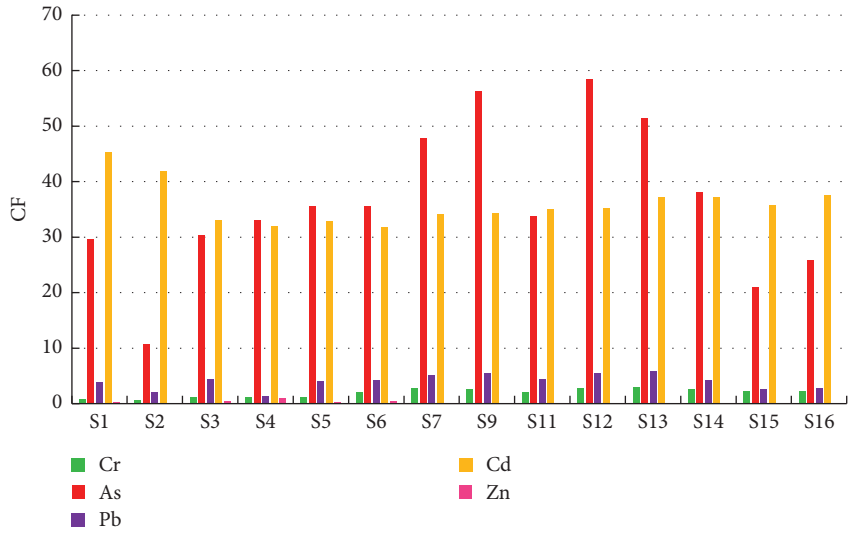

Figure 3: The column chart of the concentration factor (CF) of heavy metals in sediments.

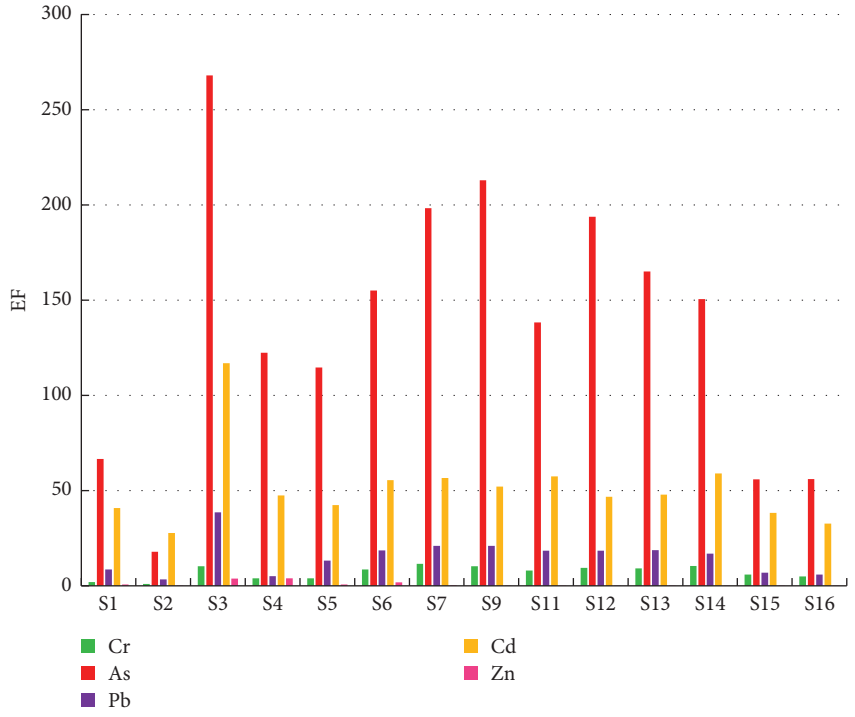

Figure 4: The column chart of the enrichment factor (EF) of heavy metals in sediments.

degree). Overall, the descending order of Cd > As > Pb > Cr > Zn for CF was found as heavy metals in the sediment of Huangshui River.

Figure 4 shows the EF values of heavy metals studied in this work. As and Cd recorded extremely high enrichment (average EF = 136.88 and 51.60, respectively). Cr indicated moderate to moderately severe enrichment ($1.04 < EF < 11.66$ with the average of 7.15). Pb recorded severe enrichment (average EF = 15.39). Zn showed no enrichment (EF < 1 except S3, S4, and S6). Since EF values represented the difference between anthropogenic and natural sources of heavy metals, the results suggested that emissions of As, Cd, Cr, and Pb from human activities had an impact on the river environment. Researchers have found similar results in other water environments [37–39].

Thus, with respect to the background concentration values, the surface river sediments are observed to be highly polluted with As and Cd. The order of the EF values was as follows: As > Cd > Pb > Cr > Zn.

The potential ecological hazard index E_r^i and comprehensive potential ecological hazard index (RI) of Cr, As, Pb, Cd, and Zn are shown in Figure 5. The E_r^i values of Cr, Pb, and Zn were less than 45, indicating low ecological risk. E_r^i for As were higher than 180 which indicated high risk

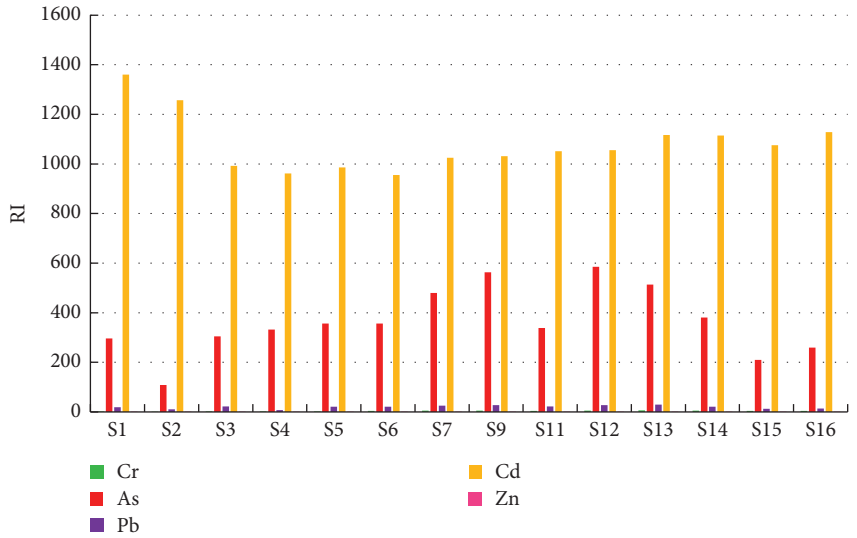

Figure 5: The column chart of the potential ecological risk index (RI) of heavy metals in sediments.

Table 4: Geoaccumulation index and pollution classification of heavy metals in sediments.

Site	Cr		As		Pb		Cd		Zn	
	I_{geo}	Classification	I_{geo}	Classification	I_{geo}	Classification	I_{geo}	Classification	I_{geo}	Classification
S1	−0.73	0	4.30	5	1.35	2	4.92	5	−2.12	0
S2	−1.25	0	2.85	3	0.45	1	4.80	5	−4.12	0
S3	−0.35	0	4.34	5	1.54	2	4.46	5	−1.75	0
S4	−0.44	0	4.47	5	−0.11	0	4.42	5	−0.48	0
S5	−0.29	0	4.57	5	1.45	2	4.45	5	−2.75	0
S6	0.41	1	4.57	5	1.51	2	4.41	5	−1.82	0
S7	0.91	1	5.00	5	1.76	2	4.51	5	−4.35	0
S9	0.86	1	5.23	6	1.88	2	4.52	5	−4.55	0
S11	0.40	1	4.49	5	1.59	2	4.55	5	−5.44	0
S12	0.93	1	5.28	6	1.89	2	4.55	5	−5.10	0
S13	0.94	1	5.10	6	1.96	2	4.63	5	−4.43	0
S14	0.82	1	4.67	5	1.50	2	4.63	5	−5.33	0
S15	0.59	1	3.81	4	0.80	1	4.58	5	−6.23	0
S16	0.62	1	4.11	5	0.86	1	4.65	5	−6.38	0

(except considerable risk for site S2). Cd has extremely serious ecological hazard risk. Considering the ecological risk index (RI) all stations was at extremely high risk, mainly due to the high content of Cd in the sediments. The order of the RI values was as follows: Cd > As > Pb > Cr > Zn. High ecological risk induced by these five heavy metals demonstrates that human activities have greatly affected the river environment. At the same time, rivers can release these pollutants again, causing ecological risks [40, 41].

Based on Table 2, the geoaccumulation index (I_{geo}) and comprehensive pollution classification of Cr, As, Pb, Cd, and Zn are given in Table 4. The I_{geo} values indicated that no sampling site was observably polluted by Zn. The upstream part was not polluted by Cr, while the middle and downstream part was mildly to moderately polluted. Two-thirds of the sampling sites were mildly to moderately polluted by Cr. All sampling sites (except S4) were moderately polluted by Pb. Both As and Cd were highly polluted and extremely polluted. The order of the I_{geo} values was as follows: Cd > As > Pb > Cr > Zn. Sediments always reflect the contamination history of water bodies [42]. It can be inferred that the heavy metals in sediments in Xining area of Huangshui River have existed for a period. This is also confirmed by previous studies [11, 16, 17, 19].

In general, there is no difference between the results of CF, I_{geo}, and RI. The only difference lies in the EF risk order of Cd and As. For the studied sediments, the four methods show medium to extreme risk.

This implies that although the total concentrations of Pb and Cr are relatively low, the high toxicity and mobility of them in sediments can lead to high risk to the Huangshui River area. The concentration of Zn in the sampling area is lower than the background concentration. Relatively small range of metal distribution indicates that these metals are mainly from natural sources [43].

4. Conclusion

Analyses of heavy metals concentrations in 14 surface sediments from Xining area of the Huangshui River led to the following order of heavy metal concentrations: As > Cr > Pb > Zn > Cd.

The concentrations of Pb, Zn, and Cr are low, which are below the risk screening values for soil contamination of agricultural land. As and Cd pollution are very serious. Their concentrations exceed the risk intervention values for soil contamination of agricultural land. The distribution of heavy metals within the studied section revealed that a fluctuating pattern, but there were some individual samples containing high proportion of certain metals. Furthermore, based on 4 different pollution indices, the order of the ecological risk is as follows: Cd > As > Pb > Cr > Zn. Cd and As are the main contributing elements to ecological risk in Xining area of Huangshui River.

The results of this study give valuable information about heavy metal distribution in surface sediments from Huangshui River. Moreover, the study suggests initiating a long-term monitoring program to improve the understanding of the behavior of such metals and the temporal changes of the environment.

Data Availability

The data used to support the findings of this study are available from the corresponding author upon request.

Conflicts of Interest

The authors declare that they have no conflicts of interest.

Acknowledgments

The authors would like to express their sincere acknowledgement to all the participants. This research was funded by Youth Innovation Team Project for Talent Introduction and Cultivation in Universities of Shandong Province.

References

[1] C. M. Bowman, F. A. Landee, and M. H. Reslock, "A chemically oriented information storage and retrieval system. I. storage and verification of structural information," *Journal of Chemical Documentation*, vol. 7, no. 1, pp. 331–354, 1967.

[2] V. Aghadadashi, M. R. Neyestani, A. Mehdinia et al., "Spatial distribution and vertical profile of heavy metals in marine sediments around Iran's special economic energy zone; arsenic as an enriched contaminant," *Marine Pollution Bulletin*, vol. 138, pp. 437–450, 2019.

[3] A. Kahal, A. S. El-Sorogy, S. Qaysi, S. Almadani, O. M. Kassem, and A. Al-Dossari, "Contamination and ecological risk assessment of the red sea coastal sediments, southwest Saudi Arabia," *Marine Pollution Bulletin*, vol. 154, Article ID 111125, 2020.

[4] M. Wu, Y. Jia, Y. Zhang et al., "Heavy metal pollution from copper smelting during the shang dynasty at the laoniupo site in the bahe river valley, guanzhong basin, China," *Journal of Geographical Sciences*, vol. 31, no. 11, pp. 1675–1693, 2021.

[5] Y. Z. Zhai, F. X. Zheng, D. F. Li, X. Y. Cao, and Y. G. Teng, "Distribution, genesis, and human health risks of groundwater heavy metals impacted by the typical setting of songnen plain of NE China," *International Journal of Environmental Research and Public Health*, vol. 19, no. 6, p. 3517, 2022.

[6] M. M. Ali, M. L. Ali, R. Proshad, S. Islam, Z. Rahman, and T. Kormoker, "Assessment of trace elements in the demersal fishes of a coastal river in Bangladesh: a public health concern," *Thalassas: International Journal of Marine Science*, vol. 36, no. 2, pp. 641–655, 2020.

[7] M. S. Hossain, M. K. Ahmed, S. Sarker, and M. S. Rahman, "Seasonal variations of trace metals from water and sediment samples in the northern Bay of Bengal," *Ecotoxicology and Environmental Safety*, vol. 193, Article ID 110347, 2020.

[8] M. Damak, R. Fourati, B. Ellech, and M. Kallel, "Assessment of organic and metallic contamination in the surface sediment of monastir bay (Eastern Tunisia): spatial distribution, potential sources, and ecological risk assessment," *Marine Pollution Bulletin*, vol. 149, Article ID 110500, 2019.

[9] Y. H. Zhang, H. B. Zhang, Z. B. Zhang et al., "pH effect on heavy metal release from a polluted sediment," *Journal of Chemistry*, vol. 2018, Article ID 7597640, 7 pages, 2018.

[10] S. An, N. Liu, X. Li, S. Zeng, X. Wang, and D. Wang, "Understanding heavy metal accumulation in roadside soils along major roads in the tibet plateau," *Science of the Total Environment*, vol. 802, Article ID 149865, 2022.

[11] Y. Qiu, C. Lu, Z. Xu, and Y. Q. Wang, "Spatio-temporal variation characteristics and analysis of water pollution sources in the huangshui river Basin," *Acta Scientiae Circumstantiae*, vol. 37, no. 8, pp. 2829–2837, 2017, in Chinese.

[12] H. S. Li, C. Y. Zhou, L. W. Meng, and L. Yang, "Continuous monitoring analysis of COD in huangshui river, xining," *Environmental Impact Assessment*, vol. 38, no. 2, pp. 75–77, 2016, in Chinese.

[13] Q. H. Wang, Z. C. Wang, and P. Li, "Water environment quality and pollution characteristics in huangshui river of Qinghai," *Journal of Qinghai Normal University (Natural Science)*, vol. 4, pp. 71–74, 2009, in Chinese.

[14] J. Wu, S. J. Lu, S. Y. Wang et al., "Water contamination survey in xining reach of huangshui river," *Journal of Environmental Health*, vol. 29, no. 12, pp. 1115-1116, 2012, in Chinese.

[15] N. Li, A. L. Chen, C. J. Yang, Y. Y. Sun, G. L. Ma, and Q. Ma, "Impact of urbanization on water quality and macrobenthos community structure upstream in the huangshui river," *Acta Ecologica Sinica*, vol. 27, no. 10, pp. 3570–3576, 2017, in Chinese.

[16] N. Li, A. L. Chen, C. J. Yang et al., "Diversity of benthic macroinvertebrates and water physical and chemical indexes in upstream of huangshui river," *Chinese Agricultural Science Bulletin*, vol. 32, no. 23, pp. 43–48, 2016, in Chinese.

[17] Z. Y. Chen and Y. Huang, "Chemical alternation index and element geochemistry of riverbed sediments from huangshui river," *Journal of Arid Land Resources & Environment*, vol. 27, no. 5, pp. 179–183, 2013, in Chinese.

[18] Z. Y. Chen, "Analysis of chemical weathering based on chemical alternation index in huangshui river Basin," *Journal of Anhui Agriculture Science*, vol. 42, no. 12, pp. 3632–3634, 2014, in Chinese.

[19] F. M. Zeng, "Assessment of heavy metal pollution in xining section of the huangshui river," *Journal of Salt Lake Research*, vol. 25, no. 2, pp. 8–12, 2017, in Chinese.

[20] O. C. Ihunwo, A. N. Dibofori-Orji, C. Olowu, and M. U. Ibezim-Ezeani, "Distribution and risk assessment of some heavy metals in surface water, sediment and grey mullet (mugil cephalus) from contaminated creek in Woji, southern Nigeria," *Marine Pollution Bulletin*, vol. 154, Article ID 111042, 2020.

[21] S. S. Fong, T. Y. Ling, N. Lee, G. Norliza, W. Y. Ee, and K. L. Ping, "Assessment of heavy metals in water, sediment, and fishes of a large tropical hydroelectric dam in sarawak, Malaysia," *Journal of Chemistry*, vol. 2016, Article ID 8923183, 10 pages, 2016.

[22] L. Hakanson, "An ecological risk index for aquatic pollution control.a sedimentological approach," *Water Research*, vol. 14, no. 8, pp. 975–1001, 1980.

[23] W. Luo, Y. Lu, J. P. Giesy et al., "Effects of land use on concentrations of metals in surface soils and ecological risk around guanting reservoir, China," *Environmental Geochemistry and Health*, vol. 29, no. 6, pp. 459–471, 2007.

[24] M. H. Sayadi, M. R. G. Sayyed, and S. Kumar, "Short-term accumulative signatures of heavy metals in river bed sediments in the industrial area, Tehran, Iran," *Environmental Monitoring and Assessment*, vol. 162, pp. 465–473, 2010.

[25] B. Amin, A. Ismail, A. Arshad, C. K. Yap, and M. S. Kamarudin, "Anthropogenic impacts on heavy metal concentrations in the coastal sediments of Dumai, Indonesia," *Environmental Monitoring and Assessment*, vol. 148, no. 1, pp. 291–305, 2009.

[26] S. Salati and F. Moore, "Assessment of heavy metal concentration in the khoshk river water and sediment, Shiraz, Southwest Iran," *Environmental Monitoring and Assessment*, vol. 164, no. 1, pp. 677–689, 2010.

[27] M. M. Ali, S. Rahman, M. S. Islam et al., "Distribution of heavy metals in water and sediment of an urban river in a developing country: a probabilistic risk assessment," *International Journal of Sediment Research*, vol. 37, no. 2, pp. 173–187, 2022.

[28] G. F. Birch and M. A. Olmos, "Sediment-bound heavy metals as indicators of human influence and biological risk in coastal water bodies," *ICES Journal of Marine Science*, vol. 65, no. 8, pp. 1407–1413, 2008.

[29] G. Muller, "Index of geoaccumulation in sediments of the rhine river," *Geojournal*, vol. 2, no. 3, pp. 108–118, 1969.

[30] P. Stoffers, G. P. Glasby, C. J. Wilson, K. R. Davis, and P. Walter, "Heavy metal pollution in wellington harbour," *New Zealand Journal of Marine & Freshwater Research*, vol. 20, no. 3, pp. 495–512, 1986.

[31] China National Environmental Monitoring Center, *Background Contents of Elements in China Soils*, Chinese Environmental Sciences Press, Beijing, China, 1990.

[32] H. Haris, L. J. Looi, A. Z. Aris et al., "Geo-accumulation index and contamination factors of heavy metals (Zn and Pb) in urban river sediment," *Environmental Geochemistry and Health*, vol. 39, no. 6, pp. 1259–1271, 2017.

[33] J. Singh and B.-K. Lee, "Reduction of environmental availability and ecological risk of heavy metals in automobile shredder residues," *Ecological Engineering*, vol. 81, pp. 76–81, 2015.

[34] Standardization Administration, *Soil Environmental Quality—Risk Control Standard for Soil Contamination of Agricultural Land, Soil Environmental Quality*, pp. 2-3, 2018.

[35] G. Zhang, J. Bai, R. Xiao et al., "Heavy metal fractions and ecological risk assessment in sediments from urban, rural and reclamation-affected rivers of the pearl river Estuary, China," *Chemosphere*, vol. 184, pp. 278–288, 2017.

[36] C. Zhang, B. Shan, W. Tang, L. Dong, W. Zhang, and Y. Pei, "Heavy metal concentrations and speciation in riverine sediments and the risks posed in three urban belts in the Haihe Basin," *Ecotoxicology and Environmental Safety*, vol. 139, pp. 263–271, 2017.

[37] L. Jian, Y. C. Lin, J. Wu, and C. Zhang, "Continental-scale spatial distribution, sources, and health risks of heavy metals in seafood: challenge for the water-food-energy nexus sustainability in coastal regions?" *Environmental Science and Pollution Research*, vol. 28, pp. 63815–63828, 2021.

[38] W. Tang, L. Sun, L. Shu, and C. Wang, "Evaluating heavy metal contamination of riverine sediment cores in different land-use areas," *Frontiers of Environmental Science & Engineering*, vol. 14, no. 6, p. 104, 2020.

[39] Z. Ma, K. Chen, Z. Yuan, J. Bi, and L. Huang, "Ecological risk assessment of heavy metals in surface sediments of six major Chinese freshwater lakes," *Journal of Environmental Quality*, vol. 42, no. 2, pp. 341–350, 2013.

[40] L. Gao, Z. Wang, S. Li, and J. Chen, "Bioavailability and toxicity of trace metals (Cd, Cr, Cu, Ni, and Zn) in sediment cores from the shima river, South China," *Chemosphere*, vol. 192, pp. 31–42, 2018.

[41] H. Arambourou, L. Llorente, I. Moreno-Ocio et al., "Exposure to heavy metal-contaminated sediments disrupts gene expression, lipid profile, and life history traits in the midge chironomus riparius," *Water Research*, vol. 168, Article ID 115165, 2020.

[42] C. K. Jain, "Metal fractionation study on bed sediments of river yamuna, India," *Water Research*, vol. 38, no. 3, pp. 569–578, 2004.

[43] L. C. Mao, L. B. Liu, N. X. Yan et al., "Factors controlling the accumulation and ecological risk of trace metal (loid)s in river sediments in agricultural field," *Chemosphere*, vol. 243, Article ID 125359, 2019.

Hindawi
Journal of Chemistry
Volume 2022, Article ID 9456026, 7 pages
https://doi.org/10.1155/2022/9456026

Research Article

Application of an Anaerobic–Anoxic–Oxic–Oxic (AAO/O) Model to the Treatment of Real Domestic Wastewater

Duc-Thuong Vo,[1] **Hoang-Vinh-Truong Phan**,[2,3] **Le-Thuy-Thuy-Trang Hoang**,[1] **Van-Kieu Nguyen**,[2,3] **Thanh-Nha Tran**,[1] **and Minh-Trung Dao**[1]

[1]*Department of Environmental Engineering, Thu Dau Mot University, Thu Dau Mot City, Binh Duong, Vietnam*
[2]*Institute of Fundamental and Applied Sciences, Duy Tan University, Ho Chi Minh 700000, Vietnam*
[3]*Faculty of Natural Sciences, Duy Tan University, Da Nang 550000, Vietnam*

Correspondence should be addressed to Minh-Trung Dao; trungdm@tdmu.edu.vn

Received 17 March 2022; Revised 6 May 2022; Accepted 24 May 2022; Published 11 June 2022

Academic Editor: Jun Wu

Untreated or inadequately treated domestic wastewater has adversely affected the aquatic environment and public health in many cities in Vietnam. A conventional anaerobic–anoxic–oxic (AAO) process is recognized as an easy-to-handle approach that constrains chemical use during the procedure. Herein, we improve an AAO system by adding more oxic orders in association with a biological membrane in order to increase the hydraulic retention time (HRT) of the oxic zone in the system. The investigated system was applied to the treatment of real domestic wastewater during 168 days of operation. The performance of the system reached a stable state after 60 days of operation. The removal efficiency of total nitrogen (TN), total phosphorus (TP), total suspended solids (TSS), biological oxygen demand (BOD_5), and chemical oxygen demand (COD) was found to be $93.6 \pm 3.0\%$, $91.9 \pm 3.5\%$, $88.6 \pm 1.2\%$, $82.6 \pm 1.4\%$, and $71.8 \pm 0.7\%$, respectively. After the operation process, the TN, TP, and TSS contents in the wastewater effluents met the A level in accordance with the QCVN 14-MT:2015/BTNMT regulation, and the effluents of COD and BOD_5 almost satisfied the requirement, with only some points being slightly higher than the limit values. The obtained data revealed that the AAO/O system was capable of treating domestic wastewater in small and medium-sized domestic wastewater treatment facilities.

1. Introduction

Wastewater treatment is one of the most pressing challenges for developing nations [1, 2]. Due to the rapid pace of population growth, organic compounds and nutrients from municipal wastewater have increased day by day and have contaminated the watercourses. More seriously, the untreated wastewater is mostly discharged into sewage sludge systems without any suitable treatment [2, 3]. Disqualified domestic wastewater is the most terrifying cause of water pollution and the leading threat to the global environment [4]. In Vietnam, the full-design capacity of the 24 existing centralized wastewater treatment plants is about 670,000 m^3/day; however, only 10% of urban wastewater is treated [5]. As a result, many cities in Vietnam have confronted negative effects not only on the quality of the surface water sources but also on the life and health of the residents [6]. Therefore, the development and application of domestic wastewater treatment before disposal is a necessary and urgent task in this developing country.

The constituents of wastewater originating from households consist of nitrogen, phosphorus, and broad groups of organic matters [7]. Common technologies for the treatment of this type of wastewater are anoxic–oxic (AO) [8, 9], AAO [10–12], University of Cape Town (UCT) [13, 14], the sequencing batch reactor (SBR) [15, 16], and membrane bioreactor (MBR) [13, 17]. When applied to domestic wastewater, they have shown relatively high performance towards several bulk parameters, including COD, TN, TP, and TSS [8, 15, 16]. Many prevalent technologies based on this combination have been developed. Each method has its own advantages and disadvantages. The most

appropriate method can be chosen based on cost-efficiency and the properties of the wastewater [18, 19]. Among those techniques, many researchers have indicated the superiority of the AAO process which involves biological processes conducted in anaerobic, anoxic, and oxic conditions [20]. This process has superior properties, such as being simpler than other simultaneous nitrogen, organics, and phosphorus removal processes. It has a short hydraulic retention time, a strong impact load resistance, and low operating management costs [21].

In the AAO process, the hydraulic retention time (HRT) is a critical operating parameter affecting the biological treatment, the infrastructure, and the operational cost in the design and operation of wastewater treatment plants (WWTPs) [22, 23]. HRT that is too short can result in less contact time between the substrates and microorganisms, thereby decreasing the treatment efficiency of the pollutants in wastewater [23, 24]. The HRT is influenced by the geometric dimensions of the reactor [25]. In order to increase the HRT in WWTPs, an additional tank volume is normally required [26], possibly leading to an increase in the overall operational cost and difficulty in controlling the HRT. Modifying a conventional AAO model is, therefore, a promising way to improve the efficiency of the system.

In this study, the AAO model was modified by adding an oxic zone in association with a biological membrane to increase the HRT in order to provide more contact time between the microorganisms and substrates. The investigated system is called the AAO/O model. The designed system was applied for the treatment of real domestic wastewater from a household in Vietnam. The investigated parameters including pH, BOD_5, COD, TN, TP, and TSS were evaluated based on the allowable pollution parameters of Vietnamese environmental standards.

2. Materials and Methods

2.1. Materials. Raw wastewater was collected from the influent waste pipe of a household located in Phu An Commune, Ben Cat town, Binh Duong Province, Vietnam. The influent ranges of pollution parameters in the investigated domestic wastewater are given in Table 1. According to Vietnamese environmental standards, the national technical regulation on domestic wastewater (QCVN 14 : 2015/MT-BTNMT) discharging into the water sources serving the tap water supply is given in Table 1. These values were used to compare and determine whether the influent and effluent of the pollution parameters satisfied the requirement in order to evaluate the effectiveness of the AAO/O system.

2.2. Reactor Setup and Operation. The applied AAO/O model was designed as a small and multisection system with an average treating capacity of 0.5 m^3/day, which is suitable for wastewater treatment of 5-member households. The designed specifications, schematic, and simulation diagrams of the studied model are given in Table 2 and Figures 1 and 2, respectively.

In the operation of the investigated AAO/O model, the influent wastewater was first discharged into an anaerobic zone for degradation of the complex organic matter. The next anoxic zone was used to reduce the nitrogen and phosphorus load from the wastewater. Then, the wastewater was further transferred to the two oxic zones in association with the biological membrane. This treatment allowed for the thorough disposal of the remaining organic matter, COD and BOD_5 content, and N and P with proportions of nutrients of $BOD_5 : N : P = 100 : 5 : 1$. The membrane offered a complete barrier to sedimentary sludge and suspended solids. At the 4th zone, the activated carbon powder was deployed as an absorbent to remove color and odor in order to enhance the quality of the effluent. Finally, sterilization of the wastewater using ozone was conducted to remove all existing harmful and pathogenic microorganisms.

2.3. Analysis Methods. The investigated parameters in this study included pH, BOD_5, COD, TN, TP, and TSS. The system treatment performance was continuously evaluated for 168 days. During this period, a qualitative measurement

Table 1: The influent range of pollution parameters and their limitation values according to Vietnamese environmental standards.

No.	Pollution parameters	Unit	Influent range of pollution parameters	Limitation values of pollution parameters according to Vietnamese environmental standards[a]
1	pH	—	5.5–7.1	6–9
2	COD	$mg{\cdot}L^{-1}$	42.9–280.2	75
3	BOD_5	$mg{\cdot}L^{-1}$	25.7–168.2	30
4	TSS	$mg{\cdot}L^{-1}$	16.4–146.0	50
5	TN	$mg{\cdot}L^{-1}$	29.1–94.1	30
6	TP	$mg{\cdot}L^{-1}$	13.8–57.2	6

[a]The national technical regulation on domestic wastewater (QCVN 14 : 2015/MT-BTNMT) discharging into the water sources serving the tap water supply.

Table 2: Designed specification of the AAO/O model.

No.	Designed specification	Unit	Threshold values	Designed values
1	Flow Q	$L{\cdot}day^{-1}$	—	200–250
2	Food to microorganism ratio (F/M)	—	0.15–0.25	—
3	MLSS	$mg{\cdot}L^{-1}$	3000–5000	—
4	Anaerobic retention time	h	0.5–1.5	1.0
5	Anoxic retention time	h	0.5–1.0	1.0
6	1st oxic retention time	h	3.5–6.0	6.0
7	2nd oxic retention time	h	3.5–6.0	6.0
8	Ozone processing time	h	—	0.1
9	Sludge circulation	$m^3{\cdot}day^{-1}$	20–50	50
10	Inner circulation	$m^3{\cdot}day^{-1}$	100–300	300

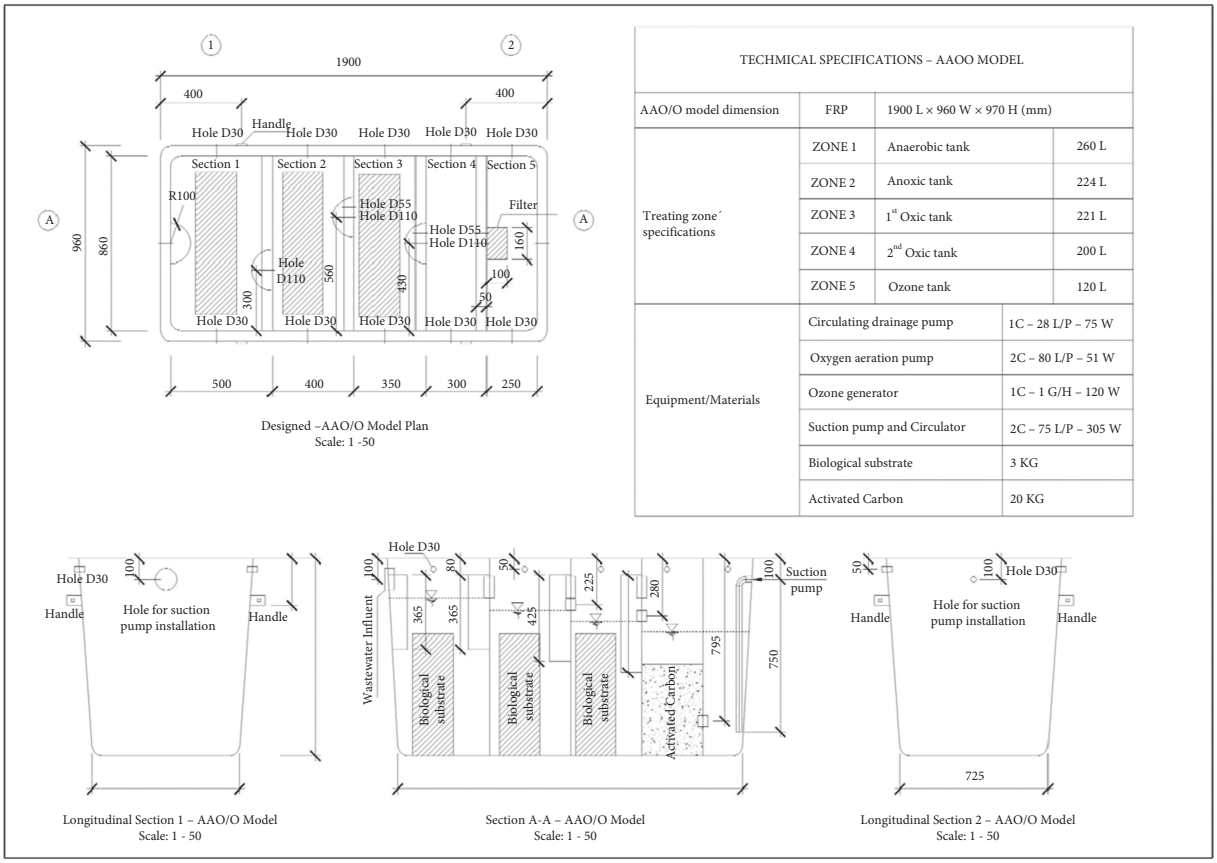

Figure 1: Schematic diagrams of the AAO/O model.

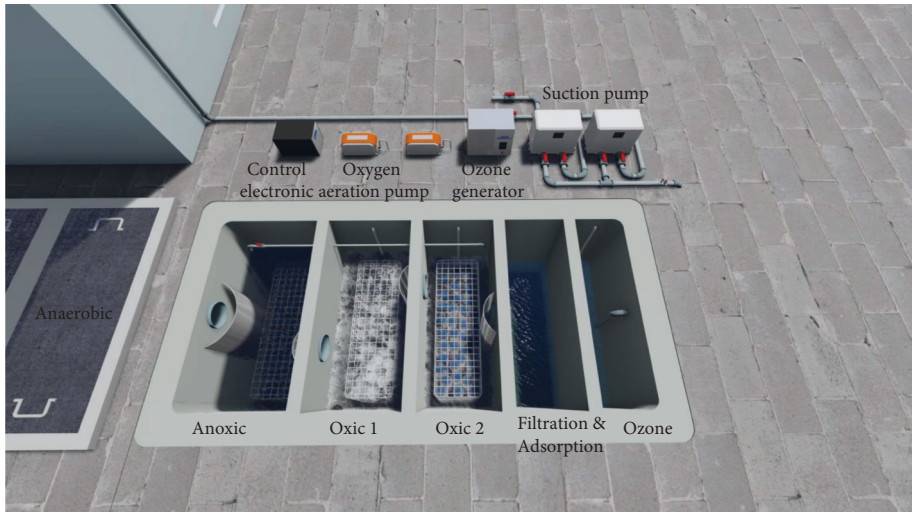

Figure 2: A simulation diagram of the AAO/O model.

was carried out every 7 days. The analysis was performed according to the standard method for the examination of water and wastewater (APHA, 2005) [27]. The pH level was monitored using a hand-held Mettler–Schwerzenbach meter (Switzerland). COD, TN, and TP were measured by UV-vis spectroscopy. The BOD_5 content was determined based on the annealing method at 20°C for 5 days. TSS was measured by filtering wastewater using 0.45 μm filter paper followed by drying at 150°C.

3. Results and Discussion

3.1. pH. The influent and effluent pH of domestic wastewater are shown in Figure 3. The influent pH during the

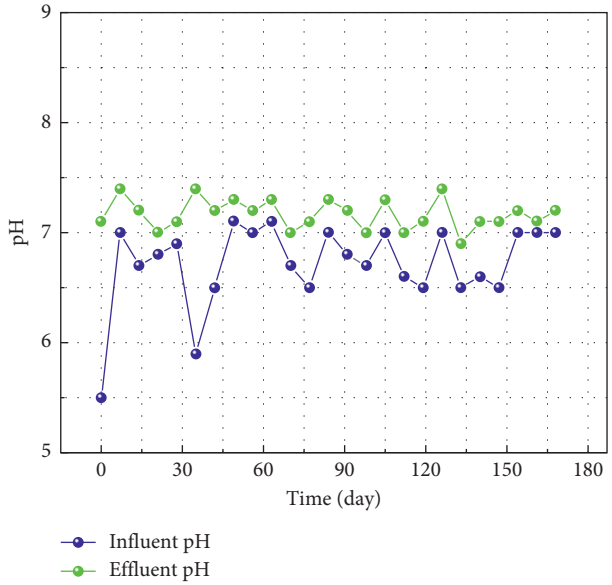

Figure 3: pH during the experimental period.

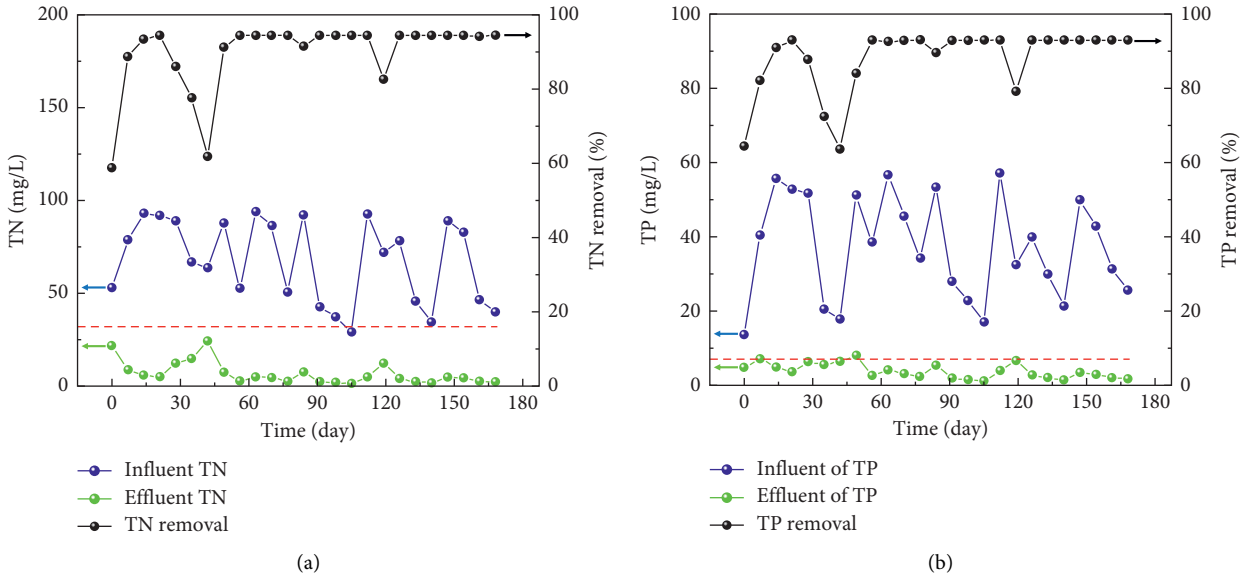

Figure 4: Nitrogen (a) and phosphorus (b) removal during the experimental period.

experimental period was in the range of 5.5–7.1, with some points out of the requirement range. These low and fluctuating values of influent pH could be due to the presence of organic matters in the wastewater entering the treatment system. After the removal of organic matters in the anaerobic tank, the pH level of wastewater was more stable for further treating processes. As a prominent parameter that strongly affects the removal capacity, the pH level in the range of 6.5–8.5 is required for the biological treating system to avoid stress on the microbial community and for optimal biological activity in both anoxic and aerobic tanks [28]. After being treated by the AAO/O system, the effluent pH range was 6.9–7.1, which satisfied the environmental standards.

3.2. Performance of the Nutrient Removal. The influent, effluent, and removal rate of TN and TP using the AAO/O system during the 168 days of operation are shown in Figures 4(a) and 4(b), respectively. The national technical regulation on domestic wastewater (QCVN 14 : 2015/MT-BTNMT) discharging into the water sources serving the tap water supply for TN (30 mg·L^{-1}) and TP (6 mg·L^{-1}) are also represented by the red dashed line in the figure. The results showed that influents of both TN and TP changed day by day and exceeded the Vietnamese environmental standards. During the first 56 days of operation, the removal rate of TN and TP was not stable, ranging 58.8–94.5% and 64.5–93.0%, respectively. This can be explained by the fact that the domestic wastewater contains high concentration of nutrients [29], and

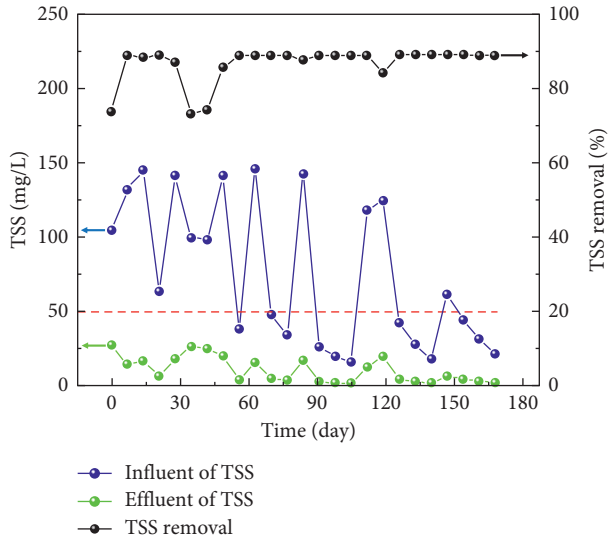

Figure 5: TSS removal during the experimental period.

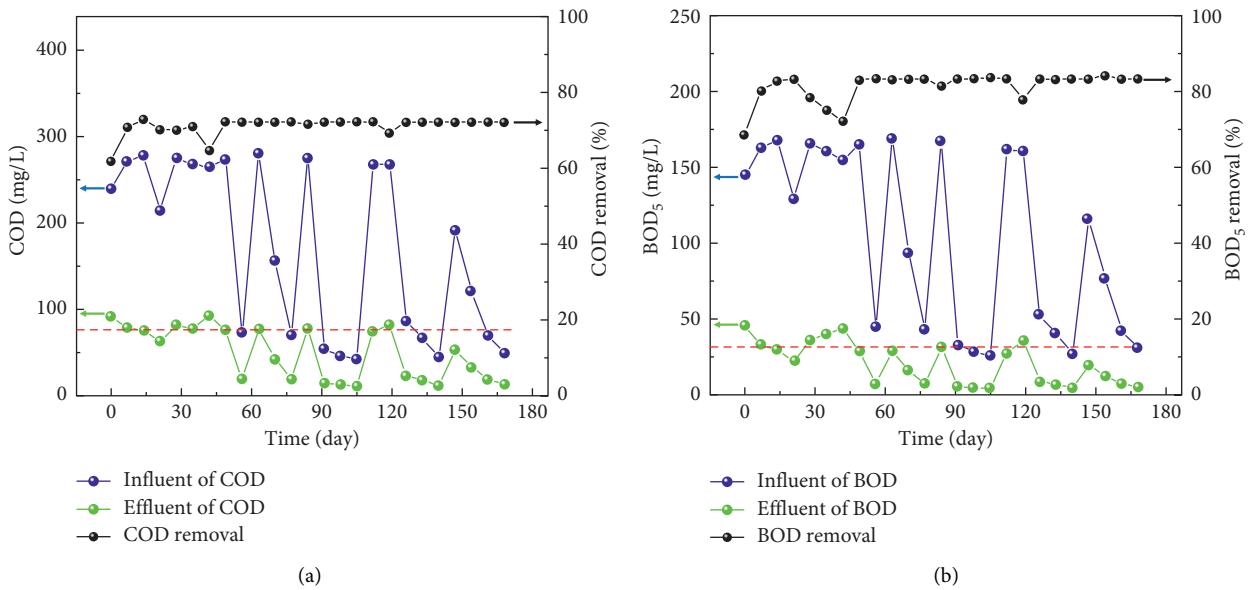

Figure 6: COD (a) and BOD_5 (b) removal during the experimental period.

the ratio of BOD_5 : N : P at 100 : 5 : 1 is required for aerobic treatment [30, 31]. The beginning period of the treatment is therefore usually needed to produce a proper mass of microorganisms in an aerobic condition and to adjust the procedure to ensure the best operating parameters. The removal efficiency of the AAO/O system for TN and TP reached a stable period after 60 days of operation, with values of 93.6 ± 3.0% and 91.9 ± 3.5%, respectively. It is worth noting that effluents of TN and TP were lower than the regulated limit standards. Therefore, the AAO/O system was found to be effective and suitable for removing nutrients in domestic wastewater.

3.3. Performance of the TSS Removal. Figure 5 shows the TSS removal performance of the AAO/O system during 168 days of operation. The influent of TSS was in the range of 16.4–146 $mg \cdot L^{-1}$, which mainly exceeded the limit value of 50 $mg \cdot L^{-1}$. Similar to the case of nutrient removal, the system maintained stable profiles after 60 days of operation with a removal efficiency of 88.6 ± 1.2%. The AAO/O system was found to be efficient for TSS removal owing to the fact that the effluent of TSS was lower than the limits of the Vietnamese standards.

3.4. Performance of Organic Removal. The removal of organic matter was mainly based on the activity of microorganisms (activated sludge) in the two oxic zones. The dissolved organic substances can be biodegraded by microorganisms, while nonbiodegradable organic compounds are removed by filtration of suspended particles. The performance of the AAO/O system in removing COD and BOD_5 is shown in

Figures 6(a) and 6(b), respectively. The BOD_5 concentration fluctuated significantly during the investigation period. This is because it depends on personal hygiene needs, such as urination and defecation from time to time of members in the family [29]. The result showed that, similar to other above parameters, both influents of COD and BOD_5 were almost higher than the limit values of the national technical regulation on domestic wastewater. In the first 56 days of operating the AAO/O system, the removal rate of COD and BOD_5 was not stable, ranging from 61.7 to 72.7% and 68.4–83.0%, respectively. The effluents of COD and BOD_5 in this period were higher than the standards. After 60 days of operation, the system became steadier with the removal efficiency of $71.8 \pm 0.7\%$ and $82.6 \pm 1.4\%$ for COD and BOD_5, respectively. With this removal efficiency, the effluents of both COD and BOD_5 almost satisfied the requirement, with only some points being slightly higher than the limit values.

The application of the investigated AAO/O system to domestic wastewater treatment yielded promising results. In particular, the removal efficiency of TN, TP, TSS, BOD_5, and COD of wastewater were $93.6 \pm 3.0\%$, $91.9 \pm 3.5\%$, $88.6 \pm 1.2\%$, $82.6 \pm 1.4\%$, and $71.8 \pm 0.7\%$, respectively. The removal efficiency of COD was found to be lower than other indices. This was because the biological method was the main technique for the wastewater treatment as the ratio of BOD/COD in the domestic wastewater was above 0.5 [32, 33]. This method is more effective for removing BOD and nutrients than COD, resulting in the higher removal rates for these indices. It should be noted that the performance of the system was not optimal during the first 56 days due to poor adaptation of microorganisms, which can lead to inefficient decomposition of contaminants. However, after around 60 days, their performance was highly optimized with stable variation, as their reproduction and expansion were already ensured. In addition to the advantage of possessing a longer HRT, the increase in the oxic order in the AAO/O model also provided a long sludge retention time that can help to prevent the loss of nitrifying bacteria and to improve the nitrification capacity of the activated sludge.

4. Conclusions

The AAO/O model was prepared by adding an oxic zone in association with a biological membrane to a conventional AAO system. The system was specifically designed for household wastewater treatment with a discharge capacity of $0.5\ m^3$/day. The removal efficiency of TN, TP, TSS, COD, and BOD_5 using the system was relatively high and almost satisfied the Vietnamese environmental standards. The qualified output can be circulated and reused for household sanitation or watering purposes. The obtained results showed that AAO/O exhibited great potential not only in maintaining water reservoirs but also in addressing notorious environmental issues.

Data Availability

The data used to support the findings of this study are included within the article.

Conflicts of Interest

The authors declare that they no conflicts of interest.

Acknowledgments

This research was funded by Thu Dau Mot University, Binh Duong Province, Vietnam, under grant number DTHV.21.4–006.

References

[1] M. A. Massoud, A. Tarhini, and J. A. Nasr, "Decentralized approaches to wastewater treatment and management: applicability in developing countries," *Journal of Environmental Management*, vol. 90, no. 1, pp. 652–659, 2009.

[2] M. Qadir, D. Wichelns, L. Raschid-Sally et al., "The challenges of wastewater irrigation in developing countries," *Agricultural Water Management*, vol. 97, no. 4, pp. 561–568, 2010.

[3] K. K. Kesari, R. Soni, Q. M. S. Jamal et al., "Wastewater treatment and reuse: a review of its applications and health implications," *Water, Air, & Soil Pollution*, vol. 232, 2021.

[4] J. Fito and K. Alemu, "Microalgae–bacteria consortium treatment technology for municipal wastewater management," *Nanotechnology for Environmental Engineering*, vol. 4, no. 1, 2019.

[5] N. B. Pham, T. Kuyama, and Y. Kataoka, *Urban Domestic Wastewater Management in Vietnam-Challenges and Opportunities*, WEPA, Redwood, CA, USA, 2014.

[6] K. T. Nguyen, H. M. Nguyen, C. K. Truong, M. B. Ahmed, Y. Huang, and J. L. Zhou, "Chemical and microbiological risk assessment of urban river water quality in Vietnam," *Environmental Geochemistry and Health*, vol. 41, no. 6, pp. 2559–2575, 2019.

[7] M. G. Lusk, G. S. Toor, Y.-Y. Yang, S. Mechtensimer, M. De, and T. A. Obreza, "A review of the fate and transport of nitrogen, phosphorus, pathogens, and trace organic chemicals in septic systems," *Critical Reviews in Environmental Science and Technology*, vol. 47, no. 7, pp. 455–541, 2017.

[8] F. Wang, J. Li, D. Bian et al., "Effect of hydraulic residence time and inlet flow distribution ratio on the pollutant removal of low-temperature municipal wastewater in multistage AO process," *Water and Environment Journal*, vol. 34, no. S1, pp. 742–752, 2020.

[9] S.-S. Yang, X.-L. Yu, M.-Q. Ding et al., "Simulating a combined lysis-cryptic and biological nitrogen removal system treating domestic wastewater at low C/N ratios using artificial neural network," *Water Research*, vol. 189, Article ID 116576, 2021.

[10] K. Zheng, H. Li, S. Wang et al., "Enhanced proteins and amino acids production based on ammonia nitrogen assimilation and sludge increment by the integration of bioadsorption with anaerobic-anoxic-oxic (AAO) process," *Chemosphere*, vol. 280, Article ID 130721, 2021.

[11] D. K. Uan, I. T. Yeom, P. Arulazhagan, and J. Rajesh Banu, "Effects of sludge pretreatment on sludge reduction in a lab-scale anaerobic/anoxic/oxic system treating domestic wastewater," *International journal of Environmental Science and Technology*, vol. 10, no. 3, pp. 495–502, 2013.

[12] J. Wang, K. Chon, X. Ren, Y. Kou, K. J. Chae, and Y. Piao, "Effects of beneficial microorganisms on nutrient removal and excess sludge production in an anaerobic-anoxic/oxic (A2O) process for municipal wastewater treatment," *Bioresource Technology*, vol. 281, pp. 90–98, 2019.

[13] G. Mannina, M. Capodici, A. Cosenza, and D. Di Trapani, "Carbon and nutrient biological removal in a University of Cape Town membrane bioreactor: analysis of a pilot plant operated under two different C/N ratios," *Chemical Engineering Journal*, vol. 296, pp. 289–299, 2016.

[14] J. Li, S. Wang, Z. Wang, Z. Zheng, and J. Zhang, "Assessing biomass activities, sludge characteristics and membrane fouling in the University of Cape Town membrane bioreactor under ferric chloride addition," *Environmental Technology & Innovation*, vol. 23, Article ID 101796, 2021.

[15] D. Xu, H. Ji, H. Ren, J. Geng, K. Li, and K. Xu, "Inhibition effect of magnetic field on nitrous oxide emission from sequencing batch reactor treating domestic wastewater at low temperature," *Journal of Environmental Sciences*, vol. 87, pp. 205–212, 2020.

[16] C. Feng, Z. Li, Y. Zhu et al., "Effect of magnetic powder on nitrous oxide emissions from a sequencing batch reactor for treating domestic wastewater at low temperatures," *Bioresource Technology*, vol. 315, Article ID 123848, 2020.

[17] C. Wang, T. C. A. Ng, and H. Y. Ng, "Comparison between novel vibrating ceramic MBR and conventional air-sparging MBR for domestic wastewater treatment: performance, fouling control and energy consumption," *Water Research*, vol. 203, Article ID 117521, 2021.

[18] P. P. Kalbar, S. Karmakar, and S. R. Asolekar, "Selection of an appropriate wastewater treatment technology: a scenario-based multiple-attribute decision-making approach," *Journal of Environmental Management*, vol. 113, pp. 158–169, 2012.

[19] R. Bashar, K. Gungor, K. G. Karthikeyan, and P. Barak, "Cost effectiveness of phosphorus removal processes in municipal wastewater treatment," *Chemosphere*, vol. 197, pp. 280–290, 2018.

[20] J. Fan, T. Tao, J. Zhang, and G. L. You, "Performance evaluation of a modified anaerobic/anoxic/oxic (A2/O) process treating low strength wastewater," *Desalination*, vol. 249, no. 2, pp. 822–827, 2009.

[21] S. Zhang, Y. Li, W. Jiao, L. Qiu, J. Zhong, and W. Sun, "Research on lateral flow treatment technology to enhance phosphorus removal of AAO process," *E3S Web of Conferences.*, vol. 53, Article ID 04029, 2018.

[22] M. Zhang, Y. Peng, C. Wang, C. Wang, W. Zhao, and W. Zeng, "Optimization denitrifying phosphorus removal at different hydraulic retention times in a novel anaerobic anoxic oxic-biological contact oxidation process," *Biochemical Engineering Journal*, vol. 106, pp. 26–36, 2016.

[23] T.-J. Chang, Y.-H. Chang, W.-L. Chao, W.-N. Jane, and Y.-T. Chang, "Effect of hydraulic retention time on electricity generation using a solid plain-graphite plate microbial fuel cell anoxic/oxic process for treating pharmaceutical sewage," *Journal of Environmental Science and Health, Part A*, vol. 53, no. 13, pp. 1185–1197, 2018.

[24] Z. Zhang, Y. Feng, H. Su et al., "Influence of operating parameters on the fate and removal of three estrogens in a laboratory-scale AAO system," *Water Science and Technology*, vol. 71, no. 11, pp. 1701–1708, 2015.

[25] M. von Sperling, M. E. Verbyla, and S. M. A. C. Oliveira, "Loading rates applied to treatment units," in *Assessment of Treatment Plant Performance and Water Quality Data: A Guide for Students, Researchers and Practitioners*, IWA Publishing, London, UK, 2020.

[26] UEPA, *Wastewater Technology Fact Sheet-Sequencing Batch Reactors*, US Environmental Protection Agency, Washington, D.C., USA, 1999.

[27] American Public Health Association, *Standard Methods for the Examination of Water and Wastewater*, American Public Health Association, Washington, D.C., USA, 2005.

[28] R. C. Rout and M. L. Devram, *Effluent Treatment by Activated Sludge Process*, IPPTA, Saharanpur, India, 2004.

[29] P. R. Rout, M. K. Shahid, R. R. Dash et al., "Nutrient removal from domestic wastewater: a comprehensive review on conventional and advanced technologies," *Journal of Environmental Management*, vol. 296, Article ID 113246, 2021.

[30] H. T. T. Bui, "Some characteristics of treatment of wastewater from paper production and recycling containing lignin in Vietnam," *Journal of Environmental Science and Engineering*, vol. 9, pp. 133–138, 2020.

[31] T. Weinpel, V. Bakos, and A. Jobbágy, "Co-treatment of a carbon deficient domestic wastewater with a dairy process effluent for a cost-effective global solution," *Periodica Polytechnica - Chemical Engineering*, vol. 62, no. 4, pp. 432–440, 2018.

[32] S. C. Deogaonkar, P. Wakode, and K. P. Rawat, "Electron beam irradiation post treatment for degradation of non biodegradable contaminants in textile wastewater," *Radiation Physics and Chemistry*, vol. 165, Article ID 108377, 2019.

[33] A. M. Al-Sulaiman and B. H. Khudair, "Correlation between BOD5 and COD for Al- Diwaniyah wastewater treatment plants to obtain the biodegradability indices," *Pakistan Journal of Biotechnology*, vol. 15, no. 2, pp. 423–427, 2018.

Hindawi
Journal of Chemistry
Volume 2022, Article ID 7704513, 9 pages
https://doi.org/10.1155/2022/7704513

Research Article

Variation of Water Quality in Ningxia Section of the Yellow River in Recent 5 Years

Yan Jin,[1] **Xinyuan Wang**,[2] **and Ya-Ping Dong**[3]

[1]*Ningxia Zhongke Jingke Test Tech., Co., Ltd, Yinchuan, Ningxia 750011, China*
[2]*School of Mathematics and Civil Engineering, Zhuhai College, Beijing Institute of Technology, Beijing, China*
[3]*Ningxia Ecological and Environmental Monitoring Center, Yinchuan, Ningxia 750002, China*

Correspondence should be addressed to Yan Jin; nxjinyan@163.com

Received 24 March 2022; Revised 6 May 2022; Accepted 23 May 2022; Published 8 June 2022

Academic Editor: Jun Wu

The Yellow River is very important for human health and social development in China to require good water quality. This study selected the Ningxia section of the Yellow River as the study area to investigate the water quality variation in 2016–2020. A total of 9 water quality parameters were monitored, and 8 parameters including pH, dissolved oxygen, biological oxygen demand, chemical oxygen demand, total phosphate, fluoride, ammonia-nitrogen, and permanganate index were in the range of Class II standard requirement. Dissolved oxygen concentrations ranged from 7.5 to 9.4 mg/L. However, total nitrogen concentrations in 2018–2020 ranged from 1.87 to 2.8 mg/L to cause the pollution. Both the Nemerow index method and the contamination degree method showed that total nitrogen with high concentration exerted the water pollution. Principal component analysis also proved this. Stricter environmental management strategies for controlling total nitrogen should be taken in the future. The findings provided some useful information for water pollution of the Ningxia section of the Yellow River.

1. Introduction

Water is considered as the origin of life and it is the critical source for human well-beings and social development [1]. Water quality is very important for water resource usage, agricultural activities, industrial production, aquaculture, and regional safety [2–6]. However, water has been frequently contaminated by diverse pollutants such as heavy metals [7], endocrine disrupting chemicals [8], antibiotic resistance genes [9], microplastics [9], and other emerging chemicals in recent decades. These pollutants have occurred in seawater, groundwater, lakes, and rivers to possibly exert the potential risks to humans [7, 9, 10]. Therefore, water pollution in terms of emerging contaminants has become a study hot-spot in recent years [7–10]. The traditional water quality parameters such as chemical oxygen demand (COD), dissolved oxygen (DO), biological oxygen demand (BOD), ammonia-nitrogen, pH, total nitrogen (TN), total phosphate (TP), permanganate index (IMn), and fluoride are important to evaluate the water quality so that these parameters have been routinely monitored for management of surface water quality. However, the investigations on water quality regarding traditional parameters are not very enough and these parameters have been often used as the influential factors for evaluating emerging pollution [11]. Therefore, water quality evaluation using traditional parameters should be paid attention.

COD is an important index to judge the water quality or effectiveness of wastewater treatment techniques [12, 13]. COD was reported to be lower than 3 mg/L in Spanish river [14]. COD in other rivers in other countries ranged from 2 to 133 mg/L while that in wastewater/sewer was in the range of 9–656 mg/L [15]. Permanganate index (IMn) is COD measured by the permanganate method which is generally used for evaluating water quality of surface water or drinking water. IMn generally shows the inorganic or organic pollution of water. Similarly, BOD which is another index to show organic pollution has also been widely paid attention. DO is another critical index for water quality and water safety. DO is related to the survival of aquatic organisms and

water ecological balance. The pH is able to indicate the acid-base degree of the aquatic environment. The animals and plants can live in water with a suitable pH range so that a lower or higher pH can indicate the deterioration of the aquatic environment. Nutrients are important for the growth of aquatic plants. However, excessive nutrients in water could induce extensive growth of plants to consume more DO and make the water quality deteriorate [16]. Ammonia-nitrogen, TN, and TP have been widely accepted as the main parameters for evaluating nutrients in water. Fluoride has widely existed in water to induce many illnesses such as kidney disease and have significant toxicity to aquatic animals [17]. Therefore, fluoride is also a critical index during water quality monitoring. Water quality can be evaluated by comparing these parameters with national water quality standards. Routine monitoring is very important for water protection and environmental management.

The Yellow River is a very important river in China. It originates from Qinghai Province, flows over 9 provinces, and enters into the Bohai Sea in Dongying of Shandong Province. The Ningxia section of the Yellow River has provided water resources for Ningxia so the water quality of this section is very critical for the regional sustainability of Ningxia. This study evaluated the water quality of the Ningxia section of the Yellow River to provide useful information on the variation of the aquatic environment in this area. The findings of this study will provide the basis for the strategy of environmental management for the Ningxia section of the Yellow River and the surrounding area in the future.

2. Materials and Methods

2.1. Chemicals, Reagents, and Analysis Method. NaOH, KI, HgI_2, MgO, HCl, $NaKC_4H_4O_6$ $4H_2O$, $Na_2S_2O_3$, $nSO_4{\cdot}7H_2O$, H_3BO_3, bromothymol blue, soluble starch, Na_2CO, NH_4Cl, H_2SO_4, $K_2Cr_2O_7$, Ag_2SO_4, $HgSO_4$, neutral resin XAD-2, CH_4O, $(NH_4)_2Fe(SO_4)_2$ $6H_2O$, $KHC_8H_4O_4$, $FeSO_4{\bullet}7H_2O$, KNO_3, $ZnSO_4$, $MnSO_4{\bullet}H2O$, $NH_2C_6H_4SO_2NH_2$, $C_{10}H_7NHC_2H_4NH_2{\bullet}2HCl$, C_2H_6O, $KAl(SO_4)_2{\cdot}12H_2O$, $KMnO_4$, $NaNO_2$, sulfamic acid, H_3PO_4, $Na_2C_2O_4$, and phenolphthalein were purchased from Shanghai Aladdin Biochemical Technology Co., Ltd.

DO was measured by a dissolved oxygen meter while pH was determined by the pH meter. NH_4^+-N was analyzed by Nessler's reagent spectrophotometric determination while TN was determined by using digestion coupling with ultraviolet spectrophotometry. IMn was determined by the permanganimetric method while COD was analyzed by the potassium dichromate method. TP was determined by the ammonium molybdate spectrophotometric method while BOD was analyzed by using the standard dilution method. Fluoride was determined by the ion selective electrode method. All detailed analysis methods referred to reference [18].

Total 6 sites of the Ningxia section of the Yellow River (Figure 1) were selected for monitoring in 2016–2020. The 6 sites were named as W1, W2, W3, W4, W5, and W6. Total 9 water quality parameters were measured.

2.2. Water Quality Evaluation Method. Water pollution of the Ningxia section of the Yellow River was evaluated by using the Nemerow index and contamination degree. The Nemerow Index was calculated according to the following equation [19]:

$$\text{Nemerrow Index} = \sqrt{\frac{(C_i/S_i)^2_{\text{mean}} + (C_i/S_i)^2_{\max}}{2}}, \quad (1)$$

where S_i refers the standard concentration of water quality parameter; C_i means the measured concentration of water quality parameter; $(C_i/S_i)_{\text{mean}}$ represents the average value of all (C_i/S_i); and $(C_i/S_i)_{\max}$ is the maximal value among all (C_i/S_i). S_i for each water quality parameter used in this study was the Class II or Class III levels of the "Surface water quality standard of China (GB 3838–2002)". Pollution evaluated by the Nemerow index could be categorized into Class I (insignificant pollution with a Nemerow index less than 1), Class II (slight pollution with a Nemerow index less than 2.5 but equal or higher than 1), Class III (moderate pollution with a Nemerow index less than 7 but equal or higher than 2.5), and Class IV (heavy pollution with a Nemerow index equal or higher than 7).

The following equation showed the calculation of *contamination degree* [20]:

$$\text{contamination degree} = \sum_{i=1}^{n} \frac{C_i}{S_i}. \quad (2)$$

The evaluation criterion included: Class I (low pollution with contamination degree less than 6), Class II (moderate pollution with contamination degree less than 12 but equal or higher than 6), Class III (considerable pollution with contamination degree less than 24 but equal or higher than 12), and Class IV (very heavy pollution with contamination degree equal or greater than 24).

2.3. Data Processing. Data were processed by using Origin 2018. Correlation analysis was performed by SPSS 19. The correlation matrix was shown as a heatmap with $^*<0.05$ and $^{**}<0.01$. Principal component analysis was performed by Origin 2018.

3. Results and Discussion

3.1. Water Quality Variation of Ningxia Section of the Yellow River during 2016–2020. The pH of 6 sites was nearly higher

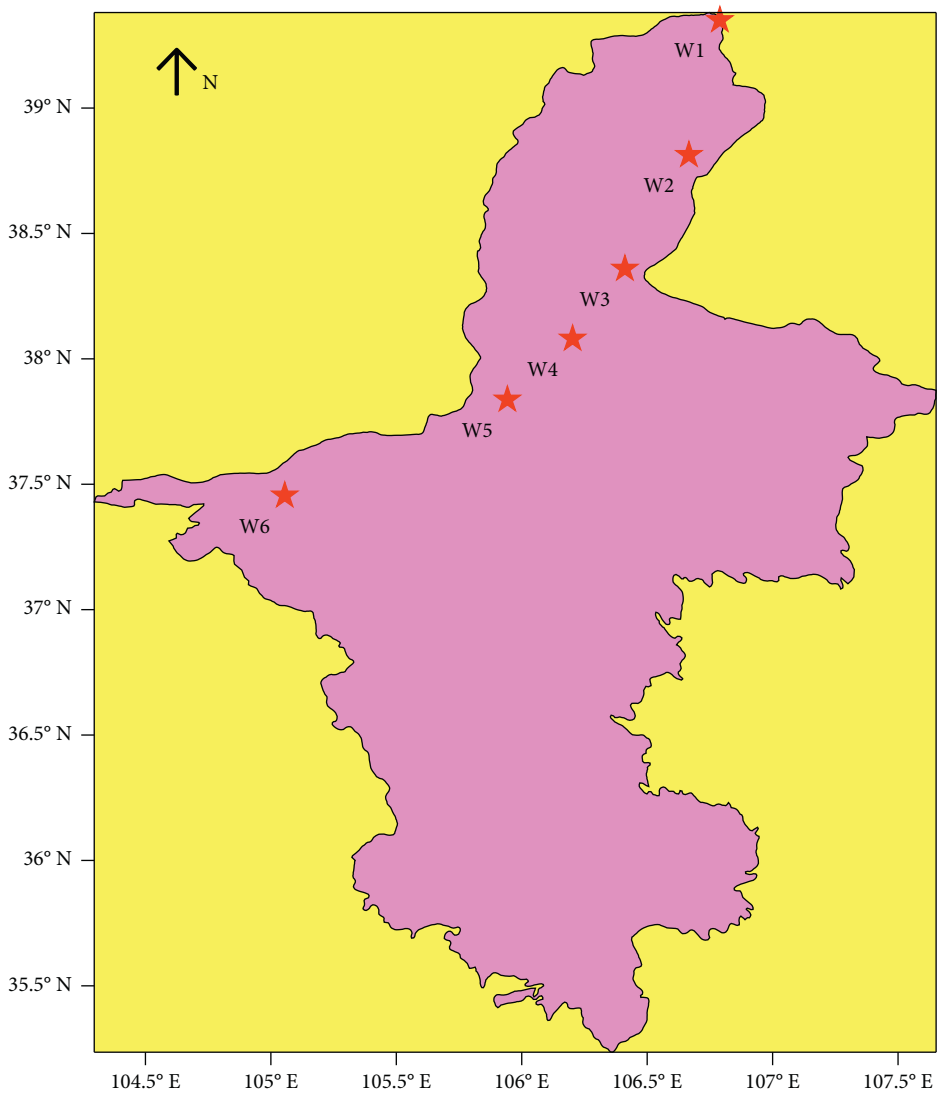

Figure 1: Sampling sites of this study.

than 8 except W6 in 2020 with a pH of 7.8 (Figure 2(a)). The pH of W1 ranged from 8 to 8.2. It was interesting that the pH of W1 showed a slightly increasing trend during 2016–2020. The pH of W2 ranged from 8 to 8.3. The pH of W2 did not show the significant variation trend during recent 5 years. The pH of W3 ranged from 8 to 8.3 and it showed a slightly decreasing trend. The pH of W4 ranged from 8 to 8.4 with the highest pH occurring in 2019. The pH of W5 ranged from 8 to 8.3 and it showed slightly increasing trend. The pH of W6 ranged from 7.8 to 8.3 with a significantly lower pH in 2020.

The DO concentration of 6 sites was nearly higher than 8.2 mg/L except W5 in 2020 with a DO concentration of 7.5 mg/L (Figure 2(b)). The DO concentration of W1 ranged from 8.2 to 9.1 mg/L while the DO concentration of W2 ranged from 8.3 to 8.9 mg/L. The DO concentration of W3 ranged from 8.4 to 9.1 mg/L and it showed a slightly increasing trend. The DO of W4 ranged from 8.4 to 9.4 mg/L with the highest DO concentration occurring in 2020. The DO concentration of W5 ranged from 7.5 to 9 mg/L and it showed significant variation in 2019 and 2020. The DO concentration of W6 ranged from 8.6 to 9.4 mg/L. The DO concentrations in 2019 and 2020 generally showed higher than before, illustrating that environmental management might take action for improving the water quality.

The IMn of 6 sites was higher than 1.8 mg/L (Figure 2(c)). The IMn of W1 ranged from 2.1 to 3 mg/L while IMn of W2 ranged from 2.1 to 2.8 mg/L. The highest IMn of W1 and W2 occurred in 2016, and IMn showed slightly decreasing trend to prove the effectiveness of environmental management strategy. The IMn of W3 ranged from 2 to 2.6 mg/L and it showed a slightly decreasing trend. The IMn of W4 ranged from 1.9 to 2.6 mg/L. The IMn of W5 ranged from 2 to 2.6 mg/L and it was stable in 2017–2020. The IMn of W6 ranged from 1.8 to 2.3 mg/L to show a slightly increasing trend. In summary, IMn values were all relatively low to illustrate the good water quality of the study area.

The BOD of 6 sites was higher than 0.8 mg/L (Figure 2(d)). The BOD of W1 ranged from 1.2 to 1.9 mg/L

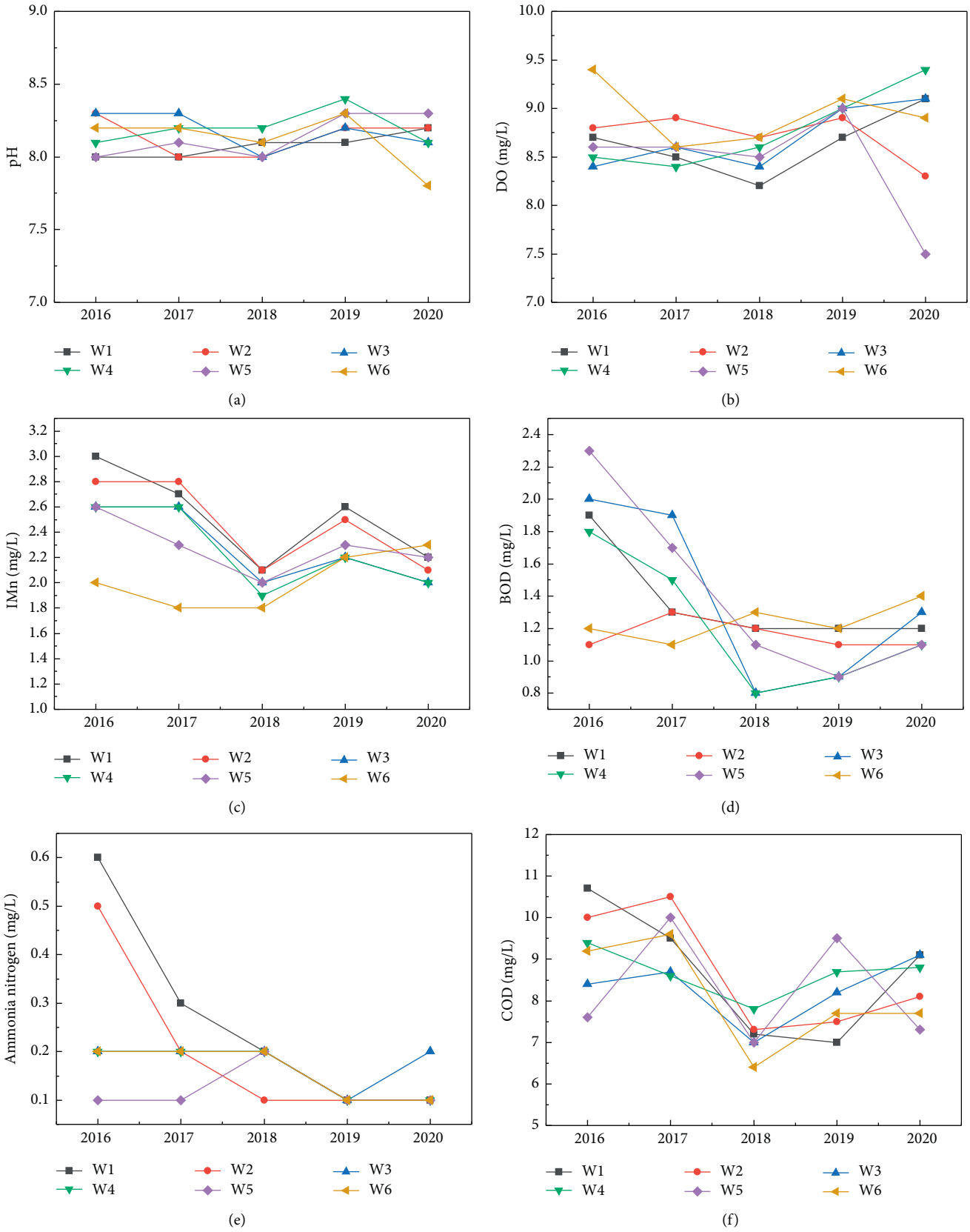

Figure 2: Continued.

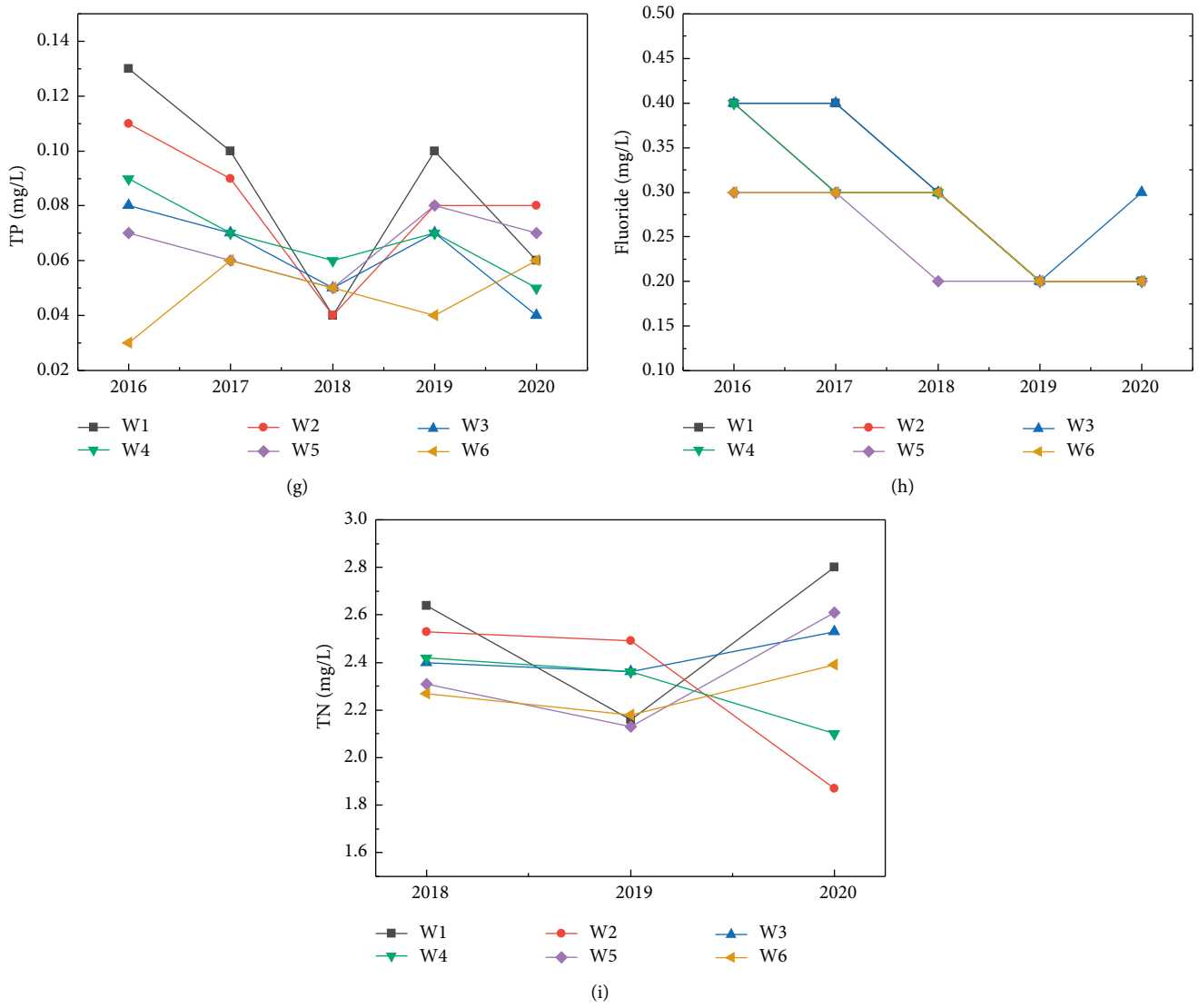

Figure 2: Variation of water quality parameters of the Ningxia section of the yellow river during 2016–2020.

with decreasing trend while the BOD of W2 ranged from 1.1 to 1.3 mg/L. The BOD of W3 ranged from 0.8 to 2 mg/L while the BOD of W4 ranged from 0.8 to 1.8 mg/L with a slightly decreasing trend. The BOD of W5 ranged from 0.9 to 2.3 mg/L while the BOD of W6 ranged from 1.2 to 1.4 mg/L. In summary, BOD values were all relatively low to illustrate the good water quality of the study area.

The ammonia-nitrogen concentrations of 6 sites were in the range of 0.1–0.6 mg/L (Figure 2(e)). The ammonia-nitrogen concentration of W1 and W2 in 2016 was 0.6 and 0.5 mg/L, respectively. The ammonia-nitrogen concentrations of the remaining sites and periods were all below 0.2 mg/L, except W1 in 2017 with 0.3 mg/L, showing good water quality.

The COD concentrations of 6 sites were in the range of 6.4–10.7 mg/L (Figure 2(f)). The COD concentrations of W1 ranged from 7 to 10.7 mg/L while the COD of W2 ranged from 7.3 to 10.5 mg/L. The COD concentrations of W3 ranged from 7 to 9.1 mg/L while the COD of W4 ranged from 7.8 to 9.4 mg/L. The COD concentrations of W5 ranged from 7.3 to 10 mg/L while COD of W6 ranged from 6.4 to 9.6 mg/L. W6 showed better water quality in terms of COD in 2018–2020. In contrast, the water quality of W1 and W2 was worse than that of other sites.

The TP concentrations of 6 sites were in the range of 0.03–0.13 mg/L (Figure 2(g)). The TP concentration of W1 and W2 in 2016 was 0.13 and 0.11 mg/L, respectively. The TP concentrations of different sites generally showed a decreasing trend especially with low concentrations in 2018–2020, showing good water quality and an effective environmental management strategy.

The fluoride concentrations of 6 sites were in the range of 0.2–0.4 mg/L (Figure 2(h)). The fluoride concentrations of all sites exhibited the decreasing trend, showing good water quality and effective environmental management strategy.

The TN concentrations of 6 sites were in the range of 1.87–2.8 mg/L (Figure 2(g)). The TN concentration of all sites in 2016 and 2017 was not measured. The TN

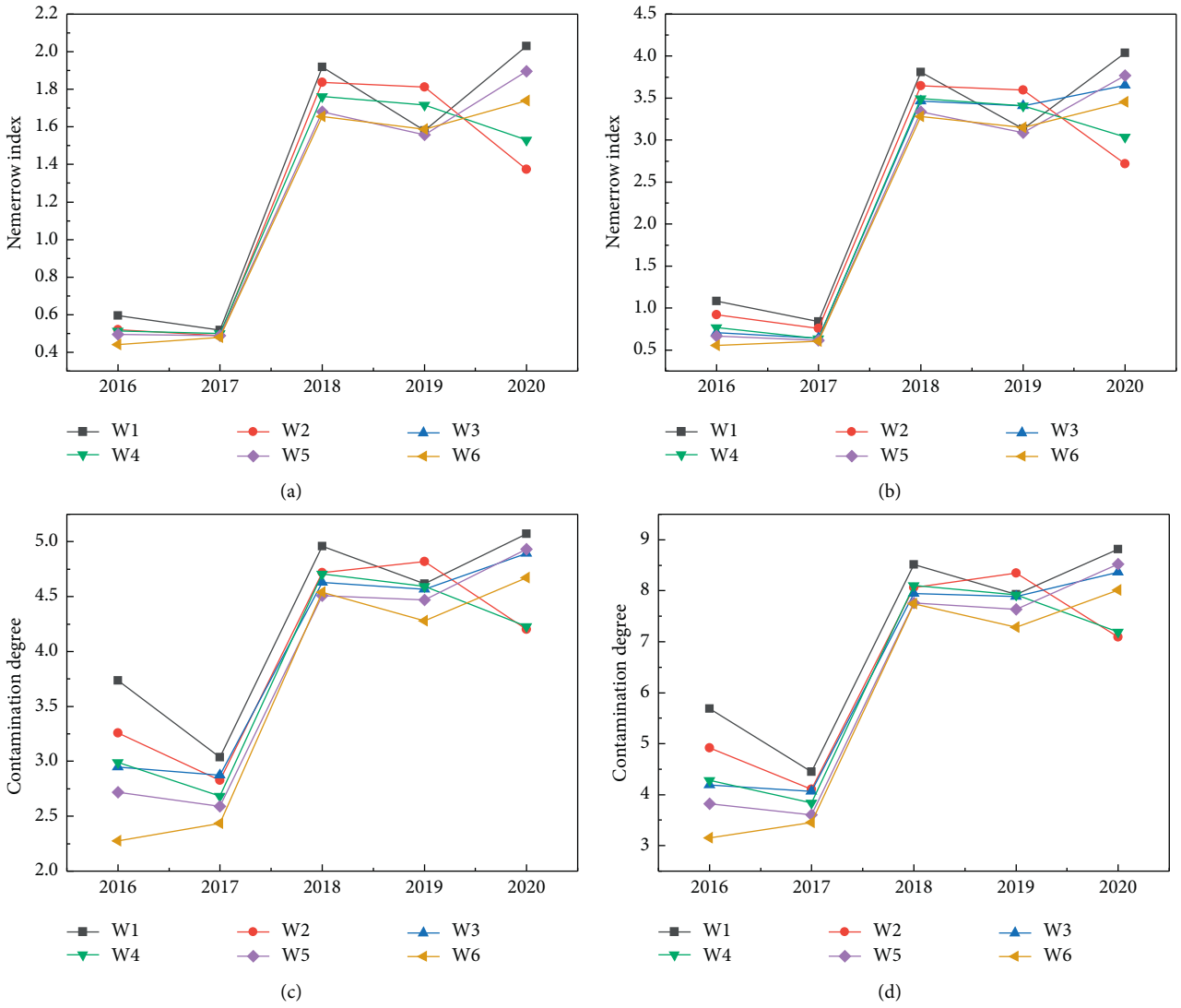

FIGURE 3: Nemerow index and contamination degree of water in the Ningxia section of the Yellow River during 2016–2020. (a) Nemerow index by using Class III; (b) Nemerow index by using Class II; (c) contamination degree by using Class III; (d) contamination degree by using Class II.

concentrations of different sites were higher than 1 mg/L in 2018–2020, which exceeded the standard of Class II and Class III, showing the possible pollution risks. Agriculture is well developed along the Ningxia section of the Yellow River, which might introduce some nitrogen pollutants into the water to cause a higher concentration of TN.

3.2. Water Pollution Variation of Ningxia Section of the Yellow River during 2016–2020. The pH, DO, IMn, BOD, ammonia-nitrogen, COD, and fluoride of all sites in 2016–2020 were below the Class II standard, showing good water quality of the study area. TP in W1 and W2 in 2016 exceeded the Class II standard but was lower than the Class III standard. The TP concentrations of all sites in 2017–2020 were below the Class II standard, showing that the water quality was greatly improved in 2017–2020 under the effective environmental management strategy. It was a little regretful to find that TN concentrations of all sites in 2018–2020 exceeded the Class III standard. TN concentrations of all sites in 2018–2020 exceeded the Class IV standard and 17 out 18 samples exceeded the Class V standard in terms of TN.

Both Nemerow index and contamination degree were used to comprehensively evaluate the water pollution of Ningxia section of the Yellow River during 2016–2020 (Figure 3). Class III (Figure 3(a) and 3(c)) and Class II (Figure 3(b) and 3(d)) standards were used as the criterion. Nemerow index values of all sites in 2016–2017 were all below 1.0 using Class III standards (Figure 3(a)), illustrating that water quality of all sites in Ningxia section of the Yellow River is good. However, Nemerow index values of all sites in 2018–2020 were higher than 1, illustrating the slight contamination occurred in the study area (Figure 3(a)). More strict criterion Class II was adopted, only W1 in 2016 showed slight contamination while W1 and W2 in 2016–2017

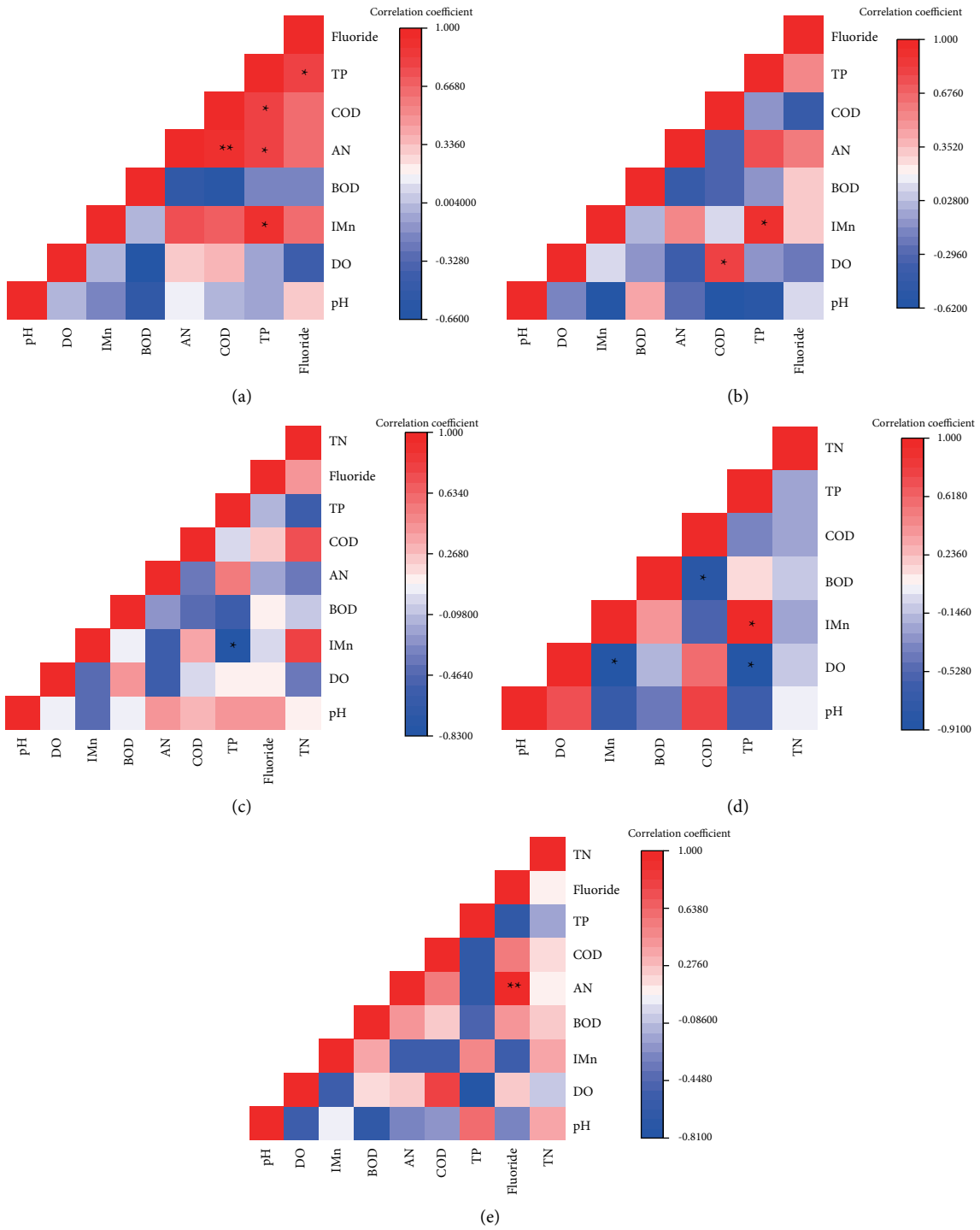

Figure 4: Correlation heatmap among the water quality parameters of the Ningxia section of the Yellow River during 2016–2020. (a) 2016; (b) 2017; (c) 2018; (d) 2019; (e) 2020. AN means ammonia-nitrogen.

showed uncontaminated state (Figure 3(b)). The remaining sites in the remaining periods all showed moderate contamination (Figure 3(b)). TN with higher concentrations in all sites in 2018–2020 served as the predominant contamination contributor.

Different from Nemerow index evaluation, contamination degree showed that all sited in 2016–2020 possessed low contamination with contamination degree less than 6 by using Class III standards (Figure 3(c)). However, all sites in 2018–2020 showed moderate water pollution by using Class II standards although these sites showed low contamination in 2016–2017 (Figure 3(d)). TN was also the major pollution contributor for the contamination degree.

Stricter criterion will obtain worse evaluation results. Taking Class II standards as the evaluation criterion, the results were worse. The worse scenario was generally used

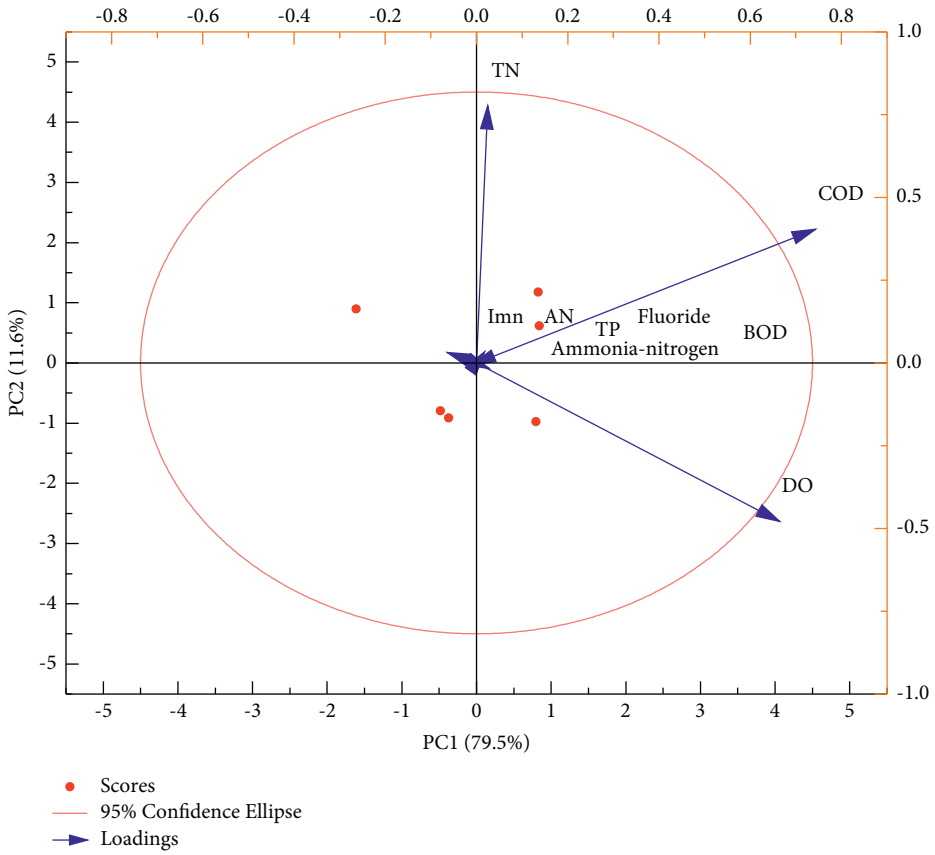

Figure 5: Principal component analysis on water quality of the Ningxia section of the Yellow River in 2020.

for the evaluation result. Therefore, the contamination degree method obtained a better evaluation result in comparison to the Nemerow index method, which might be ascribed to the fact that Nemerow index method enlarged the contribution of maximal C/S value. It should be noted that TN concentrations should be greatly decreased to be less than 1.0 even 0.5 mg/L to make the water quality become good. Therefore, more new strategies should be taken in the future. Another important point was that TN was not monitored in 2016 and 2017 so that the Nemerow index and contamination degree did not comprise TN in 2016 and 2017. More data including 2021, 2022, or longer should be used to obtain more reasonable evaluation results.

3.3. Correlation Analysis of Water Quality Parameters of Ningxia Section of the Yellow River during 2016–2020. Correlation among different water quality parameters of the Ningxia section of the Yellow River during 2016–2020 was assessed (Figure 4). Significant differences in correlation among water quality parameters occurred in different periods. Significantly positive relationship existed between COD-ammonia-nitrogen, TP-IMn, TP-ammonia-nitrogen, TP-COD, and TP-fluoride in 2016 (Figure 4(a)). Significantly positive relationship existed between COD-DO and TP-IMn in 2017 (Figure 4(b)). Tp was only significantly negatively related with IMn in 2018 (Figure 4(c)), which changed a lot with the previous 2 years. Significantly negative relationship existed between IMn-DO, COD-BOD, and TP-DO while significantly positive relationship existed between IMn and TP in 2019 (Figure 4(d)). Only fluoride was significantly positively related with ammonia-nitrogen in 2020 (Figure 4(e)).

Multiple factors might influence the correlation among different water quality parameters [21, 22]. The water quality parameters in 2016 showed the most complex relationship while those in 2018 and 2020 showed the simplest relationship. A simple relationship between water quality parameters meant more complicated factors might have an effect on the water quality.

3.4. Principal Component Analysis on Water Quality of Ningxia Section of the Yellow River. Principal component analysis was employed to determine the possible pollution source of the Ningxia section of the Yellow River (Figure 5). Data of 2020 were used considering that all parameters were monitored and the period was recent for illustrate the real situation. Two principal components were obtained after analysis with PC1 accounting for 79.5% of variation and PC2 describing 11.6% of variation (Figure 5). The first component might be agricultural activities while the second component was regarded as the domestic activities. Input of excessive nitrogen might induce the pollution of TN in the Ningxia section of the Yellow River, which might serve as the

principal component. Therefore, stricter control strategies of nutrients especially nitrogen chemicals should be taken.

4. Conclusions

The variation of water quality parameters in the Ningxia section of the Yellow River during 2016–2020 was investigated. Most of the water quality parameters were good enough to be lower than Class II or Class III standards while TN exceeded Class III in 2018–2020 to show the pollution. The Nemerow index and contamination degree showed that water pollution occurred in the Ningxia section of the Yellow River during 2018–2020 due to high-concentration TN. Stricter environmental management strategies should be taken to decrease the TN concentrations for making water quality better in the study area.

Data Availability

The data used in the study are available from the corresponding author upon request.

Conflicts of Interest

The authors declare that there are no conflicts of interest.

Acknowledgments

This study was supported by Science and Technology Project for Environmental Protection of Ningxia (Effect of pretreatment approach on monitoring TP, TN, Hg, As, and Se in Ningxia Section of the Yellow River and corresponding coping mechanisms, grant number of 202002).

References

[1] S. M. Ezzat and M. T. Moustafa, "Treating wastewater under zero waste principle using wetland mesocosms," *Frontiers of Environmental Science & Engineering*, vol. 15, no. 4, 2021.

[2] J. Lu, Y. Zhang, J. Wu, and J. Wang, "Intervention of antimicrobial peptide usage on antimicrobial resistance in aquaculture," *Journal of Hazardous Materials*, vol. 427, Article ID 128154, 2022.

[3] S. Dong, C. Yin, and X. Chen, "Toxicity-oriented water quality engineering," *Frontiers of Environmental Science & Engineering*, vol. 14, no. 5, p. 80, 2020.

[4] J. Lu, J. Wu, and C. Zhang, "Cleaner production of salt-tolerance vegetable in coastal saline soils using reclaimed water irrigation: observations from alleviated accumulation of endocrine disrupting chemicals and environmental burden," *Journal of Cleaner Production*, vol. 297, Article ID 126746, 2021.

[5] R. M. Hegde, R. M. Rego, K. M. Potla, M. D. Kurkuri, and M. Kigga, "Bio-inspired materials for defluoridation of water: a review," *Chemosphere*, vol. 253, Article ID 126657, 2020.

[6] F. Almomani, R. Bhosale, and M. Shawaqfah, "Solar oxidation of toluene over Co doped nano-catalyst," *Chemosphere*, vol. 255, Article ID 126878, 2020.

[7] J. Lu, Y. Lin, J. Wu, and C. Zhang, "Continental-scale spatial distribution, sources, and health risks of heavy metals in seafood: challenge for the water-food-energy nexus sustainability in coastal regions?" *Environmental Science and Pollution Research*, vol. 28, no. 45, pp. 63815–63828, 2021.

[8] P. Tachachartvanich, E. R. Azhagiya Singam, K. A. Durkin, M. T. Smith, and M. A. La Merrill, "Structure-based discovery of the endocrine disrupting effects of hydraulic fracturing chemicals as novel androgen receptor antagonists," *Chemosphere*, vol. 257, Article ID 127178, 2020.

[9] J. Lu, J. Wu, and J. Wang, "Metagenomic analysis on resistance genes in water and microplastics from a mariculture system," *Frontiers of Environmental Science & Engineering*, vol. 16, no. 1, 2022.

[10] H. Liu and X. Yu, "Hexavalent chromium in drinking water: Chemistry, challenges and future outlook on Sn(II)- and photocatalyst-based treatment," *Frontiers of Environmental Science & Engineering*, vol. 14, no. 5, p. 88, 2020.

[11] A. Cydzik-Kwiatkowska, K. Bernat, M. Zielinska, K. Bulkowska, and I. Wojnowska-Baryla, "Aerobic granular sludge for bisphenol A (BPA) removal from wastewater," *International Biodeterioration & Biodegradation*, vol. 122, pp. 1–11, 2017.

[12] S. Yazici Guvenc and G. Varank, "Degradation of refractory organics in concentrated leachate by the Fenton process: central composite design for process optimization," *Frontiers of Environmental Science & Engineering*, vol. 15, no. 1, 2021.

[13] M. Malhotra and A. Garg, "Characterization of value-added chemicals derived from the thermal hydrolysis and wet oxidation of sewage sludge," *Frontiers of Environmental Science & Engineering*, vol. 15, no. 1, 2021.

[14] R. Argüelles, M. Toledo, and M. A. Martín, "Study of the Tagus River and Entrepenas reservoir ecosystem around the Trillo nuclear power plant using chemometric analysis: influence on water, sediments, algae and fish," *Chemosphere*, vol. 279, Article ID 130532, 2021.

[15] M. Lepot, A. Torres, T. Hofer et al., "Calibration of UV/Vis spectrophotometers: a review and comparison of different methods to estimate TSS and total and dissolved COD concentrations in sewers, WWTPs and rivers," *Water Research*, vol. 101, pp. 519–534, 2016.

[16] A. Bechard, "Red tide at morning, tourists take warning? County-level economic effects of HABS on tourism dependent sectors," *Harmful Algae*, vol. 85, Article ID 101689, 2019.

[17] C. F. Z. Lacson, M.-C. Lu, and Y. H. Huang, "Fluoride network and circular economy as potential model for sustainable development-A review," *Chemosphere*, vol. 239, Article ID 124662, 2020.

[18] State Environmental Protection Administration, *Monitoring and Analysis Method of Water and Waste Water*, Chinese Environment Science Press, Beijing, China, 4th edition, 2004.

[19] C. T. Vu, C. Lin, C.-C. Shern, G. Yeh, V. G. Le, and H. T. Tran, "Contamination, ecological risk and source apportionment of heavy metals in sediments and water of a contaminated river in Taiwan," *Ecological Indicators*, vol. 82, pp. 32–42, 2017.

[20] Z. Sharifi, S. M. T. Hossaini, and G. Renella, "Risk assessment for sediment and stream water polluted by heavy metals released by a municipal solid waste composting plant," *Journal of Geochemical Exploration*, vol. 169, pp. 202–210, 2016.

[21] J. O. Ighalo and A. G. Adeniyi, "A comprehensive review of water quality monitoring and assessment in Nigeria," *Chemosphere*, vol. 260, Article ID 127569, 2020.

[22] A. R. Md Towfiqul Islam, M. T. Siddiqua, A. Zahid, S. S. Tasnim, and M. M. Rahman, "Drinking appraisal of coastal groundwater in Bangladesh: an approach of multi-hazards towards water security and health safety," *Chemosphere*, vol. 255, Article ID 126933, 2020.

Hindawi
Journal of Chemistry
Volume 2022, Article ID 1802204, 14 pages
https://doi.org/10.1155/2022/1802204

Research Article

Occurrence of Pharmaceutical Residues and Antibiotic-Resistant Bacteria in Water and Sediments from Major Reservoirs (Owabi and Barekese Dams) in Ghana

Joseph Nana Gyesi,[1] Bismark Anabila Nyaaba,[1] Godfred Darko,[1] Felix Charles Mills-Robertson,[2] Kodwo Miezah,[3] Nana Aboagye Acheampong,[4] Felicia Frimpong,[1] Grace Gyimah,[1] Bridget Quansah,[1] and Lawrence Sheringham Borquaye[1,5]

[1]*Department of Chemistry, Kwame Nkrumah University of Science and Technology, Kumasi, Ghana*
[2]*Department of Biochemistry and Biotechnology, Kwame Nkrumah University of Science and Technology, Kumasi, Ghana*
[3]*Department of Environmental Sciences, Kwame Nkrumah University of Science and Technology, Kumasi, Ghana*
[4]*Department of Microbiology, University for Development Studies, Nyankpala, Ghana*
[5]*Central Laboratory, Kwame Nkrumah University of Science and Technology, Kumasi, Ghana*

Correspondence should be addressed to Lawrence Sheringham Borquaye; lsborquaye.sci@knust.edu.gh

Received 2 February 2022; Revised 1 April 2022; Accepted 25 April 2022; Published 9 May 2022

Academic Editor: Jun Wu

The presence of pharmaceuticals in the environment is undesirable since their biological activity may impair ecosystem health of reservoirs that receive inflows from other water sources. This work determined the concentrations of analgesics and antibiotics, and the occurrence of antimicrobial resistance among microbes in water and sediment samples from Owabi and Barekese reservoirs—two main sources of pipe-borne water in the Kumasi metropolis in Ghana. The study also assessed the knowledge, attitude, and practice of inhabitants near these reservoirs regarding the disposal of unused and expired medicines. Out of nine targeted pharmaceuticals, four were detected in at least one sample. Five analytes (caffeine, ciprofloxacin, doxycycline, ibuprofen, and metronidazole) were below detection limit for all samples. The levels of pharmaceuticals were low, as expected, ranging from 0.06 to 36.51 μg/L in the water samples and 3.34–4.80 μg/kg in sediments. The highest detected concentration of any pharmaceutical in water was for diclofenac (107.87 μg/L), followed by metronidazole (22.23 μg/L), amoxicillin (1.86 μg/L), chloramphenicol (0.85 μg/L), and paracetamol (0.16 μg/L). Chloramphenicol recorded the highest concentration (10.22 μg/kg) in the sediments. Five bacteria isolates (*Enterobacter*, *Clostridium*, *Pseudomonas*, *Acinetobacter*, and *Klebsiella*) from the samples were resistant to all the antibiotics tested. Isolates of *Corynebacterium* and *Listeria* showed susceptibility to only doxycycline. Isolates of *Bacillus* were susceptible to only two antibiotics (erythromycin and doxycycline). All the 100 respondents interviewed admitted that they dispose of medications once they do not need them. Of those who disposed of unwanted medicines, 79% did so inappropriately. Disposal in household trash (67%) was the most common method used. Majority of respondents felt the need for a facility or program to collect unused medicines (77%), hence their willingness to pay to reduce pollution by pharmaceuticals in the environment. It is quite clear from the ecotoxicological risk assessment that a single pharmaceutical at very low level as those in this study and other works is likely to pose many ecological risks upon long-term exposure and therefore cannot be ignored.

1. Introduction

Pharmaceuticals are used primarily to prevent or treat human and animal diseases. In recent times, there has been an increase in the number of reports detailing the presence of human pharmaceuticals in water in various parts of the globe [1, 2]. In a 2002 study by the United States Geological Survey, about 80% of streams sampled in 30 American states contained trace levels of various pharmaceutical products, including hormones, steroids, and analgesics [3]. Following this report, numerous others have since been published. Even at very low concentrations, the presence of pharmaceuticals in water has raised concerns among stakeholders such as drinking-water regulators, governments, water suppliers, and the public regarding the potential risks to human health due to exposure to trace levels of pharmaceuticals via drinking water [4]. Pharmaceuticals could enter the soil and aquatic environments through wastewater effluents, landfill leachates, industrial effluents, aquaculture, and animal feedlots [5–7]. They could also enter the environment through excretion and egestion of unmetabolized drugs into wastewater collection systems and improper disposal of expired and unused medicines [8].

Pharmaceutical products are generally designed to elicit specific responses from precise biological targets. Therefore, these pharmaceutical products' effects on the environment are undesirable because their behavior in such matrices has not been studied in enough detail. The long-term effects of exposing humans, animals, plants, and other organisms in the ecosystem to pharmaceuticals remain unknown and can only be speculated to a large extent [9–11]. The presence of antibiotics in the environment could lead to an increase in the phenomenon of antimicrobial resistance. Resistance genes can develop in the environment if antibiotic residues are present; these genes can then be transferred to pathogenic bacteria. Resistance genes can be exchanged between environmental bacteria and clinical isolates [12]. Borquaye and coworkers detected amoxicillin, penicillin, and metronidazole at varying levels in leachate and soil samples from landfills in Kumasi, Ghana. Twenty-five bacteria belonging to nine genera were also isolated from leachates and soil samples in the study. Some isolated bacteria were resistant to benzylpenicillin, ampicillin, and amoxicillin. The results obtained from the study suggest that pharmaceutical residues are present in the environment and could have deleterious effects.

The Barekese and Owabi dams provide over 90% of potable water to domestic homes in the Ashanti region of Ghana. These reservoirs receive water inflow from various tributaries: Owabi, Sukobri, Akyeampomene, Pumpunase, and Afu for the Owabi reservoir [13] and Offin River for the Barekese reservoir [14]. Several dumpsites and landfill sites are located in and around the tributaries that feed the Owabi and Barekese reservoirs. Since the water treatment strategy for the management of these reservoirs does not necessarily remove chemical contaminants, water dispatched to various homes from these reservoirs could potentially contain pharmaceutical residues. Some water bottling companies also use water from these reservoirs as their raw materials to produce bottled and sachet water. The threat to the public could be substantial. There is, therefore, a need to ascertain the levels of pharmaceutical residues in these reservoirs that provide water to the Kumasi metropolis and examine the risk associated with their presence in the environment. In this work, the occurrence of antibiotics, analgesics, and antibiotic-resistant bacteria in water and sediment samples from the Owabi and Barekese dams was evaluated. The ecological risk associated with the presence of these pharmaceuticals in both water and soil samples was also investigated. A general survey on waste disposal patterns by residents in communities around the Owabi and Barekese reservoirs was also conducted.

2. Methods

2.1. Sample Collection. The Barekese and Owabi dams are in the Atwima district in the Ashanti region of Ghana. The Barekese dam, which was constructed between 1967 and 1972, stretches on latitude 6°44′N and longitude 1°42′W. The dam's catchment area measures 909 km^2 with a total volume of about 35,000,000 m^3 [14]. The Owabi dam is smaller than the Barekese dam and was constructed between 1928 and 1932. The reservoir surrounded by a forest reserve covers an area of about 69 km^2 with an approximate volume of 26,000,000 m^3 [15]. A total of 28 water and sediment samples were collected from various points in the Owabi and Barekese dams. Pre-cleaned plastic bottles (1.5 L) were rinsed with the water to be collected before samples were fetched into the bottles. For sediment samples, graduated hollow wooden sticks were immersed into the bottom of the reservoir and then withdrawn. Sediment samples collected were then placed in precleaned bottles. All samples were placed in an ice chest and returned to the laboratory for analyses. Maps of the study areas are shown in Figure 1.

2.2. Materials. All analgesics and antibiotics used for analytical and microbiological work were obtained as pure powders from Ernest Chemists (Accra, Ghana). HPLC-grade chemicals were used throughout the study. Ultrapure deionized water (18.2 MΩ) was used to prepare all solutions and calibration standards for HPLC analysis. All the solutions and samples were passed through 0.2-0.6 μm polypropylene filters before HPLC analysis.

2.3. Physicochemical Characterization. An aliquot (10 mL) of water sample was put into a clean beaker, and their pH, total dissolved solids (TDS), and electrical conductivity were measured using a Mettler Toledo (Switzerland) pH meter and a multiparametric probe (WTW, Weilheim, Germany). For soil samples, 10% (w/v) of dried pulverized sample to distilled water was prepared for the analysis [17, 18]. The pH meter was calibrated with buffers 4.01 and 7.01 before use.

2.4. Sample Preparation and Analysis. Water samples were filtered (0.45 μm pore size filters) to remove solid particles. Sample extraction and pre-concentration were done by solid-phase extraction (SPE). An HLB cartridge (6 mL, 200 mg, Green Mall, Jiangsu, China) was used in SPE analyses. SPE columns were conditioned using 5 mL distilled

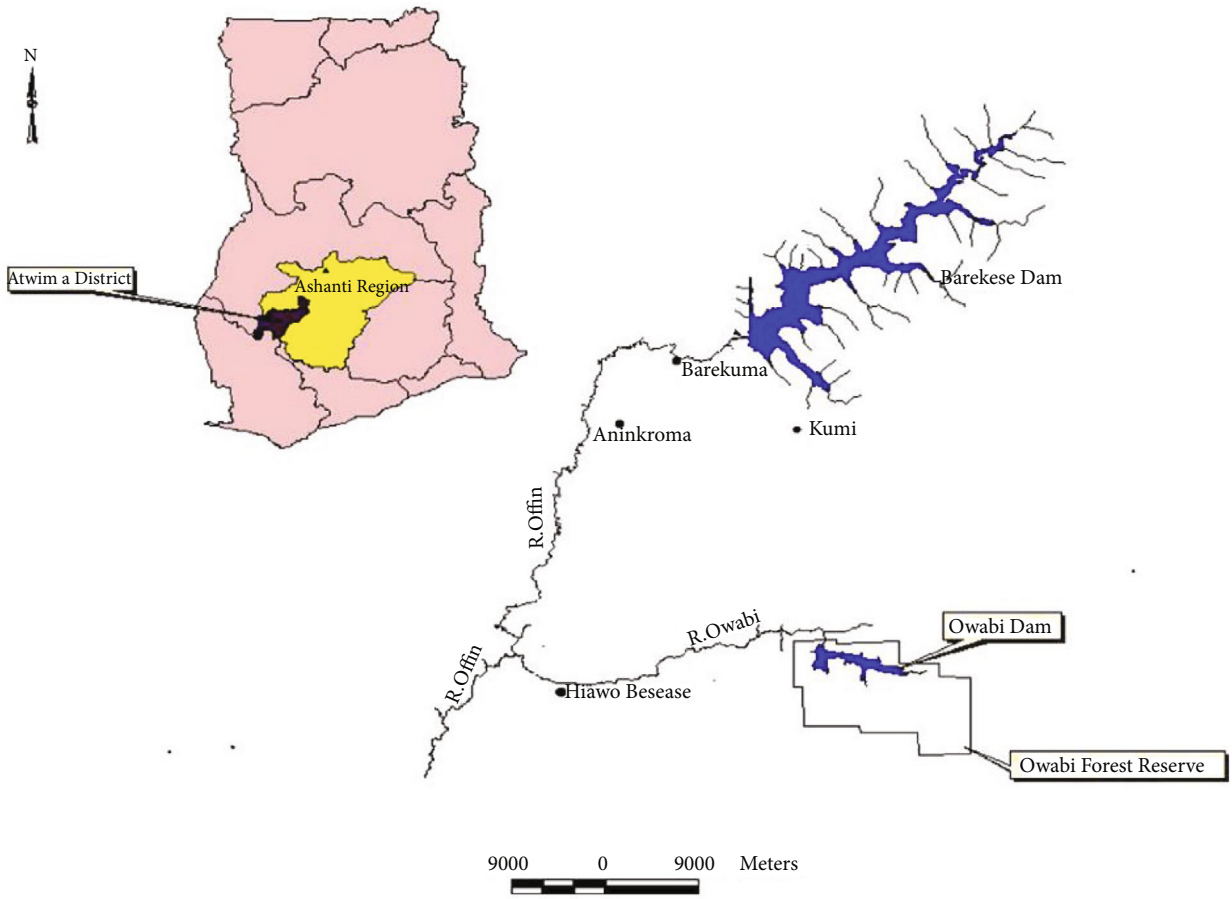

Figure 1: Map of Ghana showing the study areas in the Atiwa district in the Ashanti region [16].

water followed by 5 mL methanol. Water samples (1.5 L) were passed through the preconditioned 6 mL HLB SPE cartridges for the concentration of analytes. The SPE cartridge was then washed with 5 mL of distilled water. In the case of sediments, 100 g of an air-dried, pulverized sample was weighed into a beaker, and three successive extractions were done by sonication with 150 mL of acetonitrile. The supernatants were combined, filtered through 0.45 μm nylon membrane filters (Whatman, UK), and subjected to SPE as was done for water samples. To elute analgesics, 2 mL of methanol and 0.1% acetic acid mixture (1 : 1 v/v) was used. For antibiotics, 2 mL methanol and 0.05% trifluoroacetic acid mixture (1 : 4 v/v) was used. One milliliter of each eluate was then used in HPLC analyses .

2.5. HPLC Analyses

2.5.1. Antibiotics. Chromatographic separation was done on a Perkin Elmer Flexar HPLC coupled with a PDA detector. Separation of antibiotics was achieved on the Agilent Zorbax 300SB C18 column (250 × 4.6 mm, 5 μm). The mobile phase consisted of 0.05% trifluoroacetic acid (TFA, solvent A) and methanol (solvent B). Gradient elution was performed. Details of the gradient program are shown in Table S1. A flow rate of 1 mL/min and an injection volume of 20 μL were employed. Amoxicillin, chloramphenicol, ciprofloxacin, doxycycline, and metronidazole were monitored at 215 nm. The total runtime was 18 minutes, as shown in Figure S1A. HPLC analysis was done at ambient temperature.

2.5.2. Analgesics. Chromatographic separation of analgesics was done on the same Perkin Elmer Flexar HPLC coupled with a PDA detector. Separation of analgesics was achieved on a Phenomenex Luna C8 (150 × 4.6 mm, 5 μm) column. The mobile phase consisted of 0.1% acetic acid (A) and methanol (B). A gradient elution profile was utilized. Details of the gradient program are shown in Table S1. As with antibiotic analysis, a flow rate of 1 mL/min was employed with an injection volume of 20 μL. Peaks for paracetamol, caffeine, and diclofenac were acquired at 270 nm and that of ibuprofen at 220 nm (Figures S1B and S1C). The total runtime for analgesic analysis was 21 minutes, and all analyses were done at ambient temperature.

2.5.3. Standard Calibration and Method Validation. Five concentrations (2.5–200 μg/mL) of each standard were prepared and analyzed by HPLC, and a calibration curve was generated. This calibration curve was used to quantify analytes present in the samples. Linearity for all test samples was tested in the concentration range of 2.5–200 μg/mL. Limits of detection (LOD) and limits of quantification

(LOQ) for each of the standard drug were computed from a peak signal-to-noise ratio of 1 : 3.

2.5.4. Recoveries and Quality Assurance. A sample blank (water and soil matrices containing none of the analytes) was prepared and spiked with known concentrations of standard drugs. After the extraction and SPE clean-up procedures (as described earlier), the sample blank was analyzed by HPLC methods described earlier. The concentration of the drugs was determined from the chromatograms obtained. Standard solutions of the analytes were injected prior to analyses and also after every 10 sample runs to ensure that the HPLC system was functioning properly. Blank samples were also injected after every 5 runs to monitor any sample interference. All sample injections were made in duplicates. Each batch of analyses was prepared to include a reagent blank to check background contamination. Table S2 shows the recovery data.

2.6. Ecological Risk Assessment. The potential effects of identified pharmaceuticals on the aquatic environment were studied through ecological risk assessment. Ecological risk assessment is generally expressed with respect to hazard quotients (HQ). The predicted no-effect concentration (PNEC: the concentration of pharmaceutical at which no adverse effect is suspected to occur) values for fish, *Daphnia*, and algae were determined using data from the literature on acute toxicity. The PNEC is calculated by multiplying the EC_{50} values by an arbitrary safety factor, typically 1000 [9, 19]. The HQ was then determined by the ratio of MEC (maximum measured environmental concentration in μg/L) to PNEC, as shown in

$$\mathrm{HQ} = \frac{\mathrm{MEC}}{\mathrm{PNEC}}. \quad (1)$$

The risk ranking criteria of [20] were used in this study. According to this criterion, an $\mathrm{HQ} < 0.1$ implies a minimum risk to the organisms, $0.1 \leq \mathrm{HQ} \leq 1$ implies medium risk, and $\mathrm{HQ} \geq 1$ implies high risk [20].

2.7. Isolation and Identification of Bacteria Strains. Bacteria were isolated from water and sediment samples collected from the Barekese and Owabi reservoirs according to the method of [21]. Ten grams of each sediment sample was aseptically transferred into a sterile self-sealed bag and homogenized in 90 mL of sterile maximum recovery diluent using a pulsifier (PUL 100E; Microgen Bioproducts, UK) for 2 min. Ten-fold serial dilutions of both water and sediment samples were prepared up to 10^{-5}. An aliquot of 1 mL of each dilution was transferred into molten plate count agar (PCA) and swirled to ensure an even distribution of cells before allowing it to solidify. Inoculated media were inverted and kept in an incubator for 24 hours. A series of sub-culturing from the primary culture resulted in pure cultures of isolates. Bacterial isolates were identified based on colony characteristics and cellular morphology [22]. Identified isolates were stored in 20% glycerol broth and at -20°C, pending further analyses.

2.8. Microbial Susceptibility Assays. The susceptibility of the isolated microbes against selected antibiotics was tested in the agar disc diffusion assays. A nutrient agar media was prepared by dissolving 28 g of nutrient agar in 1 L of distilled water. The mixture was autoclaved for 40 minutes at 121°C and then cooled. Afterward, the prepared agar was poured into Petri dishes and dried. Pure cultures of isolated microbes were suspended in saline to obtain a density of 0.5 McFarland turbidity standard using the direct colony suspension. Forty microliters of the standardized colony suspension was transferred into the Petri dish and spread evenly over the entire agar surface using sterile cotton swabs. Afterward, filter paper discs (about 6 mm in diameter) containing the standard antibiotics (ampicillin, amoxicillin, cefuroxime, ciprofloxacin, doxycycline, erythromycin, gentamycin, metronidazole, and chloramphenicol) were placed on the agar surface. The filter paper disc for each standard drug was prepared using the criteria of the European Committee on Antimicrobial Susceptibility Testing (EUCAST). After the disc application on the agar plates, the plates were incubated at 37°C for 18 hours. The inhibition of growth zones was measured in millimeters. The zone diameter of each drug was interpreted using the criteria published by the EUCAST [23].

2.9. Survey on Disposal of Pharmaceuticals. Even though manufacturer packaging usually recommends disposal of unused and expired drugs by returning to the pharmacy, studies elsewhere have revealed that disposal via the sink or toilet or in regular household waste is the practice and is a potential source of human pharmaceuticals in the environment. A survey of about 100 households in and around the dams was conducted to investigate the households' disposal routes of unused and expired pharmaceuticals as a source of pharmaceutical compounds in the environment. The survey evaluated the public's level of awareness on the presence of pharmaceutical products in rivers and drinking water and knowledge on the possible impact of the presence of these pharmaceutical products in water samples. In-depth interviews were conducted with interviewers using standardized and pretested questionnaires. Ten eligible volunteers from various households were used to pretest the instrument for readability, understanding, question design, and length. The questionnaire generated sociodemographic data, their habits regarding the disposal of expired or unused medications, and their understanding of the environmental effect of medications. The questionnaires were administered to 100 household participants. Participants could either complete the survey themselves or have their responses marked by the researchers. The data was coded and input into Microsoft Excel 2016. The completeness, consistency, and reliability of the data were all examined. When respondents did not finish a question, it was considered a missing value, and only complete answers were utilized to analyze the results. Statistical analysis was performed using IBM SPSS Statistics for Windows, version 24 (IBM Corp., Armonk, N.Y., USA).

3. Results

3.1. Physicochemical Characterization. Physicochemical data of water and sediment samples used in this study are presented in Table 1. Generally, water samples obtained from the Owabi reservoir were slightly acidic with a pH range of 6.48–6.85, whereas the sediment samples ranged from slightly acidic to slightly basic (pH range of 6.24–8.93). For the samples from Barekese, all water and sediment samples were slightly acidic (pH range of 6.32–6.83). The total dissolved solids (TDS) of water and sediment samples from Owabi ranged between 90 and 94 mg/L and 26 and 58 mg/L, respectively. For samples from the Barekese reservoir, TDS ranged from 122 to 124 mg/L and 111 to 167 mg/L for water and sediment samples, respectively. The mean TDS for water from Owabi was generally lower than that of Barekese. Electrical conductivity (EC) of sediment samples from Owabi was determined to be in the range of 8.13–59.3 μS/cm while EC for water samples from the same Owabi reservoir ranged between 98.5 and 102.2 μS/cm. For the sediment samples from Barekese, the range of EC values was 124.1–239.0 μS/cm, whereas the EC of water samples from Barekese ranged between 135.9 and 138.9 μS/cm. It was observed that the mean value of EC of water samples from Barekese was greater than the mean EC recorded for Owabi samples. A similar observation was made for sediment samples from the two reservoirs.

3.2. Occurrence of Antibiotics and Analgesics. In the HPLC analysis, method linearity was evaluated in the concentration range of 2.5–200 μg/mL for both analgesics and antibiotics. A good correlation was observed for all the antibiotics and analgesics analyzed, with R^2 values between 0.98 and 0.99 recorded. For all analytes, the limits of detection (LOD) and limits of quantitation (LOQ) were determined to range between 0.031 and 0.116 μg/mL and 0.103 and 0.386 μg/mL, respectively. The LOD and LOQ were estimated based on signal-to-noise ratio of 1 : 3. The recoveries for the various analytes were high and ranged from 85.5% to 97.0% (Table 2). The elution of all analytes occurred within 19 minutes.

Of the pharmaceuticals analyzed in water samples from Barekese, chloramphenicol was the most prevalent, with a 55.56% frequency of detection. The frequency of detection for amoxicillin, diclofenac, metronidazole, and paracetamol was all 11.1% (Table 2). Caffeine, ibuprofen, ciprofloxacin, and doxycycline were not detected in any of the water samples from Barekese. The maximum concentration of chloramphenicol in water samples from Barekese was 0.85 μg/mL, whereas the maximum levels of amoxicillin, diclofenac, metronidazole, and paracetamol were 1.86, 4.36, 22.23, and 0.16 μg/mL, respectively. Caffeine, ibuprofen, doxycycline, and ciprofloxacin were not detected in water samples from Barekese. The average concentration of chloramphenicol in sediment from Barekese was 4.80 ± 3.63 μg/kg, and this was the only analyte detected in sediment samples from Barekese.

Results for the pharmaceuticals residues identified in samples from Owabi are also presented in Table 2. For the Owabi reservoir, chloramphenicol was the most frequently detected analyte, present in 77.8% of all water samples analyzed. Amoxicillin, diclofenac, and paracetamol, each at 33.3%, were detected in multiple water samples. The average concentration of amoxicillin, chloramphenicol, diclofenac, and paracetamol was 0.24 ± 0.14, 0.38 ± 0.12, 36.51 ± 68.80 , and 0.06 ± 0.08 μg/mL, respectively. Interestingly, the analytes that were not detected in Barekese water samples, namely, caffeine, ibuprofen, doxycycline, and ciprofloxacin, were undetected in water samples from Owabi. Paracetamol was the only analyte detected in sediment samples from Owabi, with a 66.67% detection frequency and an average concentration of $3.32 + 4.55$ μg/kg.

3.3. Ecological Risk Assessment. Three of the most widely used organisms in monitoring the impact of pharmaceuticals on the environment were adopted for the ecological risk assessment. The ecological risk assessment was carried out by first establishing the maximum estimated concentration for the various pharmaceuticals from the study. The corresponding predicted no-effect concentration for each analyte on each organism was obtained from the literature [9, 24–26]. The hazard quotients were computed, and the risk was established using a standard criterion [20]. The results are presented in Table 3 (water samples) and Table 4 (sediment samples). Generally, the pharmaceutical residues recorded in this study posed medium to high risk to all the three organisms investigated. The ecological risk posed by diclofenac to all organisms investigated in water was classified as high risk at both Owabi and Barekese, since the RQ was greater than 1. The levels of chloramphenicol and metronidazole in water samples from Barekese also posed high risk to all the organisms. Both paracetamol and amoxicillin posed high risk to *Daphnia* and algae, but medium risk to fish. Amoxicillin and paracetamol, however, presented a low risk to fish in water. For water samples from Owabi, amoxicillin posed a medium risk to all organisms, whereas the levels of paracetamol and chloramphenicol posed high risks to algae but a medium risk to fish. Two analytes were detected for sediment samples from Barekese and Owabi—chloramphenicol and paracetamol. Both analytes posed high risks to all organisms investigated, with RQ's far over 10 recorded in each case (Table 4).

3.4. Microorganism Isolation and Susceptibility Testing. A total of 30 pure bacteria isolates were obtained from water and soil samples in both reservoirs. Pure bacterial isolates were obtained by a series of subculturing from the primary cultures. Bacterial isolates were identified based on colony characteristics and cellular morphology. From the Gram staining reaction, 17 of the isolates were Gram-positive while 13 were Gram-negative. All isolates were rod-like in shape. Isolates were identified to belong to one of the 8 genera: *Bacillus*, *Corynebacterium*, *Pseudomonas*, *Klebsiella*, *Enterobacter*, *Listeria*, *Acinetobacter*, and *Clostridium* (Table 5). Table 6 shows the results of the antimicrobial susceptibility testing. Antibiotic susceptibility testing (AST) was performed according to EUCAST recommendations. Bacteria isolates were tested against nine antibiotics belonging to

Table 1: Physicochemical parameters of water and sediment samples from the Barekese and Owabi reservoirs.

Samples	pH		EC (μS/cm)		TDS (mg/L)	
	Range	Mean ± SD	Range	Mean ± SD	Range	Mean ± SD
Barekese, water	6.59–6.79	6.68 ± 0.07	135.9–138.9	137.10 ± 0.93	122–124	123.00 ± 0.71
Barekese, sediment	6.32–6.83	6.60 ± 0.23	124.1–239.0	175.42 ± 44.81	111–167	154.60 ± 39.49
Owabi, water	6.48–6.85	6.68 ± 0.11	98.5–102.2	32.48 ± 25.67	90–94	91.78 ± 1.48
Owabi, sediment	6.24–8.93	7.60 ± 1.35	8.13–59.3	99.38 ± 1.67	26–58	46.33 ± 17.67

Table 2: Occurrence of pharmaceutical residues in water and sediment samples from Barekese.

Reservoir	Sample type	Pharmaceutical	Range	Mean ± SD	Frequency of detection (%)
Barekese	Water (μg/L)	Amoxicillin	0.08–1.86	1.86 ± 0.00	11.11
		Chloramphenicol	0.10–0.85	0.42 ± 0.29	55.56
		Diclofenac	0.03–4.36	1.36 ± 0.00	11.11
		Metronidazole	0.06–22.23	22.23 ± 0.00	11.11
		Paracetamol	0.06–0.16	0.16 ± 0.00	11.11
	Sediment (μg/kg)	Chloramphenicol	2.78–10.22	4.80 ± 3.63	80.00
Owabi	Water (μg/L)	Amoxicillin	0.10–0.37	0.24 ± 0.13	33.3
		Chloramphenicol	0.18–0.53	0.38 ± 0.12	77.8
		Diclofenac	0.69–107.89	36.51 ± 68.80	33.3
		Paracetamol	0.01–0.15	0.06 ± 0.08	33.3
	Sediment (μg/kg)	Paracetamol	0.10–6.54	3.34 ± 4.55	66.67

Frequency of detection was computed by evaluating the ratio of the number of samples in which an analyte was detected to the total number of samples analyzed.

the classes of β-lactams (ampicillin and amoxicillin), cephalosporin (cefuroxime), fluoroquinolones (ciprofloxacin), tetracycline (doxycycline), aminoglycosides (gentamicin), macrolides (erythromycin), nitroimidazoles (metronidazole), and amphenicols (chloramphenicol). Five (*Enterobacter*, *Clostridium*, *Pseudomonas*, *Acinetobacter*, and *Klebsiella*) out of the eight isolates were resistant to all the antibiotics tested. Isolates of *Corynebacterium* and *Listeria* showed susceptibility to only doxycycline. Isolates of *Bacillus* demonstrated susceptibility to only two antibiotics (doxycycline and erythromycin) of different classes (tetracycline and macrolides).

3.5. Survey on Disposal Routes. One hundred (100) respondents participated in this study, of which 64.0% were males and the remaining 36% were females. The participants were mostly between 21 and 50 years old (79%) and had various levels of formal education, with most attaining either Middle School Leaving Certificate (JHS) (36.0%) or a Secondary Level education (29.0%). However, 23% had no formal education and have lived in the community for less than ten years. Figure 2 provides the demographic characteristics of the respondents. The majority of the respondents indicated that they disposed of both orthodox and herbal medications once they did not need them (Table S3). Antibiotic and analgesic medications, either prescription or nonprescription medicines, were the most frequently disposed medicines (Table S4). Disposal in household trash (67%) and incineration or burning (19%) were the most common methods used in getting rid of unused and expired medicines. Other methods utilized by the respondents were flushing down the sink or toilet (12%) and returning to the pharmacy (2%). To find out about the premium participants placed on issues of environmental concern, participants were asked to rank health, environment, and employment. Majority of the respondents (78%) indicated that health was extremely important to them. However, 48% of the 100 respondents ranked environment as being slightly important (Table S5). Respondents were also asked if they knew pollution of rivers and streams by pharmaceuticals was an environmental concern; to which about half of the respondents answered in the affirmative. Respondents were also asked if they were aware that they could return their unused or expired medicines to the pharmacy, and 58% of the respondents answered in the negative. Majority (60%) of respondents indicated that taking unused or expired medication to the pharmacy for disposal would be inconvenient. Respondents were asked whether they would be willing to pay to improve sewage treatments so that river and stream pollution by pharmaceuticals could be reduced, and 77% responded "yes" (Table S6).

4. Discussion

In the survey to gauge the disposal preferences of the inhabitants around the Owabi and Barekese reservoirs, a majority

Table 3: Ecological risk assessment of water samples from Barekese and Owabi reservoirs.

	Pharmaceutical	MEC (μg/L)	PNEC (μg/L)	HQ	Comment
Barekese	Amoxicillin	1.86	Fish (2.5000)	0.74	Medium risk
			Daphnia (1.1000)	1.69	High risk
			Algae (1.0000)	1.86	High risk
	Chloramphenicol	0.85	Fish (0.5400)	1.57	High risk
			Daphnia (0.5430)	1.57	High risk
			Algae (0.1850)	4.59	High risk
	Diclofenac	4.36	Fish (0.5320)	8.20	High risk
			Daphnia (0.0220)	198.18	High risk
			Algae (0.0145)	300.69	High risk
	Metronidazole	22.23	Fish (1.0350)	21.48	High risk
			Daphnia (0.1000)	222.3	High risk
			Algae (0.1250)	177.84	High risk
	Paracetamol	0.16	Fish (0.3780)	0.42	Medium risk
			Daphnia (0.0092)	17.39	High risk
			Algae (0.1340)	1.20	High risk
Owabi	Amoxicillin	0.37	Fish (2.5000)	0.15	Medium risk
			Daphnia (1.1000)	0.34	Medium risk
			Algae (1.0000)	0.37	Medium risk
	Chloramphenicol	0.53	Fish (0.5400)	0.98	Medium risk
			Daphnia (0.5430)	0.98	Medium risk
			Algae (0.1850)	2.86	High risk
	Diclofenac	107.89	Fish (0.5320)	202.80	High risk
			Daphnia (0.0220)	4904.09	High risk
			Algae (0.0145)	7440.69	High risk
	Paracetamol	0.15	Fish (0.3780)	0.40	Medium risk
			Daphnia (0.0092)	16.30	High risk
			Algae (0.1340)	1.12	High risk

RQ < 0.1 implies minimum risk, 0.1 ≤ RQ ≤ 1 implies medium risk, and RQ > 1 implies high risk [20]. MEC: maximum estimated concentration; PNEC: predicted no-effect concentration; HQ: hazard quotient.

Table 4: Ecological risk assessment of sediment samples from Barekese and Owabi reservoirs.

	Pharmaceutical	MEC (μg/kg)	PNEC (μg/kg)	HQ	Comment
Barekese	Chloramphenicol	10.22	Fish (0.5400)	18.93	High risk
			Daphnia (0.5430)	18.82	High risk
			Algae (0.1850)	55.24	High risk
Owabi	Paracetamol	6.54	Fish (0.3780)	17.30	High risk
			Daphnia (0.0092)	710.87	High risk
			Algae (0.1340)	48.81	High risk

RQ < 0.1 implies minimum risk, 0.1 ≤ RQ ≤ 1 implies medium risk, and RQ > 1 implies high risk [20]. MEC: maximum estimated concentration; PNEC: predicted no-effect concentration; HQ: hazard quotient.

(67%) of household respondents indicated that they disposed of expired or unused medicines by placing them into trash cans to be disposed of in landfills. Even though some respondents indicated periodic disposal of unwanted and expired medicines, 58% indicated that disposal was done whenever they did not need the medication. Prescription or nonprescription analgesics and antibiotics were commonly reported as unused and needing disposal. Pharmaceutical products constitute a significant component of waste generated from many homes. Additionally, some community pharmacies dispose of unused pharmaceuticals into municipal waste [27]. Analgesics and antibiotics have been reported to be frequently disposed of in large quantities by many households [28]. In literature, it has been noted that unwanted or expired medicines are most commonly dumped into trash cans, followed by subsequent disposal

Table 5: Colony morphology, cellular characteristics of isolates, and bacteria identified from water and sediment samples from Barekese and Owabi reservoirs.

Isolates	Colony morphology					Cellular characteristics		Microorganism
	Colour	Shape	Margin	Elevation	Opacity	Gram reaction	Shape	
OW1	Cream	Circular	Undulate	Umbonate		Negative	Rod	*Klebsiella* sp.
OW2	Grey	Irregular	Entire	Convex	Opaque	Positive	Rod	*Corynebacterium* sp.
OW3	Grey	Irregular	Undulate	Flat	Opaque	Positive	Rod	*Bacillus* sp.
OW4		Circular	Entire	Raised	Translucent	Negative	Rod	*Pseudomonas* sp.
OW5	Grey	Circular	Entire	Flat	Translucent	Positive	Rod	*Listeria* sp.
OS1	Grey	Irregular	Undulate	Flat	Opaque	Positive	Rod	*Bacillus* sp.
OS2	Unpigmented	Circular	Mucoid	Raised	Opaque	Negative	Rod	*Acinetobacter* sp.
OS3	Cream	Irregular	Undulate	Flat	Translucent	Positive	Rod	*Clostridium* sp.
OS4	Grey	Irregular	Undulate	Flat	Opaque	Positive	Rod	*Bacillus* sp.
OS5	Grey	Circular	Entire	Raised	Translucent	Negative	Rod	*Enterobacter* sp.
OS6		Circular	Entire	Raised	Translucent	Negative	Rod	*Pseudomonas* sp.
OS7	Grey	Irregular	Undulate	Flat	Opaque	Positive	Rod	*Bacillus* sp.
OS8	Cream	Circular	Undulate	Umbonate	Opaque	Negative	Rod	*Klebsiella* sp.
OS9	Grey	Irregular	Undulate	Flat	Opaque	Positive	Rod	*Bacillus* sp.
OS10	Grey	Circular	Entire	Flat	Translucent	Positive	Rod	*Listeria* sp.
OS11		Circular	Entire	Raised	Translucent	Negative	Rod	*Pseudomonas* sp.
OS12	Cream	Irregular	Undulate	Flat	Translucent	Positive	Rod	*Clostridium* sp.
OS13	Grey	Irregular	Entire	Convex	Opaque	Positive	Rod	*Corynebacterium*
BW1	Grey	Circular	Entire	Raised	Translucent	Negative	Rod	*Enterobacter*
BW2	Unpigmented	Circular	Mucoid	Raised	Opaque	Negative	Rod	*Acinetobacter* sp.
BW3	Grey	Irregular	Undulate	Flat	Opaque	Positive	Rod	*Bacillus* sp.
BW4		Circular	Undulate	Umbonate			Rod	*Klebsiella* sp.
BW5	Grey	Circular	Entire	Raised	Translucent	Negative	Rod	*Enterobacter* sp.
BW6	Grey	Circular	Entire	Flat	Translucent	Positive	Rod	*Listeria* sp.
BW7		Circular	Entire	Raised	Translucent		Rod	*Pseudomonas* sp.
BS1	White	Irregular	Entire	Convex	Opaque	Positive	Rod	*Corynebacterium* sp.
BS2	Grey	Circular	Entire	Raised	Translucent	Negative	Rod	*Enterobacter* sp.
BS3	Cream	Irregular	Undulate	Flat	Translucent	Positive	Rod	*Clostridium* sp.
BS4	Grey	Irregular	Undulate	Flat	Opaque	Positive	Rod	*Bacillus* sp.
BS5	Grey	Irregular	Undulate	Flat	Opaque	Positive	Rod	*Bacillus* sp.

OW: Owabi water; OS: Owabi sediment; BW: Barekese water; BS: Barekese sediment.

into dumpsites or landfills [20, 28]. The pharmaceuticals could be washed off into nearby surface waters during rainfalls or even leach into the ground to contaminate groundwater. This is no exception in communities where open defecation and indiscriminate garbage disposal are practiced; all these waste flow directly into nearby rivers and water bodies. Some of these water bodies feed the reservoirs of water treatment plants where the water is treated and dispatched to homes and factories for various uses, including drinking. Because water treatment plants do not necessarily target the removal of specific chemicals, there is the likelihood that the chemicals may be present in treated water dispatched to homes. The threat is potentially more significant for communities that consume water directly from polluted rivers and streams. Exposure to sublethal concentrations of these pharmaceuticals could harm the ecosystem and result in long-term toxic effects. The effects could be multidrug resistance (by antibiotics), interference with a drug a person might already be taking (usually by analgesics), gender binding in fish, and decline in biodiversity [11, 29, 30]. Although this study did not assess how respondents came by unwanted or expired medication, patient noncompliance, relief of symptoms/signs, medication change, and death of patient have been reported by other studies as sources of unwanted or expired medications [31–33].

The findings of this survey clearly show that respondents do not dispose of unwanted or expired medicines through proper means. Interestingly, 50% of respondents were aware that pharmaceuticals' pollution of rivers and streams was an environmental concern. Contrastively, respondents were more supportive towards greater care of the environment. The fact that 78% of respondents ranked health as extremely important while 48% ranked environment as slightly important suggests a lack of knowledge of the possible effects of

Table 6: Zones of inhibition (mm) of antibiotics against isolates and corresponding susceptibility and resistance of isolates to antibiotic.

Organisms	AMP	AML	CXM	CIP	DOX	E	GEN	MET	CHL
Bacillus sp.	R (0)	R (0)	R (0)	R (17)	S (25)	S (25)	R (10)	R (15)	R (0)
Clostridium sp.	R (8)	R (12)	R (7)	R (11)	R (0)	R (18)	R (16)	R (13)	R (11)
Klebsiella sp.	R (0)	R (0)	R (7)	10 (R)	R (0)	R (0)	R (15)	R (0)	R (10)
Corynebacterium sp.	R (0)	R (0)	R (0)	R (15)	S (24)	IP	R (0)	R (10)	R (0)
Enterobacter sp.	R (0)	R (0)	R (0)	R (16)	R (0)	R (0)	R (0)	R (0)	R (0)
Acinetobacter sp.	R (0)	R (0)	R (0)	R (9)	R (0)	R (0)	R (0)	R (0)	R (0)
Bacillus sp.	R (0)	R (0)	R (0)	R (15)	S (24)	S (25)	R (0)	R (0)	R (0)
Listeria sp.	R (0)	R (0)	R (0)	R (16)	S (22)	R (0)	R (0)	R (10)	R (0)
Pseudomonas sp.	R (0)	R (0)	R (0)	R (12)	R (0)	R (0)	IP (0)	R (0)	R (0)
Clostridium sp.	R (17)	R (18)	R (0)	R (0)	R (19)	R (8)	R (8)	R (11)	R (10)
Enterobacter sp.	R (0)	R (0)	R (0)	R (12)	R (0)	R (0)	R (0)	R (8)	R (8)

AMP: ampicillin; AML: amoxicillin; CXM: cefuroxime; CIP: ciprofloxacin; DOX: doxycycline; E: erythromycin; GEN: gentamicin; MET: metronidazole; CHL: chloramphenicol; S: susceptible; R: resistant; IP: in preparation (limited information in EUCAST database).

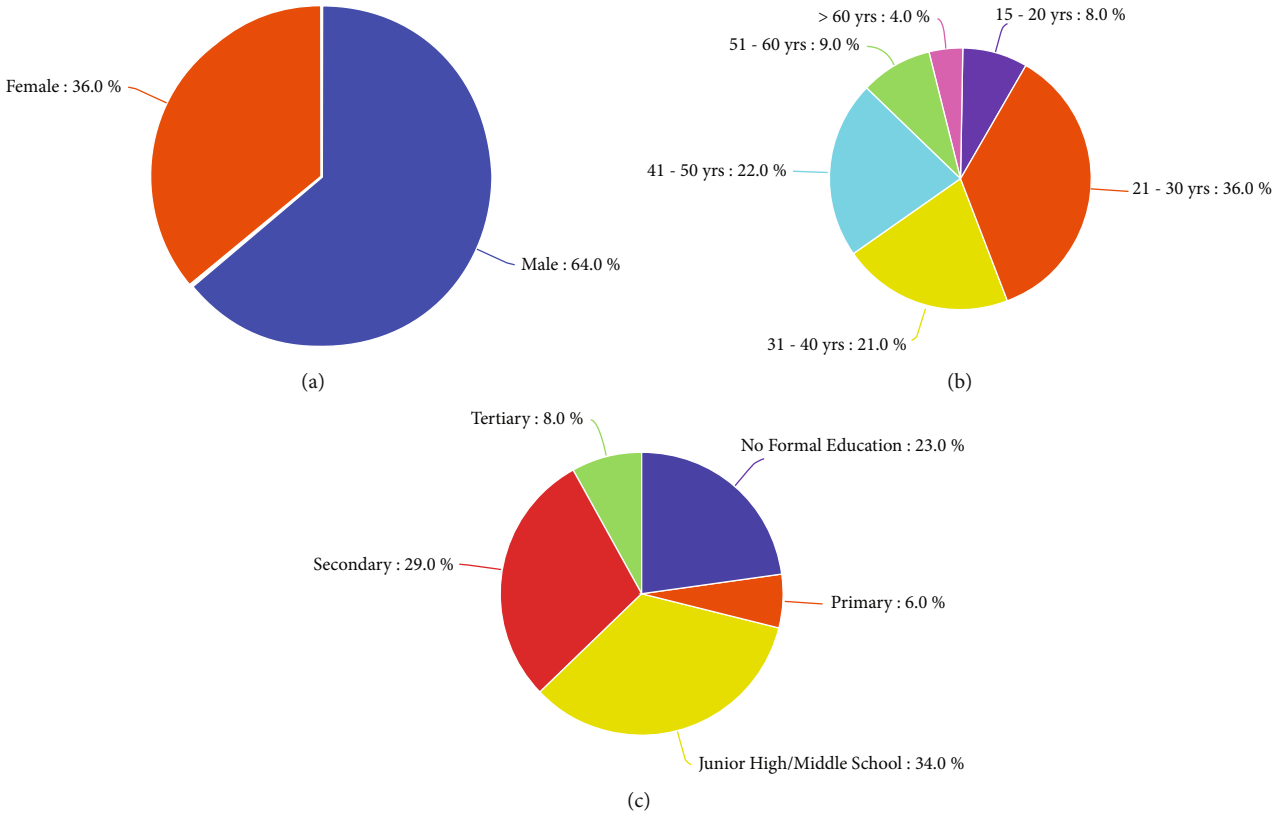

Figure 2: Demographic characteristics of respondents in household: (a) gender, (b) age, and (c) educational level of participants in the survey.

environmental problems on human health and ecosystems. There was a good correlation between respondents' awareness of the threats that pharmaceuticals pose to the environment and their willingness to pay to improve sewage treatment to minimize pollution of rivers and streams by pharmaceuticals. One strategy that has been suggested to reduce the levels of pharmaceuticals in the environment is the institution and implementation of a medicine take-back program. A search through the literature has indicated that imprudent disposal of unwanted and expired medicines is a major route through which pharmaceuticals access the environment [33–35]. There is no coordinated national outlet for the proper disposal of unused and expired drugs in Ghana. The Food and Drugs Authority (FDA) in Ghana, by the Public Health Act, 202 (Act 851), is responsible for the safe disposal of unwanted and expired drugs [36]. However, the cost and bureaucracy involved in this process are gridlocks for households looking for a safe means to dispose

of pharmaceutical waste. In 2009, the Cocoa Clinic in Accra introduced a Disposal of Unused Medicines Program (DUMP). This comprehensive medicine take-back project urges patients and staff of its parent organization to return their unused pharmaceuticals to the clinic for safe disposal. Under the FDA's supervision, the approved methods for controlled disposal of pharmaceutical waste are subsequently followed by the Cocoa Clinic for any drugs received [27, 37]. Even though this is an excellent program that can reduce the environmental presence of pharmaceuticals in Ghana, DUMP has a limited reach. The program serves only a small percentage of the Ghanaian population—personnel of the Ghana Cocoa Board and customers of the Cocoa Clinic. The larger section of the Ghanaian population still has unused and expired drugs in their possession, with the disposal of these drugs still uncontrolled. Establishing an effective medicine take-back program demands a lot of time, money, and human resources. Therefore, willingness to pay to minimize pollution by pharmaceuticals is a good indicator for a national roll-out of a Disposal of Unused Medicines Project (DUMP), as is done in countries such as New Zealand and Canada [35, 38]. A convenient location of the take-back program not only ensures environmental protection but provides details of unused pharmaceuticals valuable to the health community in optimizing its prescribing and dispensing practices to reduce the generation of unused or expired medicines [27]. The existence of a knowledge gap is therefore apparent about the above issues. These could form part of research questions for further studies as they were not explored in this study. It should be noted that the response from the survey may have been distorted as a result of the topic as a self-administered questionnaire collected data. For instance, questions regarding disposal practices, the environment, and payment to improve the environment may have been inflated to a socially desirable factor. Again, a response rate was not calculated in this study due to the fact that the number of participants approached for participation was not tracked. However, the findings of this study point clearly to the existence of improper medicine disposal practices in Ghana, which need to be addressed. This is particularly worrying as the disposal pattern identified as the primary route has been reported in other studies in Ghana [27, 39, 40].

In this study, paracetamol diclofenac, amoxicillin, metronidazole, and chloramphenicol were detected and quantified. Although most pharmaceuticals have high solubility in water and hence remain soluble in the aqueous phase, some drugs remain insoluble or attached to suspended solids in the wastewater. Since the liquid samples were filtered before extraction, the reported concentrations in this work represent only the water-soluble fraction of the analytes. The presence of pharmaceuticals in water and sediments suggests the widespread occurrence of the pharmaceuticals in both reservoirs. Paracetamol and chloramphenicol were present in all sample types. For sediment samples, only paracetamol was detected in samples from Owabi. On the other hand, only chloramphenicol was detected in sediment samples from Barekese. Individual pharmaceutical concentrations in untreated water were found to be generally low, with average concentrations ranging between 0.07 and 36.51 mg/L. The highest detected concentration of any pharmaceutical in untreated water was for diclofenac (107.87 μg/L), followed by metronidazole (22.23 μg/L), amoxicillin (1.86 μg/L), chloramphenicol (0.85 μg/L), and paracetamol (0.16 μg/L). The results of this research are in line with many other studies in the literature, which have observed low levels of pharmaceuticals in a variety of water sources. For instance, [41] detected five pharmaceuticals in influents of a municipal wastewater plant. Paracetamol, metformin, norfluoxetine, atenolol, and cephalexin were the five detected pharmaceuticals at average concentrations in a range of 1–40 μg/L. In Spain, 35 pharmaceuticals were found in the raw water at a drinking water treatment facility's intake, with levels up to 1.2 μg/L [42]. However, the levels of pharmaceuticals detected in this study were found to be higher than many other studies. In a study of 31 pharmaceuticals conducted throughout the drinking water supply system in Lisbon, the levels of pharmaceuticals detected ranged from 0.005 to 46 ng/L [43]. In Spain, pharmaceuticals were quantified in water and sediment samples from low ng/L to 168 ng/L and low ng/L to 50.3 ng/g, respectively [44]. Also, Ref. [45] quantified pharmaceuticals ranging from 0.0018 to 3 ng/L in water samples from a drinking water treatment plant. This suggests relatively higher inputs of pharmaceuticals into both reservoirs under study.

The efficiency at which pharmaceuticals are removed from water is affected by several factors, including the weather, the nature of water treatment, and its operating conditions (temperature, redox conditions, solids, and hydraulic retaining time). The physicochemical composition of most pharmaceuticals, which is acidity and high solubility in water with very low solid-liquid partition, is claimed to be the key cause. These factors often result in poor sorption of these compounds onto particles or organic matter, leaving them soluble in the aqueous phase [41]. Overall, pharmaceutical levels in the aquatic environment can be connected to specific physicochemical parameters. Physicochemical factors such as pH, temperature, conductivity, total organic carbon (TOC), and TDS can favor photodegradation and other attenuation processes [44]. The pH of all the raw water samples from both reservoirs was determined to be slightly acidic (6.32–6.89). Positively charged soil components (at pH 6) play a role in acidic pharmaceutical retention. Also, there is considerable blockage of sorption sites by humic acids at acidic pH [44]. Since the detected pharmaceuticals in this study were all acidic, the low levels of detection could be linked to the occurrence of this phenomenon. Conductivity measures the ability of the samples to conduct electricity as a result of the total effect of positive and negative ions dissolved in them. Pharmaceuticals have been found to have a stronger affinity for cationic organic matter from clay soils than anionic organic matter from sandy soils and complexation with cationic species (e.g., Ca^{2+}) [46]. The high conductivity values in this study could result in one of these two given possible phenomena leading to the low quantification levels in water samples.

The concentrations of individual pharmaceuticals in the sediments were found to have an average concentration

range of 3.34–4.80 μg/kg. The highest concentrations detected in sediment samples were 10.22 μg/kg for chloramphenicol and 6.54 μg/kg for paracetamol. This study's findings were consistent with many of the reported works in literature where low levels of pharmaceuticals have been quantified in sediments. Pharmaceuticals have been reported to be present in sediments at the outlet of a wastewater treatment plant in South Africa. Paracetamol, metronidazole, and clozapine were quantified, with concentrations as high as 18 ng/g [47]. In another study in Budapest (Hungary), naproxen and diclofenac were found in the range of 2–20 and 5–38 ng/g, respectively [48]. Although most pharmaceuticals are polar and likely to be found in the dissolved fraction, some can have specialized interactions with the solid fraction and transmitted to sediments [44]. The effects of pH on the interactions between organic matter and pH-dependent pharmaceuticals might be significant [46]. Sediment samples from Owabi were determined to be slightly acidic to basic with a pH range of 6.24–8.93. One of the five pharmaceuticals was detected in sediments from this reservoir. This is in line with the findings of [44] where pharmaceuticals were found to bond to suspended solids under basic (pH$\geq$7) conditions. However, only chloramphenicol was detected in sediments from the Barekese reservoir. The slightly acidic nature of these samples could be a possible explanation for the absence of the other pharmaceutical from the sediment samples.

Many pharmaceuticals can potentially pose long-term negative impacts on ecosystems and humans. The quantities of pharmaceuticals found in water and sediment samples might have considerable environmental consequences. The most obvious concern linked with the current study's findings is that continual exposure to antibiotics even at low levels may lead to the development of antibiotic-resistant bacteria. The occurrence of antibiotics in the environment at sublethal doses can facilitate the presence of antibiotic-resistant bacteria in the ecosystem and hence the transfer of antibiotic-resistant genes to other bacteria [29, 49]. The presence of antibiotics at these sites, in the absence or presence of other resistance selective agents such as heavy metals, disinfectants, and detergents, can create a selective pressure that causes the proliferation of antibiotic resistance genes, resulting in the development or acquisition of resistance genes among microbes, rendering current treatment regimens useless [49]. Bacteria with antibiotic resistance genes have been observed in biofilms inoculated with drinking water bacteria [29]. This points to the possibility of gene transfer to the drinking water distribution network, maybe via surface and wastewater. The adverse effects of pharmaceuticals are not limited to antibiotics. In this study, diclofenac presented the highest detected concentration. High levels of diclofenac in the environment could pose serious consequences. Unintentional exposure to diclofenac, for example, has been known to impact vultures, resulting in a significant decrease in their numbers a few years ago [50]. Diclofenac suppresses Gram-positive and Gram-negative bacteria growth by inhibiting DNA synthesis at high concentrations (50–100 mg/L), and lotic biofilms consisting of bacterial and algal communities lost about 70% of their overall initial biomass after 4 weeks of exposure to 100 g/L diclofenac [51]. Ibuprofen is reported to diminish the total bacterial biomass of a riverine biofilm community produced from rotating annular bioreactors and treated to a concentration of 10 g/L for 8 weeks [51]. Hormones such as estrogens are recognized as endocrine disruptors or modulators because they can negatively affect reproductive and sexual development, such as the feminization of male fishes at only ng/L concentrations and the sterilization frogs after progesterone exposure [46]. Conversely, Ref. [52] have reported that pharmaceuticals such as caffeine and salicylic acid can increase the yield of beet.

Thirty pure isolates (17 Gram-positive and 13 Gram-negative) bacteria were identified in water and sediment samples. *Bacillus*, *Corynebacterium*, *Pseudomonas*, *Klebsiella*, *Enterobacter*, *Listeria*, *Acinetobacter*, and *Clostridium* were among the bacteria that were identified. Various studies have also documented the isolation of bacteria from several of these genera from various locations across the world. [53] identified 101 bacteria belonging to 16 distinct genera from drinking water sources of Kohat, a northwestern district of Pakistan. They pointed out that these microbes are opportunistic pathogens and may constitute a considerable concern for public and occupational health. Borquaye et al. (2019b) isolated microbes from soil and leachate samples from active and abandoned landfill sites in Kumasi, Ghana. In a similar work carried out in Accra, Ghana, bacteria isolated included *Escherichia coli*, *Salmonella* spp., *Vibrio* spp., and *Bacillus* spp. [54]. In our study, diverse communities of microbes thriving in these sites were isolated, even though levels of antibiotics quantified were quite high in the same sites. Of the bacteria isolated from the sampling sites, *Bacillus* was the predominant genus. Five (*Enterobacter*, *Clostridium*, *Pseudomonas*, *Acinetobacter*, and *Klebsiella*) out of the eight isolates were resistant to all the antibiotics. Isolates of *Corynebacterium* and *Listeria* showed susceptibility to only doxycycline. Isolates of *Bacillus* demonstrated susceptibility to only two antibiotics (doxycycline and erythromycin). This is similar to the work done in Kumasi, where most of the bacteria isolated from landfill sites demonstrated resistance to antibiotics used in a susceptibility test. Tahrani et al. (2015b) studied resistance patterns of microbes isolated from industrial effluents in Tunisia, revealing six patterns of multidrug resistance among the 11 antibiotics tested. Also, in Nigeria, over 10% of the bacteria from the surface and underground water in six rural settlements were resistant to four or more antibiotics [55]. More so, Lu, Wu and Wang (2022) detected 18 types including 174 subtypes of antibiotic-resistant genes (ARGs) in water and microplastics of mariculture pond. Chloramphenicol-resistant genes were the dominant antimicrobial-resistant genes in their study. Although most *Bacillus* strains are not harmful to humans, prolonged contact with these microorganisms carrying resistance genes might spell tragedy. They might pass resistance genes on to other harmful organisms, wreaking havoc. Antimicrobial resistance in enteric bacteria, in particular, is a severe public health problem across the world. Skin, wounds, and the respiratory and gastrointestinal tracts are all places where *Acinetobacter* may invade. This microbe has also been linked to incidences of community-acquired infection [56].

The risks posed by the presence of the detected pharmaceuticals in the ecosystem were assessed in the ecological risk assessment study. The predicted no-effect concentration (PNEC: the concentration at which no adverse effect is suspected to occur) values for fish, *Daphnia*, and algae were determined using data from the literature on acute toxicity [9]. For water samples, HQ values for paracetamol indicated the medium risk to fish but a high risk to *Daphnia* and algae, respectively. The very high HQ values for diclofenac (HQ values $\gg 1$) imply quite a high risk to these species investigated especially against algae. Both paracetamol and chloramphenicol posed high risks to organisms in the sediments. Obviously, the worst hazard quotients were observed for diclofenac against *Daphnia* in the water samples and paracetamol on the same organism in sediment. In Pakistan, the HQ for pharmaceuticals from industrial effluents was determined. The maximum HQ values obtained in that study were with paracetamol (64 against *Daphnia*), naproxen (177 against fish), diclofenac (12,600 against *Oncorhynchus mykiss*), ibuprofen (167,300 against *Oryzias latipes*), ofloxacin (81,000 against *Pseudomonas putida)*, and ciprofloxacin (440 against *Microcystis aeruginosa*) [20]. The high HQs recorded in this study unveil a looming danger to aquatic life which needs to be addressed urgently.

5. Conclusions

This study reveals that many households in and around the Owabi and Barekese reservoirs employ improper methods to dispose of unwanted and expired medicines, where throwing medicines into trash cans with other domestic waste are the most common disposal practice. The fact that respondents ranked health as extremely important while maintaining the environment as slightly important reveals the lack of awareness of the effects of improperly disposed pharmaceuticals on human health and ecosystems. Therefore, there is a need to create greater awareness of the problem of pharmaceuticals among the public and other sectors. However, the willingness of respondents to pay for the reduction or removal of pollutants of rivers and streams indicates concern and desire to care for the environment. This study also revealed the pollution status of the two dams with pharmaceuticals. The concentration of the pharmaceuticals ranged from 0.01 to 107.89 μg/L in the water samples and 0.10 to 10.22 μg/kg in the sediments. Although some of the targeted pharmaceuticals were below the detection limit, there was a detection of at least one pharmaceutical residue in all the samples gathered from both water and sediments, indicating potential pharmaceutical pollution of the reservoirs. Since water treatment plants do not specifically target the removal of pharmaceuticals, the effect on society could be enormous. It is important to institutionalize education programs to create awareness of the proper methods for the disposal of unused and expired medicines. Regular monitoring of the reservoirs will provide accurate information on the pollution status of the reservoirs. Finally, strategies for the removal of pharmaceutical residues during water treatment should be explored.

Data Availability

All data obtained or analyzed during this study are included in this published article.

Disclosure

The funders had no role in experimental design, data collection, or interpretation of data.

Conflicts of Interest

The authors declare that they have no known competing financial interests or personal relationships that could have influenced the work reported in this paper.

Authors' Contributions

The study was designed by LSB, GD, FCM-R, and KM. All experiments were carried out by JNG, BAN, NAA, FF, GG, and BQ. The initial manuscript was drafted by JNG and BAN. LSB and GD supervised the work. All authors read and approved the final draft.

Acknowledgments

The Departments of Chemistry, Theoretical and Applied Biology, and Pharmaceutical Microbiology as well as the KNUST Central Laboratory are acknowledged for using their facilities for this study. The authors are grateful to Mr. Daniel Nimako Ampratwum of the Central Laboratory, KNUST, for technical support. This work was supported by a KNUST Research Fund (KReF 2019) grant awarded to LSB, GD, FCM-R, and KM.

Supplementary Materials

Figure S1: HPLC chromatogram for analyte standards. A: antibiotics at 215 nm; B: analgesics at 270 nm; C: analgesic at 220 nm. Peaks corresponding to specific analytes have been indicated. Table S1: HPLC flow program for the analyses of antibiotics and analgesics. Table S2: quality parameters. Table S3: frequency of disposal of prescription and nonprescription drugs. Table S4: disposal methods and medication types often disposed. Table S5: how important are health, transportation, education, environment, and jobs ($n = 100$). Table S6: respondent's willingness to better improve the environment. *(Supplementary Materials)*

References

[1] C. G. Daughton and T. A. Ternes, "Pharmaceuticals and personal care products in the environment: agents of subtle change?," *Environmental Health Perspectives*, vol. 107, supplement 6, pp. 907–938, 1999.

[2] L. S. Borquaye, E. Ekuadzi, G. Darko et al., "Occurrence of Antibiotics and Antibiotic-Resistant Bacteria in Landfill Sites in Kumasi, Ghana," *Journal of Chemistry*, vol. 2019, 10 pages, 2019.

[3] D. W. Kolpin, E. T. Furlong, M. T. Meyer et al., "Pharmaceuticals, hormones, and other organic wastewater contaminants

in U.S. streams, 1999–2000: a national reconnaissance," *Environmental Science & Technology*, vol. 36, no. 6, pp. 1202–1211, 2002.

[4] J. B. Ellis, "Pharmaceutical and personal care products (PPCPs) in urban receiving waters," *Environmental Pollution*, vol. 144, no. 1, pp. 184–189, 2006.

[5] G. D. Wright, "The antibiotic resistome: the nexus of chemical and genetic diversity," *Nature Reviews. Microbiology*, vol. 5, no. 3, pp. 175–186, 2007.

[6] A. K. Sarmah, M. T. Meyer, and A. B. A. Boxall, "A global perspective on the use, sales, exposure pathways, occurrence, fate and effects of veterinary antibiotics (VAs) in the environment," *Chemosphere*, vol. 65, no. 5, pp. 725–759, 2006.

[7] G. Darko, L. S. Borquaye, A. Acheampong, and K. Oppong, "Veterinary antibiotics in dairy products from Kumasi, Ghana," *Cogent Chemistry*, vol. 3, no. 1, p. 1343636, 2017.

[8] K. Kümmerer, "Pharmaceuticals in the environment," *Annual Review of Environment and Resources*, vol. 35, no. 1, pp. 57–75, 2010.

[9] H. Sanderson, D. J. Johnson, T. Reitsma, R. A. Brain, C. J. Wilson, and K. R. Solomon, "Ranking and prioritization of environmental risks of pharmaceuticals in surface waters," *Regulatory Toxicology and Pharmacology*, vol. 39, no. 2, pp. 158–183, 2004.

[10] M. D. Hernando, M. Mezcua, A. R. Fernández-Alba, and D. Barceló, "Environmental risk assessment of pharmaceutical residues in wastewater effluents, surface waters and sediments," *Talanta*, vol. 69, no. 2, pp. 334–342, 2006.

[11] K. Fent, A. A. Weston, and D. Caminada, "Ecotoxicology of human pharmaceuticals," *Aquatic Toxicology*, vol. 76, no. 2, pp. 122–159, 2006.

[12] N. Kemper, "Veterinary antibiotics in the aquatic and terrestrial environment," *Ecological Indicators*, vol. 8, no. 1, pp. 1–13, 2008.

[13] N. O. Boadi, L. S. Borquaye, G. Darko, D. D. Wemegah, D. Agorsor, and R. Akrofi, "Assessment of the quality of the Owabi reservoir and its tributaries," *Cogent Food & Agriculture*, vol. 4, no. 1, p. 1492360, 2018.

[14] M. K. Domfeh, F. O. K. Anyemedu, G. K. Anornu, K. A. Adjei, and S. N. Odai, "Assessment of the water balance of the Barekese reservoir in Kumasi, Ghana," *Journal of Science and Technology (Ghana)*, vol. 35, no. 3, p. 3, 2015.

[15] O. Akoto and E. Abankwa, "Evaluation of Owabi Reservoir (Ghana) water quality using factor analysis," *Lakes & Reservoirs: Research & Management*, vol. 19, no. 3, pp. 174–182, 2014.

[16] I. K. Tetteh, E. Awuah, and E. Frempong, "Post-project analysis: the use of a network diagram for environmental evaluation of the Barekese Dam, Kumasi, Ghana," *Environmental Modeling and Assessment*, vol. 11, no. 3, pp. 235–242, 2006.

[17] T. Akanchise, S. Boakye, L. S. Borquaye, M. Dodd, and G. Darko, "Distribution of heavy metals in soils from abandoned dump sites in Kumasi, Ghana," *Scientific African*, vol. 10, article e00614, 2020.

[18] N. Konwuruk, L. S. Borquaye, G. Darko, and M. Dodd, "Distribution, bioaccessibility and human health risks of toxic metals in peri- urban topsoils of the Kumasi metropolis," *Scientific African*, vol. 11, article e00701, 2021.

[19] H. Sanderson, D. J. Johnson, C. J. Wilson, R. A. Brain, and K. R. Solomon, "Probabilistic hazard assessment of environmentally occurring pharmaceuticals toxicity to fish, daphnids and algae by ECOSAR screening," *Toxicology Letters*, vol. 144, no. 3, pp. 383–395, 2003.

[20] M. Ashfaq, K. Nawaz Khan, M. Saif Ur Rehman et al., "Ecological risk assessment of pharmaceuticals in the receiving environment of pharmaceutical wastewater in Pakistan," *Ecotoxicology and Environmental Safety*, vol. 136, pp. 31–39, 2017.

[21] L. H. Galarion and W. L. Rivera, "Isolation and characterization of marine sediment bacteria capable of biocatalyzing bromination of indole," *Journal of Scientific and Industrial Research*, vol. 75, no. 6, pp. 359–364, 2016.

[22] J. G. Holt, N. R. Krieg, P. H. Sneath, J. T. Staley, and S. T. Williams, *Bergey's Manual of Determinative Bacteriology*, Baltimore,: Williams & Wilkins Co., 9th edition, 1994, https://www.biodiversitylibrary.org/item/41848.

[23] EUCAST, "EUCAST: Clinical breakpoints and dosing of antibiotics," 2021, 2022, https://www.eucast.org/clinical_breakpoints/.

[24] D. Azanu, B. Styrishave, G. Darko, J. J. Weisser, and R. C. Abaidoo, "Occurrence and risk assessment of antibiotics in water and lettuce in Ghana," *Science of the Total Environment*, vol. 622-623, pp. 293–305, 2018.

[25] C. Bouissou-Schurtz, P. Houeto, M. Guerbet et al., "Ecological risk assessment of the presence of pharmaceutical residues in a French national water survey," *Regulatory Toxicology and Pharmacology*, vol. 69, no. 3, pp. 296–303, 2014.

[26] J. Liu, G. Lu, H. Yang, T. Dang, and Z. Yan, "Ecological impact assessment of 110 micropollutants in the Yarlung Tsangpo River on the Tibetan Plateau," *Journal of Environmental Management*, vol. 262, article 110291, 2020.

[27] L. S. Borquaye, E. Ekuadzi, G. Darko et al., "Disposal of unused and expired medicines in Ghana," *Journal of Chemistry*, vol. 29, 91 pages, 2018.

[28] R. Rosal, A. Rodríguez, J. A. Perdigón-Melón et al., "Occurrence of emerging pollutants in urban wastewater and their removal through biological treatment followed by ozonation," *Water Research*, vol. 44, no. 2, pp. 578–588, 2010.

[29] O. A. Jones, J. N. Lester, and N. Voulvoulis, "Pharmaceuticals: a threat to drinking water?," *Trends in Biotechnology*, vol. 23, no. 4, pp. 163–167, 2005.

[30] S.-W. Li and A. Y.-C. Lin, "Increased acute toxicity to fish caused by pharmaceuticals in hospital effluents in a pharmaceutical mixture and after solar irradiation," *Chemosphere*, vol. 139, pp. 190–196, 2015.

[31] E. A. Abahussain, D. E. Ball, and W. C. Matowe, "Practice and opinion towards disposal of unused medication in Kuwait," *Medical Principles and Practice*, vol. 15, no. 5, pp. 352–357, 2006.

[32] S. Sonowal, C. Desai, J. D. Kapadia, and M. K. Desai, "A survey of knowledge, attitude, and practice of consumers at a tertiary care hospital regarding the disposal of unused medicines," *Journal Of Basic And Clinical Pharmacy*, vol. 8, no. 1, pp. 4–7, 2016.

[33] A. Vellinga, S. Cormican, J. Driscoll, M. Furey, M. O'Sullivan, and M. Cormican, "Public practice regarding disposal of unused medicines in Ireland," *Science of the Total Environment*, vol. 478, pp. 98–102, 2014.

[34] M. Bashaar, V. Thawani, M. A. Hassali, and F. Saleem, "Disposal practices of unused and expired pharmaceuticals among general public in Kabul," *BMC Public Health*, vol. 17, no. 1, pp. 1–8, 2017.

[35] R. Braund, B. M. Peake, and L. Shieffelbien, "Disposal practices for unused medications in New Zealand☆," *Environment International*, vol. 35, no. 6, pp. 952–955, 2009.

[36] Food and Drugs Authority, Ghana, *Guidelines for safe disposal of unwholesome products*, Food and Drugs Authority, Ghana, Accra, FDA/DRI/DMS/GL-SDP/2013/03, 2019.

[37] K. E. Ahorsu and Y. Esseku, "Emerging security challenges to Africa: the case of haphazard disposal of pharmaceuticals in Ghana," *Journal of Human Security*, vol. 13, no. 1, pp. 5–15, 2017.

[38] E. Gagnon, "Pharmaceutical disposal programs for the public: a Canadian perspective," *Ottawa, Ontario: Health Canada, Environmental Impact Initiative*, 2009.

[39] V. S. Aboagye and K. A. Kyei, "Disposal of leftover drugs in Ghana," *Asian Journal of Pharmaceutical Research*, vol. 4, no. 2, pp. 84–91, 2014.

[40] S. N. Osei-Djarbeng, G. O. Larbi, R. Abdul-Rahman, S. Osei-Asante, and R. Owusu-Antwi, "Household acquisition of medicines and disposal of expired and unused medicines at two suburbs (Bohyen and Kaase) in Kumasi-Ghana," *The Pharma Innovation*, vol. 4, no. 8, p. 85, 2015.

[41] A. Shraim, A. Diab, A. Alsuhaimi et al., "Analysis of some pharmaceuticals in municipal wastewater of Almadinah Almunawarah," *Arabian Journal of Chemistry*, vol. 10, pp. S719–S729, 2017.

[42] M. Huerta-Fontela, M. T. Galceran, and F. Ventura, "Occurrence and removal of pharmaceuticals and hormones through drinking water treatment," *Water Research*, vol. 45, no. 3, pp. 1432–1442, 2011.

[43] V. de Jesus Gaffney, C. M. M. Almeida, A. Rodrigues, E. Ferreira, M. J. Benoliel, and V. V. Cardoso, "Occurrence of pharmaceuticals in a water supply system and related human health risk assessment," *Water Research*, vol. 72, pp. 199–208, 2015.

[44] R. Moreno-González, S. Rodriguez-Mozaz, M. Gros, D. Barceló, and V. M. León, "Seasonal distribution of pharmaceuticals in marine water and sediment from a Mediterranean coastal lagoon (SE Spain)," *Environmental Research*, vol. 138, pp. 326–344, 2015.

[45] P. E. Stackelberg, J. Gibs, E. T. Furlong, M. T. Meyer, S. D. Zaugg, and R. L. Lippincott, "Efficiency of conventional drinking-water-treatment processes in removal of pharmaceuticals and other organic compounds," *Sci. Total Environ.*, vol. 377, no. 2-3, pp. 255–272, 2007.

[46] S. Mompelat, B. Le Bot, and O. Thomas, "Occurrence and fate of pharmaceutical products and by-products, from resource to drinking water," *Environment International*, vol. 35, no. 5, pp. 803–814, 2009.

[47] S. Matongo, G. Birungi, B. Moodley, and P. Ndungu, "Occurrence of selected pharmaceuticals in water and sediment of Umgeni River, KwaZulu-Natal, South Africa," *Environmental Science and Pollution Research*, vol. 22, no. 13, pp. 10298–10308, 2015.

[48] M. Varga, J. Dobor, A. Helenkár, L. Jurecska, J. Yao, and G. Záray, "Investigation of acidic pharmaceuticals in river water and sediment by microwave-assisted extraction and gas chromatography-mass spectrometry," *Microchemical Journal*, vol. 95, no. 2, pp. 353–358, 2010.

[49] J. Fick, H. Söderström, R. H. Lindberg, C. Phan, M. Tysklind, and D. G. J. Larsson, "Contamination of surface, ground, and drinking water from pharmaceutical production," *Environmental Toxicology and Chemistry*, vol. 28, no. 12, pp. 2522–2527, 2009.

[50] R. E. Green, M. A. Taggart, K. R. Senacha et al., "Rate of decline of the oriental white-backed vulture population in India estimated from a survey of diclofenac residues in carcasses of ungulates," *PLoS One*, vol. 2, no. 8, article e686, 2007.

[51] A. Barra Caracciolo, E. Topp, and P. Grenni, "Pharmaceuticals in the environment: biodegradation and effects on natural microbial communities. A review," *Journal of Pharmaceutical and Biomedical Analysis*, vol. 106, pp. 25–36, 2015.

[52] D. Papaioannou, P. H. Koukoulakis, M. Papageorgiou, D. A. Lambropoulou, and I. K. Kalavrouziotis, "Chemosphere Investigation of pharmaceutical and personal care product interactions of soil and beets (Beta vulgaris L) under the effect of wastewater reuse," *Chemosphere*, vol. 238, article 124553, 2020.

[53] T. Hussain, A. Roohi, S. Munir et al., "Biochemical characterization and identification of bacterial strains isolated from drinking water sources of Kohat, Pakistan," *African Journal of Microbiology Research*, vol. 7, no. 16, pp. 1579–1590, 2013.

[54] L. N. A. Sackey and K. Meizah, "Assesement of the quality of leachate at Sarbah landfill site at Weija in Accra," *Journal of Environmental Chemistry and Ecotoxicology*, vol. 7, no. 6, pp. 56–61, 2015.

[55] J. O. Oluyege, A. C. Dada, and A. T. Odeyemi, "Incidence of multiple antibiotic resistant Gram-negative bacteria isolated from surface and underground water sources in south western region of Nigeria," *Water Science and Technology*, vol. 59, no. 10, pp. 1929–1936, 2009.

[56] L. Tahrani, L. Soufi, I. Mehri et al., "Isolation and characterization of antibiotic-resistant bacteria from pharmaceutical industrial wastewaters," *Microbial Pathogenesis*, vol. 89, pp. 54–61, 2015.

Hindawi
Journal of Chemistry
Volume 2022, Article ID 3770935, 7 pages
https://doi.org/10.1155/2022/3770935

Research Article

Protection against the Phytotoxic Effect of Mercury Chloride by Catechin and Quercetin

Yedda M. L. S. de Matos,[1] Daniel L. M. Vasconcelos,[2] Antonio C. H. Barreto,[2] Janaína E. Rocha,[1] José B. de Araújo-Neto,[1] Fábia F. Campina,[1] Maria Milene C. da Silva,[1] Tássia T. Al Yafawi,[3] Celestina E. Sobral-Souza,[3] Jacqueline C. A. Pinheiro,[4] Saulo R. Tintino,[1] Amanda K. Sousa,[3] Raimundo N. P. Teixeira,[5] Juan C. Alvarez-Pizarro,[4] João H. da Silva,[4] Abolghasem Siyadatpanah,[6] Bonglee Kim,[7] and Henrique D. M. Coutinho[1]

[1]*Laboratory of Microbiology and Molecular Biology, Regional University of Cariri, Crato, CE, Brazil*
[2]*Department of Physics, Federal University of Ceará, Fortaleza, CE, Brazil*
[3]*University Center UNILEÃO, Juazeiro do Norte CE, Brazil*
[4]*Federal University of Cariri, Crato, CE, Brazil*
[5]*Laboratory of Analytical and Environmental Chemistry, Regional University of Cariri, Crato, CE, Brazil*
[6]*Ferdows School of Paramedical and Health, Birjand University of Medical Sciences, Birjand, Iran*
[7]*College of Korean Medicine, Kyung Hee University, Seoul 02447, Republic of Korea*

Correspondence should be addressed to Abolghasem Siyadatpanah; asiyadatpanah@yahoo.com, Bonglee Kim; bongleekim@khu.ac.kr, and Henrique D. M. Coutinho; hdmcoutinho@gmail.com

Received 11 January 2022; Revised 15 February 2022; Accepted 14 March 2022; Published 5 April 2022

Academic Editor: Jun Wu

Plants when exposed to toxic levels of metals can suffer morphological or physiological damage because toxic metals can interact with several vital molecules in the plant. One possibility to remove these contaminants from the environment is through the phytoremediation technique, since secondary metabolites produced by plants can reverse these damages. To evaluate the cytoprotective activity, the dry mass and possible damage to the membranes of *Lactuca sativa* (lettuce) seedlings subjected to different concentrations of mercury chloride in association with catechin and quercetin in suballelopathic concentration were determined. The coordination of mercury chloride with substances was also evaluated using vibrational spectroscopy (Raman and FTIR). The interaction of the mentioned flavonoids with mercury chloride was evidenced through vibrational spectroscopy. When the metal was associated with catechin and quercetin, there was an increase in dry mass of almost 3 times when compared with the $HgCl_2$ alone, demonstrating that these flavonoids act as cytoprotective agents. However, in the presence of catechin and quercetin, membrane damage caused by mercury chloride has a level similar to that observed in control plants, demonstrating none statistical difference. Comparing the highest concentration with the lowest concentration of the metal associated with quercetin, it can be seen that the intensity of the peaks in this region decreases when the concentration of the metal increases, indicating an interaction between the metallic compound and the flavonoid. In this context, the use of secondary metabolites can be an alternative in the process of remediation of areas contaminated by mercury chloride, as they mitigate the effects of mercury chloride on lettuce seedlings.

1. Introduction

One of the most worrying issues today is the rise in pollution levels, whether atmospheric, aquatic, or terrestrial, which results in harmful conditions for organisms [1]. Among the main drivers of this scenario are toxic metals, responsible for the contamination and degradation of ecosystems [2].

Mercury is among the biggest environmental contaminants, causing significant reductions in biodiversity [3]. This metal with high toxicity content is usually found in inorganic form, such as mercury chloride ($HgCl_2$), and its disposal is related, for example, to the indiscriminate elimination of effluents from mining activities, the use of chemical products in agricultural practices, foundries, and industrial activities [4].

The use of natural products with antioxidant and chelating activities is among the main alternatives to reverse or prevent the toxic effects of metals on living beings [5]. Among these, phenolic compounds form one of the largest groups of secondary metabolites with therapeutic potential [6]. Furthermore, these compounds have high antioxidant activity, inhibiting the action of reactive oxygen species (ROS), thus avoiding lipid peroxidation that damages the cellular structure of organisms [7].

Flavonoids are among the most abundant phenolic compounds in vegetables, being concentrated in the aerial part of plants, such as flowers and fruits [8]. In addition to chelation of metals and protecting the body against oxidizing agents, these polyphenols are recognized for their bioactivities, such as anti-inflammatory, antitumor, antimicrobial, cardioprotective, and enzymatic inhibition [9].

Catechin and quercetin are flavonoids that, in addition to having the aforementioned biological activities, have gastroprotective, anticancer, antiallergic, antidiabetic, antihypertensive, vasodilatory, immunomodulatory, and antineurodegenerative effects [10–12]. In addition, they denote potential applicability in the remediation of areas contaminated by toxic metals, due to their significant antioxidant activity, free radical scavenging, and chelating mechanisms [13, 14].

Studies evaluating the interaction of phenolic compounds with toxic metals such as mercury are increasing, such as the studies by [15–17] and [18] aiming at their removal from contaminated environments. Thus, the present study was aimed at evaluating the cytoprotective effect of catechin and quercetin against the toxic action of mercury chloride on *Lactuca sativa* (lettuce) seeds, as well as vibration through interaction of compounds with spectroscopy (Raman).

2. Materials and Methods

2.1. Evaluation

2.1.1. Evaluation of the Cytoprotective Effect of Flavonoids in Lactuca Sativa against Mercury Chloride. To conduct the test, Petri dishes were prepared as described by Sobral-Souza et al. [19–21]. For the concentrations used, a suballelopathic concentration of the extract and fractions (8 μg/mL) and mercury chloride ($HgCl_2$) were used, ranging from 1.25 mM to 0.05 mM. The parameters analyzed at the end of seven days were as follows: germinated seed count, germination rate index (GRI), biometrics, and occurrence of root necrosis and seedling abnormalities, following the Seed Analysis Rules Manual [22]. The tests were done in triplicate and expressed as mean.

2.1.2. Electrolyte Leak Test. The percentage of damage to stem membranes and rootlets of germinated lettuce seeds was estimated using the electrolyte leak method described by Blum and Ebercon [23]. These plant tissues were separated and incubated in 25 mL of deionized water for a period of 2 hours at a temperature of 25°C. After that time, the electrical conductivity of the incubation solution was measured using an Oakton COM 700 conductivity meter. This first electrical conductivity reading was called L_1. Then, each tissue in its respective solution will be incubated in a water bath at 75°C for 30 minutes to release the cell electrolytes and cooled to room temperature, and the electrical conductivity of the solution will be determined as previously indicated. This second reading was called L_2. The following formula was used to calculate the percentage of membrane damage: $\mathrm{VE}\,(\%) = (L_2/L_1) \times 100$, where VE = percentage of membrane damage; L_1 = initial reading; and L_2 = final reading.

2.1.3. Fourier Transform Infrared Spectroscopy. For the analysis of the samples, an infrared absorption spectrometer by Fourrier FT-IR VERTEX 70 V, of the Bruker brand, was used. A Globar source is used for the medium infrared (MIR) region equipped with DL to TGS pyroelectric detectors to capture signals emitted from the sample. This equipment has a HeNe laser source with 633 nm of wavelength that allows the calibration of the optical path of the infrared beam next to the spectrometer mirrors. This spectrometer operates with a resolution of 2 cm^{-1} and a wide-range beam divider (beamspliter) composed of silicon that allows its use for measurements in the middle region. The use of vacuum in these experiments is important to improve the sensitivity of the detector.

2.1.4. Fourier Transform Raman Spectroscopy. The FT-Raman spectrum was recorded in the wavenumber range from 40 to 4000 cm^{-1} using a compacted powder of the sample in the sample holder of a Bruker RAM II FT-Raman module coupled to the VERTEX 70 spectrometer as well as a liquid nitrogen cooled high-sensitivity Ge detector. The samples were excited with the 1064 nm line of a Nd: YAG laser and we obtained a typical resolution of ~2 cm^{-1} with accumulation of 60 scans per spectra and a nominal laser power of 150 mW.

2.2. Statistical Analysis. All determinations were performed in triplicate and the results of chemical and vegetable tests were analyzed by calculating the arithmetic means with the Bonferroni and ANOVA.

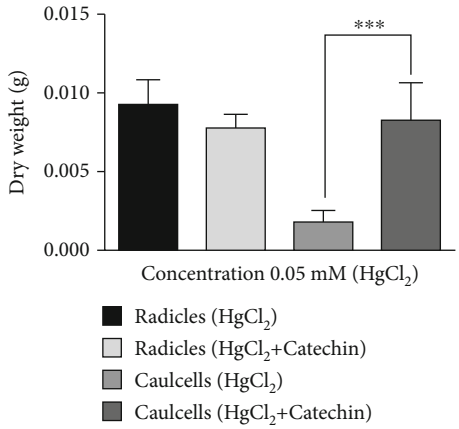

Figure 1: Effect of isolated mercury chloride ($HgCl_2$) and in association with catechin on the dry mass of radicles and stems of *Lactuca sativa*.

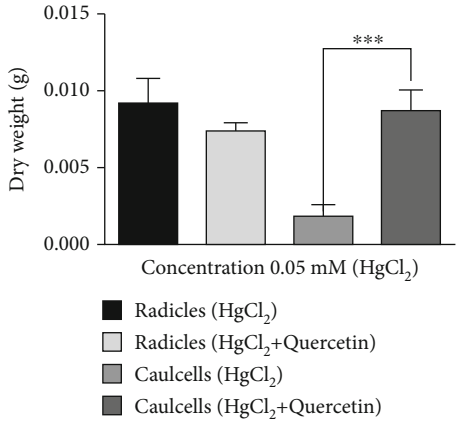

Figure 2: Effect of isolated mercury chloride ($HgCl_2$) and in association with quercetin on the dry mass of radicles and stems of *Lactuca sativa*.

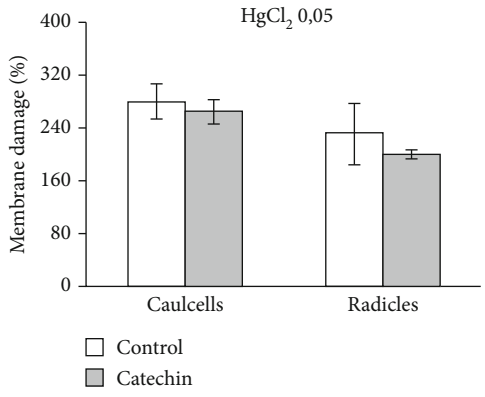

Figure 3: Membrane damage in *Lactuca sativa* caused by 0.05 mM $HgCl_2$ in the absence and presence of catechin.

3. Results

3.1. Growth of Stems and Roots. Figures 1 and 2 show the results of the action of mercury chloride on the dry mass of *L. sativa*. In the tested concentration of this metal, a reduction in the weight of the stems was observed, thus showing its interference in the development of plant tissues. However, when the metal was associated with catechin and quercetin, there was an increase in dry mass, demonstrating that these flavonoids act as cytoprotective agents, thus allowing for greater growth of the stems. When the action of mercury chloride alone or in association with the flavonoids used was evaluated, there was no interference in the dry mass of the radicles, thus showing that at a concentration of 0.05 mM, the metal did not alter the development of the plant species.

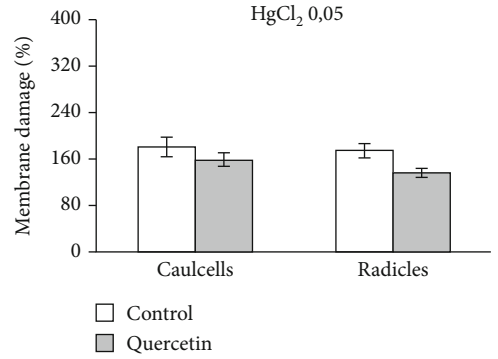

Figure 4: Membrane damage in *Lactuca sativa* caused by 0.05 mM $HgCl_2$ in the absence and presence of quercetin.

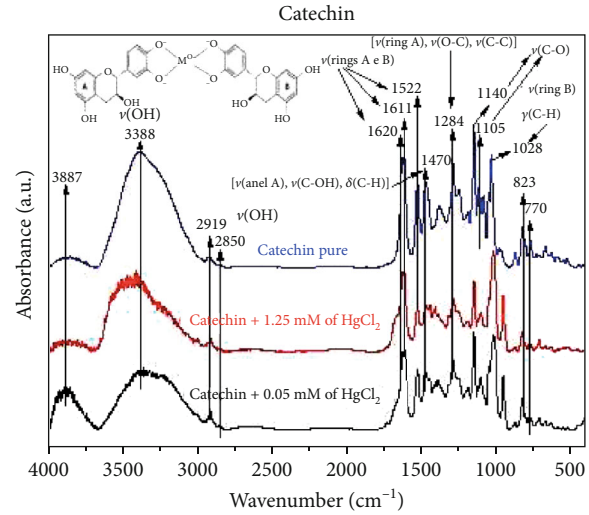

Figure 5: Spectra of pure catechin and associated mercury chloride at 0.05 mM and 1.25 mM.

3.2. Electrolyte Leaks. In this test, membrane damage in *L. sativa* caused by 0.05 mM mercury chloride in the absence and presence of catechin and quercetin was observed. Membrane damage was measured to observe the stability of *L. sativa* cell membranes as a function of mercury chloride concentrations when associated with these substances or alone. In this early stage of growth, the observation of damage to the membranes is essential and represents a good

Table 1: Characterization of the most relevant FTIR peaks of pure catechin and associated with mercury chloride.

Wavenumber (cm^{-1})			
Pure	0.05 mM $HgCl_2$	1.25 mM $HgCl_2$	Assignment
770	770	770	Deformation outside the OH group plane [24, 25]
823	823	823	δ (C-H) off plan [24, 25]
1028	1020	1020	Stretching of aromatic ring B and C-H bonds
1105	1103	1103	ν (C=O) [24, 25]
1140	1140	1140	ν (C=O) [24, 25]
1284	1284	1284	ν (ring A), ν (O-C), and ν (C-C) [24, 25]
1470	1466	1466	ν (anel A), ν (C-OH), and δ (C-H) [24, 25]
1522	1520	1520	ν (rings A and B) [24, 25]
1611	1611	1611	ν (rings A and B) [24, 25]
1620	1620	1620	ν (rings A and B) [24, 25]
2850	2850	2850	ν (O-H) [24, 25]
2919	2919	2919	ν (O-H) [24, 25]
3388			ν (O-H) [24, 25]
3887			

ν = stretching, δ = bending, r = rocking, and ω = wagging.

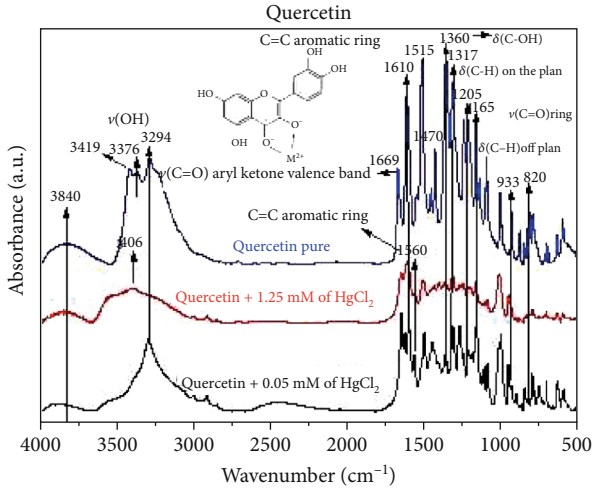

Figure 6: Spectra of pure quercetin and associated mercury chloride at 0.05 mM and 1.25 mM.

indicator to understand the toxic effect of the metal and the cytoprotective role of these flavonoids.

In Figures 3 and 4 the results show that in the presence of catechin and quercetin, membrane damage caused by mercury chloride has a level similar to that observed in the control plants (treated with water only). This preliminary result initially suggests this possible protective role of catechin and quercetin at a concentration of 0.05 mM against the toxicity of mercury chloride in both stems and radicles of *L. sativa*, this cytoprotection being statistically more relevant in the stems, which corroborates the electrolyte leakage tests.

3.3. FT Raman and FTIR Spectroscopy. The main bands characterized in the FTIR spectrum of the catechin, compared to the literature, were the stretching of the O-H bonds in the region of 3388 cm^{-1}, stretching of the C-H bonds in 2919 cm^{-1}, and aromatic ring stretch vibrations (A, B), also known as breathing vibration (Breathing). phenolic carbon-carbon bonds (1620, 1611, 1522 cm^{-1}). The peak in 1470 cm^{-1} was attributed to the stretch vibration of the connection of C-OH in phenol (A), while the peak 1284 cm^{-1} is associated with the aromatic ring A and the stretching of bonds COC and CC. The peak 1140 cm^{-1} was attributed to the stretching of the C-O link. The stretching of the aromatic ring B and C-H bonds was associated with the peak 1020 cm^{-1} [24, 25].

When observing the spectrum of pure catechin shown in Figure 5, a shift and decrease in peak intensity related to the O-H stretching occurs in the region of 3388 cm^{-1}, for the region of longest wavelength if we compare the smallest and the largest concentration with the metal.

There is a decrease in the peak intensities of 1522 cm^{-1} and 1470 cm^{-1} when catechin is put to react with $HgCl_2$ at concentrations of 0,05 and 1,25 mM. This decrease in peak intensity may be related to a possible coordination that the Hg^{2+} ion can make with the deprotonated oxygens of the phenolic groups present in the catechin structure. The decrease and small displacement of the peak in 1140 cm^{-1} also signals a possible coordination of the metallic ion with the catechin structure. A shift to lower energy frequencies is also observed in the stretch in 770 cm^{-1} referring to the out-of-plane deformation of the OH cluster (Table 1) [26].

Figure 6 shows the most relevant bands of quercetin. It is attributed to the OH stretch (Table 2) and the bands around 3400 cm^{-1}, the peak 1669 cm^{-1} is associated with the C=O vibration of the aryl ketone valence band. The peaks 1610, 1560 and 1515 cm^{-1} are associated with the C=C stretch vibration of aromatic rings. The spectrum also shows bending peaks from C-OH, in 1360 cm^{-1}, it is from OH in the phenol in 1377 cm^{-1}, in addition to CH flexion in the plane, in 1317 cm^{-1}. In 1205 cm^{-1} and 1165 cm^{-1}, we have peaks

Table 2: Characterization of the most relevant FTIR peaks of pure quercetin and associated with mercury chloride.

Wavenumber (cm^{-1})			
Pure	0.05 mM $HgCl_2$	1.25 mM $HgCl_2$	Assignment
820	820	820	δ (C-H) off plan [27, 28]
1165	1165	1165	ν (C=O) ring [27, 28]
1205	1205	1205	ν (C=O) ring [27, 28]
1317	1316	1316	δ (C-H) off plan [27, 28]
1360	1358	1357	δ (C-OH) [27, 28]
1515	1510	1510	C=C aromatic ring [27, 28]
1556	1560	1560	C=C aromatic ring [27, 28]
1610	1610	1510	C=C aromatic ring [27, 28]
1669	1654	1654	ν (C=O) aryl ketone valence band [27, 28]
3294	3294		ν (O-H) [27, 28]
3376			ν (O-H) [27, 28]
3406			ν (O-H) [27, 28]
3419			ν (O-H) [27, 28]

ν = stretching, δ = bending, r = rocking, and ω = wagging.

referring to stretch vibration C-O in the aromatic ring and bending out of plane in 820 cm^{-1} [27, 28].

It is observed by the infrared spectrum of pure quercetin and quercetin after the reaction with $HgCl_2$ at concentrations of 0,05 and 1,25 mM, a change in the band attributed to the carbonyl group which has a decrease in peak intensity in 1669 cm^{-1}. There is also a decrease in peak intensities in 1515 and 1360 cm^{-1}. This demonstrates a possible metal-to-ligand coordination from carbonyl oxygen.

The vibrational deformation originated from C-OH bonds is reflected in peaks formed in the region of 1300-1400 cm^{-1}, while the stretch deformations are located 1100 and 1200 cm^{-1} [28].

The peak reflected in the region between 3400 and 3200 cm^{-1} refers to symmetrical stretching O-H [29]. It is noticed that as there is an increase in the metal concentration, but mainly in the concentration of 1,25 mM, there is an absence of the peak absorbance. This could be due to the heavy metal binding that supposedly occurs in this radical.

4. Discussion

The results obtained about the effect of mercury chloride on the growth of *Lactuca sativa* and its dry mass are similar to those described by Rocha et al. [15–17] and Silva et al. [18], where they demonstrate the cytoprotective effect of several metabolites against the toxic action of mercury chloride.

Mercury at high levels affects seed germination and initial seedling growth, even though they have defense mechanisms against different types of stress, during germination and early development they become less tolerant [30–32]. Study with the translocation and biotoxicity of metal (oxide) nanoparticles in the wet plant system shows that *P. australis* are initially retained by the root system, followed by uptake and air transport throughout the plant [33].

Study carried out by Sobral-Souza et al. [34] showed that the presence of phenolic acids and flavonoids in samples of *Eugenia jambolana* demonstrated cytoprotective effect on the action of mercury chloride, in the stem and root development of lettuce seeds; in this study, the concentrations of mercury chloride were the same used in this research and the extract of this species also showed an expressive concentration of flavonoids in its composition.

Although the protection mechanisms using isolated substances are not fully clarified, it is preliminarily inferred that these substances may have reduced the absorption of mercury chloride by the lettuce roots or acted as an antioxidant system of the seedlings against the oxidative stress caused by this metal. Studies with the flavonoid rutin showed cytoprotection in lettuce seedlings, probably due to the antioxidant and chelating activity of this substance. Cytoprotection was verified in the eukaryotic plant model when rutin was associated with $HgCl_2$ at a concentration of 0.05 mM to promote the growth of radicles and stems, which corroborates these results [35].

Several studies have documented adverse effects caused by toxic metals in plants, such as changes in the pattern of germination and growth and morphology of radicles, stems, and leaves [36, 37]. Studies using the plant supercritical carbon dioxide (SFE) system to evaluate flavonols that play a key role in heavy metal resistance have indicated that flavonoids can improve resistance to oxidative stress by quenching the ROS [38].

[26] studying the coordination of the gallium ion, the structure of quercetin proposed that the hydroxyl group of the carbon neighboring the carbonyl has a more acidic proton, when compared to the other protons of the other phenolic groups. This fact results in a greater possibility of coordination of the metal ion occurring via carbonyl oxygen and oxygen from the deprotonated phenolic group. Probably the other phenolics should not be involved in the coordination of the metallic ion due to the lower acidity and the possible spatial impediment caused by the first complexation.

Flavonoid compounds have the ability to form complexes with metallic ions and exhibit the greatest

physiological strength, such as the association of quercetin [39]. Analyzing the infrared spectrum of isolated quercetin, it can be noted that the peaks related to the vibration of the aromatic ring are concentrated in the region of 1400 and 1600 cm^{-1}. Comparing the highest concentration with the lowest concentration of the metal associated with quercetin, it can be seen that the intensity of the peaks in this region decreases when the concentration of the metal increases, indicating an interaction between the metallic compound and the flavonoid [28, 40].

Previous studies such as the one by [41] had already demonstrated the complexation capacity of flavonoids, especially rutin, which had greater activity in the scavenging of superoxide radicals when complexed to copper and iron metals.

5. Conclusions

This study suggests that although mercury chloride causes cytotoxicity in several plant species, its complex with the flavonoids catechin and quercetin can minimize these effects, thus allowing for better plant growth, which can be observed by preserving plant tissue, *Lactuca sativa*, demonstrated by the increase in dry mass. Although these results are innovative and promising regarding the search for new alternatives for the decontamination of areas polluted by toxic metals, further studies are needed to observe the effect of their application in contaminated areas.

Data Availability

The data used to support the findings of this study are available from the corresponding author upon request.

Conflicts of Interest

The authors declare no conflict of interest.

Authors' Contributions

S.R.T., J.C.A.P., C.E.S.S., A.K.S., J.C.A.P., J.H.d.S., and H.D.M.C. were responsible for the conceptualization; Y.M.L.S.d.M. and J.B.d.A.N. were responsible for the methodology; A.K.S. was responsible for the software; D.L.M.V., A.C.H.B., F.F.C., and M.M.C.d.S. were responsible for the validation ; Y.M.L.S.d.M. was responsible for the formal analysis ; Y.M.L.S.d.M. and J.B.d.A.N. were responsible for the investigation; H.D.M.C., T.T.A.Y., A.S., and R.N.P.T. were responsible for the resources; A.K.S. was responsible for the data curation; Y.M.L.S.d.M. and J.B.d.A.N. were responsible for writing and original draft preparation; J.E.R., C.E.S.S., and B.K. were responsible for writing, reviewing, and editing; J.B.d.A.N. and M.M.C.d.S. were responsible for visualization; H.D.M.C. and J.C.A.P. were responsible for the supervision; H.D.M.C. was responsible for the project administration; A.S. and B.K were responsible for the funding acquisition. All authors have read and agreed to the published version of the manuscript.

Acknowledgments

This research was funded by the Basic Science Research Program through the National Research Foundation of Korea (NRF) funded by the Ministry of Education (NRF-2020R1I1A2066868), the National Research Foundation of Korea (NRF) grant funded by the Korea government (MSIT) (No. 2020R1A5A201941311), and a grant of the Korea Health Technology R&D Project through the Korea Health Industry Development Institute (KHIDI), funded by the Ministry of Health and Welfare, Republic of Korea (grant number: HF20C0116).

References

[1] G. L. Silveira, M. G. F. Lima, G. B. Dos Reis, M. J. Palmieri, and L. F. Andrade-Vieria, "Toxic effects of environmental pollutants: comparative investigation using _Allium cepa_ L. and _Lactuca sativa_ L.," *Chemosphere*, vol. 178, pp. 359–367, 2017.

[2] P. L. Kilunga, P. Sivalingam, A. Laffite et al., "Accumulation of toxic metals and organic micro-pollutants in sediments from tropical urban rivers, Kinshasa, Democratic Republic of the Congo," *Chemosphere*, vol. 179, pp. 37–48, 2017.

[3] Z. Niu, Y. Cao, W. Zhao, and R. Li, "Distribution and assessment of mercury (hg) in surface sediments of Futian mangrove forest, China," *Environmental Geochemistry and Health*, vol. 41, no. 1, pp. 125–134, 2019.

[4] C. N. F. Lima, T. F. Valero, N. F. Leite et al., "Acción protectora de Duguetia furfuracea (A. St.-Hil.) Saff. contra la toxicidad por cloruro de mercurio en Escherichia coli," *Rev. Cuba. de Plantas Medicinales*, vol. 19, pp. 179–188, 2014.

[5] N. F. Leite, C. E. Sobral-Souza, R. S. Albuquerque, A. I. Pinho, F. A. B. Cunha, and H. D. M. Coutinho, "Reduction of the toxic effect of mercurium chloride by chelating effect of _Psidium brownianum_ Mart. ex DC.," *International Biodeterioration & Biodegradation*, vol. 119, pp. 538–541, 2017.

[6] D. Lin, M. Xiao, J. Zhao et al., "An overview of plant phenolic compounds and their importance in human nutrition and management of type 2 diabetes," *Molecules*, vol. 21, no. 10, p. 1374, 2016.

[7] N. F. Leite, C. E. Sobral-Souza, E. F. Matias et al., "Efecto citoprotector de extractos de Eugenia jambolana y Psidium myrsinites DC. A. contra peroxidación lipídica inducida por hierro II," *Acta Toxicol. Argent.*, vol. 24, pp. 187–192, 2016.

[8] F. Perez-Vizcaino and C. G. Fraga, "Research trends in flavonoids and health," *Archives of Biochemistry and Biophysics*, vol. 646, pp. 107–112, 2018.

[9] A. N. Panche, A. D. Diwan, and S. R. Chandra, "Flavonoids: an overview," *J. Nutr. Sci.*, vol. 5, pp. 1–15, 2016.

[10] J. Ye and M. A. Augustin, "Nano- and micro-particles for delivery of catechins: physical and biological performance," *Critical Reviews in Food Science and Nutrition*, vol. 59, no. 10, pp. 1563–1579, 2019.

[11] P. V. Gadkari and M. Balaraman, "Catechins: sources, extraction and encapsulation: a review," *Food and Bioproducts Processing*, vol. 93, pp. 122–138, 2015.

[12] A. V. A. David, R. Arulmoli, and S. Parasuraman, "Overviews of biological importance of quercetin: a bioactive flavonoid," *Pharmacognosy Reviews*, vol. 10, no. 20, p. 84, 2016.

[13] J. Wu, R. Guan, G. Cao et al., "Antioxidant and antimicrobial effects of catechin liposomes on Chinese dried pork," *Journal of Food Protection*, vol. 81, no. 5, pp. 827–834, 2018.

[14] M. Lesjak, I. Beara, N. Simin et al., "Antioxidant and anti-inflammatory activities of quercetin and its derivatives," *Journal of Functional Foods*, vol. 40, pp. 68–75, 2018.

[15] J. E. Rocha, T. T. A. M. Guedes, C. F. Bezerra et al., "Identification of the gallic acid mechanism of action on mercuric chloride toxicity reduction using infrared spectroscopy and antioxidant assays," *International Biodeterioration & Biodegradation*, vol. 141, pp. 24–29, 2019.

[16] J. E. Rocha, T. T. A. M. Guedes, C. F. Bezerra et al., "Mercury chloride phytotoxicity reduction using antioxidative mechanisms evidenced by caffeic acid FTIR," *Applied Geochemistry*, vol. 104, pp. 109–115, 2019.

[17] J. E. Rocha, T. T. A. M. Guedes, C. F. Bezerra et al., "FTIR analysis of pyrogallol and phytotoxicity-reductive effect against mercury chloride," *Environmental Geochemistry and Health*, vol. 43, no. 6, pp. 2433–2442, 2021.

[18] J. P. Da Silva, M. D. S. Costa, F. F. Campina et al., "Evaluation of chelating and cytoprotective activity of vanillin against the toxic action of mercuric chloride as an alternative for phytoremediation," *Environmental Geochemistry and Health*, vol. 43, no. 4, pp. 1609–1616, 2021.

[19] C. E. Sobral-Souza, N. F. Leite, F. A. B. Cunha et al., "Cytoprotective effect against mercury chloride and bioinsecticidal activity of _Eugenia jambolana_ Lam.," *Arabian Journal of Chemistry*, vol. 7, no. 1, pp. 165–170, 2014.

[20] C. E. Sobral-Souza, N. F. Leite, F. A. B. Cunha, A. I. Pinho, J. G. M. Costa, and H. D. M. Coutinho, "Avaliação da atividade antioxidante e citoprotetora dos extratos de Eugenia uniflora Lineau e Psidium sobraleanum proença & Landrum contra metais pesados," *Rev. Cienc. Salud.*, vol. 12, no. 3, pp. 401–409, 2014.

[21] H. D. M. Coutinho, G. M. A. B. Martins, M. F. B. Morais-Braga et al., "Stryphnodendron rotundifolium Mart. As an adjuvant for the plant germination and development under toxic concentrations of $HgCl_2$ and $AlCl_2$," *Water, Air, and Soil Pollution*, vol. 228, no. 11, p. 424, 2017.

[22] Brasil Ministry of Agriculture, Department of Plant Production, *Division of Seeds and Seedlings. Rules for Seed Analysis*, LANARV/SNAD/MA, Brasilia, Brazil, 2009.

[23] A. Blum and A. Ebercon, "Cell membrane stability as a measure of drought and heat tolerance in wheat1," *Crop Science*, vol. 21, no. 1, pp. 43–47, 1981.

[24] M. M. Ramos-Tejada, J. D. G. Durán, A. Ontiveros-Ortega, M. Espinosa-Jimenez, R. Perea-Carpio, and E. Chibowski, "Investigation of alumina/(+)-catechin system properties. Part I: a study of the system by FTIR-UV-Vis spectroscopy," *Colloids and Surfaces, B: Biointerfaces*, vol. 24, no. 3-4, pp. 297–308, 2002.

[25] A. Torreggiani, Z. Jurasekova, S. Sanchez-Cortes, and M. Tamba, "Spectroscopic and pulse radiolysis studies of the antioxidant properties of (+)catechin: metal chelation and oxidizing radical scavenging," *Journal of Raman Specroscopy*, vol. 39, no. 2, pp. 265–275, 2008.

[26] V. D. N. Simões, L. R. V. Favarin, N. A. Cabeza et al., "Síntese, caracterização e estudo das propriedades de um novo complexo mononuclear contendo quercetina e íon Ga(III)," *Quimica Nova*, vol. 36, no. 4, pp. 495–501, 2013.

[27] M. Catauro, F. Papale, F. Bollino et al., "Silica/quercetin sol–gel hybrids as antioxidant dental implant materials," *Science and Technology of Advanced Materials*, vol. 16, no. 3, p. 035001, 2015.

[28] M. Heneczkowski, M. Kopacz, D. Nowak, and A. Kuzniar, "Infrared spectrum analysis of some flavonoids," *Acta Poloniae Pharmaceutica*, vol. 58, no. 6, pp. 415–420, 2001.

[29] R. M. Silverstein, G. C. Bassler, and T. C. Morrill, *Spectrometric Identification of Organic Compounds*, John Wiley & Sons, New York, United States, 7th ed. edition, 2005.

[30] S. Reetha, R. Bakiyaraj, P. Thamizhiniyan, and G. Bhuvaneswari, "Effect of cadmium nitrate and mercury chloride on germination, growth and biochemical constituents of onion seedlings (Allium cepa L.)," *Int. J. Res. Biol. Sci.*, vol. 2, pp. 182–186, 2012.

[31] N. C. Aery and S. Sarkar, "Metal species vis-à-vis seed germination and early seedling growth responses in soybean," *J. Chem. Bio. Phy. Sci.*, vol. 2, pp. 763–769, 2012.

[32] R. K. Jain, "Study of heavy metals effect in response to linum seed germination," *African Journal of Plant Science*, vol. 7, no. 3, pp. 93–109, 2013.

[33] X. Y. Yang, Q. He, F. C. Guo, X. B. Liu, and Y. Chen, "Translocation and biotoxicity of metal (oxide) nanoparticles in the wetland-plant system," *Frontiers of Environmental Science & Engineering*, vol. 15, no. 6, p. 138, 2021.

[34] C. E. Sobral-Souza, A. R. P. Silva, N. F. Leite et al., "Phytotoxicity reduction of the mercury chloride effect by natural products from _Eugenia jambolana_ Lam.: a new strategy against the toxic metal pollution," *Ecotoxicology and Environmental Safety*, vol. 170, pp. 461–467, 2019.

[35] Y. M. L. S. De Matos, J. E. Rocha, C. E. S. Souza et al., "FTIR analysis and reduction of the phytotoxic effect of mercury dichloride by rutin," *Rhizosphere*, vol. 19, article 100393, 2021.

[36] S. Silva, C. Santos, M. Matos, and O. Pinto-Carnide, "Al toxicity mechanism in tolerant and sensitive rye genotypes," *Environmental and Experimental Botany*, vol. 75, pp. 89–97, 2012.

[37] Y. Yang, X. Wei, J. Lu, J. You, W. Wang, and R. Shi, "Lead-induced phytotoxicity mechanism involved in seed germination and seedling growth of wheat (_Triticum aestivum_ L.)," *Ecotoxicology and Environmental Safety*, vol. 73, no. 8, pp. 1982–1987, 2010.

[38] X. Zhang, H. Yang, X. Wang, W. Song, and Z. Cui, "An extraction-assay system: evaluation on flavonols in plant resistance to Pb and Cd by supercritical extraction-gas chromatography," *Frontiers of Environmental Science & Engineering*, vol. 12, no. 4, pp. 6–15, 2018.

[39] A. Kumar, A. Mishra, A. K. Mishra, and H. Singh, "Quantification of the secondary metabolites by HPTLC, analgesic and antipyretic activity evaluation of Ficus racemosa L. leaves," *Oriental Pharmacy and Experimental Medicine*, vol. 19, no. 1, pp. 59–69, 2019.

[40] L. C. A. Barbosa, *Espectroscopia no infravermelho na caracterização de compostos orgânicas*, UFV, Viçosa, Brazil, 1st ed. edition, 2013.

[41] M. Y. Moridani, J. Pourahmad, H. Bui, A. Siraki, and P. J. O'brien, "Dietary flavonoid iron complexes as cytoprotective superoxide radical scavengers," *Free Radical Biology & Medicine*, vol. 34, no. 2, pp. 243–253, 2003.